SEISMIC STRENGTHENING
BY PROVIDING STRUCTURAL DIAPHRAGM

by

Renjun Wang, B.S.; M.S.

Dissertation

Presented to the Faculty of the Graduate School of

The University of Texas at Austin

in Partial Fulfillment

of the Requirements

for the Degree of

Doctor of Philosophy

The University of Texas at Austin

August 2006

Acknowledgements

I would like to especially thank Professor James O. Jirsa and Professor Sharon L. Wood for their guidance and patience. which were exceptional and vital for the accomplishment of the work described in this dissertation. I would also thank Dr. Eric B. Williamson for his suggestions in the study for this dissertation. I will always remember them for all the help and advice they gave me during my study.

In general, I would like to thank The University of Texas. Due to all the support that the university provided, I have now accomplished all my illusions and dreams. I will always have U.T. in my mind and heart.

I would like finally to thank my friends, I wish them the best future. My wife and my son are the most important part of my life, and this success is also theirs. With all of them I share this huge happiness.

Seismic Strengthening by Providing Structural Diaphragm

Publication No._____

Renjun Wang, Ph. D.

The University of Texas at Austin, 2006

Co-Supervisors: James O. Jirsa

Sharon L. Wood

There are a large number of precast frame buildings used in Turkey for industrial facilities. One-story warehouses are the most common structural configurations. Because there was little redundancy in the lateral load resisting system, many precast buildings were damaged beyond repair during the 1999 earthquakes in Turkey. In the present study, a rehabilitation scheme is proposed to add a structural diaphragm at the roof level by adding diagonal bracing. With the diaphragm action developed, the lateral forces can be transmitted among the cantilever columns, and to the vertical diagonal braces on the periphery, thus the seismic performance can be enhanced. An analysis method is also developed for the rehabilitation design.

Table of Contents

List of Tables

List of Figures

xiv

Chapter 1: Introduction

1.1 GENERAL

During earthquakes, it is essential for structures to transmit lateral forces caused by seismic motion to lateral force resisting systems (LFRS). Structural diaphragms play an important role for the transmission of forces in an earthquake. For structures with large open areas, seismic performance is often dictated by diaphragm action. Buildings with insufficient diaphragms (lack of strength or continuity) generally exhibit poor structural performance during an earthquake. One-story precast concrete frame systems commonly used as industrial buildings in Turkey represent an example of a system with inadequate diaphragm.

Since their introduction into Turkey in the 1960s, precast frame buildings have been used almost exclusively for industrial facilities. Approximately 90% of the warehouses and light industrial facilities constructed during the 1990s in Turkey were built using precast members (Karaesmen, 2001) because the structures are economical to construct and can provide large open areas for a multitude of purposes. Among precast systems, one-story structural configurations are the most common structural form.

However, the structural system was originally developed in Western Europe to carry gravity loads only (Ersoy et al. 1999), and the lateral capacity is low. Unfortunately, Turkey is located in a high seismic risk area. Even though Turkish engineers made some modifications to the connection details to improve seismic performance, their actual behavior during earthquakes was still disappointing. Structural damage and collapse of precast industrial buildings were widely reported throughout the epicentral regions of the 1999 earthquakes in Turkey.

1

So far, the research on the behavior of precast structures under seismic action is quite limited. There is an urgent need to understand the seismic response of precast systems and then to develop practical rehabilitation schemes for those existing precast buildings.

The present study is concentrated on the one-story industrial buildings in Turkey because they represent the most common form of precast constructions in the epicentral region and many of them sustained severe damage during the 1999 earthquakes. Deficiencies of this structural style are studied and a practical rehabilitation scheme for this particular structural style is presented.

1.2   EARTHQUAKES ON AUGUST 17 AND NOVEMBER 12, 1999

In 1999, two large earthquakes occurred in the Anatolian region of northwest Turkey (Figure 1.1). One struck the Marmara region with a magnitude of 7.4 on August 17, 1999. This earthquake is called the Kocaeli Earthquake or the Marmara Earthquake. The second occurred with a magnitude of 7.1 on November 12, 1999, and is called the

Figure 1.1 Map of Turkey – Region Affected by the 1999 Earthquakes (Posada, 2001)

Düzce Earthquake. The region shaken by these two earthquakes is the most densely populated in Turkey. Almost 20 million people (one third of the Turkish population) live in this region, which includes Istanbul (Scawthorn, 2000). The region is the home to about 40% of Turkey's heavy industry (Johnson, 2000). The Turkish National Security Council estimated that 115,000 buildings suffered severe damage beyond repair and more than 500,000 people were left homeless by the two earthquakes (Aschheim 2000).

The epicenter of the Kocaeli Earthquake was approximately 12 km southeast of the city of Gölcük (Ataköy, 1999), and the Düzce Earthquake originated south of Düzce. These two earthquakes were related to the collision of three tectonic plates: the Arabian, the African, and the Eurasian (Lettis, 2000). The zone is crossed by North Anatolian Fault, a strike-stripe fault extending roughly in west-east orientation (Figure 1.2), and it was the movement of this fault that resulted in these two severe earthquakes.
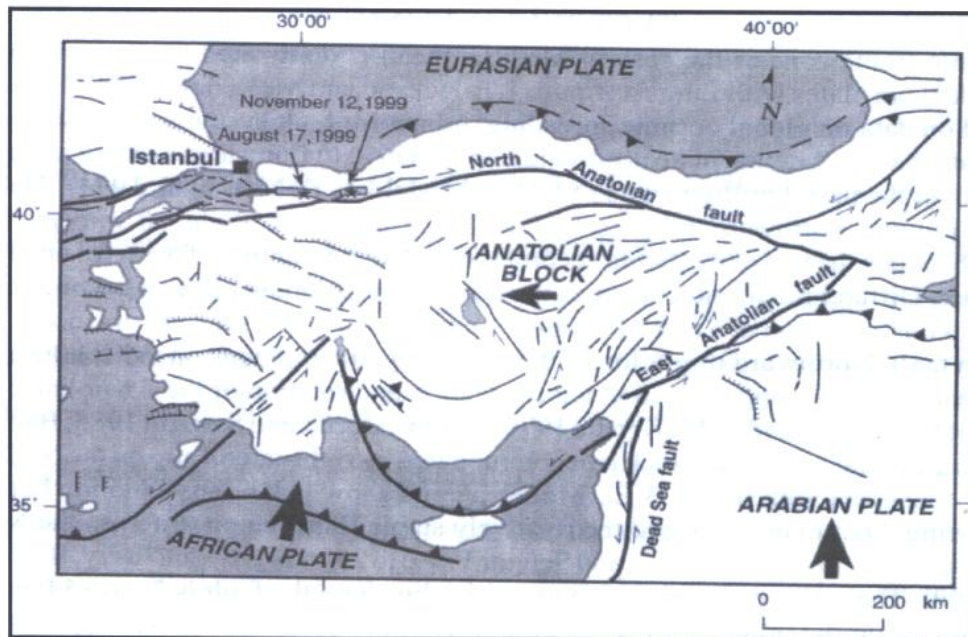
Figure 1.2 Tectonic Framework of the Anatolian Region (Lettis, 2000)

1.3   PRECAST BUILDINGS IN EPICENTRAL REGION

Precast concrete buildings are popularly used in the epicentral region because of the relatively low construction cost and the ability to provide large open areas for manufacturing. One-story frames are the most common precast structural systems used for industrial facilities. Some multi-story buildings made of precast concrete members are also present in the epicentral region.

One-story Precast Frames: Generally, the buildings are rectangular in plan with one to four bays in the transverse direction, and ten to thirty bays in the longitudinal direction (Figure 1.3 and Figure 1.4). The length of bays usually ranges from 10 to 25 meters in the transverse direction, and 6 to 8 meters in the longitudinal direction. Story height is typically 6 to 8 meters.
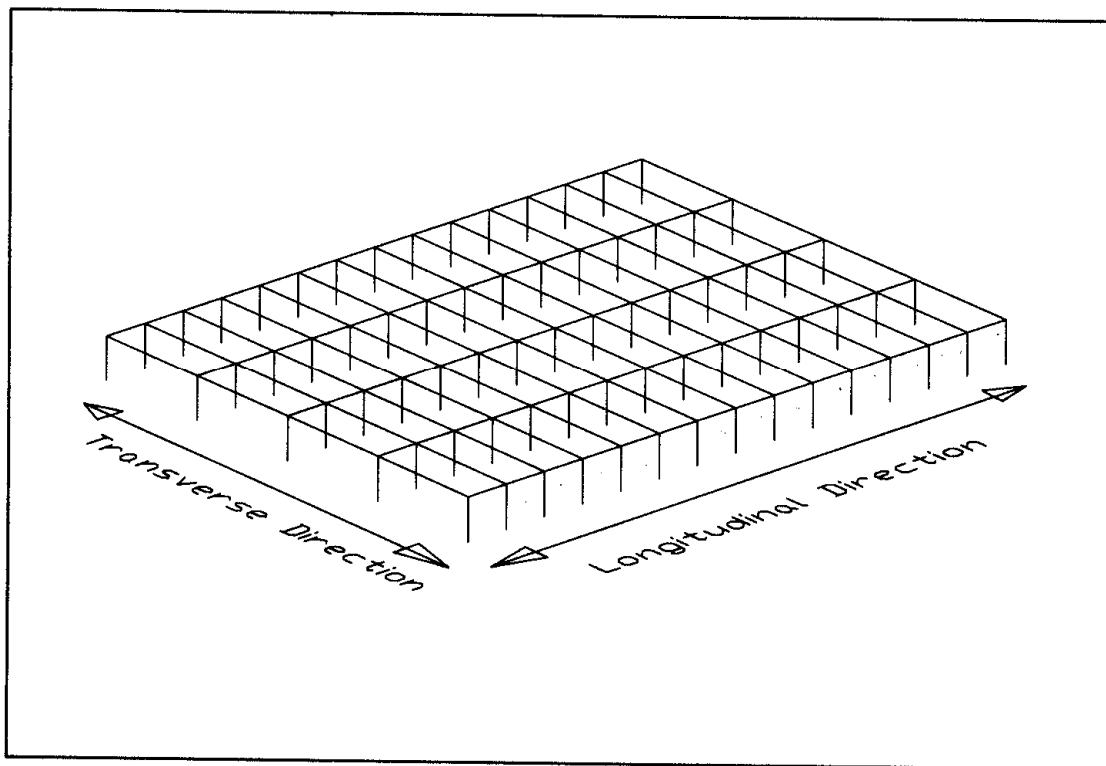
Figure 1.3 Typical Geometry of One-story Precast Frames (Posada, 2001)

4

Figure 1.4 Interior Photograph of a One-Story Precast Building

Rectangular precast columns are inserted into cast-in-place socket footings, and the gaps between the columns and the sockets are grouted. The columns support the whole structure and are assumed to be fixed at the base. Long-span roof girders, typically trapezoidal in shape, span in the transverse direction of the building. Purlins and U-shaped gutter beams (used to collect water from the roof) span in the longitudinal direction. The roof is constructed with metal decking or asbestos panels made of lightweight materials.

The columns, beams, girders and purlins are generally connected with each other using grouted pins (Figure 1.5), although some of the one-story precast concrete
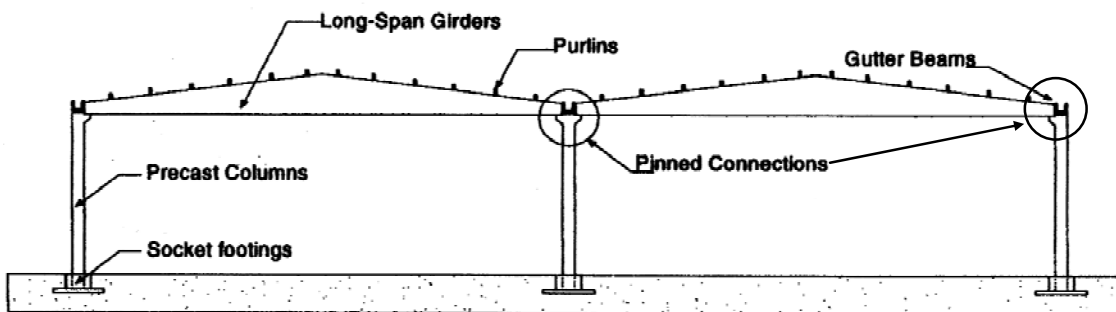
Figure 1.5 Elevation of a Typical Precast Concrete Building (Posada, 2001)

5

buildings are constructed with moment-resisting connections. In general, the lateral strength and stiffness of the building are provided only by the cantilevered columns, as the contribution from the other members is negligibly small.

Multi-Story Precast Frames: They are generally used for office and industrial purposes. Similarly to the one-story structures, these buildings are usually rectangular in plan, with precast roof girders, purlins, gutter beams and columns. The columns are precast the full height of the building up to about four stories, and lateral corbels are precast at middle stories for beam installation (Figure 1.6 and 1.7).

While the roof girders are connected to the other members (purlins and columns) using grouted pins, the beams of the middle stories are generally connected to the column corbels by moment-resisting connections. For buildings with more than four stories (sometimes even for low rise buildings), columns are connected to each other at mid-height.
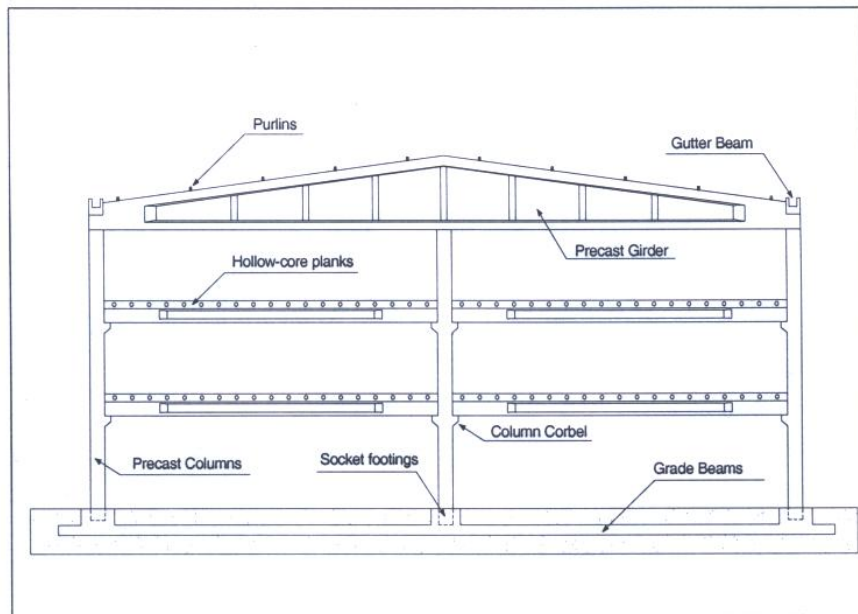
Figure 1.6 Elevation of a Typical Multi-Story Precast Frame (Posada, 2001)

6

Figure 1.7 Interior Photograph of a Multi-Story Precast Building

1.4   OBSERVED DAMAGE

Precast concrete buildings sustained considerable damage during 1999 earthquakes, especially those with precast pin-connected frames. The damage observed included:

a)   Buildings (Figure 1.8) in which all the girders fell from supports and columns sustained severe damage, and some completely collapsed. The building shown in Figure 1.8 was under construction at the time of the earthquake.

b)   Significant flexural cracking near the base of the columns indicating yielding of the column longitudinal reinforcement, some columns with inadequate flexural capacity failed at the base (Figure 1.9).

Figure 1.8 Photograph of a Completely Collapsed Precast Building

Figure 1.9 Damage Near the Base of Columns

c)   Lateral tilting of pin-connected. The grouted steel dowels used to brace roof girders were partially or completely pulled out (Figure 1.10).

d)   Concrete spalled at ends of roof girders (Figure 1.11).
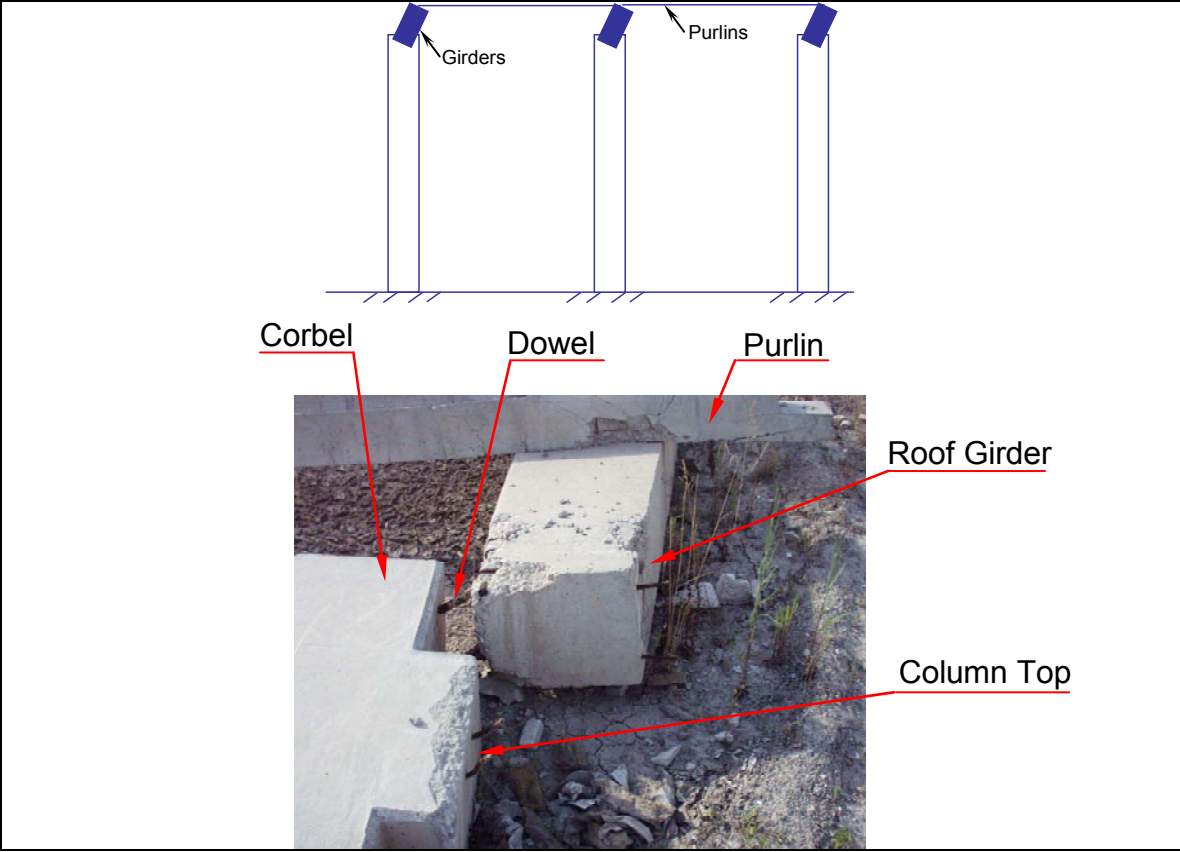
Figure 1.10 Girder Tilting and Dowel Pull-Out

Figure 1.11 Concrete Spalling

9

1.5   CAUSES OF THE OBSERVED DAMAGE

The primary analyses (Ataköy, 1999) (Ersoy,1999) conducted after the earthquakes on the industrial buildings revealed a few weaknesses that led to the observed damage. The tilting and falling of roof girders was principally due to the failure of column-girder connections. The column-girder connection represent one main difference between precast concrete frames and monolithic ones. In Figure 1.12, the details of such a connection typically used to hold roof girders to columns in precast buildings are illustrated.
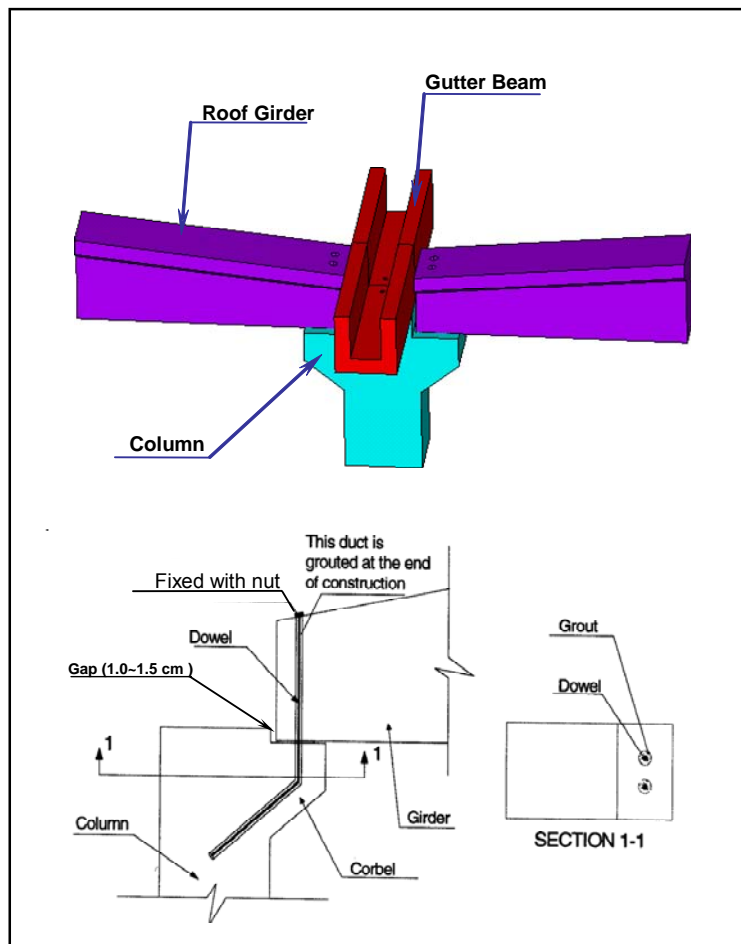
Figure 1.12 Details of a Typical Column-Girder Connection (Posada, 2001)

10

When members are cast, one or two holes are preset at each end of a roof girder, and L-shaped dowels are fixed in column corbels. During construction, the dowels are inserted through the holes at girder ends and the ducts are grouted at the end of construction. In some buildings, bolt nuts are used at dowel tips. For the purpose of easy installation, a gap of about 1.5 cm is left between the girder end and the column.

During earthquakes, several problems were identified with the column-girder connections. The ground motions in both longitudinal and transverse directions could damage the connections. When the structure was excited to in the transverse direction (parallel to the roof girder), the column rotated but the girder tended to remain horizontal because there was virtually no moment transfer between the girder and the column (Figure 1.13). As a result, the girder end impacted the side of the gutter beam as well as the top of the column corbel. This action explains concrete spalling observed at girder ends and corbel tips (Figure 1.11).
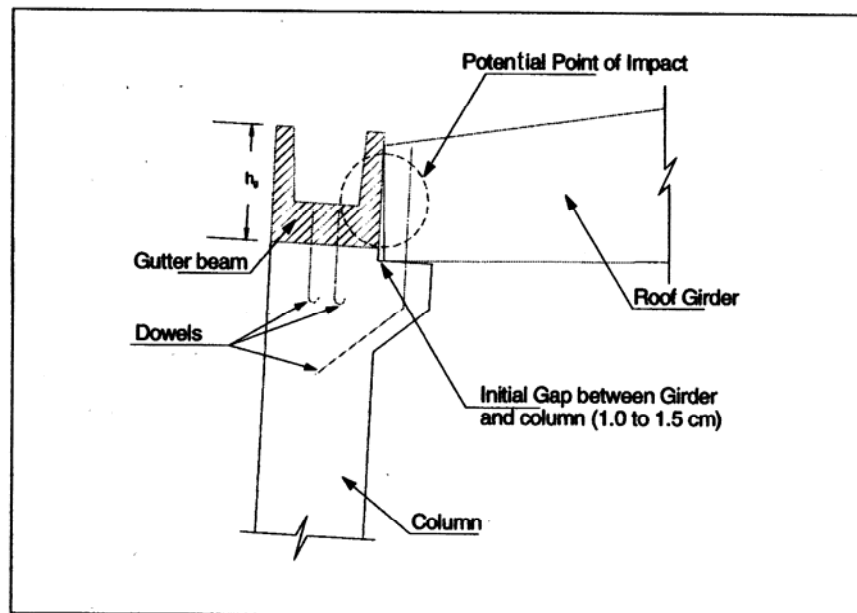
Figure 1.13 Potential Impact Problem (Posada, 2001)

Another serious consequence of the impact was the pull-out failure of the dowels. Since the grouted dowels were not grouted over a length sufficient to develop the dowels, especially when they did not have nuts at the anchored ends, they could be pulled out of the girder by the prying action caused by the column rotation. Once the dowels were pulled out of the girder, the connection was actually destroyed and consequent performance was out of control. Such a destroyed connection allowed the girder to slide on the column corbel top, and to behave more like a roller than a pin.

The most serious situation occurred when portions of the structure at different sides of this connection deflected in opposite directions and the girder was pulled from the bracket as shown in Figure 1.14 by dotted lines. This possibility existed because different portions of the structure had different dynamic characteristics, and resulted in collapse of the girders.
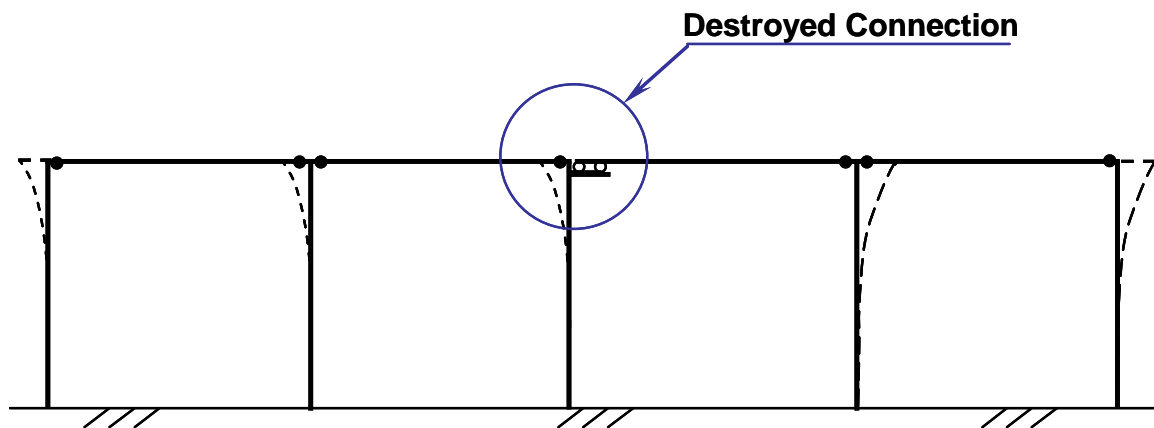
Figure 1.14 Possible Displacements (Dynamic Analysis)

The ground motion in the longitudinal direction (perpendicular to roof girders) could also contribute to connection damage. For precast industrial buildings, especially those with one story, the mass of the roof, purlins and girders represents the main part of the total. During an earthquake, a large portion of the inertial force acting on the structure is at the roof level. Analysis of the load path revealed that during earthquakes which

induced ground motion in the longitudinal direction, each roof girder had to carry a large torque due to inertial forces in roof, purlins and girders. The torque had to be offset with the moment resistance provided only by the dowels in the column-girder connections. Once again, with insufficient development length, the dowels could be pulled out from girders before yielding. Obviously, this would result in collapse of the girders.

Even if the dowels yielded during an earthquake, due to the large deformation of the dowels, tilting of girders could hardly be avoided, and the consequent P-delta effect could drive the girders from the column supports. Lack of lateral bracing of roof girders is one of the main weaknesses in these precast industrial buildings.

Another difference between precast and monolithic concrete buildings is the diaphragm. In a monolithic concrete building, the diaphragm is usually a cast-in-place floor slab. The slab is usually considered as a rigid diaphragm and lateral forces can be effectively transferred between different components connected by the slab. On the other hand, for the precast concrete industrial building studied here, the structural members assembled at right angle by dowels develop little diaphragm action, if any. Lateral load transfer between frames was almost impossible with each column working as a cantilever.

The cantilever columns were the only components that provided lateral force resisting capacity, and all lateral forces due to seismic motion had to be transferred to columns. The inadequate stiffness of columns provided an explanation for large lateral drift of precast buildings. Due to the large drift ratio, plastic hinges were formed at the column base. Columns with proper and sufficient transverse confinement were able to endure large rotations at the plastic hinge, and significant flexural cracking was observed near the base (Figure 1.9). Such columns remained standing but may have tilted after an

13

earthquake. Columns with improper or inadequate confinement were not able to survive large roof drift (Figure 1.9).

As a summary, the deficiencies which led to observed damages in the precast industrial buildings during 1999 earthquakes are listed below (Ataköy, 1999) (Ersoy,1999):

a)   The pin connections provided by grouted dowels between roof girders and columns were not adequate for ground motions in either longitudinal or transverse direction.

b)   There was no diaphragm action in the structures. Therefore lateral load transfer between frames did not exist. Each column were working alone as a cantilever.

c)   The columns were the only lateral force resisting components. Little redundant resistance was provided. But the columns were neither stiff enough to limit the lateral drift nor strong enough to resist the lateral load due to seismic action.

1.6   SCOPE AND OBJECTIVE

Although a huge number of precast concrete structures have been built in Turkey, which is located in a high seismic region, and the number is still growing rapidly, the research that has been devoted to the behavior of precast structures under earthquakes is limited. It should be stated that there is a serious lack of practical seismic rehabilitation schemes for existing precast structures.

The classical techniques used in seismic rehabilitation of cast-in-place reinforced concrete structures can hardly be applied directly to the precast structures. As no horizontal diaphragm action is present, widely used schemes, such as reinforced concrete shear walls, infilled vertical bracing frames, etc, can not work effectively in precast industrial buildings because there is no mechanism to transfer the lateral load to these

additional lateral force resisting systems (LFRS). Horizontal diaphragms play a key role in the seismic rehabilitation of precast industrial buildings.

Because one-story industrial buildings were widely used in the epicentral zone of 1999 earthquakes and because many of them sustained severe structural damage or collapse during the earthquakes, this study is devoted to one-story precast concrete industrial buildings only.

Based on the foregoing descriptions, a structure in this study scope have the following features:

a) One-story frame built of precast concrete members

b) Large open area

c) Weak pin connections

d) Girder overturning risk

e) No diaphragm action

f) Inadequate lateral force resisting capacity

A successful rehabilitation scheme for the existing precast industrial buildings should reduce the roof drift, prevent the roof members from separating from supports, and prevent the girders from overturning. The rehabilitation operation should minimize the adverse influence to the current use of the existing buildings.

In the present study, a practical rehabilitation scheme which introduces a new type of structural diaphragm is proposed. The diaphragm is provided by horizontally adding tension-only steel braces at the roof level. As such, it is a "soft" diaphragm with particular characteristics and a rational analysis method is obviously needed to ensure the safety, efficiency and economy of the design.

The implementation issues of the objectives of this study include:

- Development of a diaphragm for the existing precast buildings, so that the lateral forces can be transferred between different lateral force resisting members.

- Addition of a redundant lateral force resisting system. The lateral force resisting capacity of the existing structures is inadequate. Alternate lateral force resisting system is required for redundancy.

- Strengthening of the connections at the top of columns. The strengthened connections should be able to prevent the roof members from sliding from supports.

- Formulation of an analysis method for the rehabilitation design. This will includes the determination of fundamental period, estimation of maximum seismic displacement, and calculation of internal forces, etc.

Chapter 2: Ground Motions and Prototype Building

2.1   INTRODUCTION

In order to obtain the elastic response spectra for the rehabilitation, fifteen ground motion records of the 1999 earthquakes in Turkey were analyzed. Based on the elastic analysis results, an acceleration response spectrum and a displacement response spectrum were selected for further study of the behavior of one-story precast industrial buildings.

A typical one-story precast building is selected as the prototype of the study. The properties of construction materials and members are summarized according to the detailed structural drawings provided by the precast producer.

2.2   GROUND MOTION RECORDS

A large number of ground motions on various types of soil were recorded during the 1999 earthquakes by eight stations located within 50 km of the epicenters. The epicentral distances of these stations and corresponding recorded peak horizontal accelerations of ground motions are illustrated in Figure 2.1 (Posada, 2001). The Gebze, Arcelik and Sakarya records were obtained on stiff soil, İzmit on rock, and the others were recorded on soft alluvial soil deposits. Most records indicate peak ground motion accelerations less than 0.5 g, while for records from Bolu, located 42 km from the epicenter of Düzce earthquake, peak accelerations in both directions (normal and parallel to the fault) are larger than 0.7 g. According to Anderson (2000), site response caused by sediment amplification and the directivity-focusing phenomenon may have contributed to the large peak accelerations in Bolu.
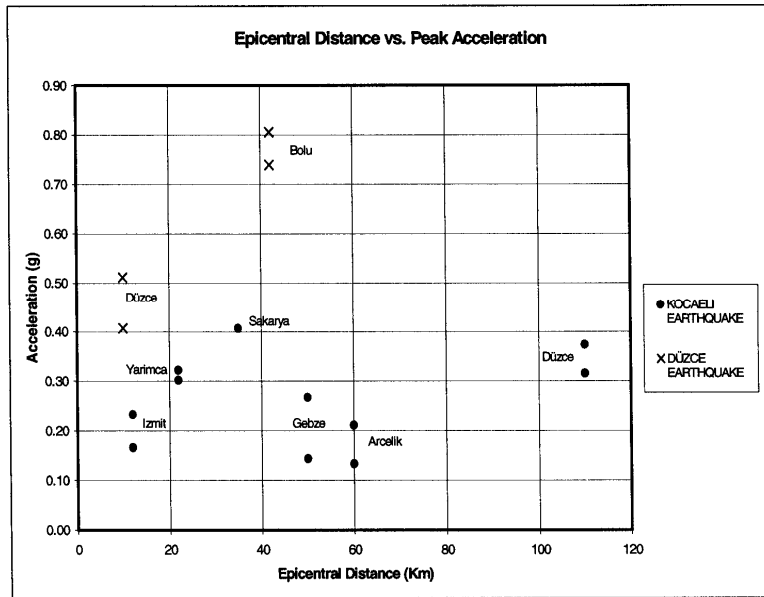
Figure 2.1 Ground Motion Records Used in the Study (Posada, 2001)

Table 2.1 Ground Motions Considered in This Study (Posada, 2001)

Earthquake	Station	Comp.	Peak Acc (g)	Epicentral Distance (km)	Distance to fault rupture plane (km)	Soil Conds.
Kocaeli	Arcelik (ARC)	000	0.21	60	17	Stiff Soil
		090	0.13			
	Düzce (DZC)	180	0.32	110	14.2	Soft Soil
		270	0.37			
	Gebze (GBZ)	000	0.27	50	17	Stiff Soil
		270	0.14			
	İzmit (IZT)	090	0.23	12	7.7	Rock
		180	0.17			
	Sakarya (SKR)	090	0.41	35	3.3	Stiff Soil
	Yarimca (YPT)	330	0.32	22	4.4	Soft Soil
		348	0.30			
Düzce	Bolu (BOL)	000	0.74	42	19.9	Soft Soil
		090	0.81			
	Düzce (DZC)	180	0.41	10	8.3	Soft Soil
		270	0.51			

18

From the available ground motion records, 15 (5 from stiff soil and 10 from soft soil) are selected for this study and summarized in Table 2.1 (Posada, 2001). The accelerograms from the 15 records are presented in Appendix A (Posada, 2001).

2.3   RESPONSE SPECTRA

For the 15 ground motion records, Posada (2001) calculated elastic acceleration, velocity and displacement response spectra using a 2% damping ratio (Appendix B). Maximum, minimum and average acceleration and displacement spectra for stiff soil/rock are plotted in Figure 2.2. Spectra for soft soil are shown in Figure 2.3.

The maximum acceleration/displacement spectra represent the most critical situations that the structures would experience during earthquakes. As expected, comparison between response spectra for stiff soil/rock and those for soft soil shows that ground motions at soft soil sites control. In this study, only spectra for soft soil are considered, and an idealized acceleration spectrum was selected to represent the maximum soft soil acceleration spectrum (Figure 2.3). Based on this idealized acceleration spectrum, a displacement spectrum was calculated.

For the idealized acceleration spectrum (T is the fundamental period of a structure):

$$S_{a,s} = 2.5\,g \qquad\qquad \text{Maximum considered acceleration at short period}$$

$$S_{a,1} = 1.25\,g \qquad\qquad \text{Maximum considered acceleration at 1 sec period}$$

$$T_s = \frac{S_{a,1}}{S_{a,s}} = 0.5\,\text{sec} \qquad \begin{array}{l}\text{Period at intersection of constant} \\ \text{acceleration and constant velocity} \\ \text{regions of spectrum.}\end{array} \qquad (2.1)$$

$$T_0 = 0.2T_s = 0.1\,\text{sec} \qquad\qquad\qquad\qquad\qquad\qquad (2.2)$$

$$S_a = S_{a,s}\left(0.4 + 0.6\frac{T}{T_0}\right) \quad \text{If } T \le T_0 \qquad\qquad\qquad (2.3a)$$

19
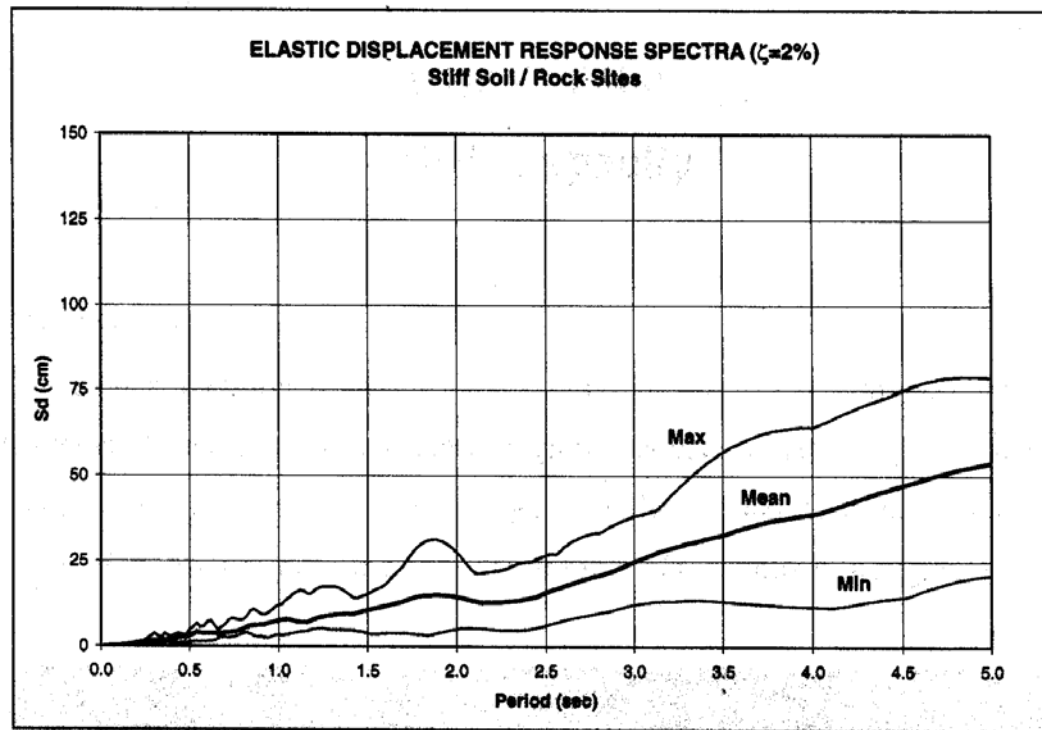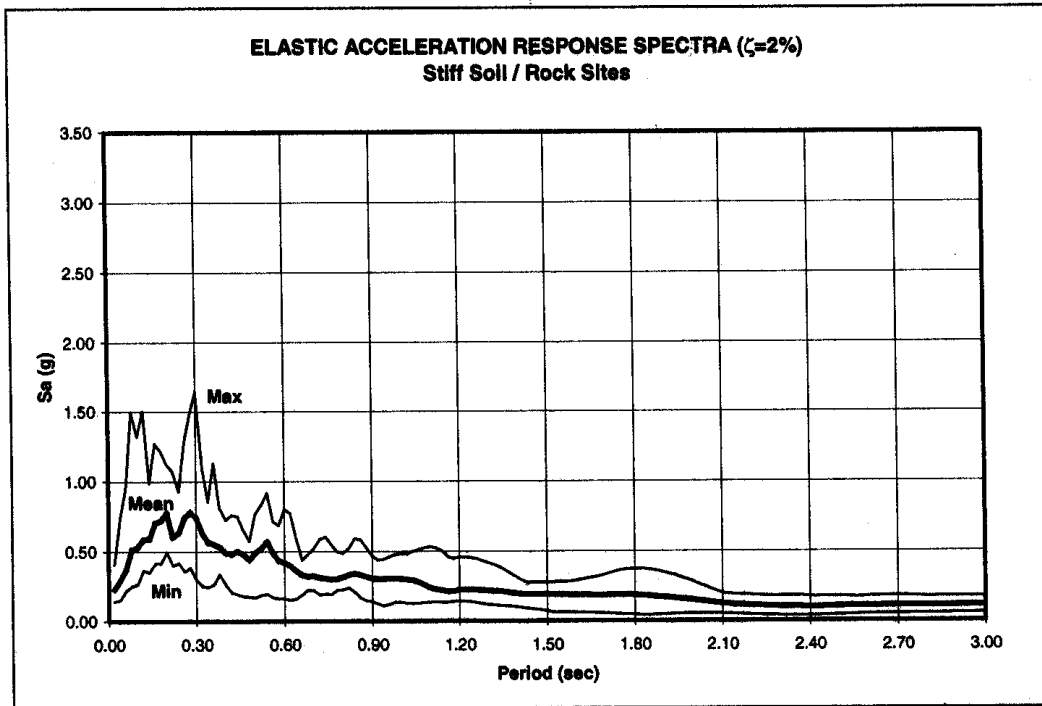
Figure 2.2 Response Spectra for Stiff Soil/Rock Sites (Posada, 2001)

20
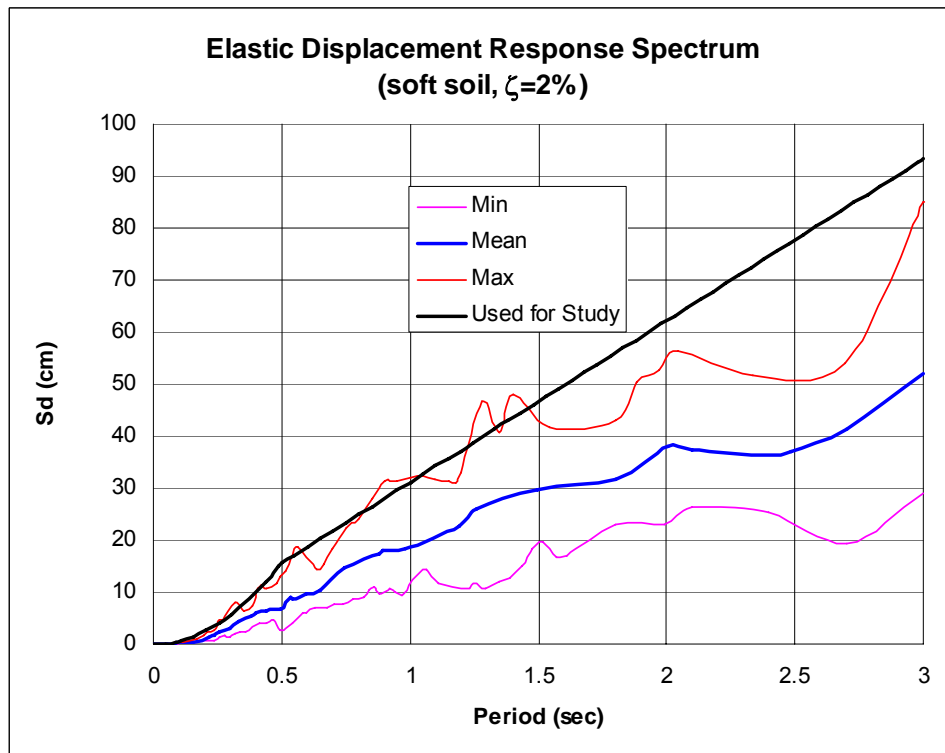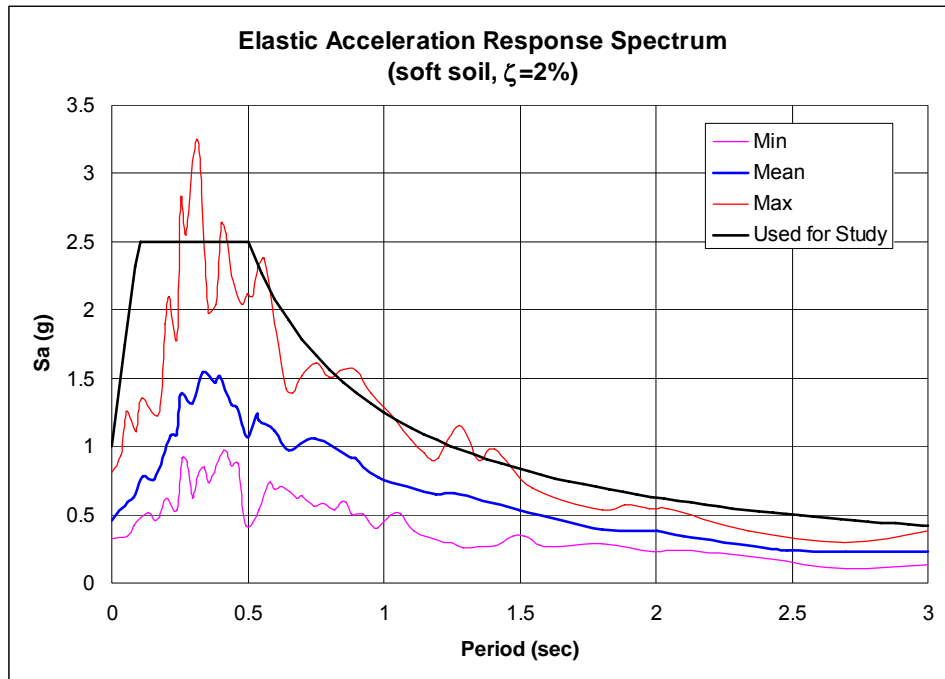
Figure 2.3 Response Spectra for Soft Soil Sites

$$S_a = S_{a,s} = 2.5g \qquad \text{If } T_0 < T \leq T_s \qquad\qquad (2.3b)$$

$$S_a = \frac{S_{a,1}}{T} \qquad\qquad \text{If } T > T_s \qquad\qquad (2.3c)$$

Spectral displacement is calculated by:

$$S_d = \frac{S_a T^2}{4\pi^2} \qquad\qquad (2.3d)$$

The fundamental natural periods of one-story industrial buildings are typically between 0.9 sec and 1.6 sec (Ersoy, 1999), which correspond to Eq. 2.3c. The resulting spectral displacement corresponding to this period region is proportional to the fundamental period.

2.4   PROTOTYPE BUILDING

A one-story precast industrial building selected as the prototype for this study is shown in Figure 2.4. The building is near Adapazari and detailed structural drawings were available. A simplified version of this building was selected as the prototype building for this investigation. The prototype is considered to be representative of one-story precast systems in the epicentrial region. It is rectangular in plan with multiple bays in both directions (Figure 2.5). The structure consists of precast columns, roof girders, gutter beams and purlins. The column base sockets were cast in place and the roof is made of lightweight metal decking. The main geometric features of the prototype building are listed below:

a)   14 bays in longitudinal direction, 7.5 m center-to-center spacing

b)   4 bays in transverse direction, 20 m center to center spacing

c)   Precast 7.0 m high columns fixed in sockets

d)   Trapezoidal roof girders span along the transverse axis of the building

e)   Purlins and U-shaped gutter beams span in the longitudinal direction (purlins only partially shown in Figure 2.5)

Figure 2.4 Prototype Building
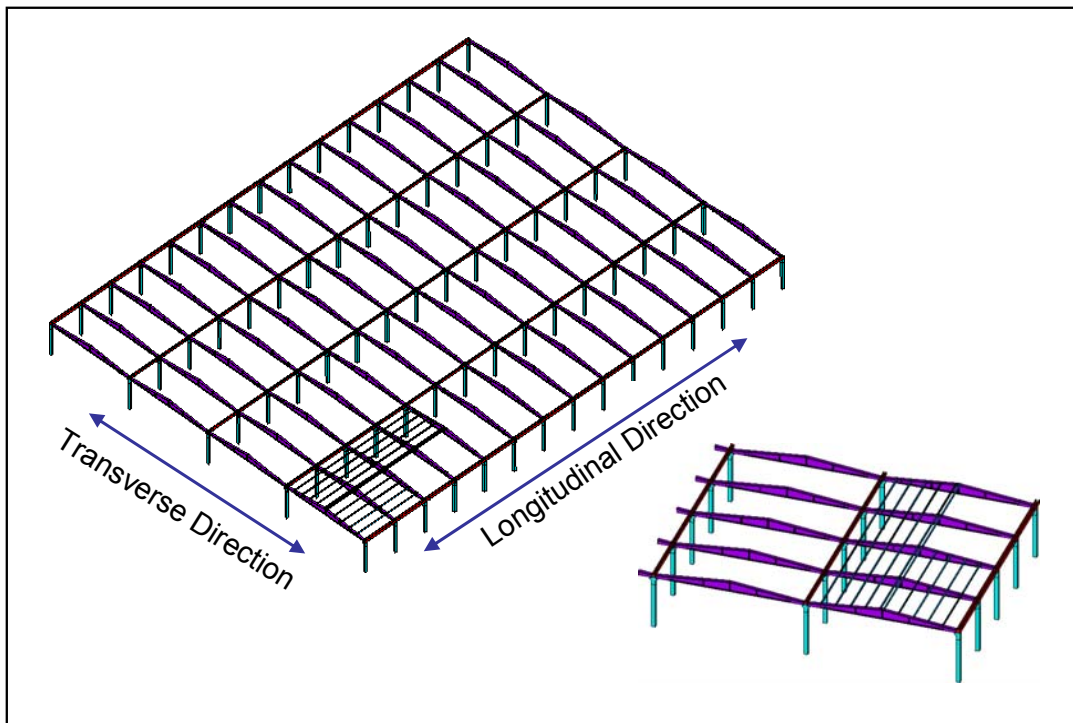
Figure 2.5 Prototype Frame

2.4.1 Materials

Concrete: normal weight for all concrete members, mass density ρ_c = 2,400 kg/m^3; specific compressive strength f'$_c$ = 30 MPa.

Reinforcement: G420 steel; yield stress f_y = 420 MPa; tensile strength f_u = 500 MPa; modulus of elasticity E_s = 200 GPa;

Roof Material: mass density of the roof is assumed to be ρ_R = 24 kg/m^2.

2.4.2 Members and Connections

Columns: The dimensions of a precast column are shown in Figure 2.6. As columns were the only components that provided lateral force resisting capacity in the original structures, the cross section and reinforcement are also included in the figure. The longer edge of the column cross section coincides with the transverse direction of the
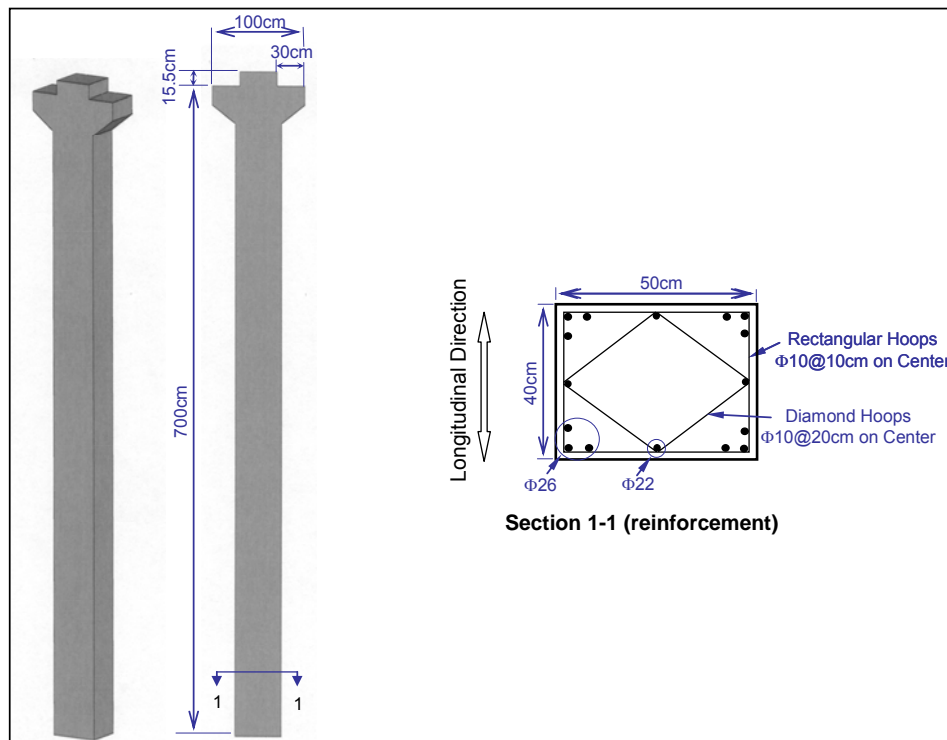
Figure 2.6 Column of Prototype Building

24

structure. According to the structural drawings, 135 degree hooks were used for the transverse reinforcement, however this detail is not common in the epicentral region.

Girders: Because the connections between girders and columns are pinned, the roof girders provide little moment resisting capacity to the system. However, due to their size, they contribute considerable mass, and large inertial force to the structure. Figure 2.7 gives the detailed dimensions of a typical roof girder. Because the roof girders are as long as 20 m, prestressed bars were used for the reinforcement.
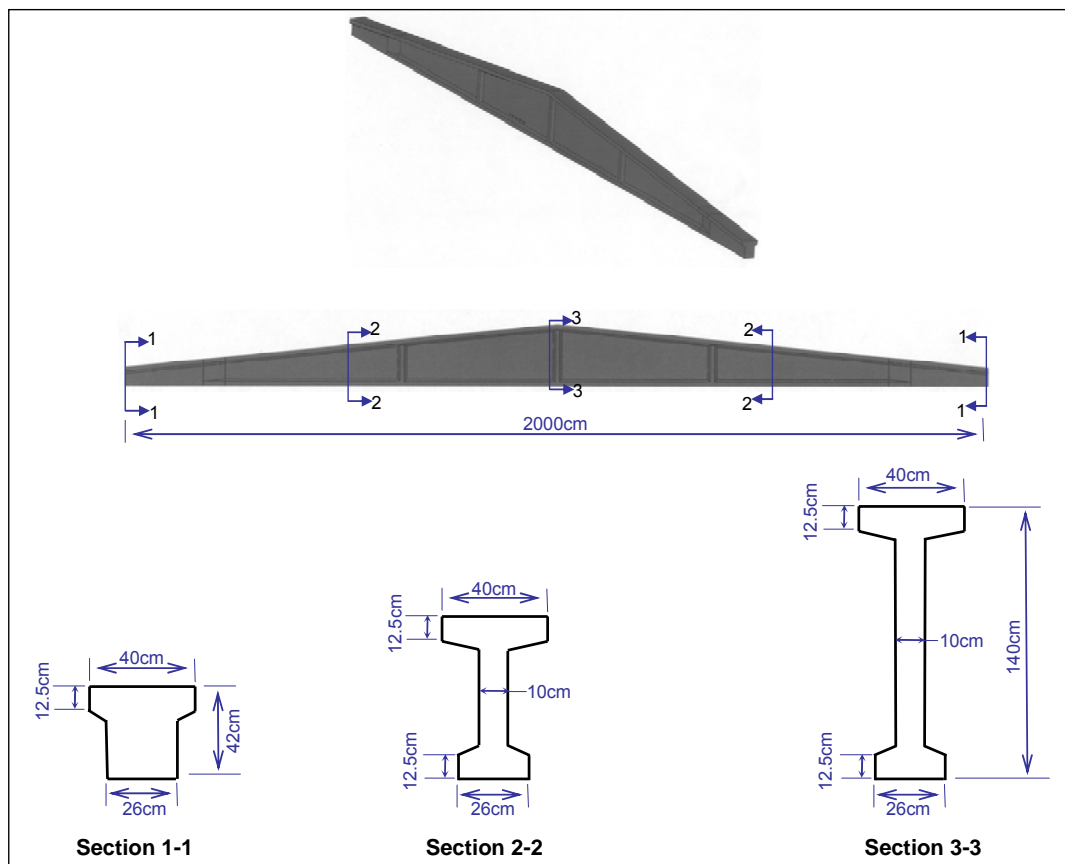
Figure 2.7 Roof Girder of Prototype Building

Gutter Beams and Purlins: Figure 2.8 shows dimensions of a gutter and a purlin respectively.
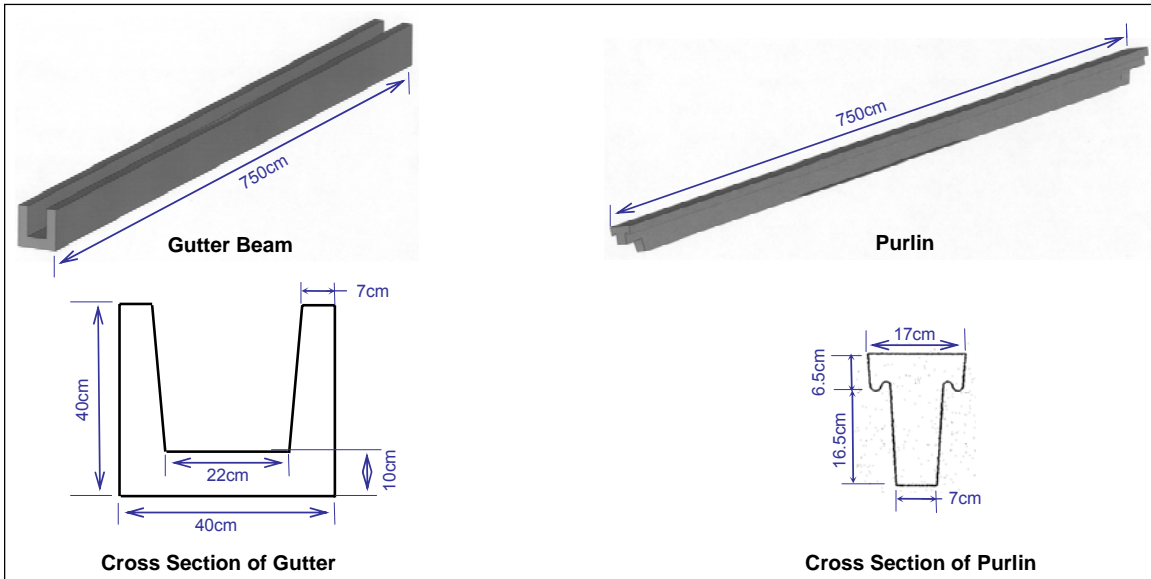
Figure 2.8 Gutter Beam and Purlin of Prototype Building

Connections: The connections used in the prototype building are shown in Figure 2.9. For a girder-column connection, two Φ26 dowels were grouted. One Φ16 dowel and one Φ20 dowel were used respectively for purlin-girder connection and gutter-column
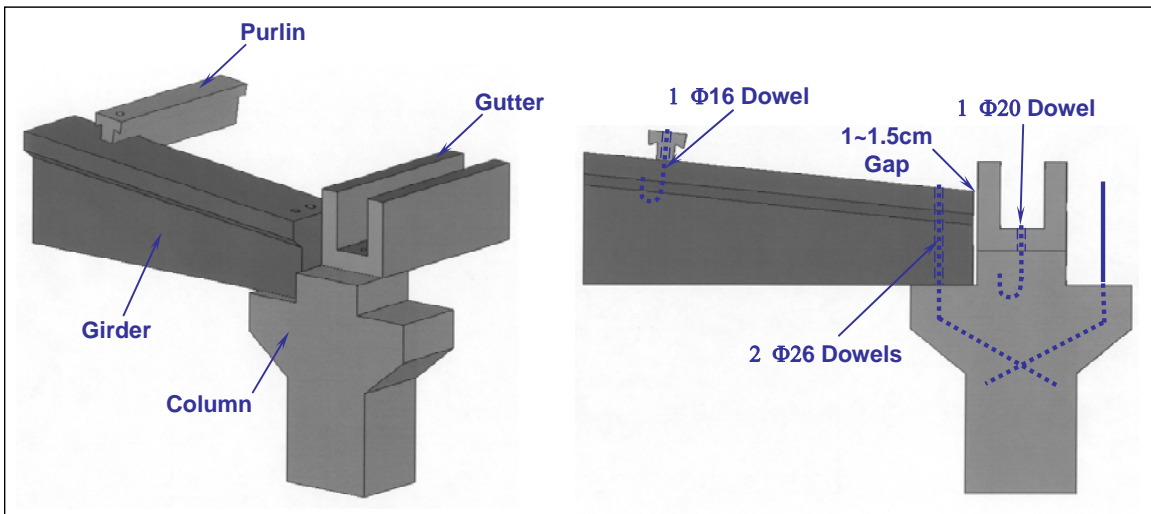
Figure 2.9 Connections of Prototype Building

connection. For the convenience of assembly, a gap of 1 to 1.5 cm is generally present between the column and the girder end. It should be mentioned that because of the short development length of the connection dowels, the girders, gutters and purlins can carry little axial tension, but can carry compression.

Chapter 3: Overview of Rehabilitation Scheme

3.1   INTRODUCTION

During an earthquake, when a structure undergoes inelastic response, it is usually deformation rather than force that controls the damage of structural members. For one-story precast industrial buildings, the estimation of the maximum roof drift, which is directly related to the deformation in the cantilevered columns, plays an essential role in the seismic evaluation.

In this chapter, the seismic performance of the as-built prototype building is evaluated. The analyses give an estimation of the maximum displacements that the structure is likely to experience during the considered earthquakes. Further investigation indicates that the structure needs to be strengthened in both longitudinal and transverse directions.

Based on these results, the concept for a rehabilitation scheme to develop a horizontal roof diaphragm using tension-only braces is proposed at the end of this chapter.

3.2   SEISMIC PERFORMANCE OF THE ORIGINAL PROTOTYPE STRUCTURE

Because there will be no diaphragm action in the prototype structure during an earthquake, the inertial forces caused by the seismic motion can not be transferred among different elements of the frame. As a result, each column will work individually as an isolated cantilever. This makes the calculations quite straightforward to estimate the drift of the structure at the roof. The critical column is the one that carries the largest mass, and it is idealized as a single-degree-freedom (SDOF) system. The maximum deflection of this SDOF oscillator corresponds directly to the maximum roof drift of the structure.

All interior columns of the prototype building carry roughly the same amount of mass, which is larger than that of any of the peripheral columns. The maximum lumped mass at the roof level for an interior column is calculated as:

Roof: (20 m × 7.5 m): 24 kg/m^2 × 2 0 m × 7.5 m = 3600 kg;

Purlins: (10 purlins): 428.4 kg/purlin × 10 purlins = 4284 kg;

Girder: (1 girder): 7578 kg;

Gutter: (1 gutter): 1584 kg;

Column: (upper half of a column): 3360 kg/column × 0.5 column = 1680 kg.

Total mass: **18726 kg**.

A column will act as a cantilever with the maximum bending moment occurring at the base. The flexural deformation of the column is then modeled by assuming elastic curvature over its height and concentrating the inelastic rotation at the base plastic hinge (Figure 3.1). FEMA-356 suggests that the equivalent length of the plastic hinge may be conservatively taken as l_p = 0.5 h, where h is the section depth. In order to obtain the necessary parameters (stiffness, plastic hinge properties, etc) for this SDOF oscillator, the properties of the column (materials, dimensions) are required.

Lumped Mass, m

Elastic Column, EI

H

Plastic Hinge
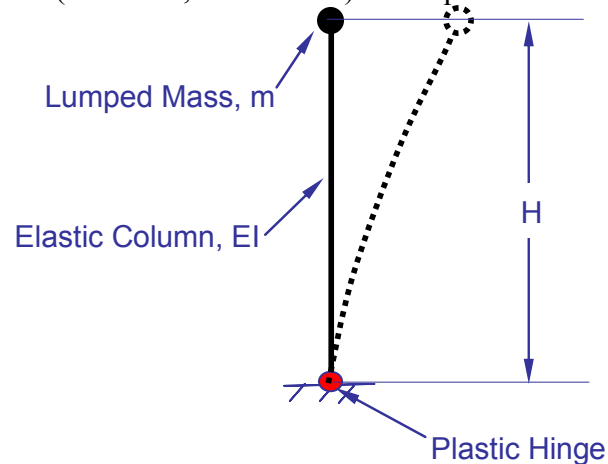
Figure 3.1 SDOF Oscillator

29

3.2.1 Column Properties

Reinforcing Steel: As indicated in Section 2.4.1, Grade 420 reinforcing steel was used with yield stress f_y = 420 MPa and elasticity modulus E_s = 200 GPa. In the calculation, the constitutive relation of the reinforcing steel is idealized using an elasto-plastic model with strain hardening at 1% strain. The slope of hardening curve is 5% of the initial modulus of elasticity (Figure 3.2). The steel properties under compression are assumed similar to those under tension.
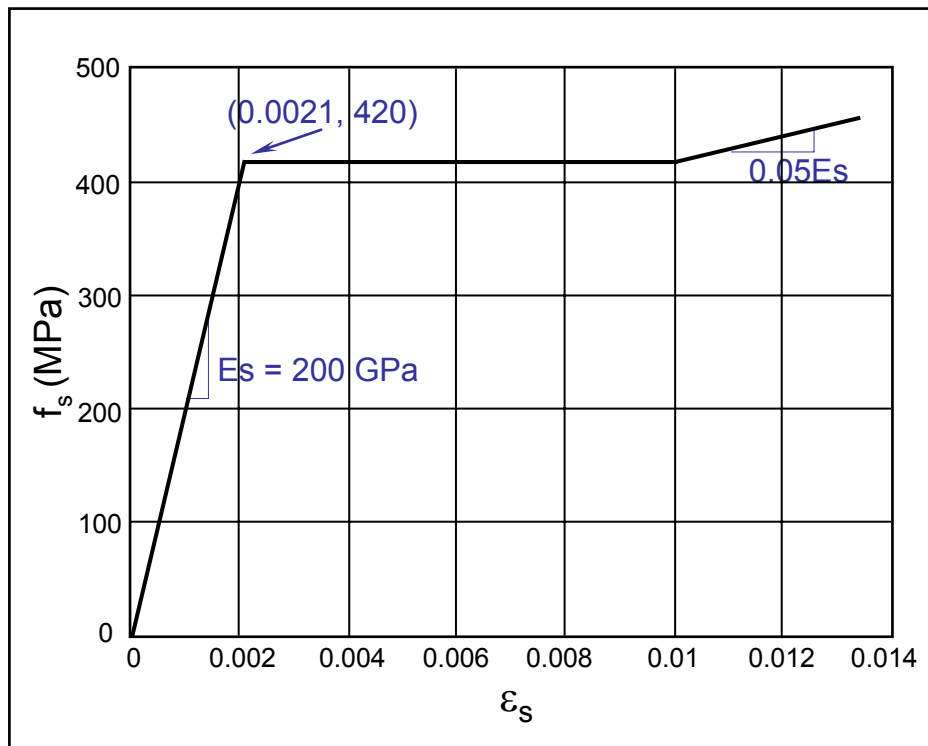
Figure 3.2 Constitutive Model of Reinforcing Steel

Concrete: As shown in Figure 2.6, the transverse reinforcement of the columns was provided with two groups of hoops, one consisting of rectangular hoops, and the other, diamond hoops. Both groups were made of Φ10 bars with 135 degree hooks. In the region one meter long from the base support, the center to center spacing of the

rectangular hoops is 10 cm and that of the diamond ones is 20 cm. In the rest of the column, the spacing of the transverse reinforcing hoops is 20 cm for rectangular hoops and 40 cm for diamond ones.

The confining effect of the diamond hoops is limited because the area of the enclosed concrete is small and the hoop spacing is larger than one-quarter of the minimum column dimension, 40 cm. To simplify the calculation, the effect of the diamond hoops is ignored. According to ACI 318-05, the provided rectangular hoops satisfy the requirements for a beam in a special moment resisting frame, but this transverse confinement does not satisfy the requirements for a column, as the total cross-sectional area A_{sh} of a rectangular hoop is only 1.6 cm^2, less than required 4.2 cm^2.

The column was modeled using two types of concrete: unconfined cover and laterally confined core. The modified Kent and Park (1971) model was used to construct the stress-strain relations for both types of concrete.

With the tension strength ignored, the parameters for the modified Kent and Park model are described as follows.

$$\kappa = 1 + \frac{\rho_s f_{yh}}{f'_c} \tag{3.1a}$$

$$\varepsilon_0 = 0.002\kappa \tag{3.1b}$$

$$Z = \frac{0.5}{\dfrac{3 + 0.29f'_c}{145f'_c - 1000} + 0.75\rho_s \sqrt{\dfrac{h'}{s_h}} - 0.002\kappa} \tag{3.1c}$$

$$\varepsilon_u = 0.004 + 0.9\rho_s \frac{f_{yh}}{300} \tag{3.1d}$$

$$f_{max} = \kappa f'_c \tag{3.1e}$$

$$f_u = f_{max} - \kappa Z f'_c \left(\varepsilon_u - \varepsilon_0 \right) \tag{3.1f}$$

where,

ε_0: Concrete strain at maximum stress;

31

κ :   Strength increase factor due to confinement;

Z: Strain softening slope;

f'_c :   Concrete specific compressive strength (MPa);

f_{yh}:   Yield stress of stirrups (MPa);

ρ_s: Volume ratio of hoop reinforcement to core concrete measured to outside of stirrups;

s_h :   Center to center spacing of stirrups;

h' :   Width of core concrete measured to outside of stirrups;

ε_u: Ultimate compressive strain of concrete;

f_{max}:   Maximum stress in concrete;

f_u: Concrete stress at ultimate strain ε_u.

The concrete stress-strain relation follows a quadratic curve with peak at ε_0 when strain is not larger than ε_0, and then a descending straight line when strain is between ε_0 and ε_u. For strain beyond ε_u, the core concrete carries constant compression, while the cover concrete carries no compression.

Following the listed formulation, the parameters of unconfined concrete cover are calculated below, and illustrated in Figure 3.3. This constitutive model is also used for concrete in the roof girders and gutter beams.

$\rho_s = 0$

$f'_c = 30$ MPa

$\varepsilon_0 = 0.002$

$f_{max} = 30$ MPa

$\varepsilon_u = 0.004$

$f_u = 9.9$ MPa
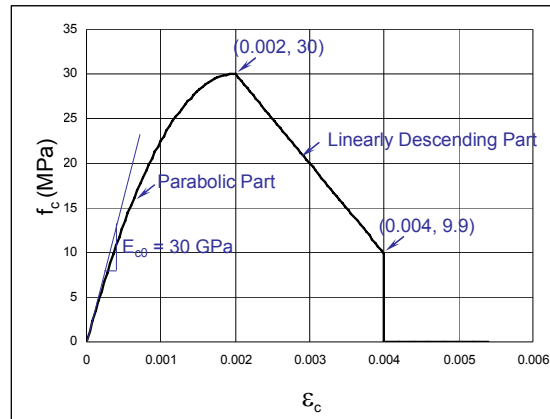
Figure 3.3 Stress-Strain Relation of Concrete Cover

Similarly, the constitutive model for confined core concrete is constructed as below (Figure 3.4).

$\rho_s = 0.0085$

$f'_c = 30$ MPa

$\varepsilon_0 = 0.00223$

$f_{max} = 33.5$ MPa

$\varepsilon_u = 0.0146$

$f_u = 19.1$ MPa
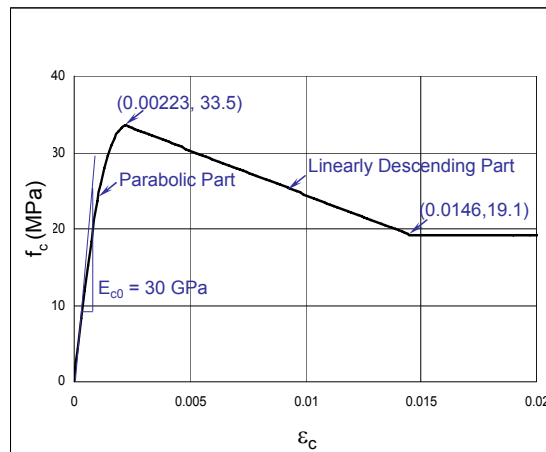
Figure 3.4 Stress-Strain Relation of Concrete Core

33

Column section: Based on the dimensions shown in Figure 2.6 and material models described above, the moment-curvature relationships of the column section about its two main axes are calculated and shown in Figure 3.5. To simplify the behavior of the column section about both axes, bilinear models shown in Figure 3.5 are used in this study.
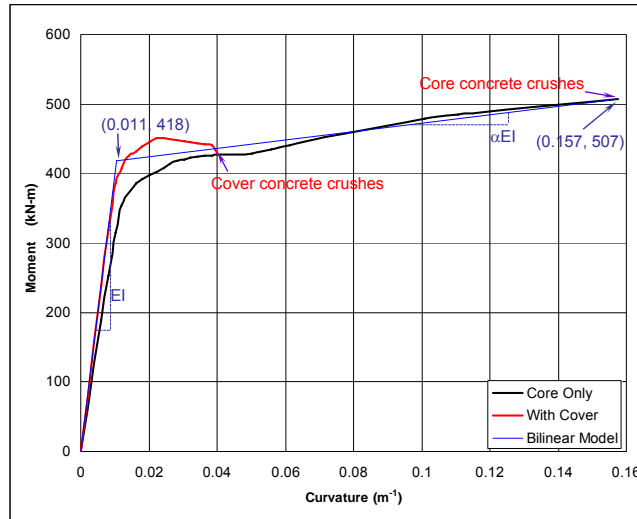
(a) About Weak Axis
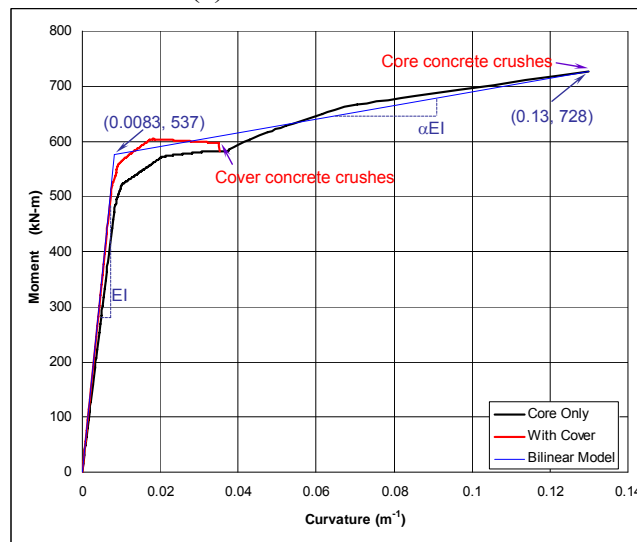
(b) About Strong Axis

Figure 3.5 Moment-Curvature Relationships for Column Cross Section

Initially, the moment increases proportionally to the curvature with a slope EI until yielding is reached. Beyond yielding, the moment increases, but the slope drops to αEI, where α is a constant less than 1.0. When a column is deformed in the transverse direction, its cross sections rotates about their strong axes (the longitudinal axis of the structure). For deflection in the longitudinal direction of the structure, the column is bent about their weak axes (the transverse direction of the structure)..

The main parameters of the SDOF oscillator shown in Figure 3.1 are calculated and listed in Table 3.1.

Table 3.1   Parameters of the SDOF Oscillator Model of Column

For flexure in longitudinal direction	
Flexural rigidity	EI = 38000 kN•m^2
Stiffness ratio beyond yielding	α = 0.016
Yield moment	M_y = 418 kN•m
Flexural strength	M_u = 507 kN•m
Rotational capacity of plastic hinge	θ_u =(0.157 - 0.011) × 0.4 × 0.5 = 0 0.029 rad
Post-yield slope of plastic hinge	K_m = (507 – 418) / 0.029 = 3069 kN•m / rad
For flexure in transverse direction	
Flexural rigidity	EI = 64699 kN•m^2
Stiffness ratio beyond yielding	α = 0.024
Yield moment	M_y = 537 kN•m
Flexural strength	M_u = 728 kN•m
Rotational capacity of plastic hinge	θ_u = (0.13 – 0.0083)) × 0.5 × 0.5 = 0.030 rad
Post-yield slope of plastic hinge	K_m = (728 – 537) / 0.03 = 6367 kN•m / rad

3.2.2 Displacement Estimation Strategy

During earthquakes, especially strong earthquakes, the columns of the one-story precast industrial building are likely to respond in the inelastic range. As the inelastic behavior is related to the deformation history, even for the SDOF oscillator as shown in Figure 3.1, the calculation of the maximum displacement can be very complicated.

Shimazaki and Sozen (1984) conducted a parametric study of the seismic response of reinforced concrete buildings with various initial structural stiffness and strength characteristics subjected to different types of ground motions. They indicated that:

if $\dfrac{T_i}{T_s} + \dfrac{V_p}{V_e} \geq 1.0$, the inelastic displacement response of a reinforced building can

be satisfactorily estimated using the elastic response spectrum for a 2% damping ratio,

where:

T_i : fundamental natural period of the reinforced concrete structure

T_s : period corresponding to the boundary of the constant spectral velocity and constant spectral acceleration regions (refer to section 2.3)

V_p : base-shear capacity of the structure

V_e : maximum elastic base shear corresponding to the initial stiffness of the structure (Figure 3.6).

The fundamental natural periods of one-story industrial buildings are typically between 0.9 sec and 1.6 sec (Ersoy, 1999). The value of T_s for the idealized acceleration response spectrum of is 0.5 sec (Section 2.3). Therefore, the required condition can be satisfied, and the maximum displacement of the one-story industrial buildings can be simply estimated using elastic response spectrum with a damping ratio of 2%, and the

characteristics of the plastic hinge is not needed to find the maximum displacement of the SDOF oscillator.
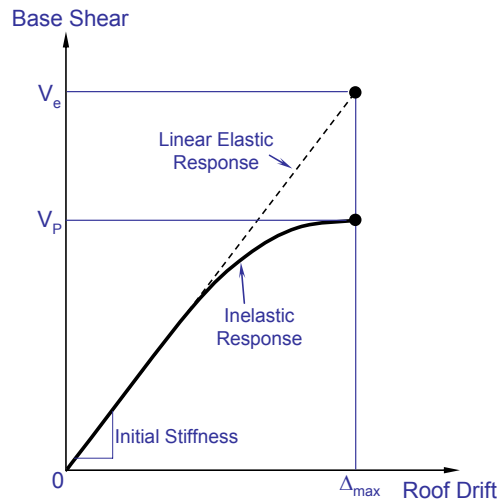
Figure 3.6 Definition of V_P and V_e

3.2.3 Column Deformation in the Longitudinal Direction

When the ground motion coincides with the longitudinal direction of the prototype structure, the maximum roof displacement can be estimated as follows.

Lumped Mass: $\qquad$ m = 18726 kg

Column Flexural Rigidity: $\qquad$ $EI = 38000 \text{ kN} \cdot \text{m}^2$

Column Height: $\qquad$ H = 7 m

Initial Stiffness of Oscillator: $\qquad$ $k = \dfrac{3EI}{H^3} = 332 \text{ kN/m}$

Fundamental Natural Period: $\qquad$ $T_i = 2\pi\sqrt{\dfrac{m}{k}} = 1.49 \text{ sec}$ $\qquad$ (larger than $T_s = 0.5$ sec)

Spectral Acceleration at T_i: $\qquad$ $S_a = \dfrac{1.25g}{T_i} = 0.84 \text{ g}$

Spectral Displacement at T_i: $\qquad$ $S_d = \dfrac{S_a T_i^2}{4\pi^2} = \mathbf{46.3 \text{ cm}}$

37

Using the estimated deformation of the top of the column, the behavior of the column in the longitudinal direction can be further investigated. Considering the moment diagram along the column, it is obvious that the inelastic deformation will be concentrated in the region near the column base. To represent this phenomenon, as stated in Section 3.1.1, the deformation of a column is considered in two parts: the elastic deformation of the column trunk and the inelastic rotation at the base. Obviously, the rotation of the plastic hinge controls the damage of the column. Estimation of rotational capacity is of a critical value in the seismic analysis of structures.

The relation between the plastic rotation and the top deflection of the column (Figure 3.7) is developed as follows.

1)   For a given lateral force P, calculate the maximum bending moment at column base, $M = P \cdot H$;

2)   Using the bilinear model shown in Figure 3.5, find the curvature ϕ corresponding to the moment M using:

$$\phi = \frac{M}{EI} \qquad \text{if } M \leq M_y = 418 \text{ kN} \cdot \text{m, where EI} = 38000 \text{ kN} \cdot \text{m}^2$$

$$\phi = \frac{M_y}{EI} + \frac{M - M_y}{\alpha EI} \qquad \text{if } M \geq M_y, \text{ where } \alpha = 0.016$$

3)   Calculate the rotation angle of the plastic hinge using:

$$\theta_p = 0 \qquad \text{if } \phi \leq \phi_y = 0.011 \text{ m}^{-1}$$

$$\theta_p = \frac{h}{2}(\phi - \phi_y) \qquad \text{if } \phi > \phi_y, \text{ where } h = 40 \text{ cm}$$

4)   Calculate the elastic deflection at the top of the column using:

$$\Delta_e = \frac{PH^3}{3EI}$$

5)   Calculate the inelastic displacement at the top of the column due to rotation of plastic hinge:

$$\Delta_p = \theta_p H$$

38

6) Calculate the total deflection at the top of the column:

$$\Delta = \Delta_e + \Delta_p$$

7) Plot $\Delta \sim \theta_P$ curve.
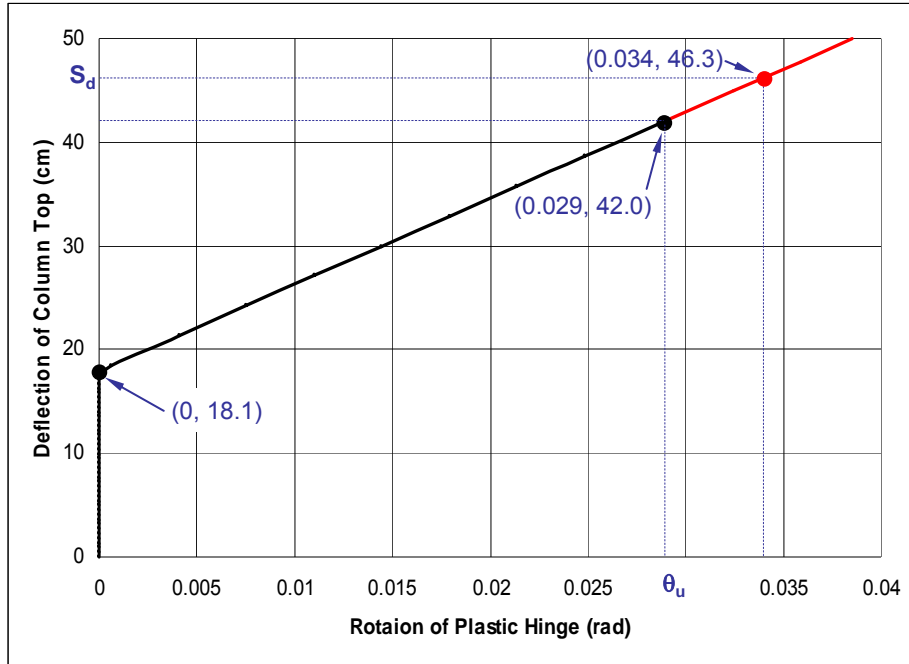
Figure 3.7   Relation Between Roof Drift and Plastic Hinge Rotation (Longitudinal)

From Figure 3.7, it can be seen that when the displacement at the column top is smaller than 18.1 cm, the rotation of the plastic hinge remains zero, which means that the column remains elastic. When the roof drift exceeds 18.1 cm, the rotation of the plastic hinge increases proportionally with the roof drift. The rotation angle can be calculated by:

$$\theta_p = 0 \qquad \text{if } \Delta \leq 18.1 \text{ cm}$$

$$\theta_p = 1.21 \times 10^{-3}(\Delta - 18.1) \quad \text{If } \Delta > 18.1 \text{ cm, where } \Delta \text{ is measured in cm}$$

According to this relation, when the column top drifts 46.3 cm, which is the spectral displacement at period T_i, the corresponding rotation of the plastic hinge will be 0.034 rad. This rotation exceeds 0.029 rad, the computed rotational capacity of the plastic hinge. It is likely that the concrete at the column base crushes at such a large deformation.

39

This situation can be stated in another way. Under ground motions in the longitudinal direction, the ultimate deflection of the column top corresponding to the rotation capacity of the plastic hinge is $\Delta = 18.1 + \dfrac{0.029}{1.21 \times 10^{-3}} = 42.0$ (cm). The expected maximum roof drift is 46.3 cm, larger than 42.0 cm, the maximum roof drift that the column can sustain. The column is likely to collapse under the estimated drift.

In summary, the prototype building can not survive the considered earthquake motion if oriented along the longitudinal direction of the structure.

3.2.4 Column Deformation in the Transverse Direction

For a building with square columns, the seismic response of the columns to the earthquake oriented along the transverse direction will be the same as that when ground motion is in the longitudinal direction. The cross section of the columns of the prototype building is rectangular with longer dimension in the transverse direction, therefore the column response to the earthquake oriented along the transverse direction also needs to be checked. In the transverse direction, because of the higher moment inertia, the columns have higher stiffness, and thus will have shorter period and lower seismic deflection level. The maximum transverse roof drift is estimated as follows.

Lumped Mass: $\qquad\qquad\qquad$ m = 18726 kg

Column Flexural Rigidity: $\qquad$ EI = 64700 kN•m^2

Column Height: $\qquad\qquad\;$ H = 7 m

Initial Stiffness of Oscillator: $\quad k = \dfrac{3EI}{H^3} = 566 \text{ kN/m}$

Fundamental Natural Period: $\quad T_i = 2\pi\sqrt{\dfrac{m}{k}} = 1.14 \text{ sec}$ $\qquad$ (larger than $T_s = 0.5 \text{ sec}$)

Spectral Acceleration at T_i: $\quad S_a = \dfrac{1.25g}{T_i} = 1.10 \text{ g}$

Spectral Displacement at T_i: $\quad S_d = \dfrac{S_a T_i^{\,2}}{4\pi^2} = \mathbf{35.5 \text{ cm}}$

40

Similarly, the relation between the roof drift and plastic hinge rotation in the transverse direction is developed (Figure 3.8) with $EI = 64700$ kN·m^2, $M_y = 537$ kN·m, $\phi_y = 0.0083$ m^{-1} and h = 50 cm.
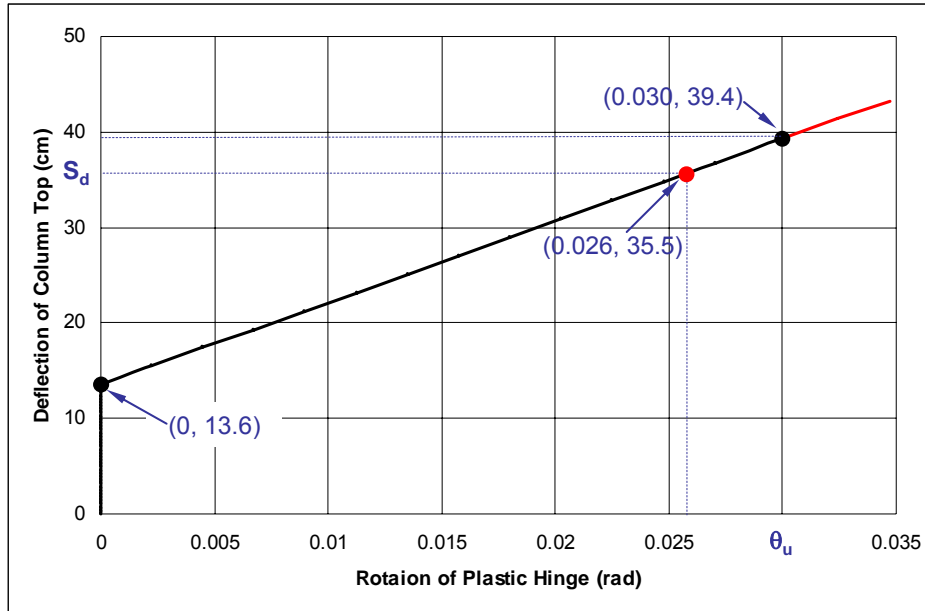
Figure 3.8 Relation Between Roof Drift and Plastic Hinge Rotation (Transverse)

From Figure 3.8, the maximum elastic displacement of the column top in the transverse direction is 13.6 cm, and beyond that level, the relation between the roof drift and plastic hinge rotation can be formulated as $\theta_p = 1.18 \times 10^{-3}(\Delta - 13.6)$ rad, where Δ is measured in cm. As calculated in Section 3.1.1, the rotation capacity of the column in the transverse direction is 0.030 rad. This rotation will correspond to a roof drift of 39.4 cm in the transverse direction. The estimated maximum displacement, 35.5 cm, is smaller than the maximum roof drift that columns can endure.

The prototype building would be expected to survive a considered earthquake in the transverse direction. However, the existing structure may be in high risk of failure during an earthquake in the transverse direction because:

41

1)   There is no roof diaphragm action developed in the structure, thus each column tends to work individually. Because of the variation of mass distribution, material properties, etc, different columns may have different dynamic characteristics (period, amplitude, etc). For an example, the mass carried by a peripheral column is only roughly 60% of that carried by an interior column. The period of this oscillator will be only 0.88 sec, considerably shorter than 1.14 sec, the period of an interior oscillator. If all the columns in the structure do not move together, the weak connections between girders, gutters and columns could be easily damaged and result in collapse of roof members.

2)   0.030 rad is the ultimate rotational capacity of the plastic hinge in the transverse direction, which means this is the point where the concrete crushes and column collapses. 0.026 rad is near this ultimate capacity. If for some reason (quality variation, non-uniformly distributed mass, etc), some of the columns are damaged and their capacity is lost, the lateral forces have to be redistributed to other members. This is not likely to be accomplished even if diaphragm action is developed because most columns are close to their ultimate capacity, and their capacity to carry additional forces is almost negligible.

It then can be concluded that even in the transverse direction, the prototype building will have little margin against failure until diaphragm and alternate lateral force resisting elements are both provided. In that way, even if the plastic hinges in some columns are seriously damaged and have little moment resisting capacity, they can still support gravity loads if the diaphragm redistributes lateral forces to unstressed columns and the building will be less likely to collapse.

3.3   OVERVIEW OF PROPOSED REHABILITATION SCHEME

The traditional seismic rehabilitation schemes for cast-in-place buildings are classified into two categories: local rehabilitation and global rehabilitation. A local scheme does not include the introduction of a new lateral force resisting system, i.e. all

the work will be performed on the existing members, connections and systems to enhance their strength, stiffness, ductility, etc. On the other hand, a scheme is considered the global rehabilitation if it adds new elements of the lateral force resisting system (shear walls, vertical bracings, etc) to the existing structure.

Several local rehabilitation schemes have already been proposed for one-story precast industrial buildings in Turkey. Since the columns are the only members that provide lateral force resisting capacity for the structures, local rehabilitation was concentrated on the cantilever columns. One proposed scheme involves partially jacketing the lower portion of all columns with reinforced concrete. This scheme would enhance the flexural stiffness of the columns and lower the fundamental period of the frame. However, analyses by Ersoy (2000) revealed that with a partial reinforced concrete jacket, the moment at the upper end of the jacketed region could be even greater than that at the column base when the jacket is absent because the lower fundamental period leads to higher inertial forces.

Another proposed approach involves steel jacketing of all columns. Steel angles are added at each column corner, and connected using steel plates. Due to the presence of the column sockets (Figure 1.5), the steel angles at column corners can not be properly connected to the foundation to transfer the moment, thus the jacket does not increase the column stiffness much and the roof drift can not be reduced. The ductility of the columns might be improved depending on how well the angle-plate assembly confines the concrete.

The classical global rehabilitation techniques that work effectively for cast-in-place reinforced concrete structures can not be applied directly to the precast structures. Since a global rehabilitation introduces new LFRS to the existing structure, there has to be some mechanism provided to transfer the lateral load from the existing structures to

43

the additional system. In this case, diaphragm action is required for global rehabilitation. Unfortunately, as described before, the absence of diaphragm is one of the main deficiencies of the precast concrete industrial buildings.

3.3.1 Basic Idea of Proposed Rehabilitation Scheme

Because local rehabilitation can not meet the seismic requirements for precast concrete industrial buildings in the epicentral zone in Turkey, a global scheme is proposed in this study. In order to avoid adverse effects on the industrial operations in the existing buildings, vertical diagonal steel bracing is proposed along the periphery of the structures (Figure 3.9). The diagonal braces will provide additional lateral force resistance during earthquakes. For a conceptional study, it is assumed that braces will be installed between all adjacent peripheral columns, but in a real structure, some bays will not be braced where doors and other openings for access are needed.
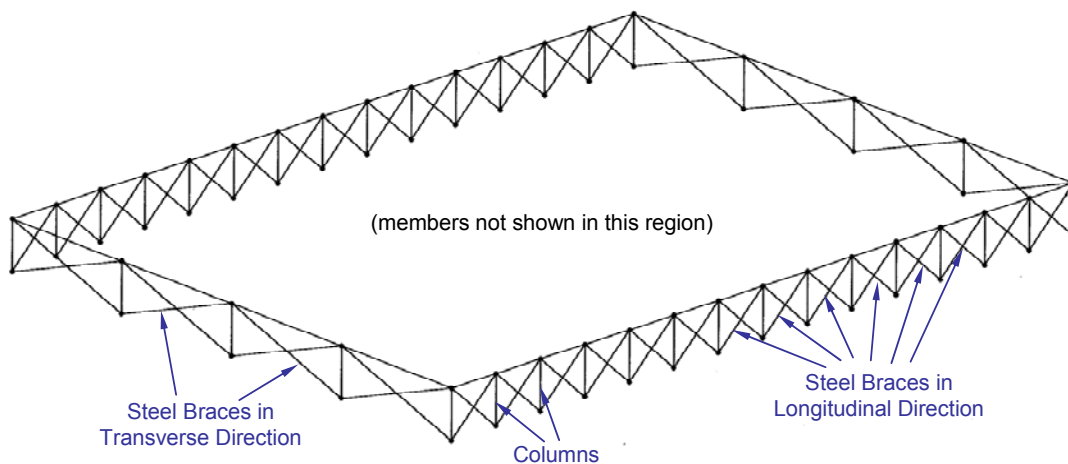
Figure 3.9 Peripheral Bracing

In order to transfer the lateral forces within the precast frame to the added peripheral braces, it is necessary to introduce a diaphragm action. The basic idea for the diaphragm is shown with a wood model in Figure 3.10.
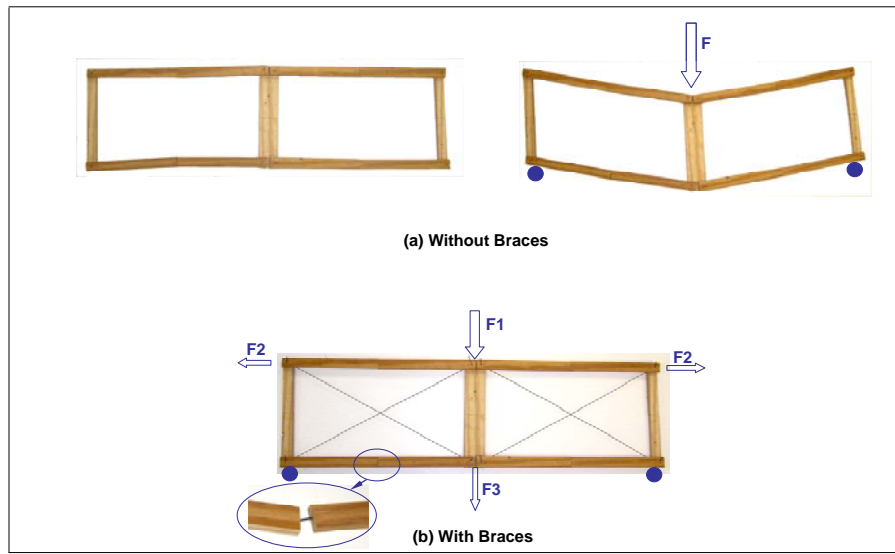
Figure 3.10   Simple Diaphragm Model

The wood frame in Figure 3.10(a) was used to model the existing roof frame of the prototype building, thus the columns were not included. The horizontal wood members represented roof girders, and the vertical ones, gutter beams. Steel pins were used for all the connections which could carry no moment. Because the girders and gutters in the prototype building can carry little tensile force due to the weak connections, the wood members were cut the middle, holes were drilled on each side of the cuttings, and steel pins were inserted inside the holes. In this way, all the members could carry no tensile force but do well for compressive loads.

With the vertical peripheral braces, the lateral motion of the columns on the periphery of the prototype building will be restrained. In Figure 3.10, the restraint to the boundary elements was realized by holding the two members at the ends of the model (right figure of Figure 3.10(a)). This model can not carry any lateral force at its middle, as there exists no lateral force transferring mechanism.

By adding diagonal tension-only steel braces as shown in Figure 3.10(b), the transfer of lateral forces can be accomplished. With the diagonal braces, the model can

45

carry external lateral forces in all directions as a whole. The only problem with the wood model was the stability. Because all the members were cut at the middle, they might buckle at the cutting under small compressive forces. However, this will not happen in the real structures because all members are precast integrally.

3.3.2   A Few Considerations about the Rehabilitation

Based on the introduction of the physical model in Section 3.3.1, it is expected that, if diagonal braces are added to the roof frame of a one-story industrial building immediately under the girders, a diaphragm could be formed by diagonal steel braces carrying tensile forces and precast concrete members (girders and gutters) carrying compressive forces. Through the diaphragm, the lateral force in the building may be transferred to the vertical diagonal braces added on the periphery of the structure. Figure 3.11 shows the top view of the braced prototype building.
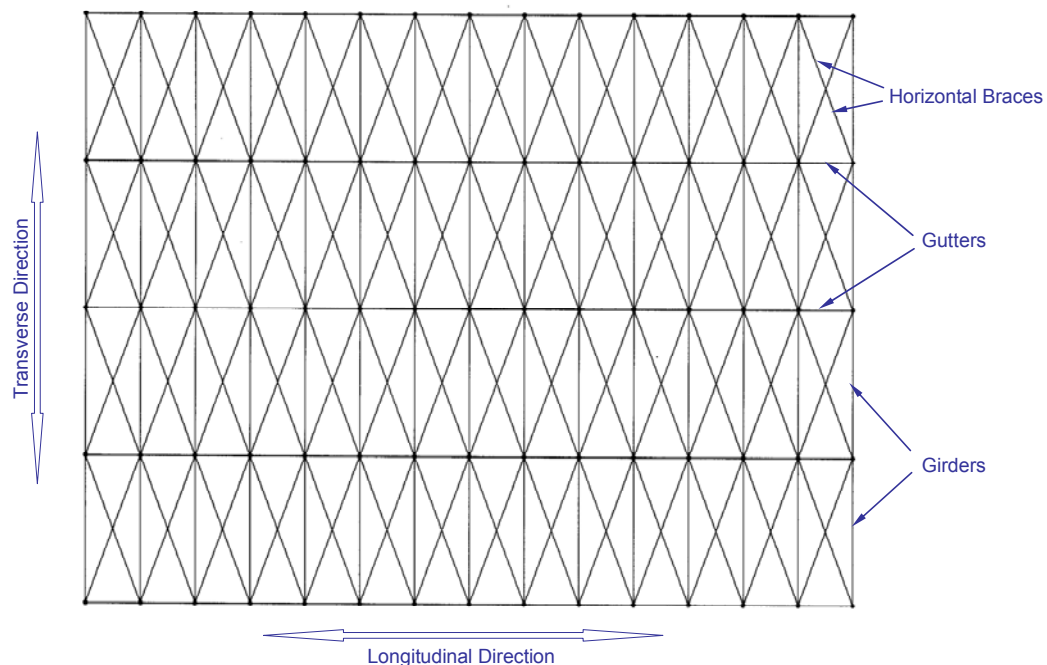
Figure 3.11 Braced Roof Frame of Prototype Building

46

To fully develop this rehabilitation system, analyses will be needed to size the braces and to determine the feasibility of introducing the new elements on to an existing structure. Before proceeding with the analyses of the prototype building with the proposed diaphragm bracing, a few points should be clarified:

1)   As calculated in Section 3.2, the maximum roof drifts which the columns could endure are 42.0 cm in longitudinal direction and 39.4 cm in transverse direction, and the corresponding plastic hinge rotations are respectively 0.029 rad and 0.030 rad. With the diaphragm bracing, the plastic hinge rotations should not exceed **0.025 rad** in both directions. The limiting rotation corresponds to **38.8 cm** longitudinal and **34.8 cm** transverse roof drifts respectively. With the vertical bracings working as a redundant LFRS, 0.025 rad is considered an acceptable level for the plastic hinge rotations.

2)   The diagonal horizontal braces should be installed through the centerlines of the columns, otherwise the twisting effect of these braces to the columns will definitely complicate the problem.

3)   It is important for the horizontal braces remain elastic. In case a few braces yield, there would be a large relative displacement between nodes associated with a same roof member (Figure 3.12). The roof members and connections can sustain small tensile deformation only. For the case shown in Figure 3.12, it is likely that the relative displacement would be too large and connections would be damaged and roof girders and gutters would fall from their supports.

4)   The vertical braces on the periphery are allowed to undergo yielding. The lateral displacements of the peripheral columns restrained by the vertical steel bracing are expected to be small. Even if the braces yield, the columns themselves should remain in the elastic range, thus the overall resistance will be still increasing as increased although the stiffness is reduced.
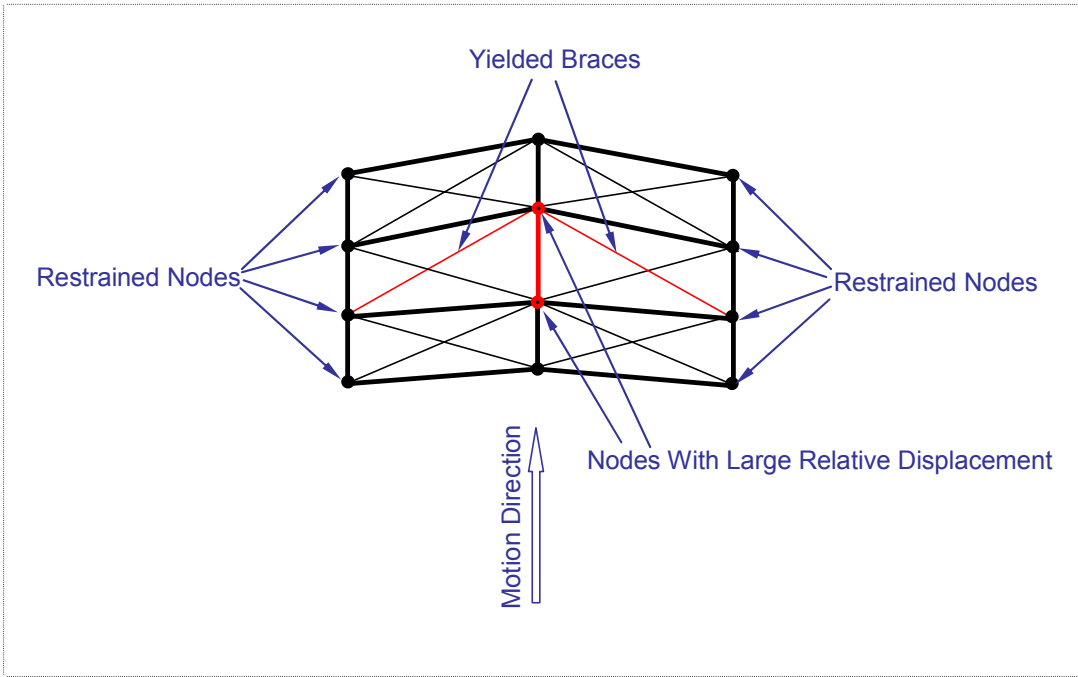
Figure 3.12   Potential Damage if Braces Yield

Chapter 4: Analytical Models

4.1   INTRODUCTION

As mentioned in Section 1.6, considerable strengthening work is required at the girder-column and gutter-column connections. However, before the details of the rehabilitation scheme are determined, the demands placed on the connections can not be determined. Therefore, the connections discussed in this chapter will be modeled as pins in the analyses. The procedures used to strengthen the connections will not be discussed until a practical rehabilitation scheme has been established.

In order to simulate the static and dynamic behavior of the prototype building, two different structural models were created. Both are capable of modeling the inelastic response of the structure. The first was developed using the finite element program SAP2000 This model will be used for static and modal analyses of the structure. Although static (elastic and inelastic) analysis and modal analysis can be easily conducted with the SAP2000 model, the program is not well suited for inelastic dynamic analyses. The computational platform OpenSees (Open System for Earthquake Engineering Simulation) was selected for the inelastic dynamic analyses. With the promising technique of fiber element, OpenSees model can efficiently calculate the inelastic properties of reinforced concrete members and thus simulate the inelastic dynamic response of concrete structures.

4.2   SAP2000 MODEL

In the SAP2000 model, all columns are modeled as cantilevers with the base fixed. The girder-column and gutter-column connections are modeled as pins using frame releases for bending moment as well as twisting torque. With these releases, the girders

and gutter beams may be simplified as truss members, which could carry axial force and deformation only.

SAP2000 model will be used for elastic modal analysis and nonlinear static analysis. Neither analysis considers the inelastic cyclic response of the materials. Therefore, the inelastic hysteretic properties of the materials are not included.

4.2.1 Mass

The roof, purlins, roof girders and gutter beams contribute the majority of the building mass. During an earthquake, the inertial force due to this distributed mass will be roughly uniformly applied along the girders and gutters, thus inducing moment and shear in members. However, since there were no flexural or shear problems observed with roof girders or gutter beams (Ersoy, 1999), it is believed that both girders and gutters had adequate flexural and shear capacity to resisting the induced bending moments and shear forces. To investigate the effect of the distribution of mass on the structural performance, a variety of SAP2000 models was built for different structural configurations with different mass models. The basic idea is shown in Figure 4.1. For a particular structure, two models were built, one with mass lumped at the member ends (Figure 4.1(a)), and the other with mass distributed along the members (Figure 4.1(b)). Then modal analyses were conducted on the two models respectively. The periods and mode shapes of the different models were compared.

The analyses indicated that if a structural member does not experience large flexure, using different mass distribution does not result in considerable difference of structural response. Because the roof members are not expected to sustain large flexure, they can be modeled with mass lumped at their ends. The difference of the periods using different mass models is within 2%.

(a) 3 Bays x 3 Bays (Top View)
(Lumped Mass, T = 0.93 sec)

(b) 3 Bays x 3 Bays (Top View)
(Distributed Mass, T = 0.94 sec)
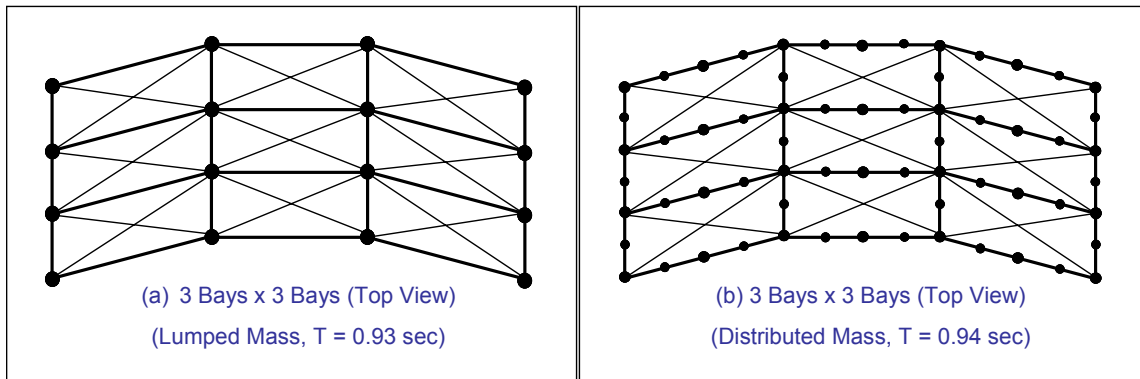
Figure 4.1 Effect of Mass Distribution on Structural Performance

For the columns which mainly experiences flexure, lumped mass model overestimates the effective mass, thus leads to larger periods. The period using lumped mass model is usually 5% larger than that using distributed model. However, because a larger period leads to a conservative design, for the purpose of simplifying the analyses, lumped mass is used in the SAP2000 models in this study. Purlins and the roof are not included in the model, except that their mass is computed and lumped at the upper joints of columns.

From the information given in Section 2.4, the mass of the precast members can be calculated respectively. The mass of a girder is 7578 kg, a column, 3360 kg, a gutter, 1584 kg, and a purlin, 428 kg. The density of the roof is assumed to be 24 kg/m^2. The amounts of mass lumped at the upper joints of columns are listed in Table 4.1

Table 4.1 Lumped Mass at Upper Joints of Columns (unit: kg)

Location of Column	Interior	At Ends of Long. Lines	At Ends of Trans. Lines	At Corners
Mass from Roof	3600	1800	1800	900
Mass from Girders	7578	7578	3798	3789
Mass from Gutters	1584	792	1584	792
Mass from Purlins	4284	2142	2142	1071
Mass from Column	1680	1680	1680	1680
Total Mass	**18726**	**13992**	**10995**	**8232**

4.2.2 Member Models

Roof Girders and Gutter Beams: With the pinned connections and lumped mass at upper ends of the columns, the roof girders and gutters mainly experience axial forces and axial deformation during seismic motion. As the deformation in roof girders and gutter beams is expected to be lower than the yield level of materials (concrete and steel reinforcement), the girders and gutters are simplified as uniform elastic trusses in the SAP2000 model.

Another fact that should be stated is that because of the weakness of the connections, the girders and gutter beams could carry little tensile forces. For the purpose of simplification, roof girders and gutter beams are modeled as compression-only members, i.e. when the strain in these members is tensile, the corresponding axial force remains zero.

The actual cross section area of the roof girder varies along its length. In the SAP2000 model, the area of the smallest cross section, 0.13 m^2 (Figure 2.7), is used through its length. The initial elasticity modulus of the concrete material shown in Figure 3.3, 30 GPa, is used for models of girders and gutters. The cross section area of gutters is 0.08m^2.

Columns: The columns mainly experience lateral deflection during earthquake, thus their flexural properties have to be considered. The maximum axial load on a single column is not larger than 184 kN, only 3.6% of the product of the concrete specified compressive strength and the cross section area of the column. Therefore the effect of the axial force on its flexural properties is not considered.

The column model used for SAP2000 analyses is exactly the same as illustrated in Section 3.2, i.e. each column is modeled as an elastic cantilever with a plastic hinge at the base. The relevant parameters are listed in Table 3.1.

Braces: As indicated in Section 3.3.2, it is important to keep the horizontal roof braces within elastic range. However, before the analyses have been conducted, the highest stress level in these braces is unknown. Therefore in the analytical models, the yield stress of both vertical and horizontal braces is assumed to be 690 MPa. This value was selected to be representive of Dywidag bars. If the results indicate that the maximum tensile stress in the bracing cables is less than yield, lower strength materials will be considered for economic reason.

Because the braces can not accommodate large deformations, the strain hardening of the material is not included in the material model. The idealized stress strain relationship for the brace material is given in Figure 4.2. As all braces are modeled as tension-only members, when the strain is negative (compression), the stress remains zero.
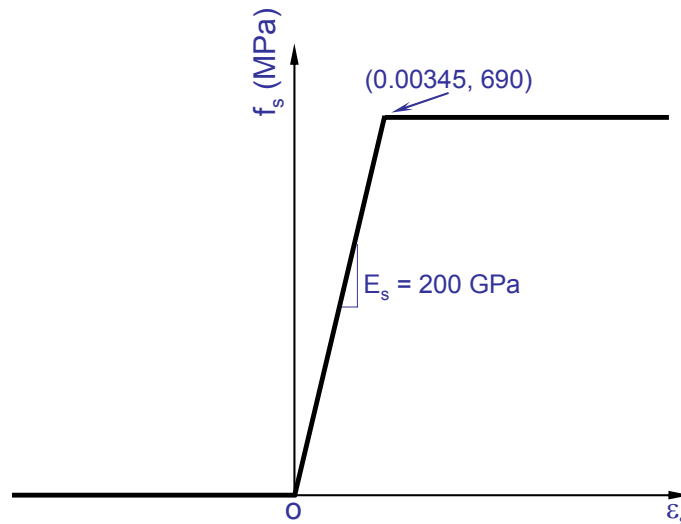
Figure 4.2 Stress-Strain Relation of Braces

4.2.3 Structural Model

The characteristics of the SAP2000 model of the prototype building are summarized in Figure 4.3.
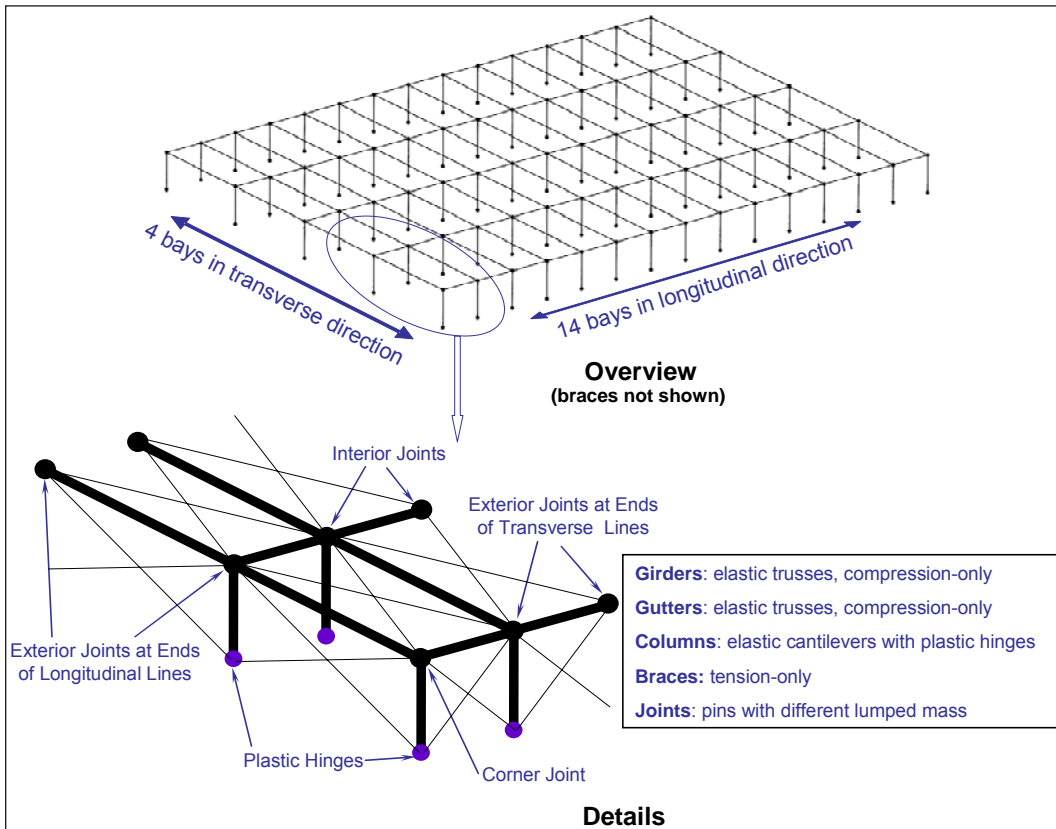
Figure 4.3 Summary of SAP2000 Model

4.3 OPENSEES MODEL

Similarly to the SAP2000 model, the columns are idealized as cantilevers with base fixed in the OpenSees model. At the top of the columns, connections are simplified as pins with no capacity to resist rotations. In this study, the OpenSees model is used mainly for the inelastic dynamic analyses (time-history analyses) of structures, thus the hysteretic properties of materials and structural members must be included in the model.

4.3.1 Material Models

Reinforcing Steel: The longitudinal reinforcing steel in columns is idealized using kinematic strain hardening model (STEEL01 in OpenSees platform)(Figure 4.4).

From the monotonic envelope shown in Figure 4.4 (a), it can be seen that the hardening starts as soon as the strain reaches yielding level. This is different from that shown in Figure 3.2, in which hardening starts at a strain of 0.01. Therefore, the hardening modulus ratio is selected as 2% in the OpenSees model, relatively lower than 5% used for SAP2000 model.
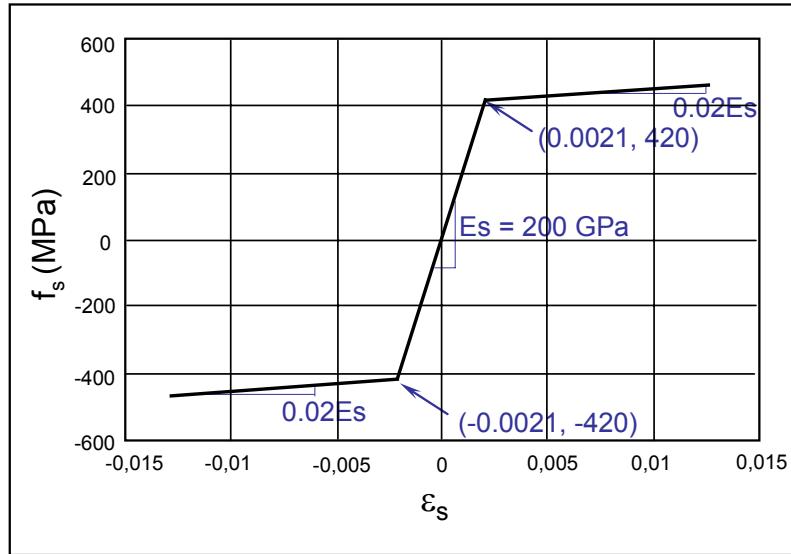
(a) Monotonic Envelope
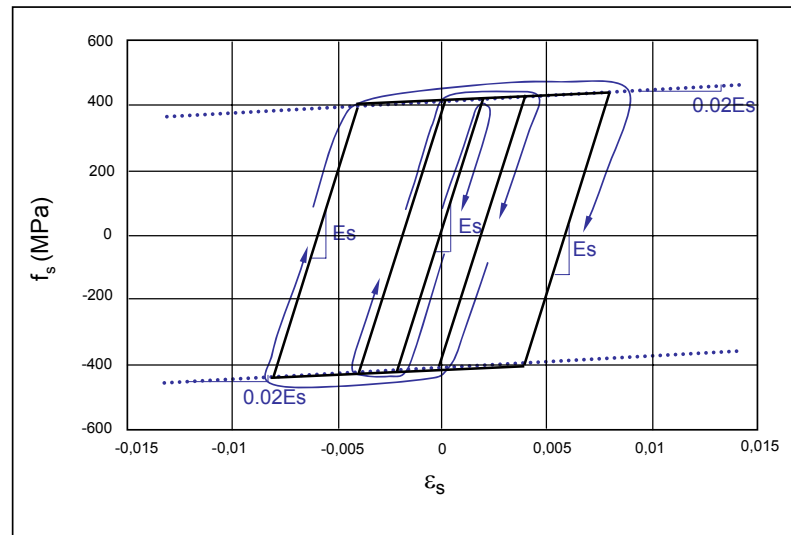
(b) Hysteretic Behavior

Figure 4.4 Hysteretic Model of Steel

55

Figure 4.4(b) shows the performance of the steel model under cyclic loading. This figure indicates the hysteretic properties of the reinforcement model as follows:

a)   If the cyclic loading starts at the initial status of the material, and the maximum strain does not exceed the yielding level ε_y (0.0021), the stress-strain relation remains linear proportional with a constant slope E_s;

b)   When the cyclic loading goes beyond the yielding point ε_y, the backbone of the stress-strain relation curves coincides with the monotonic envelope shown in Figure 4.3 (a);

c)   From the most recent reversal point, the curve goes with a constant slope E_s until it reaches the monotonic envelope.

Concrete: The material model CONCRETE01 in OpenSees platform was selected to construct the stress-strain relationship of the concrete material. The monotonic envelopes were acquired using modified Kent and Park model (Figure 3.3 and 3.4).

The hysteretic behavior of concrete is modeled with degraded linear unloading/reloading stiffness and no tensile strength according to the work of Karsan and Jirsa (1969) (Figure 4.5).
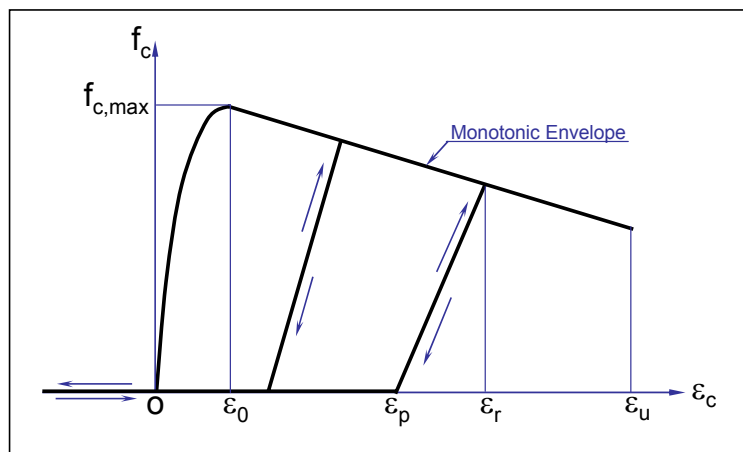
Figure 4.5 Hysteretic Concrete Stress-Strain Relation

56

The following rules govern the stress-strain relationship:

a)   Unloading from a point on the backbone curve takes place along a straight line connecting the point ε_r, at which unloading starts, to a point ε_p on the strain axis. The location of ε_p is given by the equations (Karsan and Jirsa, 1969):

$$\varepsilon_p = (0.145\,\upsilon^2 + 0.13\,\upsilon) \bullet \varepsilon_0$$

where ε_0 is the strain level corresponding to the maximum compressive stress in concrete, and υ is the ductility calculated with $\upsilon = \varepsilon_r / \varepsilon_0$.

b)   The concrete stress remains zero when strain is smaller than that at complete unloading (ε_p) since the tensile resistance of the concrete is ignored.

c)   On a reloading in compression, the stress in concrete is zero before the strain reaches the previous complete unloading point (ε_p). Once the strain goes beyond ε_p, reloading continues along the previous unloading path. Here, the fact is neglected that, in reality, unloading and reloading follow nonlinear paths, which together form a hysteresis loop. The calculations show this simplification has a minor influence on the hysteretic response of a reinforced concrete member (Taucer,1991).

d)   The proposed hysteretic model of concrete in compression does not account for the damage of concrete during cyclic motions. All the concrete members involved in this study are precast, and it can be assumed this kind of concrete damage is small since the quality of precast concrete members can be controlled more easily than cast-in-place ones.

4.3.2 Mass

In the OpenSees model, the mass of the roof, purlins, girders and gutters is lumped at the upper joints of columns. However, the mass of the columns is distributed along the columns because this would be more realistic and the fiber element method (discussed in Section 4.3.3) used for column model can deal with distributed mass

conveniently. The mass lumped at the top of columns is then 17046 kg for an interior column, 9315 kg for a column at an end of longitudinal lines, 12312 kg for a column at an end of transverse lines, and 6552 kg for a corner column.

4.3.3 Member Models

Roof Girders and Gutter Beams: As described in forgoing sections, there was no flexural or shear damage observed with girders or gutters (Ersoy, 1999), and it is believed that the deformation in both girders and gutters were small. Therefore, these members were modeled as uniform elastic beams with rectangular cross sections in the OpenSees model. The cross section of the girder model evenly is 40 cm high and 32.5 cm wide. The total mass of the girder is distributed to the two joints at its ends. The cross section of the gutter beam is 20 cm high and 40 cm wide. The initial modulus of elasticity of concrete (30 GPa) is used for both girders and gutters.

Columns: In order to simulate the hysteretic response of the cantilever columns, the only members that carry lateral loads in the original structure, flexibility-based fiber elements were adopted to model the precast columns. The fiber element method is actually an extension of the traditional finite element method. The basic idea of this model is that an element is monitored at several cross sections located at numerical integration points and each section is subdivided into a number of fibers where each fiber is free to experience different states of stress and strain (Figure 4.6). Under a certain deformed configuration, the strains in different fibers of a cross section are calculated separately assuming member cross sections remain plane and corresponding stresses are obtained from the stress-strain relationships. The components of the overall force at the cross section are then obtained by integrating of the response of all fibers.
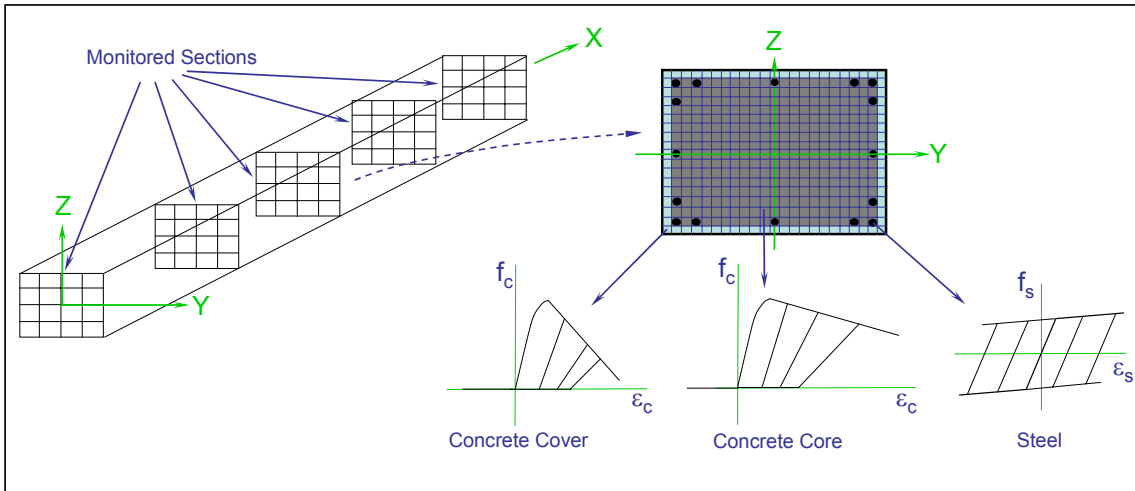
Figure 4.6 Fiber Element

The detailed formulation of fiber element method is out of the scope of this study, but this method has been integrated in the OpenSees framework. For detailed strategy of fiber element method, refer to Taucer (1991).

Based on the material models and with fiber element method, the moment-curvature relationships calculated for a column section under monotonic loading in both directions are shown in Figure 4.7. As a comparison, the models used in SAP2000 model are also included.

During an earthquake, columns in the one-story precast industrial buildings respond to the seismic motion of the ground as oscillators with the base fixed. Figure 4.8 shows the response simulations of a column in the prototype building when its top is under displacement-controlled cyclic excitations. In the calculations, the material models proposed in Section 4.3.1 and fiber element method are used for the flexural properties of the column in both directions (longitudinal and transverse). The maximum displacement sequence followed by the cyclic excitation in the longitudinal direction is 25 cm, 35 cm, 35 cm, 38 cm, 38 cm, in the transverse direction, 25 cm, 30 cm, 30 cm, 35 cm, 35 cm.
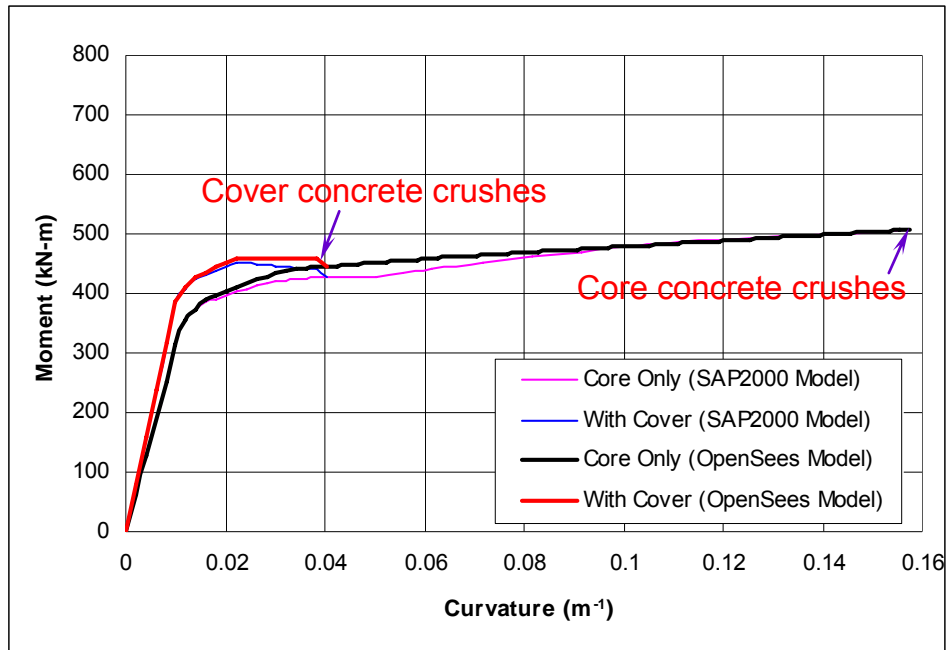
(a) About Weak Axis
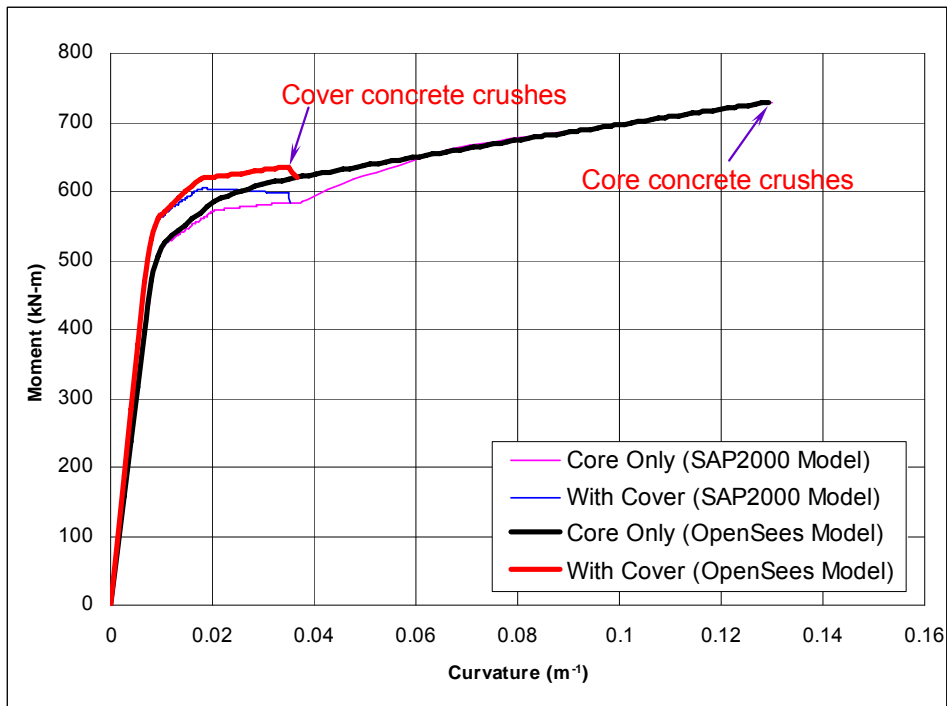
(b) About Strong Axis

Figure 4.7 Moment-Curvature Relation of Column Section

60
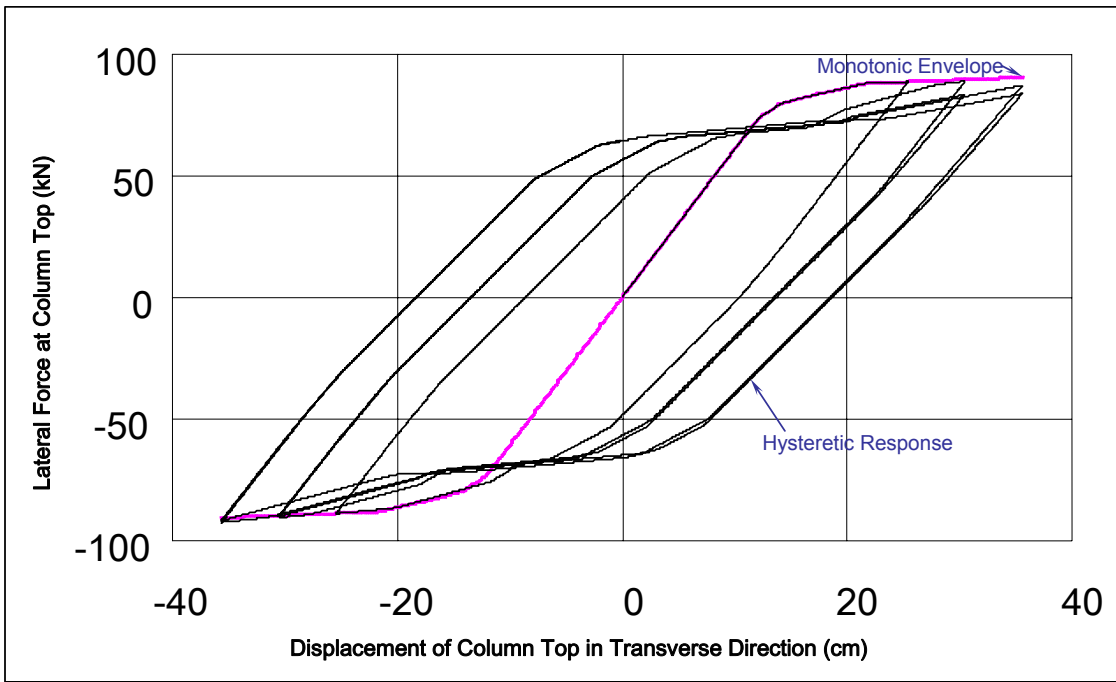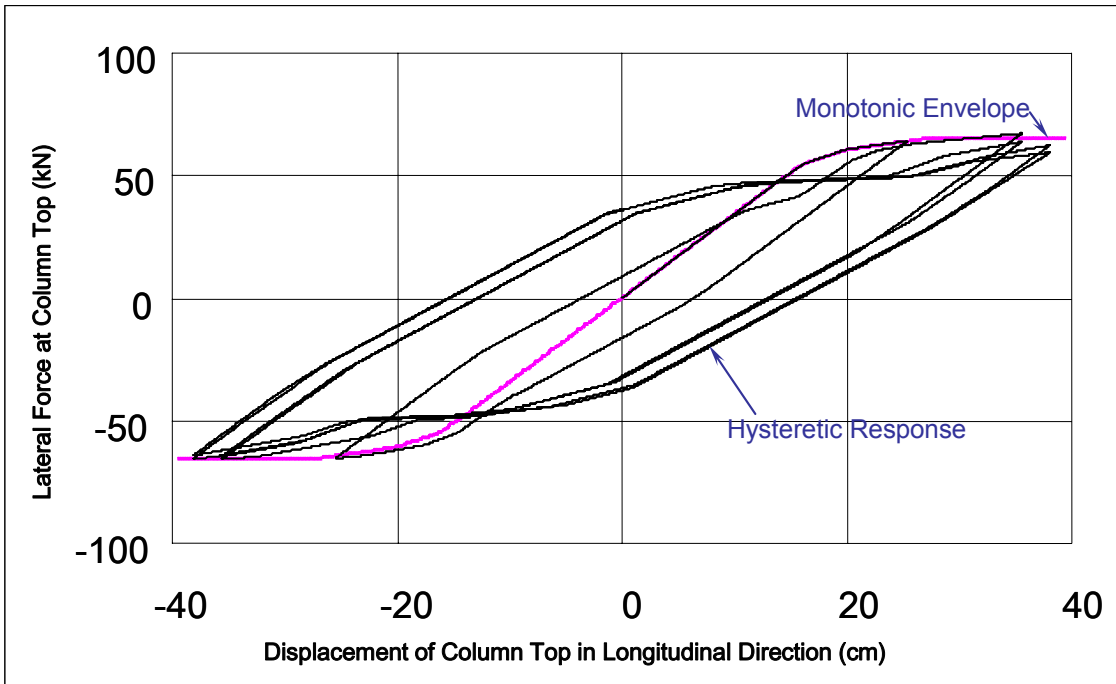
Figure 4.8 Force-Displacement Response of Column under Cyclic Excitations

61

Braces: All braces are modeled as tension-only truss elements without strain hardening. Under cyclic loading, the relation between the stress and strain in the braces is given in Figure 4.9. The slope E_s for both unloading and reloading remains constant.
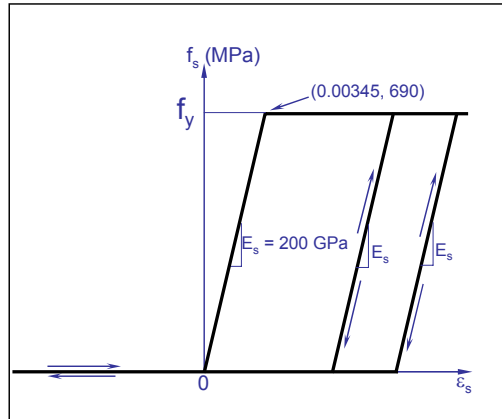
Figure 4.9 Hysteretic Behavior of Braces

4.3.4   Structural Model

The overall OpenSees model is analogous to the one shown in Figure 4.3. The main differences between these two analytical models are listed below:

a)   The hysteretic properties of all members are included in the OpenSees Model;

b)   These are no concentrated plastic hinges included in the OpenSees model. By using a fiber model, the inelastic response of the column is distributed along the length, not concentrated at the base.

4.4   SEISMIC ANALYSIS METHOD

In order to analyze the response of structures under earthquakes, a lot of analysis methods were developed by foregoing engineers and researchers. For a particular structure, one or more of three types of analysis are usually used: modal analysis, static analysis and time history analysis.

The modal analysis is completely based on the linear elastic behavior of structures. All the properties used for a modal analysis are corresponding to the initial status of the structure, therefore no inelastic response can be included. However, modal analysis can provide a lot of valuable features of the structure for further analyses, such as fundamental period T, shape of the first mode vibration, etc. Especially, the elastic modal analysis could estimate the maximum seismic displacement of the structure which actually responds inelastically during earthquakes (Shimazaki and Sozen, 1984).

Static analysis tries to estimate the dynamic performance of a structure by investigating the structural response under static loads with proper patterns and amplitudes. Inelasticity of structural members can be considered in static analyses. This method is actually built on the assumption that the first mode vibration dominates the structural performance during an earthquake. Therefore the estimation of the fundamental period and the shape of the first mode of a considered structure plays an essential role in the static analyses. This method is the most popular in the engineering field since it is easy to conduct.

The analytical model for time history analysis will include the most detailed information (elasticity, plasticity, hysteresis, etc.) of the structure. A recorded ground motion will be input to the structural model as excitation and the real time response of the structure will be monitored. This type of analysis is the most realistic of the three as it simulates the structural responses to real earthquakes. However, time analysis is usually too complicated and it takes a lot of computation time. It is generally used to verify the results from other analyses.

The detailed formulations of these three methods are illustrated in Appendix C.

Chapter 5: Tensioned String Analogy

5.1 INTRODUCTION

It has been emphasized that the static methods are the most popular in the industrial field and the easiest to be performed. Also stressed was the essential role of the fundamental period and the shape of the first mode of a considered structure. A one-story precast industrial building generally comprises a big degree of freedom represented by the displacements at the top of all the columns. This implies that a mode shape will possess a lot of components even though only one displacement component for each node is included, e.g., for a one-story building with 4 bays × 10 bays, at least 55 components have to be included to represent a single mode shape, which is almost impossible to be estimated without proper simplifications.

In this chapter, based on the mode shape observations of the prototype building, a series of modifications are suggested to the structural model, and a concise procedure based on the vibration of a tensioned string is developed to estimate the shape of the first mode. Using the proposed procedure, the fundamental period and the first mode shape of a one-story precast building strengthened by adding roof diaphragm could be easily estimated to a fairly high accuracy.

With the aid of the tensioned string analogy, the seismic response maxima of a series of strengthened one-story precast structures with different configurations are calculated and compared to the results from the full scale time history analyses. With these response maxima, the detailed strengthening scheme could be determined by performing the static push-over procedure on the analytical model built in Section 4.2. This chapter introduces the tensioned string analogy only, then push-over analyses and the final rehabilitation scheme for the prototype building will be discussed in Chapter 6.

5.2   **OBSERVATIONS OF MODE SHAPES**

With the analytical model built in Section 4.2, the shape of the first mode of the prototype structure could be conveniently calculated using SAP2000 software. By increasing or decreasing the numbers of the bays in both directions, different structural configurations are considered in the analyses. The two principal characteristics observed on the mode shapes of all structural configurations are illustrated as follows.

1)   When the system vibrates in the longitudinal direction of the structure, for the upper joints of all the columns located in a same line orienting in the longitudinal direction, the difference of their modal displacements is negligibly small. The same statement can be made for the vibration in the transverse direction. This characteristic is illustrated by the top views given in Figure 5.1, which is based on a 14 bay × 4 bay structure. In figure 5.1(a), joints are located in 5 longitudinal lines L1 to L5, and the joints in each of the 5 lines will have almost the same longitudinal displacements. In Figure 5.1(b), there are 5 joints with very close transverse displacements in each of the 15 transverse lines.

The same phenomenon was observed in all the structural configurations with different numbers of bays, different column stiffness, different brace sizes, and etc. The displacement difference increases where the brace size undergoes abrupt variation. But even the cross section area of the braces is decreased by a half in a particular region, the ratio of this difference over the joint displacement will be within 3%.

The displacement difference also increases if the column size changes dramatically within a considered line. However, in the real engineering, the dramatic size change is usually unexpected within the columns in a same line. Instead, columns of the same size are often used for a single building. Therefore, the effect of the column size variation on the mode shapes could be usually ignored.

65

L1
L2
L3
L4
L5

(a) Longitudinal Motion

T1 T2 T3 T4 T5 T6 T7 T8 T9 T10 T11 T12 T13 T14 T15
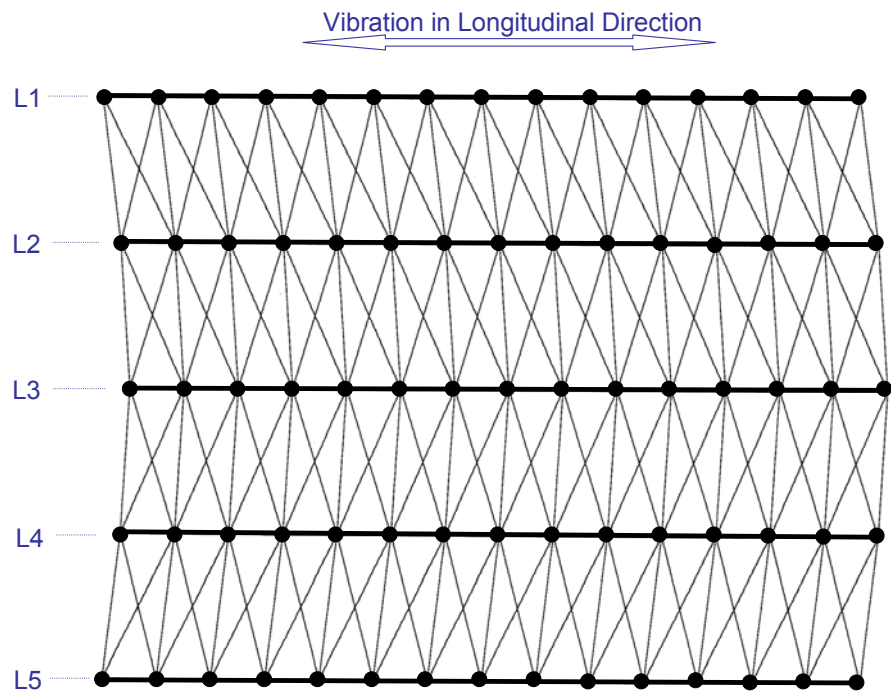
Vibration in Transverse Direction
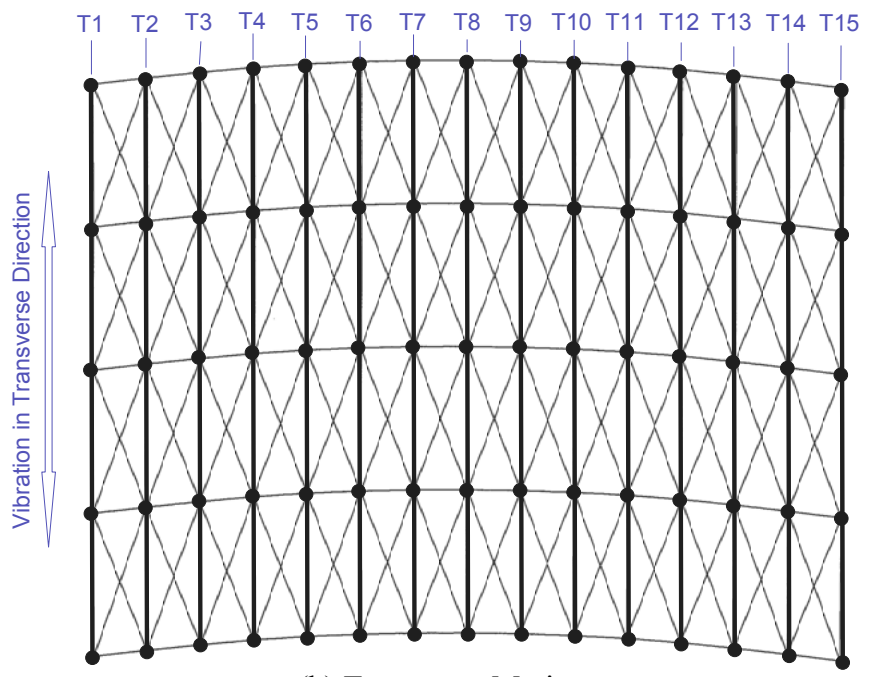
(b) Transverse Motion

Figure 5.1 First Mode Shapes

66

From this observation, it can be concluded that when the motion in either direction (longitudinal or transverse) is considered, as long as the roof braces work in elastic range, all the joints located in a same line orienting in the motion direction can be considered as having the same displacement. In other words, they can be dealt with as one node. This simplification reduces the degree of freedom (DOF) of the system dramatically. For example, a one-story industrial building with 10 bays in the longitudinal direction and 3 bays in the transverse direction can be simplified to an 11 DOF system in the transverse direction and a 4 DOF system in the longitudinal direction , instead of 44 DOF ones.

2)   The mode shapes are insensitive to the column stiffness if only all columns are of the same size. To explain this phenomenon, the transverse vibrations of the structure with 14 bays $\times$ 4 bays were first investigated. The diameters of the roof braces and the vertical braces were assumed to be 26 mm and 29 mm respectively. The column stiffness was adjusted by multiplying their original stiffness (EI = 64700 kN•m^2) with a factor τ, which varied between 0 and 3.0. At different values of τ, the shapes of the first transverse modes were recorded. As described above, the displacements of the joints in each same transverse line were almost identical, therefore the structure was simplified as a MDOF of 15 nodes with lumped mass m_1 through m_{15}. The deformed shape of any longitudinal line (Figure 5.1b) could represent the mode shape $\{\varphi\}$. The mode shapes were then normalized such that $\sum_{j=1}^{15} m_j \varphi_j^2 = 10^6$. The number 10^6 was selected for the purpose that the resulted mode shape turned out with numbers which were convenient for expression, i.e. they were neither too large nor too small. The resulted shapes corresponding to $\tau = 0.0, 0.5, 1.0, 2.0$ and 3.0 are shown in Figure 5.2, where $\tau = 0.0$ implies the column stiffness effect is ignored and $\tau = 1.0$ represents the actual structure.

67
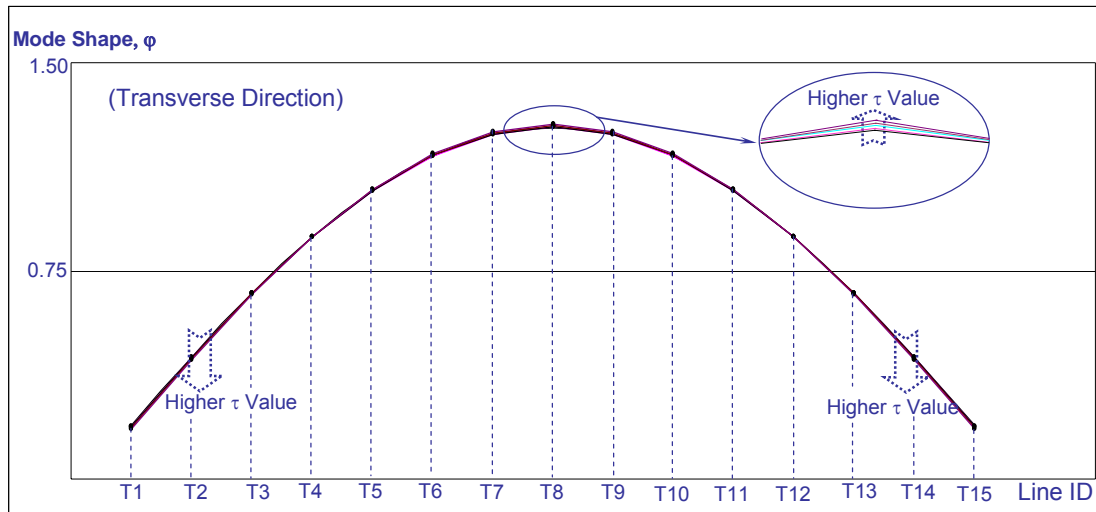
Figure 5.2 Effect of Column Stiffness on Mode Shape (14 bays × 4 bays)

Figure 5.2 shows that the effect of column stiffness on the mode shape is limited as the 5 curves are so close to each other that they look like one curve. When the value of τ increases, the deformed shape becomes more curved, i.e., the displacements at two ends decrease and that at the middle goes up. Although the column stiffness varies over a huge span, the maximum difference of modal displacement is within 8%.

This phenomenon could be explained by the particularities of the mass matrix and the stiffness matrix of this special structural style. As described above, since the displacement difference of the nodes in each transverse line is negligible, the structure was simplified to a system with 15 degrees of freedom. From the information in Section 4.2.1, the mass of the first and the fifteenth node (T1 and T15 in Figure 5.1) will respectively 58440 kg, which includes 2 corner joints and 3 transversely exterior joints. This mass is 75% of that of an interior node, 78168 kg, which includes 2 longitudinally exterior joints and 3 interior joints. The mass matrix of the 15 DOF system then has a form:

$$[M] = m^* \begin{bmatrix} 0.75 & 0 & 0 & 0 \\ 0 & 1 & 0 & 0 \\ & & \ddots & \\ 0 & 0 & 1 & 0 \\ 0 & 0 & 0 & 0.75 \end{bmatrix} \approx m^*[I] \tag{5.1}$$

where m^* represents the mass of an interior node.

In the meantime, if all the columns have the same stiffness, the stiffness matrix of the 15 DOF system will be in the form:

$$[K] = [K_B] + k_C[I] \tag{5.2}$$

where $[K_B]$ is the contribution from bracing and k_C is the overall stiffness of 5 columns in each transverse line.

Assuming $\{\varphi\}$ represents the shape of the first mode associated with angular frequency ω of this system, by the definition of mode shape, Eq. 5.3 below must apply.

$$[K]\{\varphi\} = [M]\omega^2\{\varphi\} \tag{5.3}$$

If the stiffness of each column is increased by the same amount, the stiffness matrix for the new system can be written in the form:

$$[K'] = [K] + \Delta k_C[I] \tag{5.4}$$

To verify that $\{\varphi\}$ is also a mode shape of the new system, consider the product of matrix $[K']$ and the mode shape $\{\varphi\}$:

$$[K']\{\varphi\} = [K]\{\varphi\} + \Delta k_C[I]\{\varphi\} \tag{5.5}$$

Substituting Eq. 5.3 into Eq. 5.5, and considering the form of the mass matrix given in Eq. 5.1, Eq. 5.5 becomes:

$$[K']\{\varphi\} = [M]\omega^2\{\varphi\} + \frac{\Delta k_C}{m^*}[M]\{\varphi\} = [M]\left(\omega^2 + \frac{\Delta k_C}{m^*}\right)\{\varphi\} = [M](\omega')^2\{\varphi\} \tag{5.6}$$

where $(\omega')^2 = \omega^2 + \frac{\Delta k_C}{m^*}$.

Eq. 5.6 indicates that $\{\varphi\}$ must be a mode shape of the new system with a new angular frequency of ω'. In the same way, it can be shown that these two systems with different column stiffness possess the same shapes for all modes.

The only approximation used in the derivation above is in Eq. 5.1 because with the described simplification, the actual mass matrix in Eq. 5.1 is not a multiple of the unit matrix. Instead, for a regular one-story precast industrial building, with the same simplification applied for Eq. 5.1, the mass of the first and the last node will be 0.60 ~ 0.80 times that of an interior node. Therefore approximating the mass matrix as a multiple of the unit matrix introduces some error to the mode shape calculation.

However, with the vertical bracing added to the periphery of the structure, the seismic displacement of these two exterior nodes is remarkably reduced, thus the mode shape becomes less sensitive to the mass of these two end nodes. The extreme situation is when the vertical braces are so over-sized that the exterior columns do not deform related to the ground during an earthquake and the end nodes could be idealized as fixed. In this situation, the mode shape becomes independent of the mass of the two end nodes. With finite stiffness of the vertical bracing, it is expected that errors in the mode shapes decreases as the number of bays increases because the closer to a multiple of a unit matrix the mass matrix will be.

To clarify if the effect of the columns to the mode shapes can be neglected in the calculation, another structural model with only 3 bays in each direction was built. Once again, the diameters of the roof braces and the vertical braces were assumed to be 26 mm and 29 mm respectively. The same procedures by which Figure 5.2 was obtained were conducted on the fundamental mode shapes with τ varying from 0.0 to 3.0 in both directions of this 3 bay $\times$ 3 bay structure, and the results are shown in Figure 5.3.
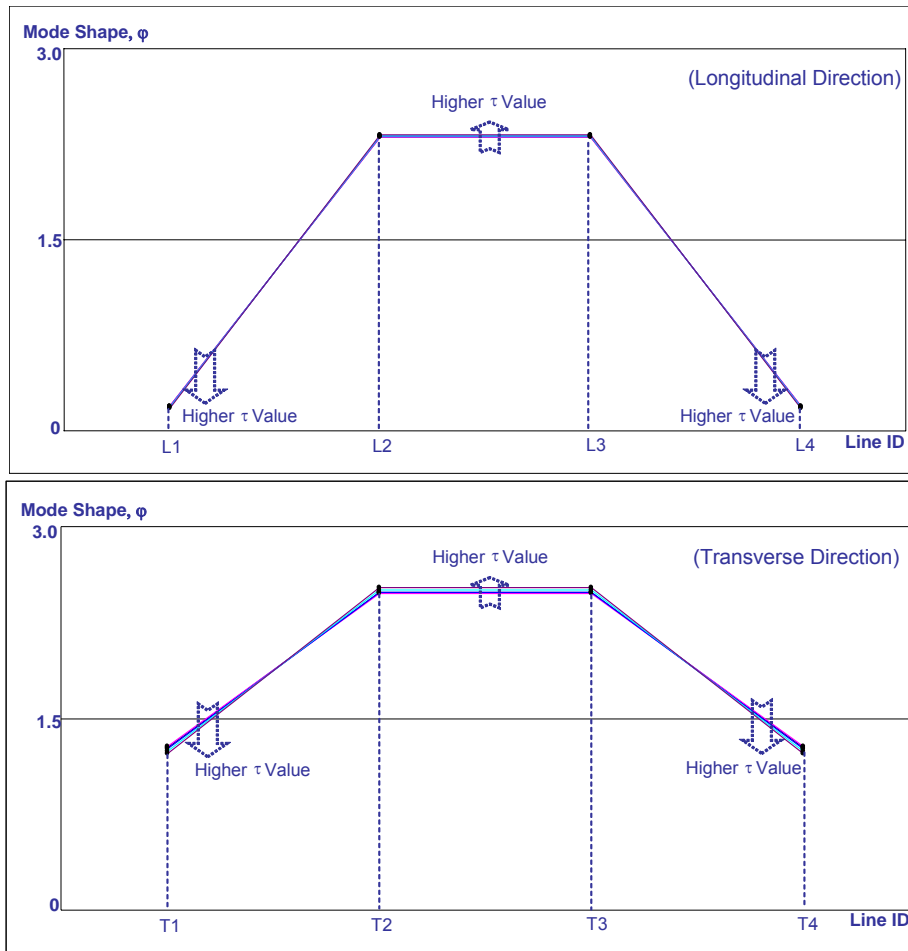
Figure 5.3 Effect of Column Stiffness on Mode Shapes (3bays × 3 bays)

In Figure 5.3, the column stiffness effect in the longitudinal direction is smaller than that in the transverse direction. This is a reasonable result considering that the longitudinal movement of the nodes on the periphery is reduced by the vertical braces more effectively than that in the transverse direction. As expected, the mode shape with 3 bays in the transverse direction is more sensitive to the column stiffness than with 14 bays. But the maximum difference of modal displacement is still within 10% although the column stiffness varies over such a large range. The columns still can be ignored in the estimation of the mode shape.

To summarize the observations on the mode shapes of one-story precast industrial buildings strengthened by horizontal diaphragm bracing as well as vertical peripheral braces, conclusions can be stated as follows:

1) In the estimation of the mode shapes in either longitudinal or transverse direction, all the nodes located in a same line orienting in the motion direction may be considered to have the same displacement, i.e. they can be dealt with as one single node.

2) The effect of the column stiffness can be ignored as long as all columns have roughly the same stiffness.

5.3 TENSIONED STRING ANALOGY

Several formulations have been developed to estimate the mode shapes of structures. The formulation recommended in ASCE 7 can not be used for the one-story precast industrial building strengthened using diaphragm braces, because there is only one story and the displacement of the roof can not be represented by only one quantity when the deformation of the diaphragm itself can not be neglected. The shape of the soft diaphragm shows up as an essential part of the mode shape estimation.

If the displacements at the two ends of a diaphragm are negligibly small compared to that of the other parts, the diaphragm can be approximated as a shear beam. The first mode of a uniform, simply supported beam is $\varphi(x) = \sin\left(\dfrac{\pi x}{L}\right)$ as shown in Figure 5.4.
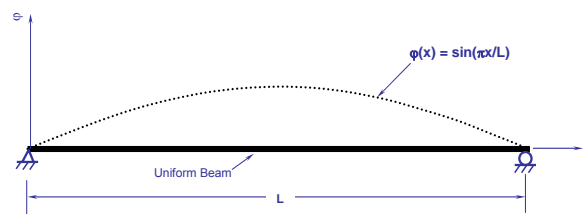
Figure 5.4 Mode Shape of Uniform Beam

72

Two obstacles prevent the sine formulation from being used to estimate the mode shape of the diaphragm strengthened buildings in this study:

1)   The displacements of the diaphragm ends, i.e. the exterior column lines, are usually not negligible, and these displacements have to be included in the mode shape estimation, especially when the cross-section area of the vertical braces is small;

2)   When the sizes of the horizontal braces within the diaphragm vary, the diaphragm stiffness is not a constant.

The formulation used in this study is based on the tensioned string model and is built from the observation on the mass and stiffness matrixes of the strengthened structures. Using the simplification described in Section 5.2, in the estimation of the mode shape of a structure including N bays under consideration, only the stiffness of the braces (vertical and horizontal) need to be considered, and the structure can be simplified as a MDOF system with N+1 nodes (refer to Figure 5.1). The mass matrix can be calculated by simply adding the mass of the joints in corresponding lines:

$$[M] = m^* \begin{bmatrix} \alpha & 0 & & 0 & 0 \\ 0 & 1 & & 0 & 0 \\ & & \ddots & & \\ 0 & 0 & & 1 & 0 \\ 0 & 0 & & 0 & \alpha \end{bmatrix} \tag{5.7}$$

where α is the ratio of the mass of an end node to the mass of an interior node, and it is generally between 0.6 and 0.8.

The stiffness matrix can be constructed using the indirect method. When node 1 displaces by a unit distance and the other nodes remain unmoved, node 1 will be restrained by the peripheral vertical braces and the horizontal braces connecting node 1 and 2. These two forces can be notated as $k_{w,1}$ and $k_{D,1}$, where the subscript "W" means "Wall", and "D", "Diaphragm" . The other end node N+1 can be handled similarly and

the corresponding forces can be notated as $k_{w,2}$ and $k_{D,N.}$ The interior node j $(1 < j < N+1)$ will be subjected to the forces coming from the adjacent diaphragm brace groups, $k_{D,(j-1)}$ and $k_{D,j}$. According to the indirect method, the system stiffness matrix is in the form:

$$[K] = \begin{bmatrix} k_{W,1}+k_{D,1} & -k_{D,1} & 0 & 0 & 0 & 0 \\ -k_{D,1} & k_{D,1}+k_{D,2} & -k_{D,2} & 0 & 0 & 0 \\ 0 & -k_{D,2} & k_{D,2}+k_{D,3} & 0 & 0 & 0 \\ & & & \ddots & & \\ 0 & 0 & 0 & k_{D,(N-2)}+k_{D,(N-1)} & -k_{D,(N-1)} & 0 \\ 0 & 0 & 0 & -k_{D,(N-1)} & k_{D,(N-1)}+k_{D,N} & -k_{D,N} \\ 0 & 0 & 0 & 0 & -k_{D,N} & k_{D,N}+k_{W,2} \end{bmatrix} \tag{5.8}$$

To investigate the effect of vertical braces on the mode shape, temporarily assuming all horizontal braces are of the same size and the same vertical braces are used at both ends, the stiffness matrix becomes:

$$[K] = \begin{bmatrix} k_W+k_D & -k_D & 0 & 0 & 0 & 0 \\ -k_D & 2k_D & -k_D & 0 & 0 & 0 \\ 0 & -k_D & 2k_D & 0 & 0 & 0 \\ & & & \ddots & & \\ 0 & 0 & 0 & 2k_D & -k_D & 0 \\ 0 & 0 & 0 & -k_D & 2k_D & -k_D \\ 0 & 0 & 0 & 0 & -k_D & k_W+k_D \end{bmatrix} \tag{5.9}$$

where k_W and k_D represent the stiffness of vertical and horizontal braces respectively. The mode shape is determined by Eq. 5.7 and Eq. 5.9.

Consider the tensioned string shown in Figure 5.5(a), in which the tension force is assumed to be Γ and the mass density is set to ρ. When vibrating with small amplitude, the tension in the string can be considered as constant through the whole length L.

To perform numerical analysis, supposing the string is divided into N+2 segments shown in Figure 5.5(b) where λ is selected in such a way that $2\dfrac{k_D}{k_W}\lambda + N\lambda = L$, and assuming each segment remains straight during the vibration, the mass matrix of this N+1 DOF system will be:
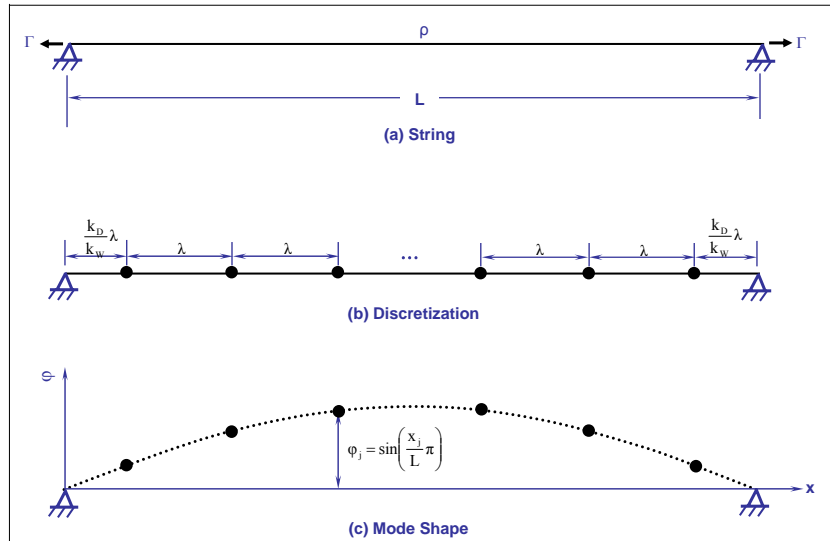
Figure 5.5 Tensioned String Model

$$[M'] = m' \begin{bmatrix} \beta & 0 & 0 & & 0 & 0 & 0 \\ 0 & 1 & 0 & & 0 & 0 & 0 \\ 0 & 0 & 1 & & 0 & 0 & 0 \\ & & & \ddots & & & \\ 0 & 0 & 0 & & 1 & 0 & 0 \\ 0 & 0 & 0 & & 0 & 1 & 0 \\ 0 & 0 & 0 & & 0 & 0 & \beta \end{bmatrix} \tag{5.10}$$

where $m' = \rho\lambda$ and $\beta = 0.5 + 0.5\dfrac{k_D}{k_W}$.

The stiffness of a string segment is proportional to the tension Γ and inversely proportional to the segment length. With the assumption that Γ remains constant during small amplitude vibration, the stiffness matrix of the system shown in Figure 5.5(b) is:

$$[K'] = \begin{bmatrix} \dfrac{k_W}{k_D}k'_D + k'_D & -k'_D & 0 & 0 & 0 & 0 \\ -k'_D & 2k'_D & & 0 & 0 & 0 \\ 0 & -k'_D & 2k'_D & 0 & 0 & 0 \\ & & & \ddots & & \\ 0 & 0 & 0 & 2k'_D & -k'_D & 0 \\ 0 & 0 & 0 & -k'_D & 2k'_D & -k'_D \\ 0 & 0 & 0 & 0 & -k'_D & \dfrac{k_W}{k_D}k'_D + k'_D \end{bmatrix} \tag{5.11}$$

where $k'_D = \dfrac{\Gamma}{\lambda}$.

75

Comparison of Eq. 5.11 with Eq. 5.9 shows that if Γ is selected in such a way that $k'_D = k_D$, i.e. $\Gamma = k_D\lambda$, the stiffness matrix in Eq. 5.11 becomes exactly the same as that of the one-story structure shown in Eq. 5.9.

For Eq. 5.10 and Eq. 5.7, if the density of the string is selected as $\rho = \dfrac{m^*}{\lambda}$, the only different item between $[M']$ given in Eq. 5.10 and $[M]$ in Eq. 5.7 is α and β. α is generally between 0.6 and 0.8. The β value is related to the ratio of k_D over k_W by $\beta = 0.5 + 0.5\dfrac{k_D}{k_W}$.

When $k_D \le k_W$, β is valued between 0.5 and 1.0. As β is now close to α, the effect of the difference between α and β on the mode shape is expected to be negligible. The mode shape of the strengthened one-story industrial building may be estimated by a tensioned string. The shape of the first mode of such a string coincides with a sine function (Figure 5.5(c)).

$$\varphi_j = \sin\left(\frac{x_j}{L}\pi\right) = \sin\left(\frac{\frac{k_D}{k_W}\lambda + (j-1)\lambda}{L}\pi\right)$$

$$= \sin\left(\frac{\frac{k_D}{k_W}\lambda + (j-1)\lambda}{\frac{2k_D}{k_W}\lambda + N\lambda}\pi\right) = \sin\left(\frac{\frac{1}{k_W} + \frac{j-1}{k_D}}{\frac{2}{k_W} + \frac{N}{k_D}}\pi\right) \qquad (5.12)$$

The mode shape determined by Eq. 5.12 is equivalent to that of the idealized tensioned string shown in Figure 5.6, where the length of each string segment is the reciprocal of the stiffness of the corresponding diaphragm or vertical bracing. The total length of the tensioned string is then $L = \dfrac{2}{k_W} + \dfrac{N}{k_D}$, and the mode shape is exactly the same as that given by Eq.5.12.
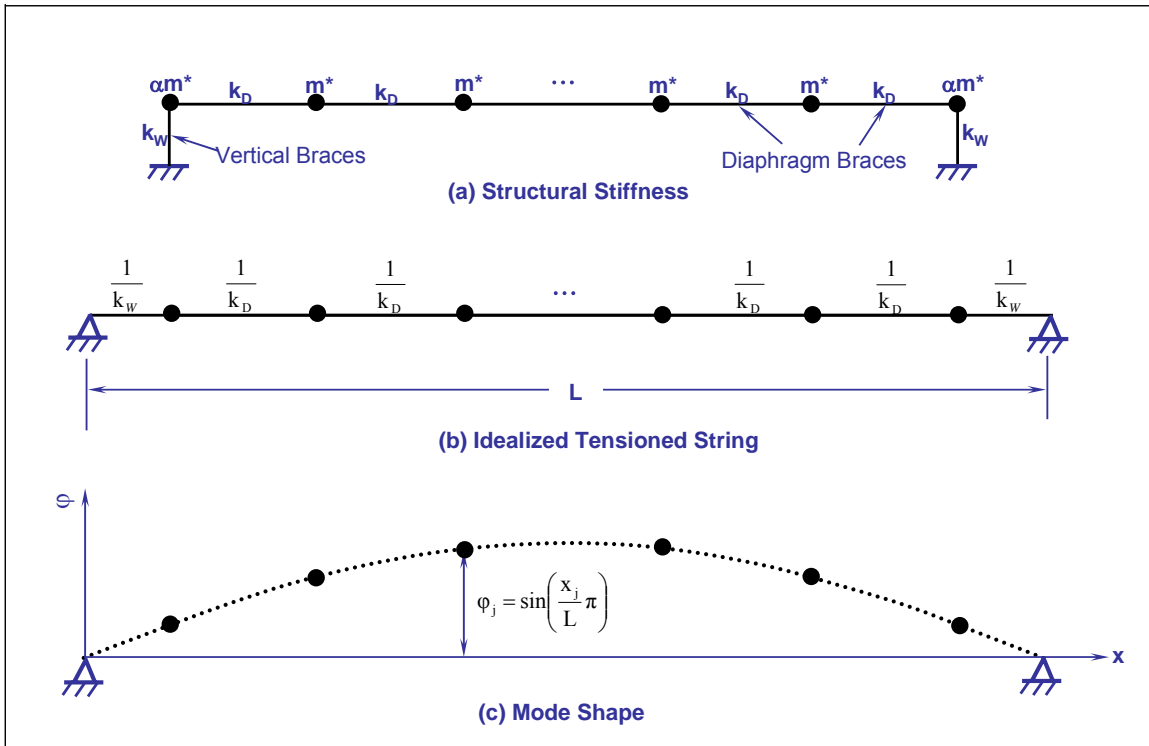
Figure 5.6   Analogical Tensioned String for Mode Shape

So far, the tensioned string analogy is developed assuming $k_D \leq k_W$. As for the feasibility of this method on structures with $k_D > k_W$, the physical response of the structure needs to be considered. When k_D is much larger than k_W, the value of β in Eq. 5.10 will be much larger than α in Eq. 5.7, thus the string model can not represent the actual structure any more. However, the string model is not developed to analyze the seismic response of the structure. Instead, it is expected to estimate the mode shape only. Possessing quite different mass matrixes does not necessarily mean having quite different mode shapes. Actually, it is impossible to calculate all the structural response with the columns out of consideration even when β is exactly the same as α because the columns are not in the account yet.

77

When $k_D \gg k_W$, in the tensioned string model, the segment length corresponding to the vertical braces will be much larger than that of a diaphragm section, i.e. $\dfrac{1}{k_W} \gg \dfrac{1}{k_D}$. As a result, all the nodes will be relatively concentrated in the middle region of the string because the first segment and the last one are much longer than the others (Figure 5.7). When the mode shape is calculated using Eq. 5.12, the displacements of all nodes will be close to each other. This is exactly what physically happens on the actual structure with stiff diaphragm but soft peripheral vertical braces.
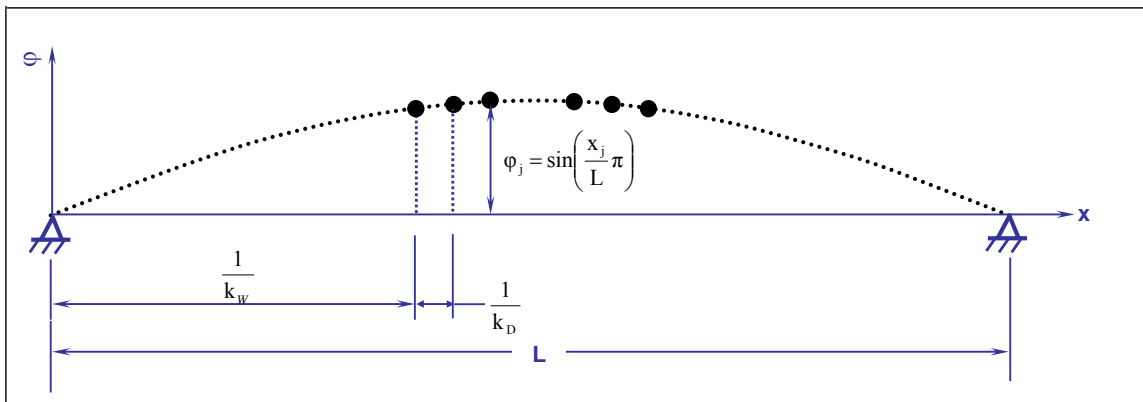
Figure 5.7   Tensioned String Model for $k_D \gg k_W$

The physical meaning of $k_D \gg k_W$ is a stiff diaphragm together with soft vertical bracing. The diaphragm tries to make all joints move together, while the vertical bracing reduces the displacements of the end nodes. Because the diaphragm is much stiffer than the vertical bracing, the final displacements of the nodes would be close to each other, just like what the tensioned string model predicts. The tensioned string analogy might be still used to estimate the mode shape.

Unfortunately, the applicability of the tensioned string analogy when $k_D \gg k_W$ can hardly be proven by strict analytical derivation. However, the applicability can be verified by analysis results on a verity of structural configurations. The same thing

78

happens when the tensioned string analogy is used on structures with diaphragm braces of different sizes.

When the sizes of the horizontal braces vary within the diaphragm, different bays will generally have different diaphragm stiffness, e.g. $k_{D,1} \neq k_{D,3}$. Even further, the two vertical brace groups might have different stiffness $\left(k_{W,1} \neq k_{W,2}\right)$ (Figure 5.8) for some reason. In this case, the tensioned string shown in Figure 5.6(b) is modified by replacing each segment length with the reciprocal of the corresponding stiffness.

In Figure 5.8(b), it can be seen that the distance between two adjacent nodes varies on the analogical string, although nodes in the actual structure (Figure 5.8(a)) are still uniformly spaced. With varying diaphragm stiffness, the applicability of the tensioned string analogy needs to be verified by analysis results on different structural cases, as it can hardly be proven by analytical derivation.
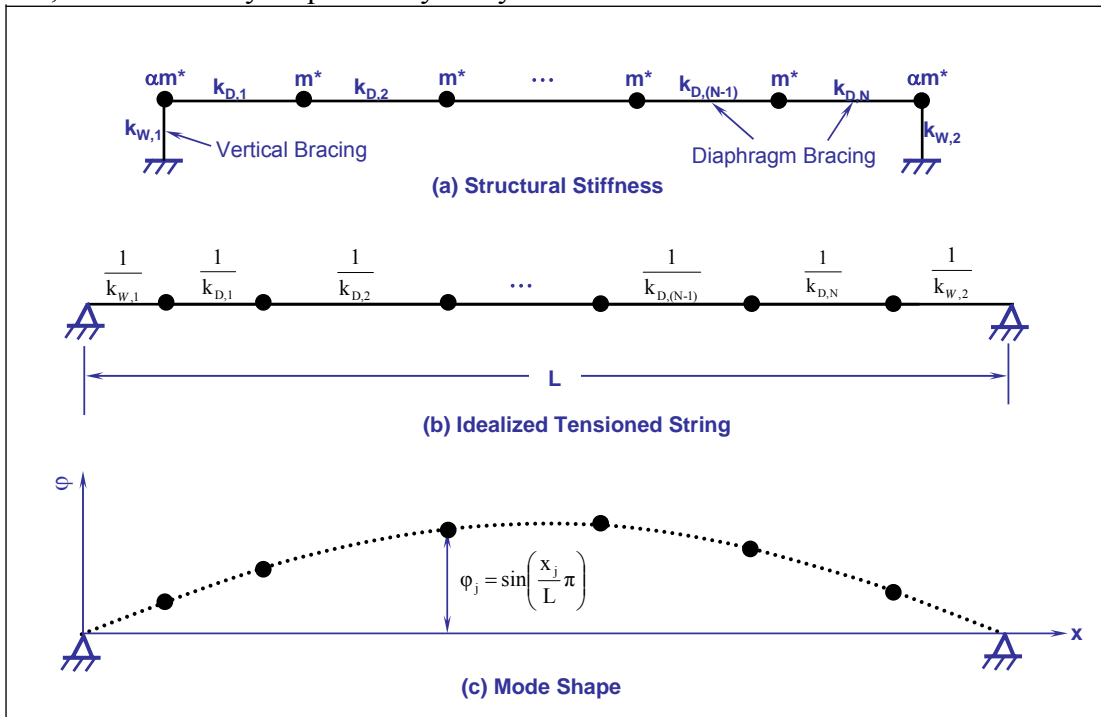
Figure 5.8   Tensioned String Model for Varying Stiffness

5.4   VERIFICATION OF TENSIONED STRING ANALOGY

To verify the described tensioned string analogy, a series of SAP2000 models were constructed with different numbers of bays in each direction, different column sizes and different brace sizes. The mode shapes of these structural models were estimated using the tensioned string analogy, and compared with the modal analysis results from SAP2000 program. As an example, the calculation of the longitudinal mode shape for a 13 bay × 3 bay (N = 3) structure with uniform 26 mm diaphragm braces and 13 mm vertical braces is illustrated in Figure 5.9.
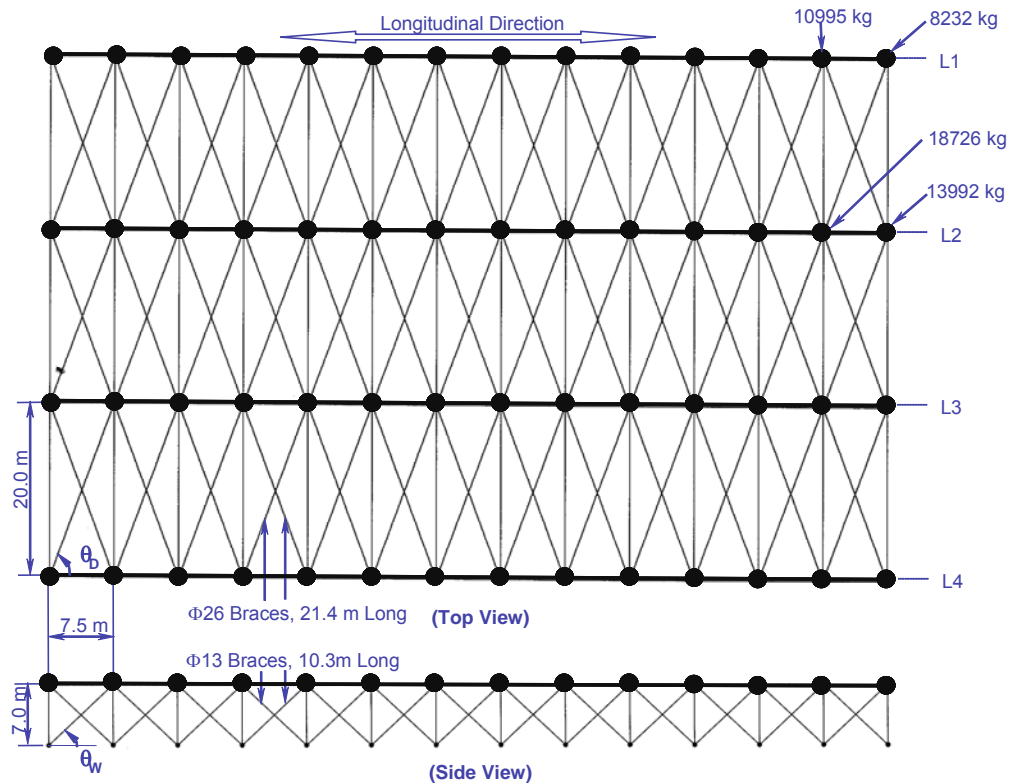
Figure 5.9 Parameters of 13 Bay × 3 Bay Structure

The structure was simplified to a MDOF system with 4 nodes, L1, L2, L3 and L4.

Mass of node L1 and L4: $m_1 = m_4 = 8232 \text{ kg} \times 2 + 10995 \text{ kg} \times 12 = 148404 \text{ kg}$

Mass of node L2 and L3: $m_2 = m_3 = 13992 \text{ kg} \times 2 + 18726 \text{ kg} \times 12 = 252696 \text{ kg}$

Stiffness of the diaphragm (the diaphragm force between two adjacent nodes, e.g. L1 and L2, when one of them is fixed but the other displaces by a unit in the longitudinal direction):

$$k_D = \frac{E_s A_D}{L_D} \cos^2\theta_D \times n = \frac{200 \text{ GPa} \times 531 \text{ mm}^2}{21.36 \text{ m}} \left(\frac{7.5}{21.36}\right)^2 \times 13 = 7969 \text{ kN/m}.$$

where E_s is the elasticity modulus of diaphragm brace material, A_D is the cross section area of the diaphragm braces, L_D is the length of the diaphragm bracing bars, θ_D is the slope of the braces shown in Figure 5.9, n is the number of the bays in the motion direction.

Stiffness of the vertical bracing (the overall force on L1 or L4 from the vertical bracing when L1 or L4 displaces by a unit in the longitudinal direction):

$$k_W = \frac{E_s A_W}{L_W} \cos^2\theta_W \times n = \frac{200 \text{ GPa} \times 132.7 \text{ mm}^2}{10.26 \text{ m}} \left(\frac{7.5}{10.26}\right)^2 \times 13 = 17969 \text{ kN/m}$$

The stiffness ratio: $\dfrac{k_D}{k_W} = 0.44$.

According to tensioned string analogy, the locations of the nodes on the tensioned string are calculated, $\{x\} = \{5.565, 18.113, 30.662, 43.211\}^T \times 10^{-5} \text{ (m/kN)}$ and the total length of the string $L = 48.776 \times 10^{-5} \text{ (m/kN)}$. The mode shape is then estimated using:

$$\{\varphi'\} = \sin\left(\frac{\{x\}}{L}\pi\right) = \{0.35, 0.92, 0.92, 0.35\}^T$$

Normalized so that $\displaystyle\sum_{j=1}^{4} m_j \varphi_j^2 = 10^6$, the longitudinal mode shape of such a 13 bay × 3 bay structure is then estimated as $\{\varphi\} = \{0.51, 1.35, 1.35, 0.51\}^T$. The modal analysis result from SAP2000 program for the same structure is $\{\varphi^*\} = \{0.43, 1.37, 1.37, 0.43\}^T$.

The comparison of the mode shapes calculated using tensioned string analogy with those by analyses using SAP2000 program was performed for 3 categories, i.e.

$k_D \le k_W$ with uniform diaphragm bracing, $k_D > k_W$ with uniform diaphragm bracing, and with varying brace sizes in diaphragm as well as in vertical bracing. To evaluate the accuracy of the estimations, an error index e is defined as:

$$e = \sqrt{\frac{\sum_{j=1}^{N+1}(\varphi_j - \varphi_j^*)^2}{N+1}} \Bigg/ \left(\frac{\sum_{j=1}^{N+1}|m_j\varphi_j^*|}{\sum_{j=1}^{N+1}m_j} \right) \tag{5.13}$$

where N is the number of bays under consideration, vector $\{\varphi\}$ is the estimated mode shape using tensioned string analogy, $\{\varphi^*\}$ represents the result from SAP2000, $\sum_{j=1}^{N+1}m_j$ is the total mass of the whole system, and the denominator of Eq. 5.13 is actually the modal displacement of mass center of the system.

5.4.1   Stiff End Frames and Uniform Diaphragm Braces
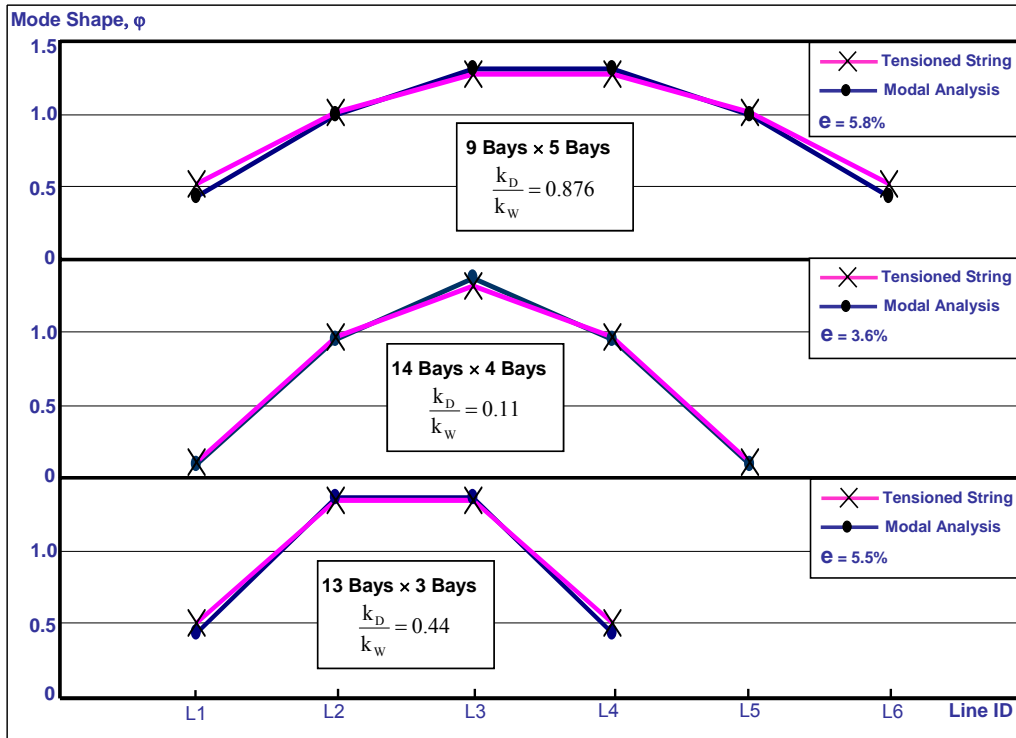
Figure 5.10   Mode Shapes of Structures When $k_D \le k_W$ (longitudinal)
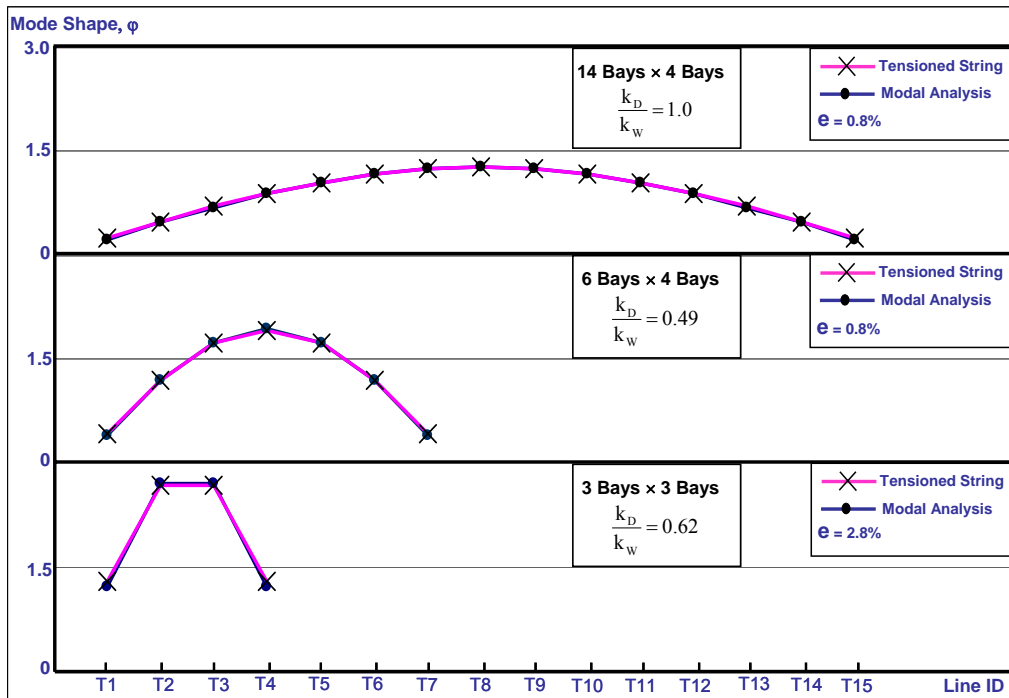
Figure 5.11 Mode Shapes of Structures when $k_D \le k_W$ (transverse)

Given in Figure 5.10 and Figure 5.11 are typical mode shapes of structures with uniform roof diaphragms and larger vertical bracing stiffness compared to that of the diaphragm. The comparisons indicate that the tensioned string analogy estimates the mode shape fairly accurately. The maximum error index e_{max} occurs in the longitudinal direction and it is within 6%.

5.4.2 Flexible End Frames and Uniform Diaphragm Braces

Figure 5.12 and Figure 5.13 indicate that for a structure which has strong diaphragm but relatively weaker peripheral vertical braces, the accuracy of the mode shape prediction using tensioned string analogy decreases compared to the cases in which $k_D \le k_W$. The maximum error index e increases from 6% to 8%. As an estimation
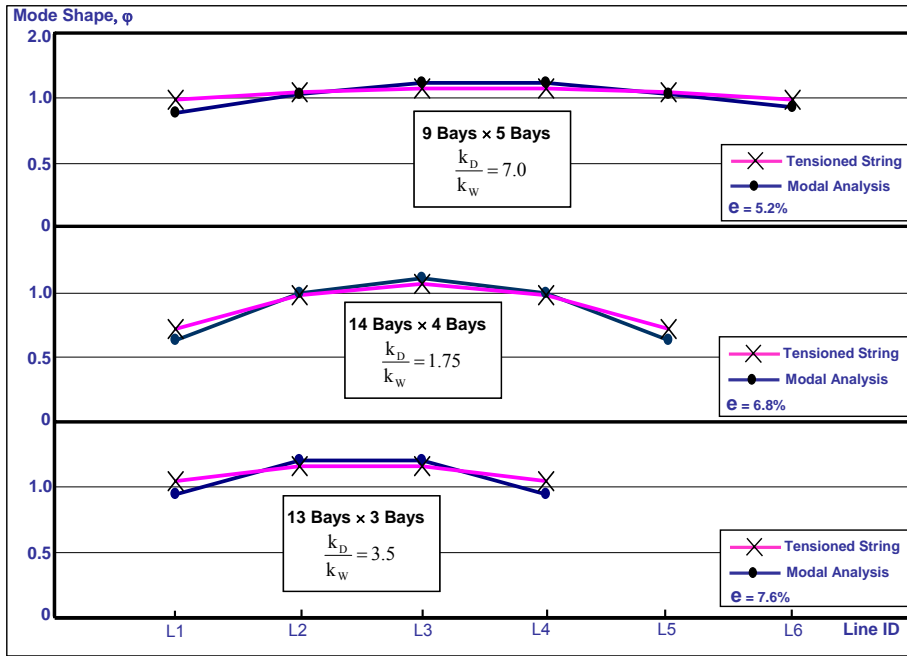
Figure 5.12 Mode Shapes of Structures when $k_D > k_W$ (longitudinal)
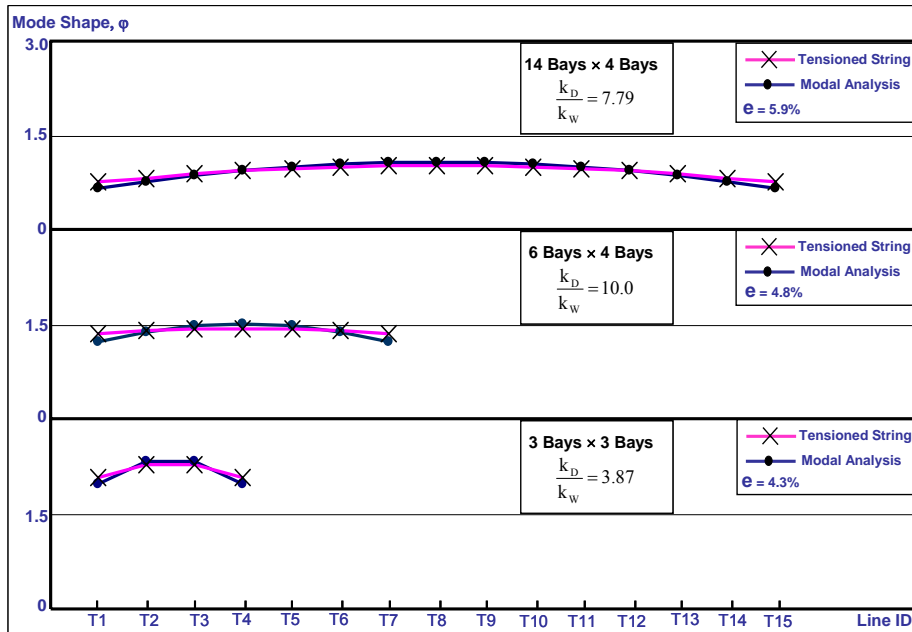
Figure 5.13   Mode Shapes of Structures when $k_D > k_W$ (transverse)

84

of the mode shapes, tensioned string analogy still works fine when $k_D > k_W$ although it can hardly be proved by analytic derivation.

5.4.3 Diaphragm Braces of Varying Sizes

In order to check if the application of tensioned string analogy could be extended to one-story industrial precast structures strengthened using braces of varying sizes, a series of special cases were investigated and Figure 5.14 shows some of the typical mode shape estimations. The main parameters of these four special cases are gathered in Table 5.1. It should be mentioned that the listed configurations are only for the purpose of verifying the feasibility of the tensioned string analogy, thus from a point of engineering view, some of them will never take place in the real engineering.

Table 5.1 Parameters of Special Cases

	Numbers of Bays (Long. × Trans.)	Considered Direction	Description on Bracing
Case 1	9 × 5	Transverse	Vertical: $\Phi26$ for $k_{W,1}$ and $k_{W,2}$ Diaphragm: $\Phi13$ for $k_{D,3}$, $k_{D,4}$, $k_{D,6}$, $k_{D,7}$ $\Phi26$ for the others
Case 2	6 × 4	Transverse	Vertical: $2 \times \Phi26$ for $k_{W,1}$ $4 \times \Phi26$ for $k_{W,2}$ Diaphragm: $\Phi13$ for $k_{D,2}$, $k_{D,6}$ $\Phi26$ for the others
Case 3	10 × 4	Longitudinal	Vertical: $\Phi26$ for $k_{W,1}$ and $k_{W,2}$. Diaphragm: $\Phi13$ for $k_{D,2}$, $k_{D,3}$ $\Phi26$ for $k_{D,1}$, $k_{D,4}$
Case 4	14 × 4	Longitudinal	Vertical: $\Phi18$ for $k_{W,1}$ $\Phi26$ for $k_{W,2}$ Diaphragm: $\Phi13$ for $k_{D,4}$ $\Phi26$ for the others
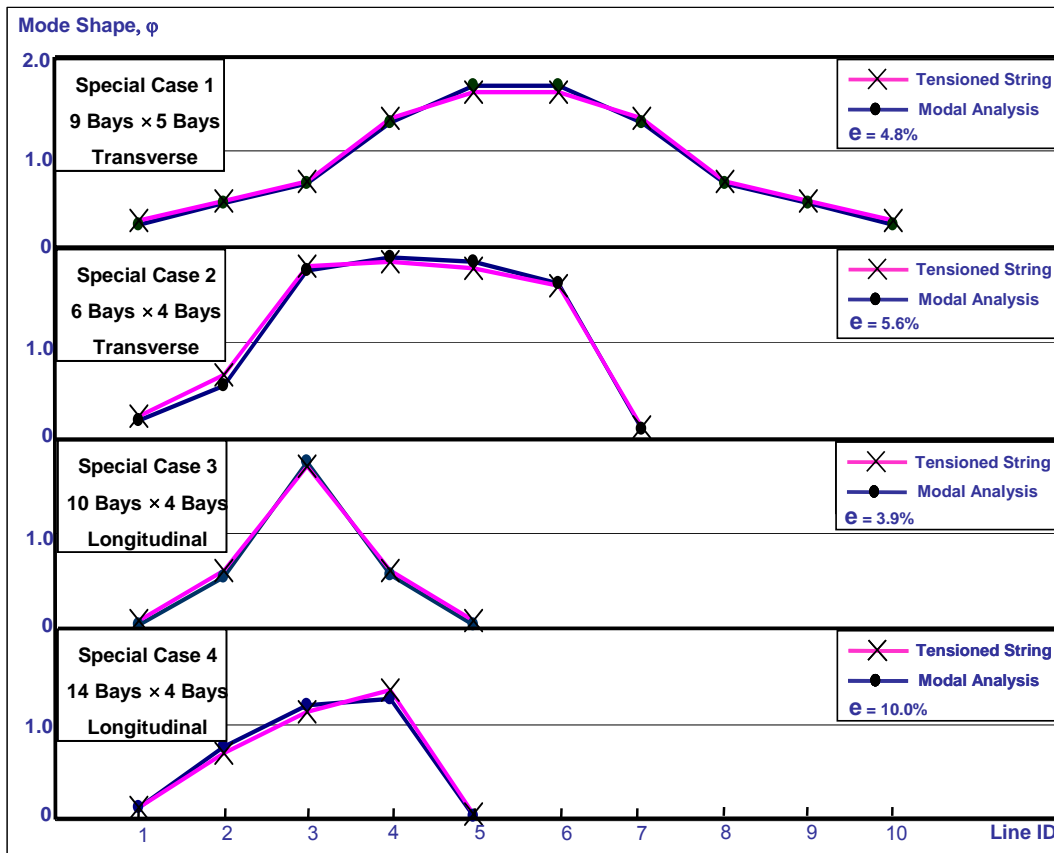
Figure 5.14 Mode Shapes for Special Cases

The results given in Figure 5.14 indicate that when the tensioned string analogy is applied on structures with arbitrarily selected strengthening braces, it can still estimate the mode shapes with fine accuracy, especially for symmetric structures. Although the maximum error index e increases to 10% for unsymmetrical structures, considering that the actual buildings usually select symmetric structures, it can be concluded that the tensioned string analogy can be extended to the one-story industrial precast buildings with arbitrarily selected strengthening braces.

86

5.5   FUNDAMENTAL PERIOD ESTIMATION

Through all the illustrations given in last section, a concise method of mode shape estimation for bracing strengthened one-story precast industrial buildings is established. As emphasized before, another essential factor for the seismic analysis of a structure is the fundamental period T, i.e. the natural period of the first mode. In contrast to the mode shape estimation, the effect of the column stiffness has to be included in the calculation of the fundamental period. Eq. 5.6 shows the column stiffness k_C takes an important part in the determination of the angular frequency ω, which is another expression form of the natural period T.

With the mode shape $\{\varphi\}$ determined, if this mode is the only one under the consideration, the system could be easily dealt with as a SDOF system. Because all the nodes move together with the mode shape, if the displacement of one node is determined, the displacements of all the others can be calculated using the mode shape. Then resistance provided by the columns and vertical braces can be respectively calculated according to their stiffness. Using the displacements and the resistance, the initial stiffness corresponding to the mode shape can be estimated.

When a structure deforms to a shape represented by $\{\varphi\}$, the total resistance P provided by columns and vertical braces can be determined using:

$$P = k_{W,1}\varphi_1 + k_{W,2}\varphi_{N+1} + \sum_{j=1}^{N+1} k_{C,j}\varphi_j \tag{5.14}$$

where $k_{C,j}$ represents the total stiffness involving all the columns involved with node j.

The displacement of the mass center is calculated using:

$$\overline{\varphi} = \frac{\sum_{j=1}^{N+1} m_j \varphi_j}{m}, \quad m = \sum_{j=1}^{N+1} m_j \tag{5.15}$$

87

where m is the total mass of the whole system. Then the overall initial stiffness of the system can be calculated using:

$$k = \frac{P}{\varphi}$$

(5.16)

The fundamental period T as well as the angular frequency can be determined by:

$$T = 2\pi\sqrt{\frac{m}{k}}, \quad \omega = \sqrt{\frac{k}{m}}$$

(5.17)

Eq. 5.17 could be obtained mathematically from Eq. C.8 in Appendix C, but the derivation from Eq. 5.14 through 5.17 clearly shows the physical meaning of each quantity.

As an example, the calculation of fundamental period T of the 13 bay × 3 bay structure shown in Figure 5.9 is given as follows.

The mass of each node has already been determined:

$$\{m\} = \{148404\,\text{kg}, 252696\,\text{kg}, 252696\,\text{kg}, 148404\,\text{kg}\}^T, \text{ so } m = \sum_{j=1}^{4} m_j = 802200\,\text{kg}.$$

Also known is the stiffness of the two vertical brace groups: $k_{W,1} = k_{W,2} = 17969\,\text{kN/m}$.

The column stiffness $k_{C,j}$ can be calculated with the column flexural stiffness EI given in Section 4.2.2:

$$k_{C,j} = \frac{3EI}{H^3} \times (n+1) = \frac{3 \times 38000\,\text{KN} \bullet \text{m}^2}{(7\,\text{m})^3} \times 14 = 4653\,\text{kN/m}, \text{ where H is the column}$$

height and n is the number of the bays in the motion direction, thus n+1 is actually the number of columns belonging to each node. As the mode shape has been estimated to be $\{\varphi\} = \{0.51, 1.35, 1.35, 0.51\}^T$, the calculations can follow Eq. 5.14 through 5.17.

$$P = k_{W,1}\varphi_1 + k_{W,2}\varphi_{N+1} + \sum_{j=1}^{N+1} k_{C,j}\varphi_j = 2 \times 17969 \times 0.51 + 4653 \times 2 \times (0.51 + 1.35) = 35638\,(\text{kN})$$

$$\overline{\varphi} = \frac{\displaystyle\sum_{j=1}^{N+1} m_j\varphi_j}{m} = \frac{2 \times 148404 \times 0.51 + 2 \times 252696 \times 1.35}{802200} = 1.04\,(\text{m})$$

88

$$k = \frac{P}{\varphi} = \frac{35638}{1.04} = 34267 \, (\text{kN/m})$$

$$T = 2\pi\sqrt{\frac{m}{k}} = 2 \times 3.142 \times \sqrt{\frac{802200}{34267 \times 10^3}} = 0.96 \, (\text{sec}),$$ which is very close to the modal

analysis result calculated using SAP2000, 1.00 sec.

5.6 MAXIMUM DISPLACEMENT ESTIMATION

As described above, with the mode shape predicted using the proposed tensioned string analogy, a one-story precast industrial building strengthened by diaphragm bracing can be considered as a SDOF system with mass m calculated by Eq. 5.15 and stiffness k determined by Eq. 5.16, and its fundamental period can be estimated using Eq. 5.17. The two features essential for maximum seismic displacement estimation are both available now. Because the seismic response of a structure is generally dominated by the first mode, it has been widely accepted to estimate the maximum displacement with the first mode response. According to the conclusion of Shimazaki and Sozen (1984) (refer to Section 3.2.2), the maximum displacement of the one-story industrial buildings can be simply estimated using the elastic spectral displacement for damping ratio 2%.

The elastic displacement response spectrum of the considered earthquakes has been developed in Section 2.3 (Figure 2.3). For a fundamental period T determined using the procedure introduced in Section 5.5, the corresponding spectral displacement S_d can be conveniently read from Figure 2.3 or calculated using Eq. 2.3. According to the conclusion of C.2 of Appendix C, the corresponding maximum displacement of the MDOF system with N+1 nodes can be calculated using:

$$\{u_{max}\} = rS_d\{\varphi\} \tag{5.18}$$

where r is the participation factor of the first mode defined as:

$$r = \frac{\sum_{j=1}^{N+1} m_j \varphi_j}{\sum_{j=1}^{N+1} m_j \varphi_j^2} \tag{5.19}$$

Eq. 5.18 can be written in another form:

$$\{u_{max}\} = \frac{\sum_{j=1}^{N+1} m_j \varphi_j}{\sum_{j=1}^{N+1} m_j \varphi_j^2} S_d \{\varphi\} = \frac{\left(\sum_{j=1}^{N+1} m_j \varphi_j\right)^2}{\sum_{j=1}^{N+1} m_j \varphi_j^2} \frac{S_d \{\varphi\}}{\sum_{j=1}^{N+1} m_j \varphi_j} = m_e \frac{S_d \{\varphi\}}{\sum_{j=1}^{N+1} m_j \varphi_j}$$

$$= \frac{m_e}{m} \frac{S_d \{\varphi\}}{\left(\sum_{j=1}^{N+1} m_j \varphi_j\right)\Big/ m} = \frac{\rho_e S_d}{\overline{\varphi}} \{\varphi\} \tag{5.20}$$

where m_e is the effective mass of the first mode, m is the total mass of the system. $\rho_e = \dfrac{m_e}{m}$ is called effective mass ratio, $\overline{\varphi}$ was defined in Eq. 5.15.

Once again, the calculation of the maximum displacement of the structure shown in Figure 5.9 is listed below for an instance.

$$\{m\} = \{148404 \text{ kg}, 252696 \text{ kg}, 252696 \text{ kg}, 148404 \text{ kg}\}^T$$

$$m = \sum_{j=1}^{4} m_j = 802200 \text{ kg}$$

$$\{\varphi\} = \{0.51, 1.35, 1.35, 0.51\}^T$$

$$T = 0.96 \text{ sec}$$

$$S_a = \frac{1.25}{0.96} g = 1.30 g \text{ (refer to Eq. 2.3(c))}$$

$$S_d = \frac{S_a T^2}{4\pi^2} = 29.8 \text{ cm (refer to Eq. 2.3(d))}$$

$$\sum_{j=1}^{4} m_j \varphi_j = 833651 \text{ kg}$$

$$\overline{\varphi} = \frac{\sum_{j=1}^{4} m_j \varphi_j}{m} = 1.04$$

$$\sum_{j=1}^{4} m_j \varphi_j^2 = 998277 \, \text{kg}$$

$$m_e = 696173 \, \text{kg}$$

$$\rho_e = \frac{m_e}{m} = 86.8\%$$

$$\{u_{max}\} = \frac{\rho_e S_d}{\overline{\varphi}} \{\varphi\} = \{12.7, 33.6, 33.6, 12.7\}^T (\text{cm}).$$

5.7 COMPARISON OF RESULTS BY DIFFERENT ANALYSIS METHODS

With the establishment of the tensioned string analogy, three numerical methods are available now to calculate the maximum displacements of the bracing strengthened one-story precast industrial buildings during the considered earthquakes: modal analysis, time history analysis, and the tensioned string analogy. The tensioned string analogy is the simplest and does not require a 3 dimensional computer model to be developed. It can be conveniently carried out using a Microsoft Excel spreadsheet, which has been widely used in engineering for design. With the help of the spreadsheet, another merit of this method shows up, that is its great flexibility. For a given response spectrum, the maximum displacements of a precast structure strengthened with different braces can be quickly obtained by changing the respective stiffness quantities, thus the primary strengthening scheme could be determined according to the allowable structural roof drift. However, before such a spreadsheet is used as a design tool, it is important to assess the accuracy of the displacement estimates.

As indicated in Chapter 4, the time history analysis is the most realistic method to simulate the seismic response of structures because the analytical model used for time history analyses includes the most detailed information of the structure and the analyses are conducted with the records of real earthquakes. Therefore if the results of the simple tensioned string analogy are comparable to those from time history analyses, the doubt

91

about the feasibility of the new method to the real engineering could be removed to a great extent.

With the stated consideration, a series of time history analyses were performed by introducing the earthquake records described in Chapter 2 to the analytical models of various one-story precast industrial buildings strengthened by vertical and diaphragm bracing. Because the response displacements for the records at soft soil sites are much larger than those for stiff soil sites and the response spectra used for the displacement estimations were developed based on the soft soil records, the soft soil records were used as principal excitations of the time history analyses. The response displacement of each joint at each time step under each forcing ground motion was recorded, and then the maximum displacements were determined.

The time history analysis results of the 16 structural cases whose mode shapes are given in Figure 5.10 through 5.14 are illustrated in this section. For clearness, the cases are renamed as Case 1 through Case 16, and re-classified to two categories according to the direction in which the seismic motion are considered.

Category 1: Case 1 ~ Case 8, longitudinal motion. The main parameters of these 8 structures are listed in Table 5.2.

For the Case 1 through Case 8 listed in Table 5.2, the fundamental periods calculated respectively using modal analysis and the tensioned string analogy are given in Table 5.3, and the maximum displacements from the time history analyses are illustrated in Figure 5.15. The displacement estimations of modal analyses and those using tensioned string analogy are also given together for comparison. The naming of lines coincides with Figure 5.1(a).

Table 5.2 Brace Sizes for Longitudinal Cases

	Numbers of Bays (Long. × Trans.)	**Brace Sizes**
Case 1	13 × 3	Vertical: $\Phi 13$ Diaphragm: $\Phi 26$
Case 2	13 × 3	Vertical: $\Phi 6$ Diaphragm: $2 \times \Phi 26$
Case 3	14 × 4	Vertical: $\Phi 26$ Diaphragm: $\Phi 26$
Case 4	14 × 4	Vertical: $\Phi 26$ Diaphragm: $2 \times \Phi 26$
Case 5	9 × 5	Vertical: $\Phi 9$ Diaphragm: $\Phi 26$
Case 6	9 × 5	Vertical: $\Phi 6$ Diaphragm: $4 \times \Phi 26$
Case 7	14 × 4	Vertical: $\Phi 18$ for $k_{W,1}$, $\Phi 26$ for $k_{W,2}$ Diaphragm: $\Phi 13$ for $k_{D,4}$, $\Phi 26$ for the others
Case 8	10 × 4	Vertical: $\Phi 26$ for $k_{W,1}$ and $k_{W,2}$. Diaphragm: $\Phi 13$ for $k_{D,2}$, $k_{D,3}$, $\Phi 26$ for $k_{D,1}$, $k_{D,4}$

Table 5.3 Parameters of Longitudinal Cases

Case No.	1	2	3	4	5	6	7	8
T by Modal Analysis (sec)	1.00	1.10	1.06	1.10	1.22	1.20	1.19	1.16
T by Tensioned String (sec)	0.96	1.08	1.03	1.07	1.19	1.18	1.14	1.14
Max. Spectral Acc. from Ground Motion Record (g)	1.28	1.05	1.19	1.05	0.96	0.93	0.9	0.93
Acc. from Idealized Spectrum (g)	1.30	1.16	1.21	1.17	1.05	1.06	1.10	1.10
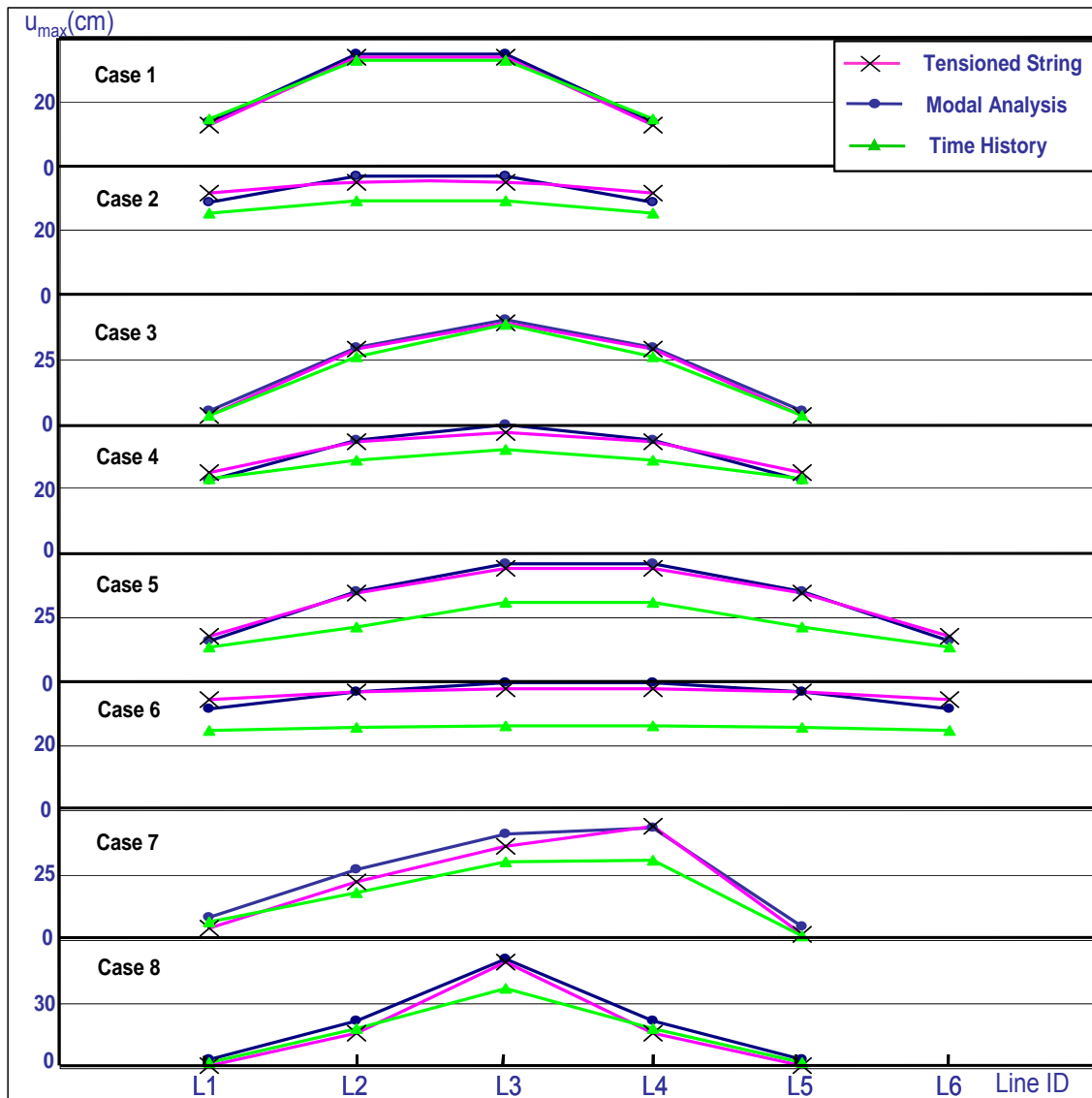
Figure 5.15 Maximum Longitudinal Displacements By Different Methods

Category 2: Case 9 ~ Case 16, transverse motions. The main parameters of these 8 structures are listed in Table 5.4.

Table 5.5 gives the calculated periods of Case 9 through Case 16 respectively using modal analysis and the tensioned string analogy. Figure 5.16 shows the maximum displacements of Case 9 through Case 16 using different methods. The line naming rule is similar to that shown Figure 5.1(b).

94

Table 5.4 Brace Sizes for Transverse Cases

	Numbers of Bays (Long. × Trans.)	Cross Section Areas of Braces
Case 9	3 × 3	Vertical: Φ32 Diaphragm: Φ26
Case 10	3 × 3	Vertical: Φ13 Diaphragm: Φ26
Case 11	6 × 4	Vertical: 2 × Φ26 Diaphragm: Φ26
Case 12	6 × 4	Vertical: Φ8 Diaphragm: Φ26
Case 13	14 × 4	Vertical: Φ26 Diaphragm: Φ26
Case 14	14 × 4	Vertical: Φ9 Diaphragm: Φ26
Case 15	6 × 4	Vertical: 2 × Φ26 for $k_{W,1}$, 4 × Φ26 for $k_{W,2}$ Diaphragm: Φ13 for $k_{D,2}$, $k_{D,6}$, Φ26 for the others
Case 16	9 × 5	Vertical: Φ26 for $k_{W,1}$ and $k_{W,2}$ Diaphragm: Φ13 for $k_{D,3}$, $k_{D,4}$, $k_{D,6}$, $k_{D,7}$ Φ26 for the others

Table 5.5 Parameters of Transverse Cases

Case No.	9	10	11	12	13	14	15	16
T by Modal Analysis (sec)	0.50	0.73	0.69	0.91	0.92	0.96	0.81	0.89
T by Tensioned String (sec)	0.49	0.72	0.69	0.90	0.91	0.96	0.78	0.89
Max. Spectral Acc. from Ground Motion Record (g)	2.10	1.59	1.48	1.53	1.50	1.37	1.49	1.56
Acc. from Idealized Spectrum (g)	2.50	1.74	1.81	1.39	1.37	1.30	1.60	1.40

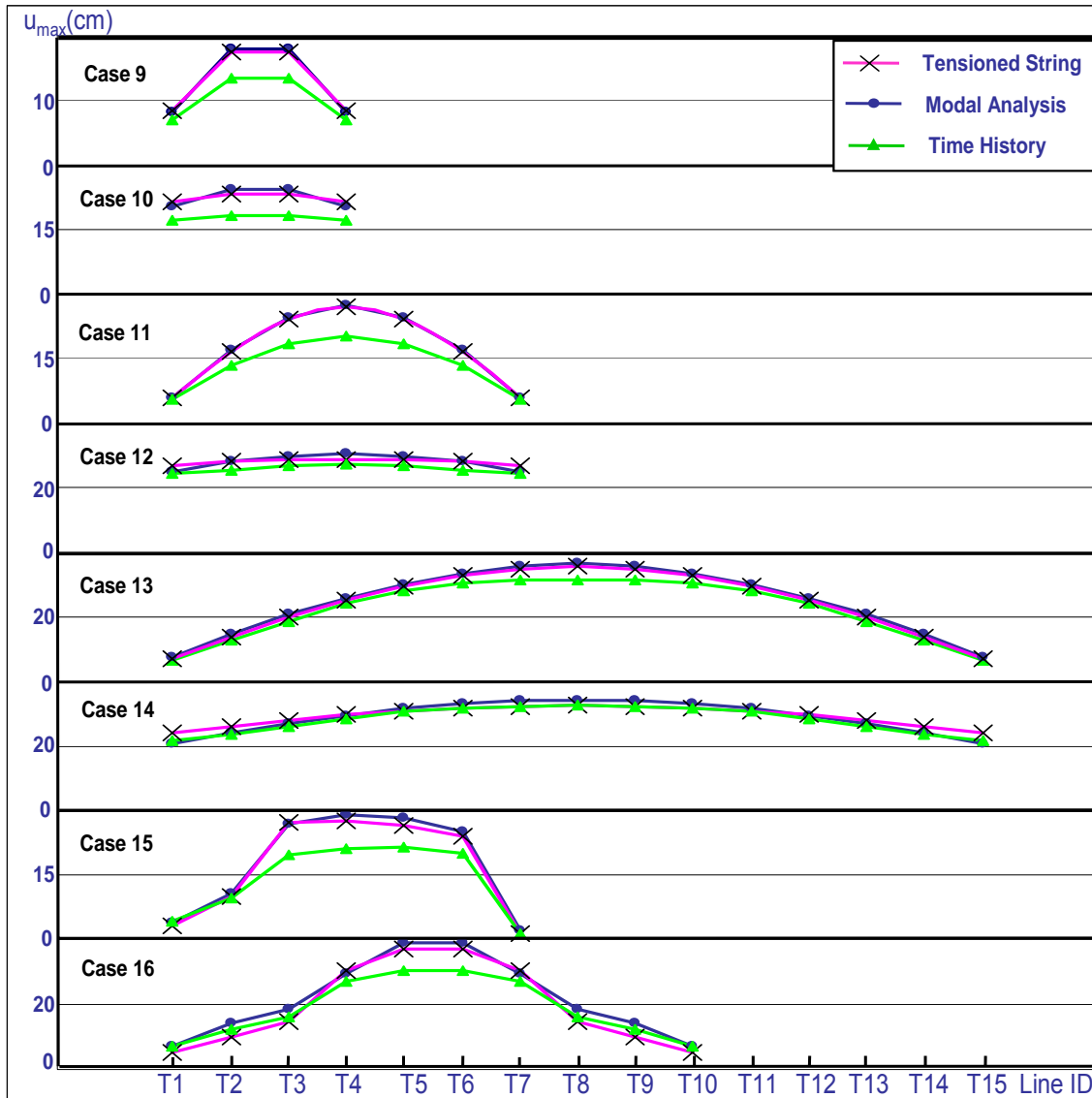Figure 5.16   Maximum Transverse Displacements By Different Methods

Figure 5.15 and 5.16 indicate that the displacement estimates provided by tensioned string analogy are always close to those from modal analyses. Compared to time history analyses, tensioned string analogy gives larger displacement estimates, which lead to conservative design. This difference can be explained with two reasons:

96

1)   In the OpenSees model used for time history analyses, the mass of the columns was distributed along the columns. However, in the calculations using string analogy, a half of the mass of the columns was assumed lumped at the upper joints of the columns. The string analogy overestimated the effective mass of the system, thus led to longer periods and larger displacements. If the same lumped mass is used in the OpenSees model, the time history analyses will result in larger displacements by 8% to 15%.

2)   The idealized spectrum used for tensioned string analogy was not the simple envelope of the spectra from the ground motion records (Figure 2.3), but the time history analyses were conducted using these individual ground motion records. From Table 5.3 and Table 5.5, it can be seen that for most cases, the accelerations used for string analogy are larger than the actual maximum accelerations from the ground motion records which were used for time history analyses. This gives another reason why string analogy usually provides conservative estimates.

It should be stated that at some particular periods, the maximum spectral acceleration from the ground motion records may be much higher than the idealized value for design, e.g. at the period of 1.28 sec. in Figure 2.3. The calculated maximum displacements using time history analyses at these periods might be higher than the estimated results using the idealized spectrum. But for properly developed design spectrum and feasible estimation method, the time-history result should not be larger than the estimation by a considerable amount.

Chapter 6: Push-Over Analyses and Rehabilitation Scheme

6.1 INTRODUCTION

Using the tensioned string analogy for an existing one-story precast structure, it is convenient to track the changes of the maximum seismic displacements with the modifications of the brace sizes, thus the brace sizes can be selected to satisfy the displacement requirements.

For the prototype building introduced in Chapter 2, the brace sizes are selected using the tensioned string analogy. Static push-over analyses are then conducted to the estimated maximum displacements to determine detailed requirements for each structural member. With the detailed results, the braces can be optimized, and the details of the connections at the top of columns can be determined. The strengthened structure is checked to see if the second order effect (P-delta effect) can be neglected.

6.2 DISPLACEMENT REQUIREMENTS

For the 14 bay × 4 bay prototype building, two displacement requirements need to be satisfied:

1)   Maximum drift: As mentioned in Section 3.3.2, the maximum rotation of the plastic hinges at the column base should not be larger than 0.025 rad, thus the maximum displacements of the top of the columns should not exceed 38.8 cm in the longitudinal direction and 34.8 cm in the transverse direction.

2)   Yielding of diaphragm braces: it was previously stated that the diaphragm braces should remain elastic, thus the relative displacement of any two adjacent column lines in the direction of motion needs to be controlled.

6.2.1 Longitudinal Direction

When the relative displacement between two adjacent longitudinal lines is Δ_R (Figure 6.1), the strain in the tension brace will be:

$$\varepsilon = \frac{\sqrt{(7.5\,\text{m} + \Delta_R)^2 + (20\,\text{m})^2}}{\sqrt{(7.5\,\text{m})^2 + (20\,\text{m})^2}} - 1 \tag{6.1}$$
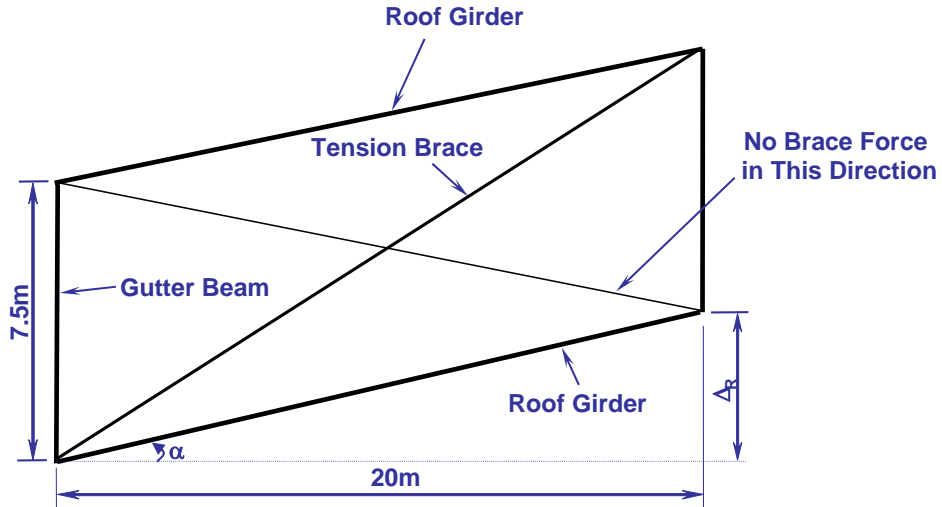
Figure 6.1 Relation Between Brace Strain and Relative Displacement

Eq.6.1 can be rewritten in another form:

$$\Delta_R = \sqrt{456.25(1+\varepsilon)^2 - 400} - 7.5 \quad (\text{m}) \tag{6.2}$$

The constitutive relationship of the brace material was shown in Figure 4.1 with $\varepsilon_y = 0.00345$. Using Eq. 6.2, the maximum relative displacement under which the brace remains within the elastic range can be calculated:

$$\Delta_{R,max} = \sqrt{456.25(1 + 0.00345)^2 - 400} - 7.5 \quad (\text{m}) = 20.7\,\text{cm}$$

The corresponding rotation of the roof girder is: $\alpha = \arcsin\left(\dfrac{20.7\,\text{cm}}{20\,\text{m}}\right) = 0.01\,\text{rad} = 0.6^{\circ}$.

6.2.2 Transverse Direction

Similarly, the maximum relative transverse displacement under which the brace remains elastic is determined to be 7.9 cm.

99

6.3   BRACE SIZE SELECTION

Simultaneously considering the displacement requirements in both longitudinal and transverse directions, the brace sizes for the prototype building can be selected using the tensioned string analogy. A spreadsheet was developed to calculate the changes of the maximum nodal displacements as modifications were made to the brace sizes. The brace sizes were modified until the displacement requirements discussed in Section 6.2 were satisfied. One of the acceptable selections is shown in Figure 6.2. It should be stated that the selection of the brace sizes is not unique. Shown in Figure 6.2 is an optimized one that considers using minimum sizes of bars and saving materials. The braces are added symmetrically to the existing structure about both longitudinal and transverse axes. In Figure 6.2, for each rectangle between line L2 and L4, one Φ29 steel bar is required in each diagonal direction. For each of the eight rectangles at the structure corners, two Φ26
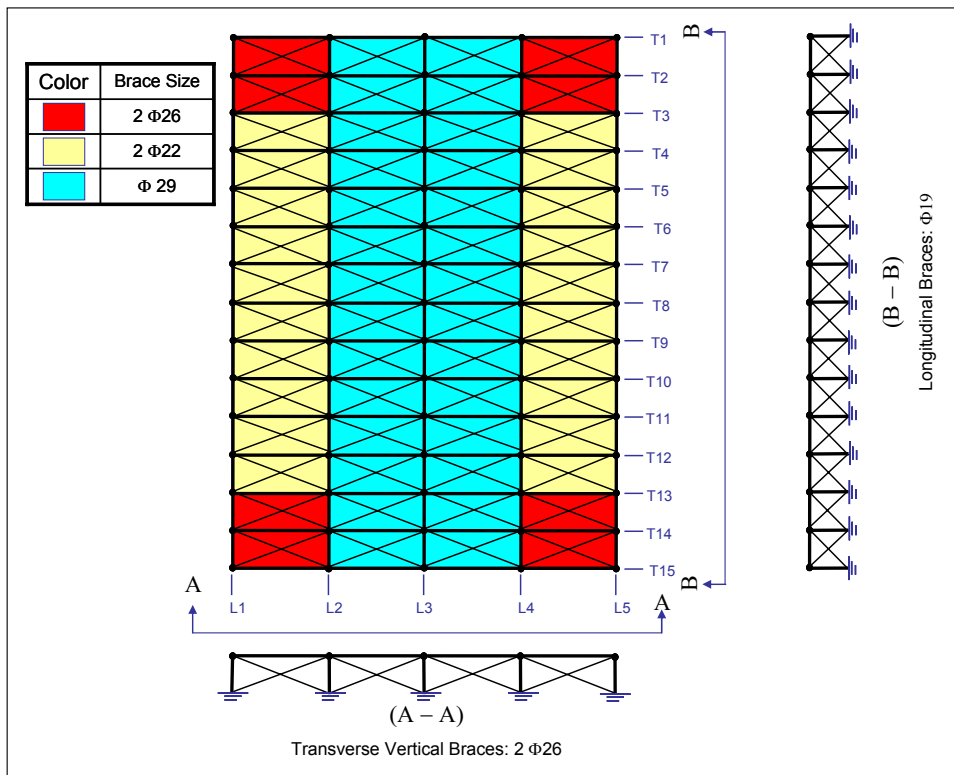

Figure 6.2   Brace Sizes

steel bars are used in each diagonal direction, and for exterior rectangles between line T3 and T13, double Φ22 bars are suggested.

Table 6.1 gives the results using the tensioned string analogy for seismic motion in the longitudinal direction. Because of the symmetry, only the results of line L1, L2 and L3 are listed. For comparison, the displacements and period calculated using modal analysis are also listed.

The analysis results calculated for transverse motion are given in Table 6.2.

Table 6.1 Analysis Results of Longitudinal Motion

Line ID	Nodal Mass m_j (10^3 kg)	Mode Shape φ_j	Max. Displacements $U_{max,j}$ (cm)		Period T (sec)	
			String Analogy	Modal Analysis	String Analogy	Modal Analysis
L1	159.4	0.26	7.5	8.3		
L2	271.4	0.95	27.5	28.2	0.96	0.98
L3	271.4	1.34	38.6	39.5		

Table 6.2 Analysis Results of Transverse Motion

Line ID	Nodal Mass m_j (10^3 kg)	Mode Shape φ_j	Max. Displacements $U_{max,j}$ (cm)		Period T (sec)	
			String Analogy	Modal Analysis	String Analogy	Modal Analysis
T1	58.4	0.19	5.0	5.5		
T2	78.2	0.42	11.1	12.5		
T3	78.2	0.64	16.8	18.1		
T4	78.2	0.86	22.7	23.5		
T5	78.2	1.05	27.7	27.9	0.87	0.87
T6	78.2	1.19	31.4	31.7		
T7	78.2	1.28	33.7	34.3		
T8	78.2	1.31	34.5	35.3		

6.4 STATIC PUSH-OVER ANALYSES

For the prototype structure with the proposed rehabilitation shown in Figure 6.2, static push-over analyses were conducted for both longitudinal and transverse directions following the steps described in Section C.3 of Appendix C using SAP2000 software.

6.4.1 Longitudinal Direction

Load Pattern: The lateral force imposed on each column upper joint was proportional to the product of the mass lumped at the joint and the corresponding component of the predicted mode shape. The load pattern is illustrated in Figure 6.3, where η is a load amplifier, which will increase from 0 until the displacement at the control node reaches the target displacement. Because of the symmetry, only a quarter of the roof is shown.
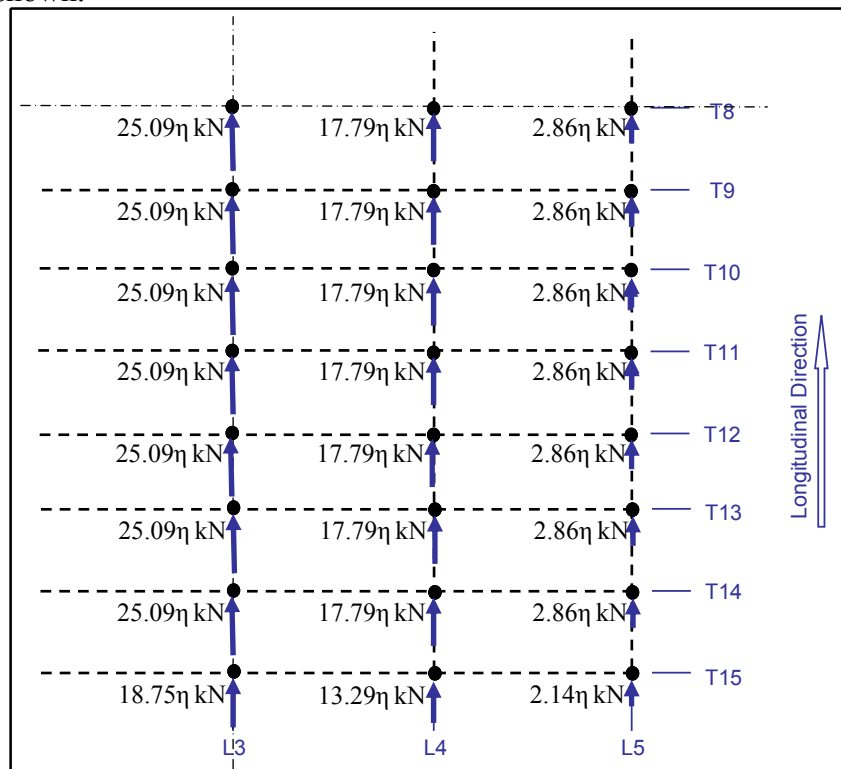

Figure 6.3   Load Pattern in Longitudinal Direction

102

Control Node: The displacement of node at the mass center, i.e. the intersection of line L3 and T8, was selected to be the control value.

Target Displacement Δ_t: The load amplifier η was increased from 0 until the displacement at the control node reached Δ_t = 38.6 cm, the maximum displacement predicted by the tensioned string analogy.

Analysis Results: With η = 8.50, the target displacement Δ_t was reached. As the base shear corresponding to $\eta = 1$ is 962 kN, the maximum base shear that the structure experienced in the push-over was $V_{max} = 962\,kN \times 8.5 = 8177\,kN$. The base shear (V) vs the displacement (Δ) at the control node is shown in Figure 6.4(a). The final deformed shape of the roof and internal forces in roof members are shown in Figure 6.4(b). Because of the symmetry, only half of the roof is shown.

The important results from the longitudinal push-over analysis are listed as follows:

1)   All the diaphragm braces remained elastic. A maximum strain, 2.8 $\mu\varepsilon$, was reached in the two exterior bays. The maximum strain in the two interior bays was 1.7 $\mu\varepsilon$.

2)   Most roof girders were in compression, and the maximum compressive strain was 0.18 $\mu\varepsilon$. There were gaps formed between the columns and the two middle girders in line T1, and the width of the gaps was 1 to 2 cm.

3)   All gutter beams were in compression, and the maximum compressive strain was 0.09 $\mu\varepsilon$.

4)   All longitudinal vertical braces yielded, and the maximum strain was 8.2 $\mu\varepsilon$. For such a strain, it can be assumed that the strain hardening effect is negligible.

5)   Plastic hinges developed for all columns in line L2, L3 and L4. Columns in line L1 and L5 remained elastic.

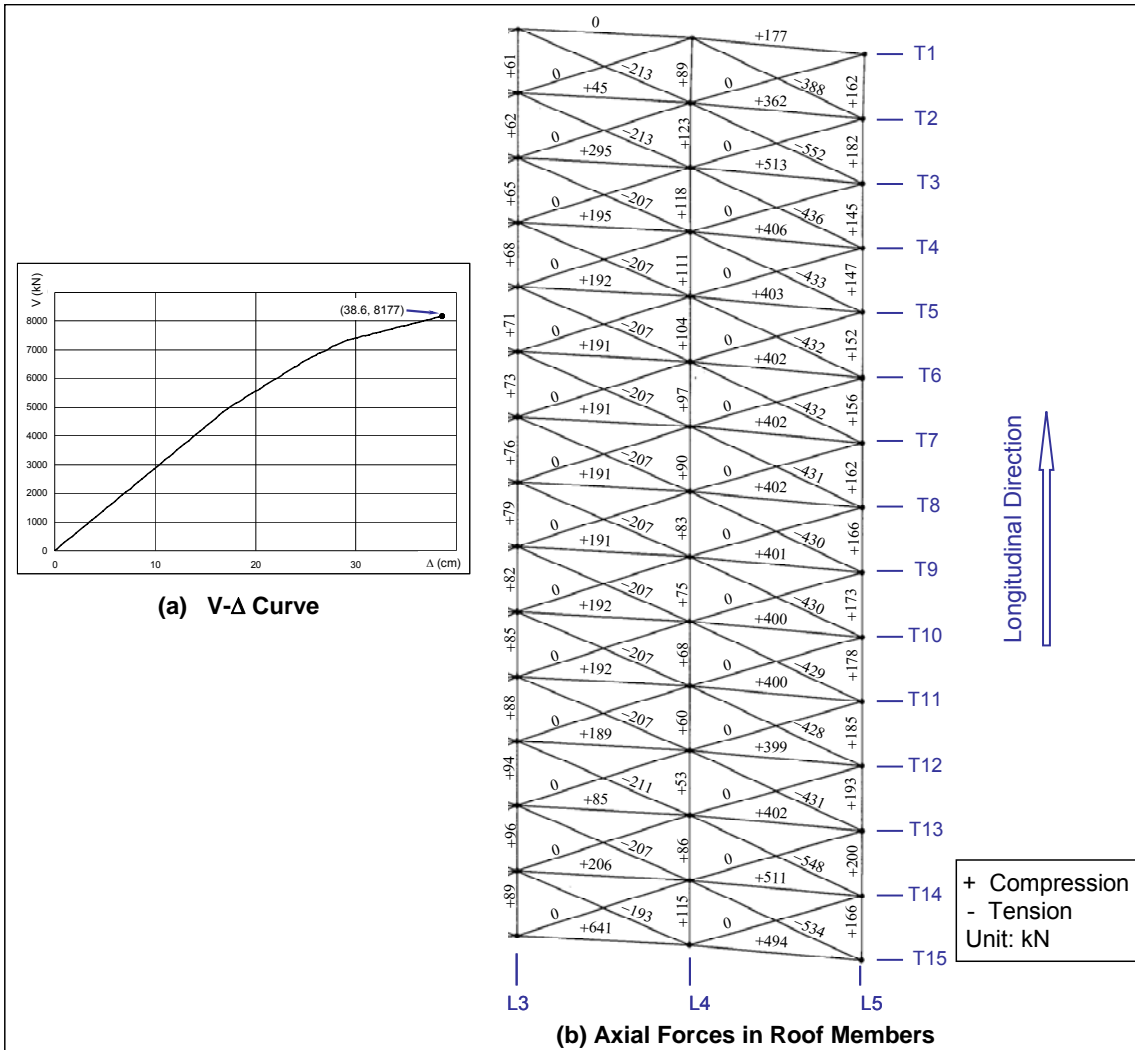Figure 6.4   Results of Push-Over Analysis in Longitudinal Direction

6.4.2   Transverse Direction

Load Pattern: The load pattern in the transverse direction is illustrated in Figure 6.5

Control Node: The displacement of the joint at the mass center, i.e. the intersection of line L3 and T8, was selected to be monitored.
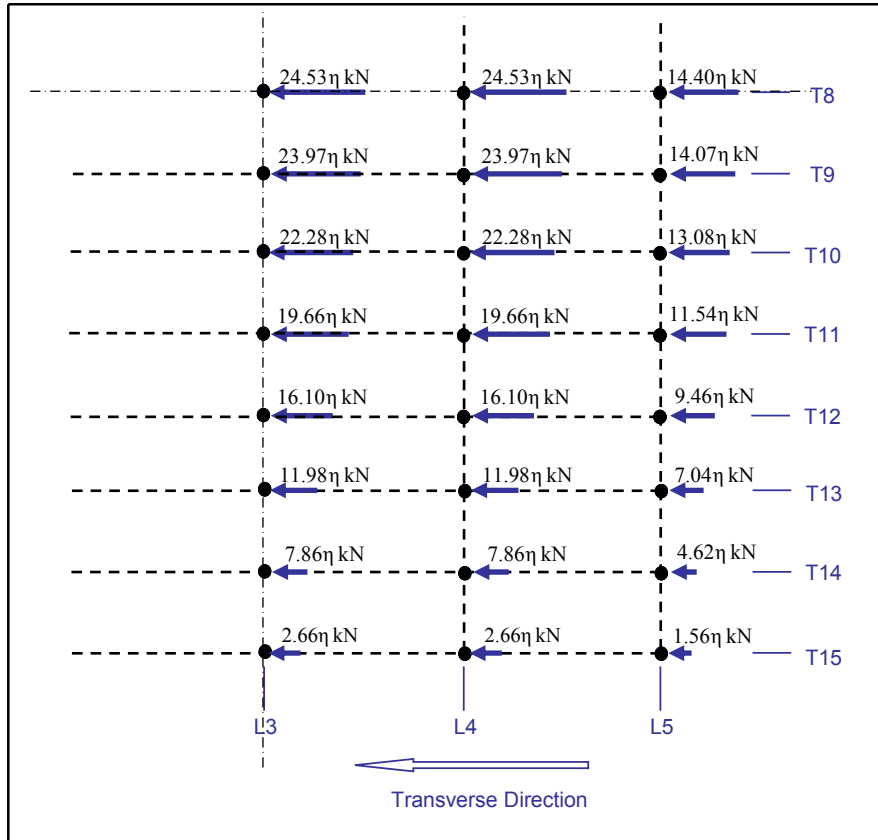
Figure 6.5   Load Pattern in Transverse Direction

Target Displacement Δ_t: The load amplifier η was increased from 0 until the displacement of the control node reached $\Delta_t = 34.5$ cm.

Analysis Results: When η was 8.68, the target displacement Δ_t was reached. As the base shear value corresponding to $\eta = 1$ is 975 kN, the maximum base shear was $V_{max} = 975 \text{ kN} \times 8.68 = 8463 \text{ kN}$. The analysis results are illustrated in Figure 6.6.

The important results from the transverse push-over analysis are listed as follows:

1)   All the diaphragm braces remained elastic. The maximum strain, 2.8 $\mu\varepsilon$, occurred in the bays between line T3 and T4, as well as those between line T12 and T13. The maximum strain in the bays between line T5 and T11 was 2.0 $\mu\varepsilon$.

105

(a) V-Δ Curve

(b) Axial Forces in Roof Members
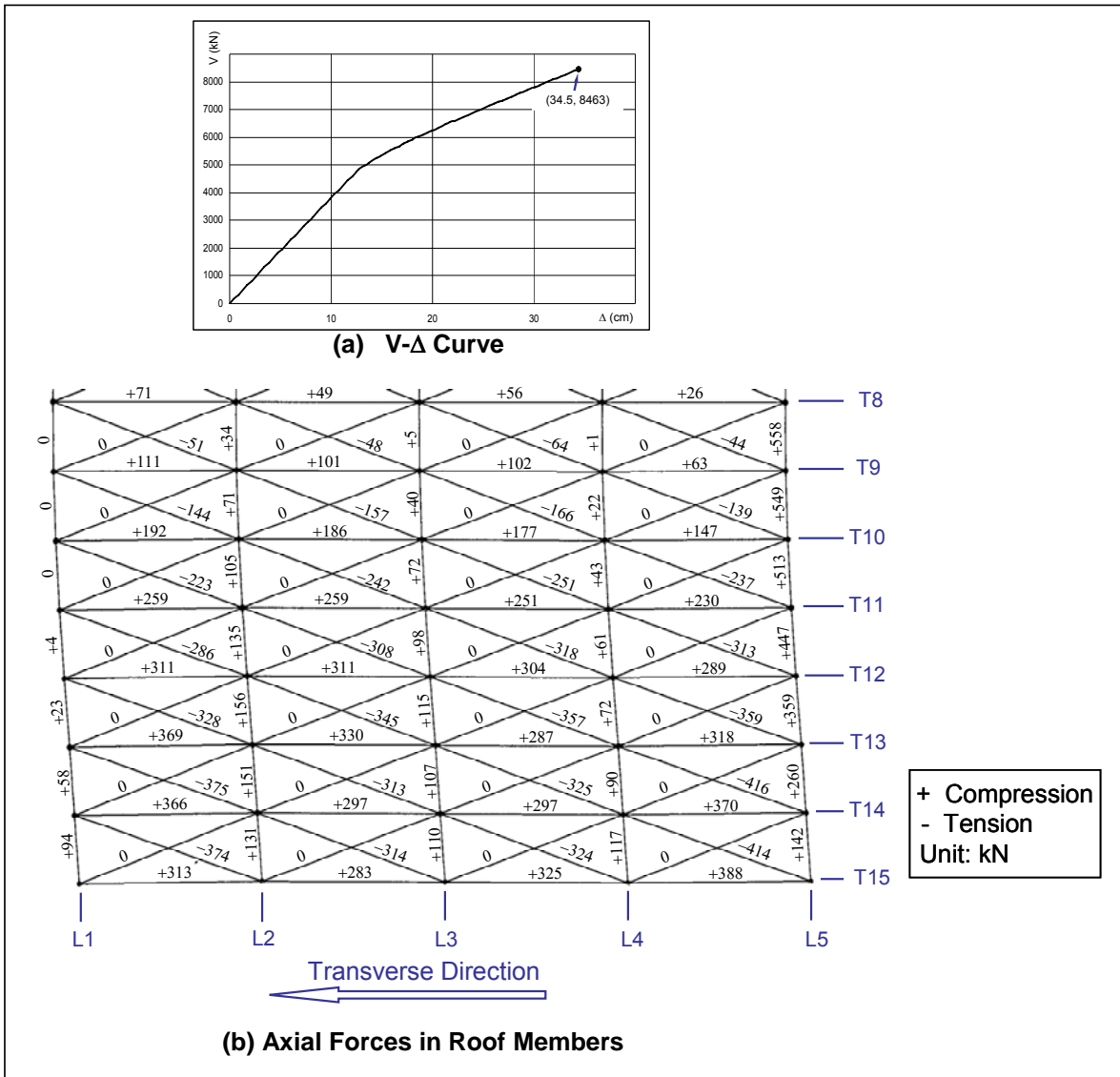
Figure 6.6   Results of Push-Over Analysis in Transverse Direction

2)   Most gutter beams were in compression, and the maximum compressive strain was 0.25 με. Gaps formed between columns and the 6 gutters in the middle of line L1, and the maximum opening was 1.5 cm.

3)   All roof girders were in compression, and the maximum compressive strain was 0.1 με.

106

4) All transverse vertical braces remained elastic, and the maximum strain was 1.9 $\mu\varepsilon$.

5) Plastic hinges developed in all columns in lines T3 through T13, but columns in line T1, T2, T14 and L5 remained elastic.

6.5 DISCUSSION OF PUSH-OVER ANALYSIS RESULTS

Selection of Braces: The results of the push-over analyses indicate that the selected braces shown in Figure 6.2 are needed for the prototype building to survive the considered earthquakes. For the selected brace system, the connections at the upper joints of the columns must work as pins. In the central region of the structure, where strains in the diaphragm braces are low, other steel material with lower yield stress could be considered, e.g. G420 steel. However, the sizes of the diaphragm braces in the central region can not be reduced since size reduction will change the stiffness of the structure. Thus the mode shape, period and the maximum displacement would change. The same situation occurs for the transverse vertical bracing. For this structure, both strength and stiffness need to be considered. The higher yield stress is needed to provide strength, while larger sizes are selected for stiffness.

Consideration about Gutters and Girders: Most gutter beams and roof girders are subjected to compression. The compressive strain in these members will be less than 0.25 $\mu\varepsilon$ so that there will be no inelasticity in the gutters and girders. In order for the girders and gutters to participate the diaphragm action as soon as the structure deforms, gaps between the columns and girder ends and between adjacent gutter ends, should be grouted (Figure 2.9).

Gaps would form between structural members on the periphery. Although it was assumed that the girders and gutters could not carry any tensile force, the width of the openings was quite small (2 cm) compared with the dimension of the column corbel (25

cm). It can be concluded that the risk of girders and gutters to slide off supports can be ignored.

P-Delta Effect: In the longitudinal direction, with the maximum roof deflection, the total second order moment at the base of columns due to the selfweight of the structure will be 2897 kN•m, and the moment due to the inertial forces will be 57239 kN•m. The second order moment is only 5% of the moment due to the inertial forces. The moment ratio in the transverse direction is 4%, even smaller than in the longitudinal direction. Generally, when the second order moment is less than 10% of that caused by the inertial forces, the P-delta effect can be neglected (ASCE 7-05, 2006). Although the structure of the prototype building is relatively soft considering fundamental periods of 0.96 sec and 0.87 sec, the selfweight of the total building is not large as it consists of only one story, thus the second order effect is not substantial. Therefore the P-delta effect is not included in the analyses of the present study.

Overturning of Girders: When the seismic motion is in the longitudinal direction, a roof girder will be subjected to overturning moment because the inertial force is not applied at the support (Figure 6.7). Overturning of roof girders was observed in buildings under construction at the time of the 1999 earthquakes. Preventing the girder overturning is one of the rehabilitation issues that must be considered.

To estimate the maximum overturning moment, the amplitude of the maximum inertial force applied to the girder is needed. Using the results of the push-over analyses, the inertial force can be determined by considering the maximum accelerations at the two ends of the girder as shown in Figure 6.7.

When longitudinal movement occurs, the total lateral forces applied on the longitudinal lines L1 through L5 consists of three parts, one from columns, one from

108

diaphragm braces and one from vertical braces. Because of symmetry, only line L1, L2 and L3 will be considered here.
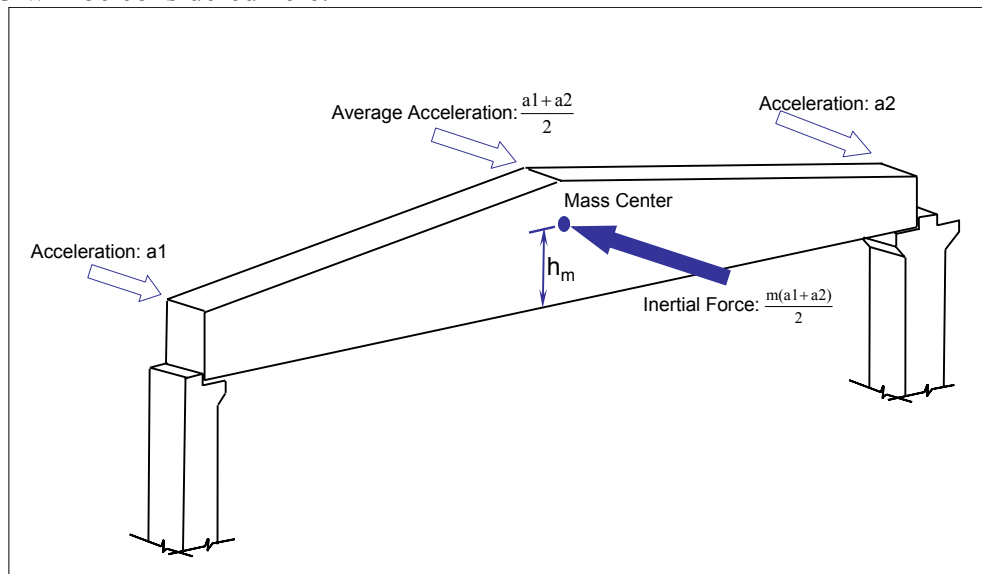

Figure 6.7   Overturning of Girder

Line L1:

Total mass in the line: $m = 159408\,\text{kg}$

Lateral force from columns: $F_C = 570\,\text{kN}$

Lateral force from vertical braces: $F_V = 2006\,\text{kN}$

Lateral force from diaphragm braces connecting L1 and L2: $F_{D,12} = -2230\,\text{kN}$

Then the maximum acceleration of L1 can be calculated as:

$$a_{L1} = \frac{(570 + 2006 - 2230) \times 1000}{159408} = 2.17\left(\text{m/s}^2\right)$$

Line L2:

Total mass in the line: $m = 271442\,\text{kg}$

Lateral force from columns: $F_C = 975\,\text{kN}$

Lateral force from diaphragm braces connecting L1 and L2: $F_{D,21} = 2230\,\text{kN}$

Lateral force from diaphragm braces connecting L2 and L3: $F_{D,23} = -1018\,\text{kN}$

109

Then the maximum acceleration of L1 can be calculated as:

$$a_{L2} = \frac{(975 + 2230 - 1018) \times 1000}{271442} = 8.06 \, (m/s^2)$$

Line L3

Total mass in the line: $\qquad m = 271442 \, kg$

Lateral force from columns: $\qquad F_C = 1058 \, kN$

Lateral force from diaphragm braces connecting L2 and L3: $\quad F_{D,32} = 1018 \, kN$

Lateral force from diaphragm braces connecting L3 and L4: $\quad F_{D,34} = 1018 \, kN$

Then the maximum acceleration of L1 can be calculated as:

$$a_{L3} = \frac{(1058 + 1018 + 1018) \times 1000}{271442} = 11.40 \, (m/s^2)$$

The roof girders in the two exterior bays will be subjected to an average acceleration $\frac{a_{L1} + a_{L2}}{2} = 5.12 \, m/s^2$, and that in the two interior bays will be $\frac{a_{L2} + a_{L3}}{2} = 9.73 \, m/s^2$. Therefore, the girders in interior bays are more likely to overturn.

For a single roof girder in the interior bays, the supported roof portion and 10 purlins will move simultaneously together with the girder. The total mass of the assembly of the girder with the purlins and roof portion is 15760 kg from Section 4.2.1, and the height of the mass center from the bottom of the girder is $h_m = 75 \, cm$ (Figure 6.7), which is calculated according to the dimension given in Figure 2.7. The maximum overturning moment a girder will experience during the considered earthquake is:

$$M_{OT} = 17560 \, kg \times 9.73 \, m/s^2 \times 75 \, cm = 115.0 \, kN \bullet m \tag{6.3}$$

In the same way, the overturning moment of a girder in the two exterior bays will be 67.5 kN•m. The overturning moments must be resisted at the column-girder connections.

6.6 CONNECTION STRENGTHENING

In the previous chapters, all the connections were assumed to be pins. For the strengthened connections at the top of the columns to be able to act as pins, they must posses capacities listed as follows:

a)   to prevent the girders from overturning

b)   to prevent the girders and gutters from sliding on the top of columns

c)   to transfer large tensile forces from the diaphragm and the vertical braces

Axial compressive forces developed in the girders can be transferred to the column directly as shown in Figure 6.8(a). No force will act on strengthening elements.

The equilibrium of the two gutters meeting at the top of a column is shown in Figure 6.8(b). The two gutters may have different axial force C_1 and C_2 acting in them. A force equal to $C_2 - C_1$ has to be resisted by the column through strengthening elements, otherwise the gutters may slide on the top of the column. The push-over analyses indicated the maximum value of $C_2 - C_1$ is 117 kN.
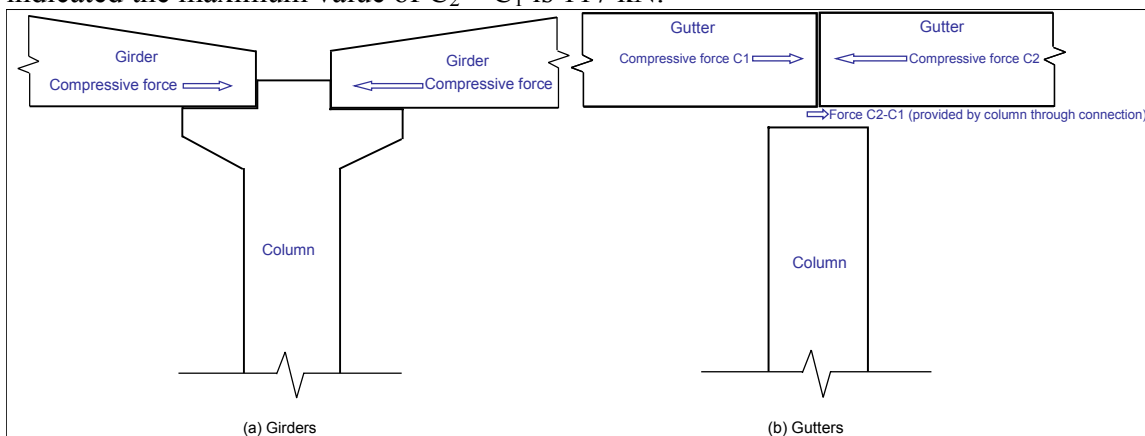

Figure 6.8   Slide Prevention of Girders and Gutters

Therefore the forces that need to be considered for a strengthened connection are:

a)   overturning moments of the girder(s)

111

b)   axial forces in the two gutters meeting at the connection

c)   tensile forces from the diaphragm and vertical braces

The detailed force requirements for the connections can be determined from the push-over analyses. All the forces need to be considered for a typical interior connection are shown in Figure 6.9. For connections at some special locations, e.g. connections at the corners of the structure, one or more of the roof members shown in Figure 6.9 may be absent, thus the associated forces will not exist.
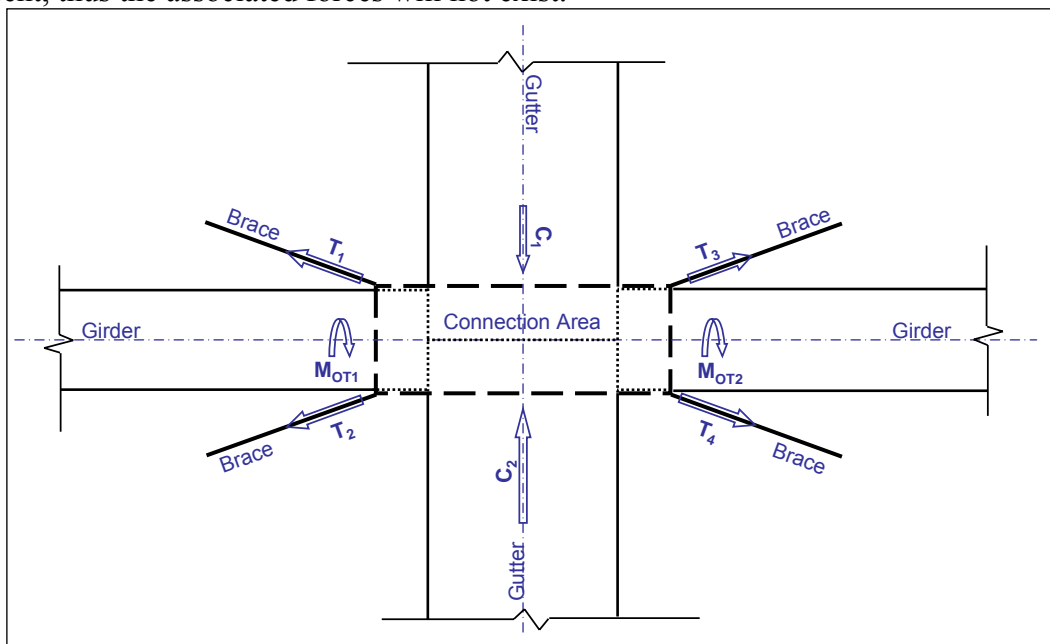

Figure 6.9 Forces Considered for a Typical Connection

The installation of the strengthening elements also needs to be considered. This construction depends on the existing configuration of the original structure, and to make the rehabilitation scheme acceptable, the strengthening operation must be as simple as possible. Strengthening of the connections will be discussed in four categories: interior, exterior at the ends of the transverse lines, exterior at the ends of longitudinal lines and corner connection.

6.6.1   Interior Connections

There are 39 interior connections in the prototype structure. Considering all the requirements discussed above, a strengthening scheme is proposed as shown in Figure 6.10. A clamping device made of steel plates will be installed on the column corbels (Figure 6.10(b)). The clamp consists of two identical parts connected with 8 bolts, 4 on each side.
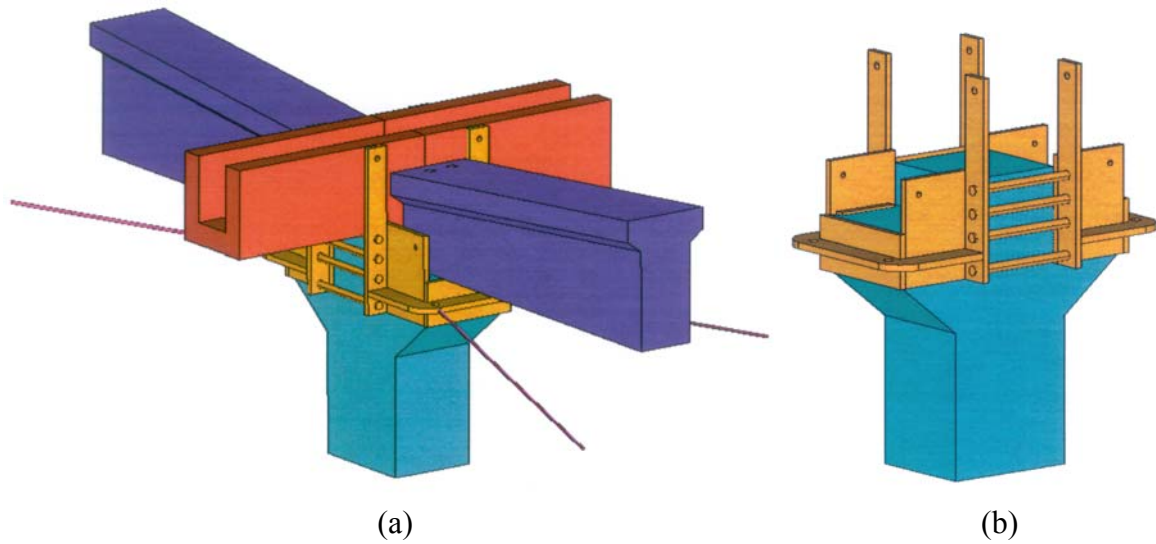
(a)   (b)

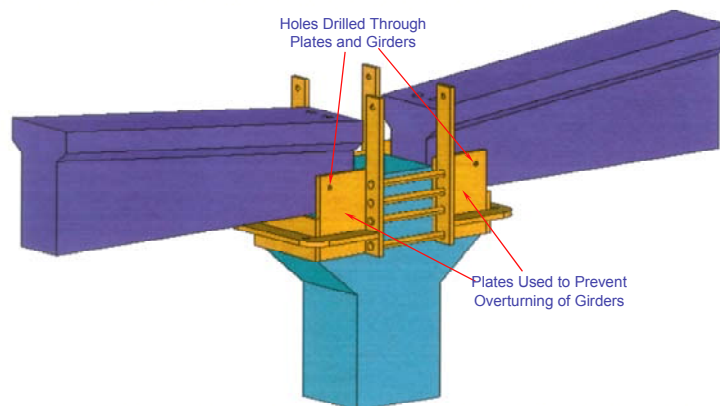Figure 6.10 Strengthening for Interior Connections

Figure 6.11   Plates Used to Prevent Overturning of Girders

Overturning Prevention: Four vertical plates are used to prevent the overturning of the roof girders (Figure 6.11). A hole is drilled in each of the plates, and at the same places, the roof girders are drilled through, thus bolts can be inserted through of the holes at the girder ends. After the gaps between the roof girders and steel plates are filled using washers, the roof girders and the steel plates are bound together by nuts. The holes in roof girders should be grouted for better efficiency.

Gutter Slide Prevention: The four steel plates used for the bolts that connect the two parts of the clamps extend to the top level of gutter beams (Figure 6.12). Analogous to what is done for roof girders, holes are drilled in the steel plates as well as gutter beams, and the components are bound together with bolts. Because the gutters are used to gather water from building roof, the holes should not be drilled in the lower part of the gutters. Holes in gutters should be grouted after the installation.
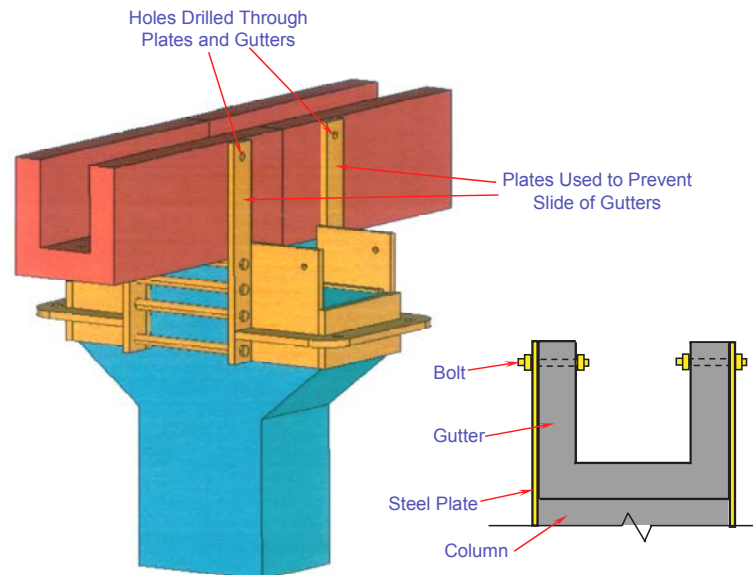

Figure 6.12   Plates Used to Prevent Slide of Gutters

Transfer of Tensile Forces from Braces: Horizontal flanges are used to anchor the diaphragm braces (Figure 6.13). The locations of holes must be carefully determined to avoid additional twisting of the columns. Local stress concentration will occur around

114

the hole, and its extent depends on the technique used for the diaphragm brace attachment. A variety of measures can be taken for this issue. In this study, steel nuts are welded at the top and bottom of the flange coaxially with the drilled holes.
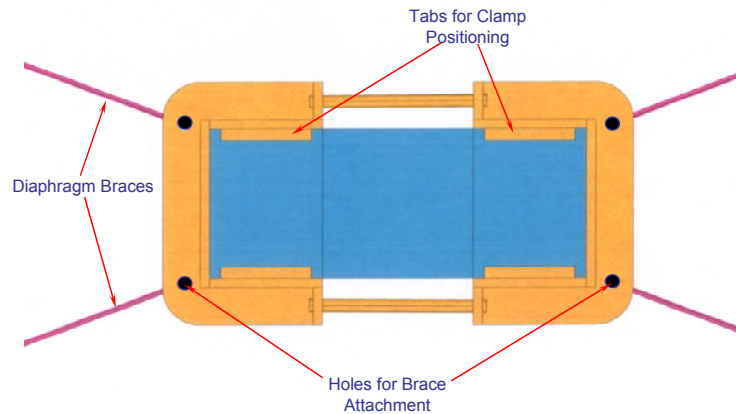

Figure 6.13   Top View of a Clamp

Installation: Four, 10-mm thick steel tabs are welded at the interior side of the clamp to help the clamp ride on the corbels (Figure 6.13). The width of the girder bottom is 26 cm while that of the column corbel is 40 cm, thus the width of the four steel strips can be 3 cm.

Finally gaps between girders and columns and between adjacent gutters should be grouted. The locations of the holes should be selected to avoid cutting the reinforcing steel bars in the precast members.

A variety of load combinations are obtained from the push-over analyses to determine the thickness of the clamp plates. It turns out that three typical cases are the most critical for the device. For convenience of expression, they are numbered Case 1, Case 2 and Case 3.
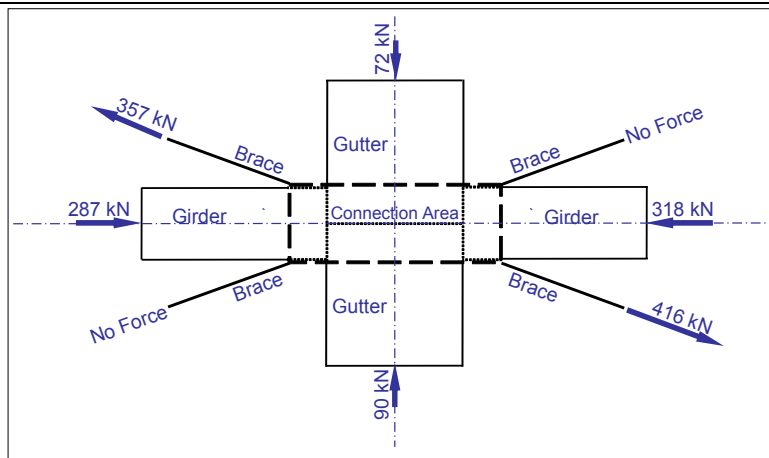
Case 1 and Case 2 are from the longitudinal push-over analysis. Case 1 (Figure 6.14 (a)) is taken at the joint in line L4 at line T2, and Case 2 (Figure 6.14(b)), line L3 at line T2. Case 3 (Figure 6.14(c)) takes place in line T13 at line L4 in the transverse push-
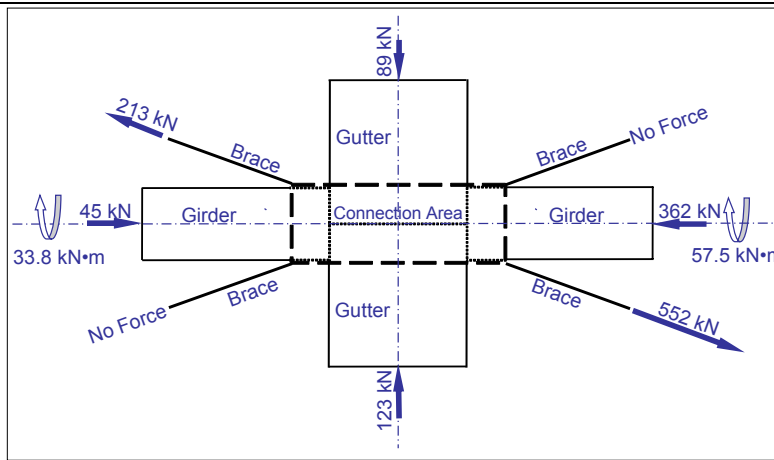
(a) Case 1 (Joint in Line L4 at Line T2 in Figure 6.4)
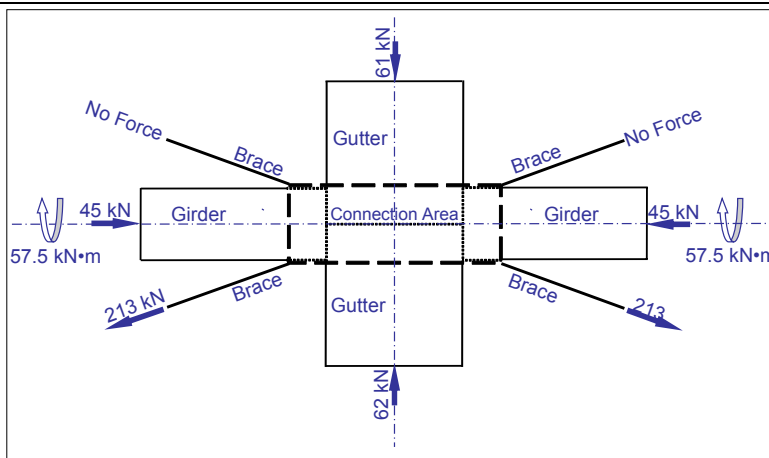
(b) Case 2 (Joint in Line L3 at Line T2 in Figure 6.4)

(c) Case 3 (Joint in Line T13 at Line L4 in Figure 6.6)

Figure 6.14 Critical Load Combinations for Interior Connection

over analysis, therefore there is no overturning moment. It should be mentioned that the axial forces from girders will be transferred to the column directly, and thus do not influence the design of the clamp.

6.6.2 Exterior Connections at Ends of Transverse Lines

Compared to the interior connection illustrated in Figure 6.9, for an exterior column at the ends of transverse lines T2 through T14, there is only one girder at that connection, but two vertical braces are anchored to each clamp. The clamps are modified
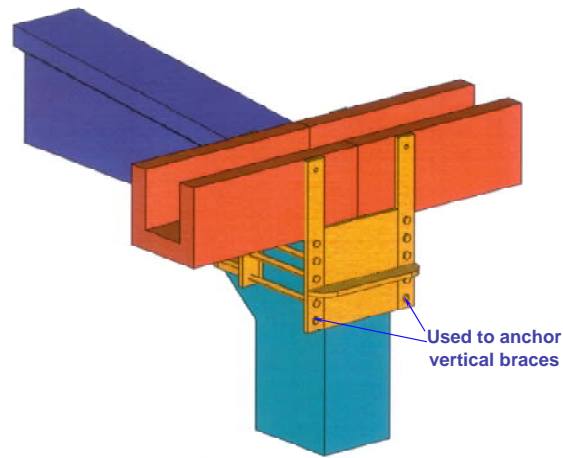

Figure 6.15 Exterior Connection at Ends of Transverse Lines

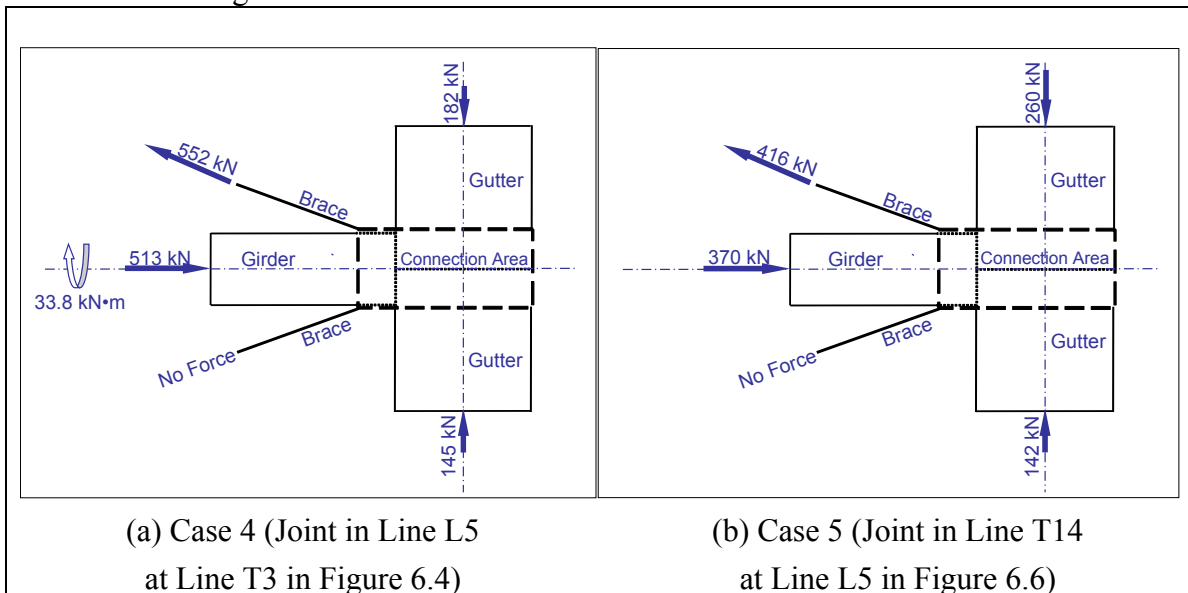| (a) Case 4 (Joint in Line L5	(b) Case 5 (Joint in Line T14
at Line T3 in Figure 6.4)	at Line L5 in Figure 6.6)

Figure 6.16 Critical Load Combinations for Connections at Ends of Transverse Lines

accordingly (Figure 6.15). The most critical load combinations are illustrated in Figure 6.16, and numbered as Case 4 and Case 5.

6.6.3 Exterior Connections at Ends of Longitudinal Lines

An exterior connection at ends of longitudinal line L2, L3 and L4 has a gutter beam on only one side (Figure 6.17). In order to balance the compressive force from the
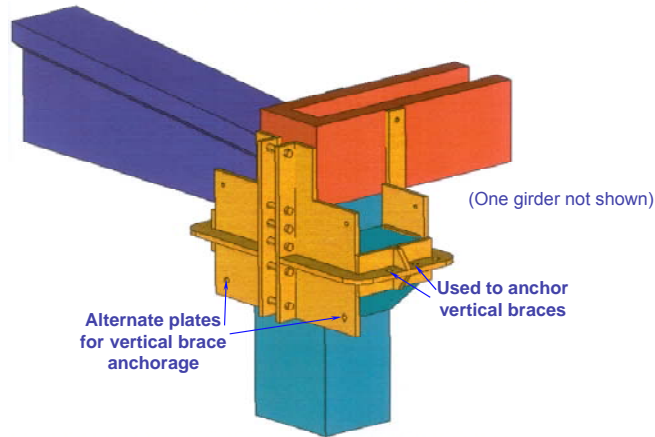

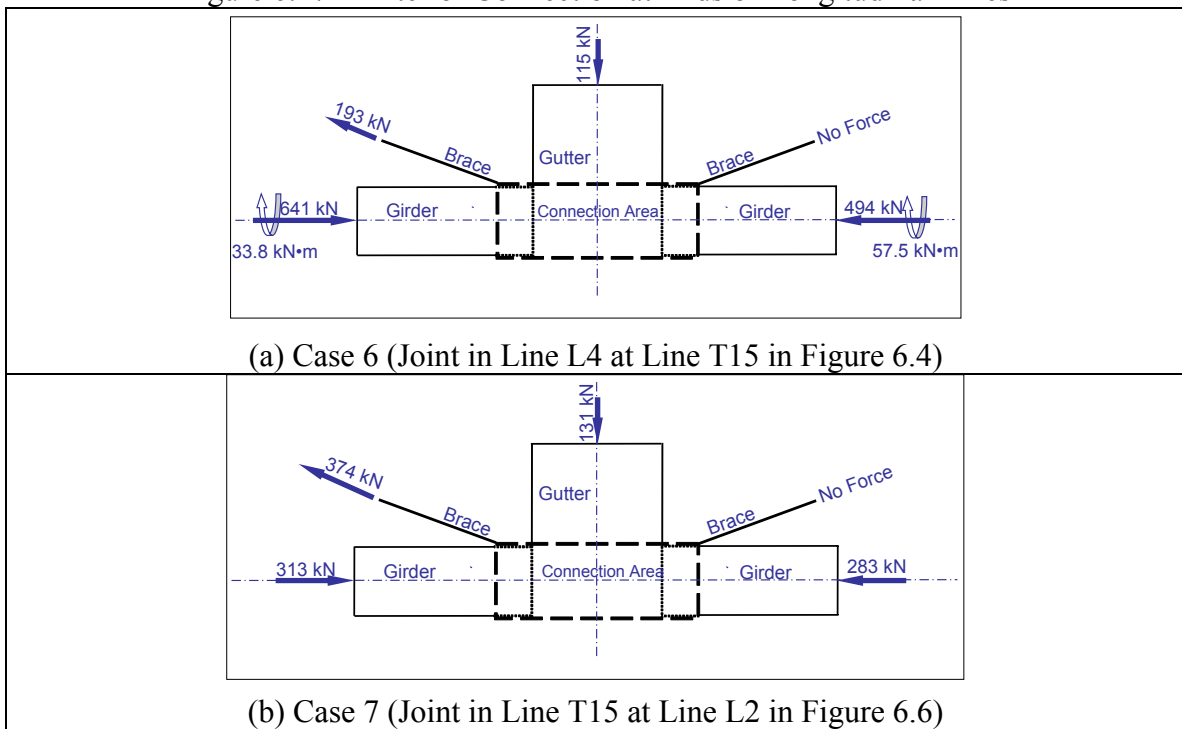Figure 6.17   Exterior Connection at Ends of Longitudinal Lines

(a) Case 6 (Joint in Line L4 at Line T15 in Figure 6.4)

(b) Case 7 (Joint in Line T15 at Line L2 in Figure 6.6)

Figure 6.18 Critical Load Combinations for Connections at Ends of Longitudinal Lines

118

gutter, the clamp has to be stronger on its exterior side. Alternate plates for vertical brace anchorage are provided in case openings are requires for access, and thus more braces are required in the bays adjacent to the openings. The most critical load combinations are shown in Figure 18 and numbered as Case 6 and Case 7.

6.6.4   Corner Connections

Only one roof girder and one gutter beam join at each of the four corner connections (Figure 6.19). The most critical load combinations for corner connections are illustrated in Figure 6.20 and numbered as Case 8 and Case 9.
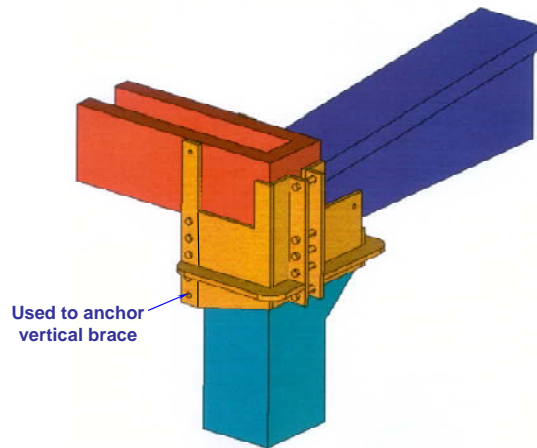

Figure 6.19   Corner Connection

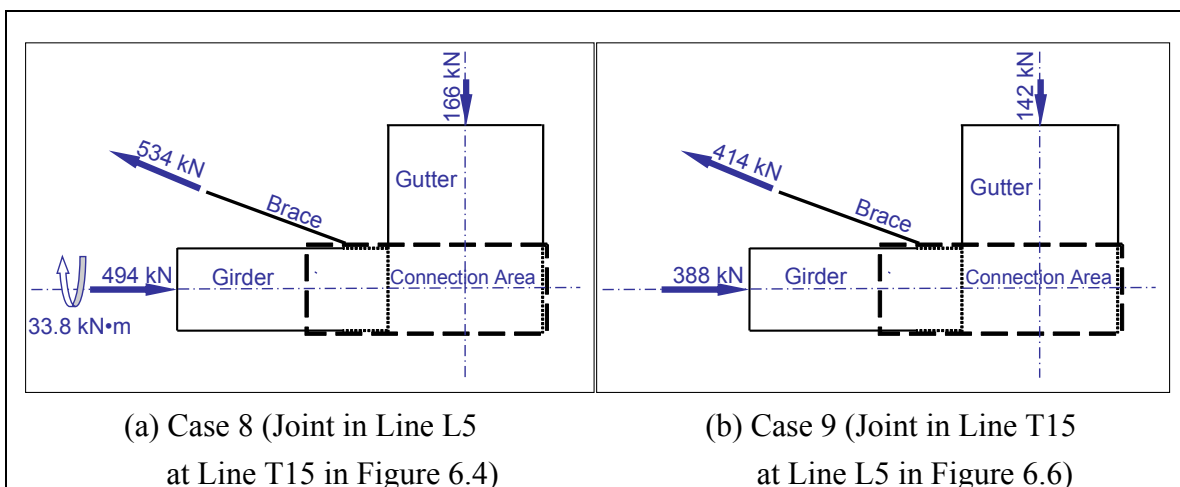| (a) Case 8 (Joint in Line L5	(b) Case 9 (Joint in Line T15
at Line T15 in Figure 6.4)	at Line L5 in Figure 6.6)

Figure 6.20 Critical Load Combinations for Corner Connections

6.6.5   Determination of Plate Sizes

In order to determine the required sizes of the plates for the four kinds of clamps, finite element models were develped using ANSYS software. All plates were modeled using shell elements and the yield stress of the steel material was assumed to be 345 MPa. For all the bolts, 620 MPa yield stress was used.

The analysis results reveal that $\Phi 26$ bolts are required to bind together the two parts of a clamp, $\Phi 23$ bolts to prevent the girder overturning, and $\Phi 10$ bolts to balance the compressive forces in gutters. To bear the stress concentration around the diaphragm brace installation holes, 1.5-cm thick nuts should be welded on each side of the flange.

Figure 6.21 gives the resulting dimensions of the clamps for all four types of connections. For an interior connection (Figure 6.10), the two parts connected by the 8 bolts are identical (Figure 6.21(a)). For an exterior one at ends of transverse line T2 to T14 (Figure 6.15), its two parts are very different. One is the same as shown in Figure 6.21(a), the other one is shown in Figure 6.21(b). The two parts of an exterior connection at ends of longitudinal line L2, L3 or L4 are twins to each other (Figure 6.17), and its dimensions are shown in Figure 6.21(c). One part of a corner connection shown in Figure 6.19 is dimensioned in Figure 6.21(d), and the dimension of the other part of it is the same as Figure 6.21(c). Using the shown steel clamps, all the connections can be modeled as pins as assumed in analyses conducted. The stress distributions in the clamps under the load case 1 through case 9 are given in Appendix D.

The technique of strengthening connections in the precast concrete buildings using steel clamps has been adopted in some buildings in Turkey (Figure 6.22). Although the proposed strengthening clamps are more complicated, the fact that similar types of clamps have been installed implies that this rehabilitation scheme economical and

120

constructible. No added diaphragms were observed, but the proposed braces are the easiest to be installed in the field.
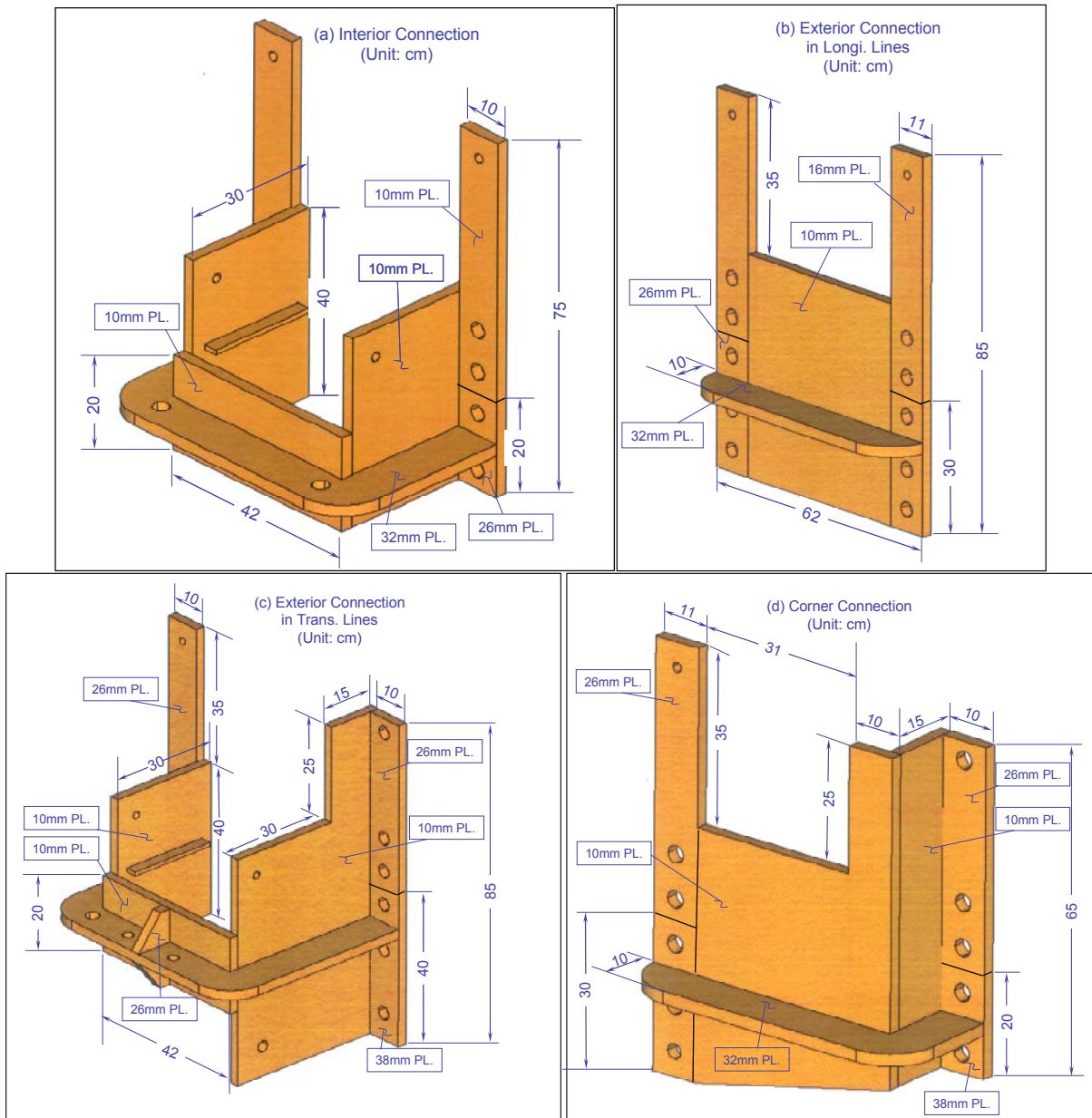

Figure 6.21 Dimensions of Connection Clamps

Figure 6.22 Steel Clamps Used to Retrofit Connections

6.7 COLUMN HINGE REQUIREMENT

It should be noted that because the diaphragm itself is flexible, with a rehabilitation scheme consisting of only adding diaphragm braces and peripheral vertical braces, the reduction in maximum roof drift may not be sufficient if column core is not well confined at the base, where maximum moment occurs. For the prototype building of this study, 135 degree hooks were indicated on the design drawings for the transverse reinforcement in the columns, so that the columns have considerable ductility. However this transverse reinforcement detail is not common in the epicentral region.

Transverse hoops with 90° hooks were used for the columns of most precast concrete buildings in the epicentral region in Turkey. When the concrete cover spalled at the base of the columns during an earthquake, the hoops opened and confinement of the concrete core was diminished or destroyed. The maximum strain that the core can endure in such a case may be almost the same as the cover and the ductility of the columns will be dramatically lower than that of the prototype building. Using diaphragm bracing and peripheral vertical braces only can not reduce the roof drift to an allowable level for the brittle columns.

122

Supplementary measures can be taken to improve the flexural ductility of the columns. For example, the base region of the columns can be jacketed by placing steel angles at the column corners and connecting the angles with steel strips (Figure 6.23).
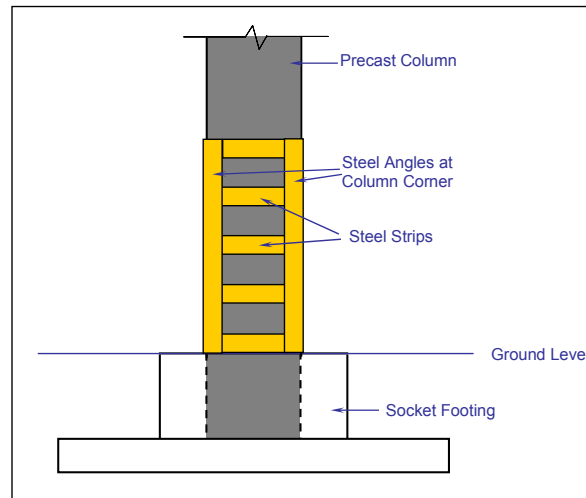

Figure 6.23 Steel Jacketing at Base of Column

This procedure is being used in the epicentral region in Turkey. The steel jacketing offers additional confinement to the column concrete, increases the ultimate strain capacity, and enhances the maximum allowable deflection. The diaphragm bracing and the additional LFRS then can be designed based on the enhanced column ductility. Not all the columns of the structure will experience the same deflection during an earthquake or have the same details. Therefore, the angle jacketing can be applied only where it is necessary.

It should be stated that for columns with large rectangular cross section, the efficiency of the confinement of steel jacketing decreases (Aboutaha, 1994). Under compression, the steel tabs will bend outwards, and thus can not provide sufficient confinement to the concrete in the middle of the edge (Figure 6.24(a)). In this case, steel dowels are suggested to be anchored inside the concrete, and washers and bolts are used to restrain the deformation of the steel tabs (Figure 6.24(b)). With the steel dowels, the

123

confinement to the concrete can be improved and the ductility of the columns can be enhanced.
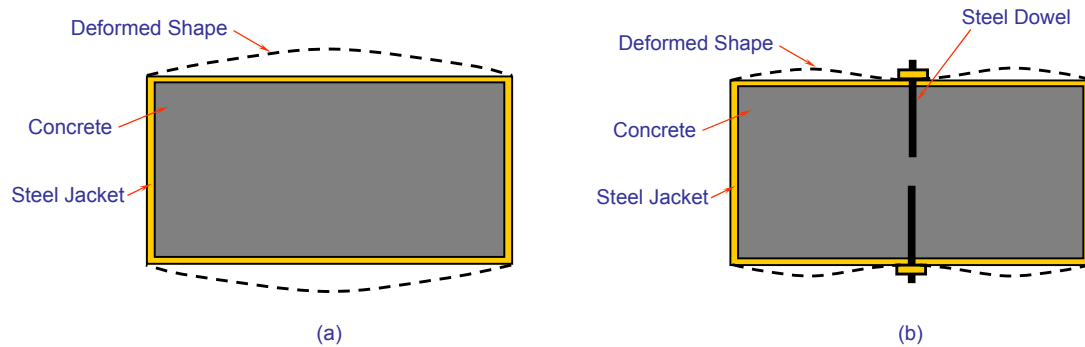

Figure 6.24 Rectangular Steel Jackets for Large Column

6.8   RESULTS BY OTHER ANALYSIS METHODS

All the rehabilitation procedures above for the prototype building were based on the results from the tensioned string analogy. Other methods such as modal analysis and time history analysis could also be performed on the rehabilitated building, and the results could be used to verify the applicability of the string analogy. As indicated before, the most important features that could be used for the comparison are the nodal displacements. The forces provided by modal analyses are of limited value because modal analyses do not consider the inelasticity of the structure. A time history analysis does provide real time force information, which could be compared with that from the push-over analyses.

6.8.1   Displacement

The displacement results by different methods are listed in Table 6.3 and illustrated in Figure 6.25. Modal analysis was more conservative than the tensioned string analogy or time history analysis.

Table 6.3   Maximum Displacements by Different Methods

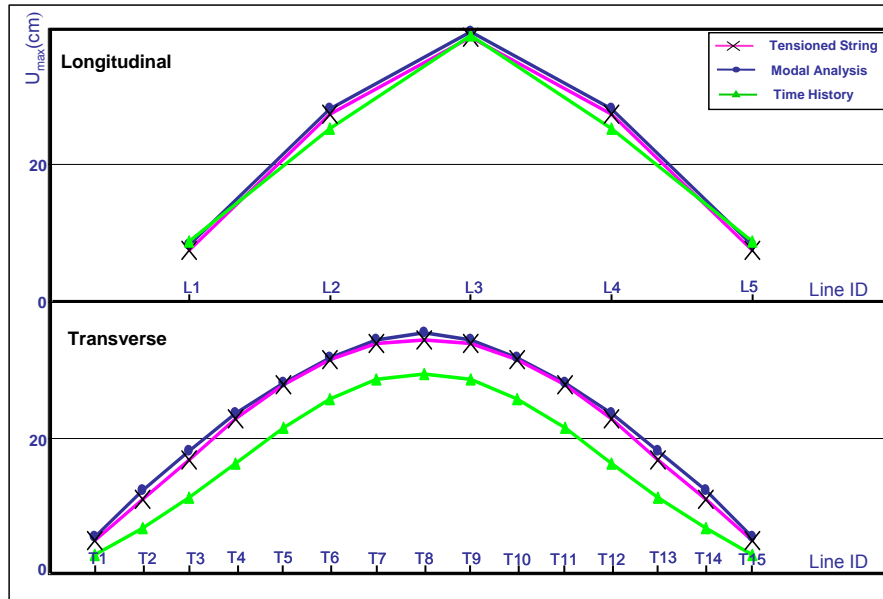| Line ID	Longitudinal Motion (unit: cm)		
	Tensioned String	Modal Analysis (SAP2000)	Time History Analysis (OpenSees)
L1	7.5	8.3	8.8
L2	27.5	28.2	25.3
L3	38.6	39.5	38.9
Line ID	Transverse Motion (unit: cm)		
	Tensioned String	Modal Analysis (SAP2000)	Time History Analysis (OpenSees)
T1	5.0	5.5	3.0
T2	11.1	12.5	6.9
T3	16.8	18.1	11.2
T4	22.7	23.5	16.3
T5	27.7	27.9	21.5
T6	31.4	31.7	25.8
T7	33.7	34.3	28.6
T8	34.5	35.3	29.3

Figure 6.25   Comparison of Displacements by Different Methods

6.8.2   Other Features

Other features of interest include internal forces, strains, relative extensions that are important for the design details. All are closely related to the nodal displacements. For motion in the transverse direction, since the maximum displacements resulting from the time-history analyses are significantly smaller than the estimations from the other methods, it is expected that the maxima other than displacement, e.g. maximum strain in bracing, from the time-history analyses will be also smaller than the estimations using modal analyses and the string analogy. Therefore, only the results under the longitudinal ground motion are compared because the maximum displacement from the time-history analyses is almost the same as the estimations.

  Maximum Strain in Diaphragm Braces: The maximum strain in the diaphragm braces from the time-history analysis is 2.7 $\mu\varepsilon$, very close to the push-over analysis result, 2.8 $\mu\varepsilon$. From the time-history analyses, the maximum strain in the horizontal braces in the two bays between L2 and L4 is 2.0 $\mu\varepsilon$, slightly higher than the estimated result, 1.7 $\mu\varepsilon$. All the analyses indicate the elastic behavior of the diaphragm.

  Gaps Between Columns and Girders: The time-history analyses reveal that all gaps might occur between columns and girders on the periphery, the width of the openings will be less than 1.5 cm. All the interior girders only experience elastic compression.

  Gutter Beams: All analyses indicate small strain in gutter beams under longitudinal motions; 0.09 $\mu\varepsilon$ from push-over analysis, and 0.11 $\mu\varepsilon$ from time-history analyses.

  Vertical Bracing: Similar to the push-over analysis, the time-history analyses reveal yielding of the vertical braces in line L1 and L5, and maximum strain in the

vertical braces turns out as 6.3 $\mu\varepsilon$, less than the level 10 $\mu\varepsilon$ for which strain hardening effects need to be considered. Strain hardening effects are assumed to be negligible.

Columns: Because the maximum roof drift from time history analyses are almost the same as that from the string analogy, the response of the columns from time history analyses is almost the same as that from the push-over analyses.

It should be stated that it would not be necessary to check every design with time-history analyses, but the results are compared here to provide verification of the proposed analysis method.

6.9   EFFECT OF GROUND MOTION DIRECTION

The response of the rehabilitated prototype building to earthquake motions in transverse and longitudinal directions has been completely analyzed. Since earthquake motions could be imposed in any direction, some additional analyses were made to check if the building with the proposed rehabilitation would be adequate for considered earthquakes in other directions. The angle of motions from the longitudinal axis of the structure is shown in Figure 6.26. Additional time-history analyses were conducted on the
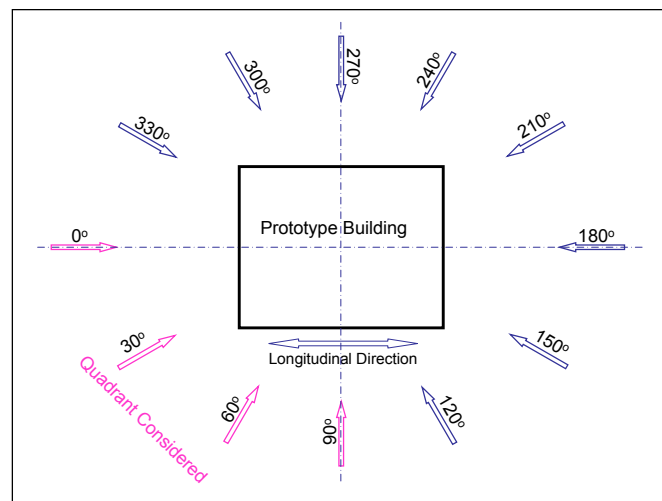

Figure 6.26   Earthquake Directions

rehabilitated structure using the OpenSees model. Because of the symmetry of the structure, earthquakes in directions between 0° and 90° were considered.

When earthquake ground motions are skewed relative to the longitudinal or transverse direction of the structure, the responding motion of the structure is much more complicated. Columns will be subjected to bidirectional forces. However, the key feature that controls collapse of the columns and thus the failure of the structure is the maximum strain in the concrete core at the column base. With the fiber element method used in the OpenSees model, the strain in the concrete core of the columns can be calculated. In order to clarify which direction is the most critical for the prototype building, the maximum strains in the concrete core of the columns under earthquake ground motions at angle 0°, 30°, 60° and 90° are listed in Table 6.4.

Table 6.4   Maximum Strain in the Concrete Core of the Columns

Direction	0°	30°	60°	90°
Max. Concrete Strain ($\mu\varepsilon$)	13	12	11	9.8

For earthquake ground motions in the longitudinal direction of the structure (0° angle in Table 6.4), the concrete core of the structural columns experienced the highest strain. For all the other considered directions, the diaphragm braces always remained elastic, and the maximum column strain were less critical. From the analyses conducted on the response of the structure under earthquakes in the longitudinal direction, the proposed rehabilitation should be adequate for ground motions in any direction.

Chapter 7: Summary and Conclusions

7.1 SCOPE

In this study, the seismic performance of typical one-story precast industrial buildings in Turkey was studied. Because the connections between the precast units were not detailed for earthquakes, significant deficiencies in the seismic response of these structures have been identified. Specifically,

1) The lateral force resisting capacity of the buildings was inadequate. All the lateral force due to seismic motion had to be resisted by cantilever columns. There was no redundancy in the system. The expected seismic deflection was close to or beyond the deformation capacity of the columns. As some of the columns became damaged, their lateral force resisting capacity decreased. Since the lateral capacity of the columns was the same throughout and the forces imposed were nearly the same, no redistribution of forces was possible.

2) The roof system could not develop diaphragm action. Because the connections between the columns and roof girders, between columns and gutter beams were simple pins, the lateral load due to the seismic motions could not be transferred to alternate lateral force resisting elements, making rehabilitation difficult or impossible.

3) Other local weaknesses have also been identified. The connections were insufficient to keep roof members from separating from the columns. There was little resistance to overturning of the roof girders.

7.2 REHABILITATION SCHEME

The global rehabilitation scheme proposed in this study provides a diaphragm to the existing precast industrial buildings through the addition of diagonal steel braces in a

horizontal plane right under the roof girders. Diagonal steel braces, together with the existing roof system, establish a flexible diaphragm that transmits lateral load between elements to peripheral frames. To conduct the design, an analysis based on a tensioned string analogy was developed to estimate the maximum displacements in the structure under earthquake actions. Using the tensioned string analogy and static push-over analysis, requirements for a rehabilitation scheme needed that would reduce the risk of failure of the existing structural members can be determined.

7.2.1 Tensioned String Analogy

Using the tensioned string analogy, the first mode shape, fundamental period, and maximum displacements of the structure can be determined. The following properties of the system (in order) are needed:

- Total mass and the mass distribution of the structure

- Stiffness of diaphragm bracing and the additional lateral force resisting system

- Equivalent length of the analogous tensioned string

- Shape of the first mode

- Modal displacement of the mass center using elastic response spectra

- Overall structural stiffness corresponding the first mode

- Fundamental period and corresponding spectral acceleration

- Effective mass ratio

- Spectral displacement

- Maximum seismic displacements

The tensioned string analogy offers three major advantages:

a) The calculations are fairly straightforward. No analytical model is required and hand calculations can be used.

130

b)   The analysis procedure can be adopted to a variety of structures. A spreadsheet can be developed to determine the changes of the desired parameters, such as period and maximum nodal displacements, as modifications are made to a particular structure.

c)   Results obtained using the tensioned string analogy compare closely with other more complex methods, especially for symmetric structures with stiff lateral force resisting systems.

The main deficiency of the tensioned string analogy is that, in the estimation of mode shapes, only the spatial variation of the stiffness of the structural components is considered. The mass distribution is not taken into account. This will result in some error because the mode shapes are associated with both stiffness and mass. This disadvantage can be ameliorated to a certain extent through the use of push-over analyses to check deformation level because the load pattern used in the push-over analysis is associated with the mass distribution.

Another disadvantage of the tensioned string analogy is that it considers only the first mode of a structure. If the first mode of a system activates most of the mass of a structural system, the estimated results will be quite close to those from a modal analysis. For a general existing building such as the prototype of this study, the effective mass ratio of the first mode is larger than 80%, and the tensioned string analogy gives satisfactory estimation. For special structures in which there are abrupt variation of stiffness and mass distribution, the effective mass ratio of the first mode may be even smaller than 60%. If the effective mass ratio of the first mode is lower than 75%, FEMA 356(2000) suggests referring to the results of modal analysis, in which at least 90% of the total mass will be included.

7.2.2 Static Push-Over Analyses

The static push-over analysis was used to determine the detailed requirements for new and existing structural members. The push-over analysis is carried out as follows:

- Develop an analytical model that include inelasticity in some or all structural members

- Determine load pattern based on mass distribution and the shape of the first mode

- Select a control node, usually one where maximum displacements occurs. The displacement estimated by the tensioned string analogy is used as the target displacement for the push-over analysis

- Increase the lateral load proportionally, keeping the load pattern constant, and monitor the displacement of the control node until the target displacement is reached

- Investigate detailed deformations, and internal forces in structural members.

7.3   CONCLUSIONS

Through the present study, the following conclusions can be stated:

1)   The poor performance of existing precast industrial buildings in Turkey can be corrected. The roof drift can be reduced, overturning of the girders can be avoided, and sliding of the roof members from supports can be prevented.

2)   A horizontal diaphragm can be provided by adding diagonal steel braces at the roof level. Diaphragm action can be developed by introducing new diagonal braces that act together with the existing roof system, so that the lateral forces can be transferred among different lateral force resisting members.

3)   Redundant lateral force resisting systems can be provided by adding vertical diagonal braces on the periphery of the structure. With diaphragm action developed, lateral forces can be transferred to these peripheral vertical braces.

4)   The existing poor connections can be improved. By adding properly designed steel clamping devices, the connections can prevent the roof members from separating from the columns, and the roof girders from overturning.

5)   The required analysis for the rehabilitation design can be conveniently conducted using tensioned string analogy. The calculations are straightforward and the results are close to those from other analyses using complex methods.

6)   The proposed rehabilitation scheme can be readily constructed and minimally interfere with the current occupancy of the buildings. The strengthening elements are not too large to install and they can be added sequentially to produce the new systems.

7.4   FUTURE RESEARCH

The main accomplishment of this study is a technique for adding a structural diaphragm at the roof level in an existing one-story precast building. It should be noted that in the development of this rehabilitation scheme, many features were simplified or even ignored. Some simplifications may lead to a conservative design, and as a consequence, the resulting rehabilitation scheme may be inefficient.

In order to develop comprehensive rehabilitation schemes for existing precast industrial buildings with different configurations, further research is required in the following areas:

1)   Investigate the effect of the moment and tension resistance of the strengthened connections. In this study, the connections were simplified as perfect pins which were assumed to carry no moment. The capacity of the connections to resist tension was also ignored. However, with the strengthening clamps, the connections will have some capacity to resist moment and tension. The research of the effect of this capacity on the performance of the structures may help to improve the rehabilitation.

133

2)   Consider the sensitivity of the structural performance to the twisting of columns. It was assumed that the horizontal braces were aligned with the centerline of the columns, and twisting was not considered. But because of the tolerances of the members and the construction, the twisting of the columns is unavoidable. The effect of the twisting on the structural performance should be considered.

3)   Investigate the feasibility of the proposed rehabilitation scheme to precast structures with steel trusses or girders (Figure 7.1). In some industrial buildings, rather then precast concrete girders, steel trusses or girders were used. Compared with precast girders, the steel members will be more flexible, The feasibility of the proposed rehabilitation as well as the analysis method should be verified before use.

Figure 7.1 Industrial Buildings with Steel Trusses or Girders

Appendix A: Seismic Acceleration Records

A.1   ACCELERATION RECORDS FORM KOCAELI EARTHQUAKE
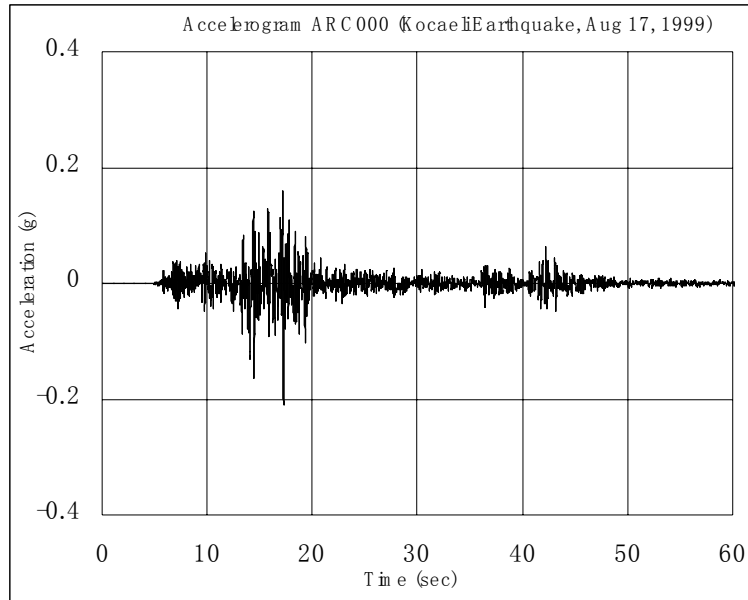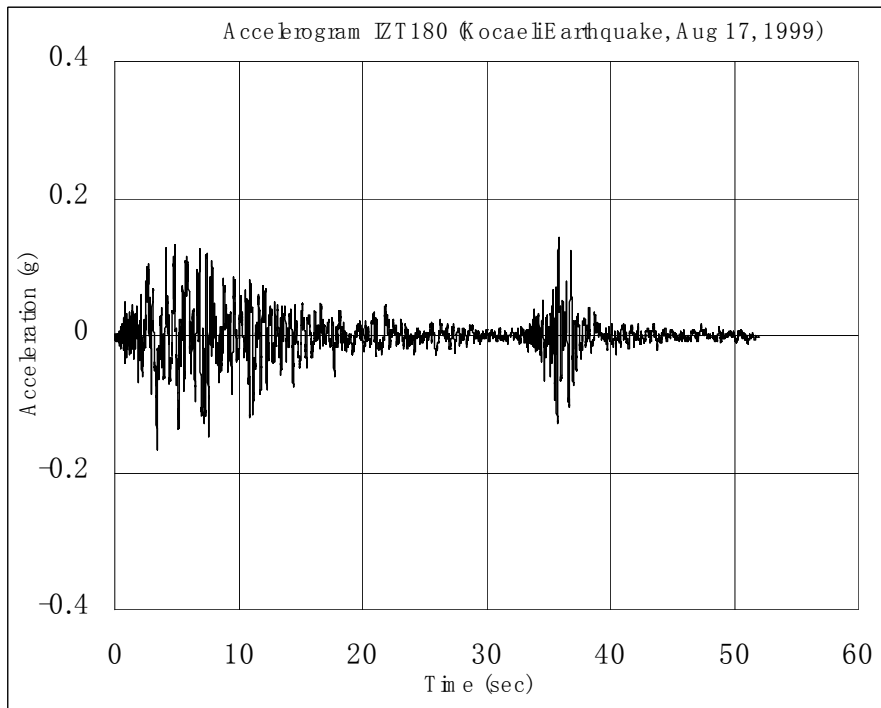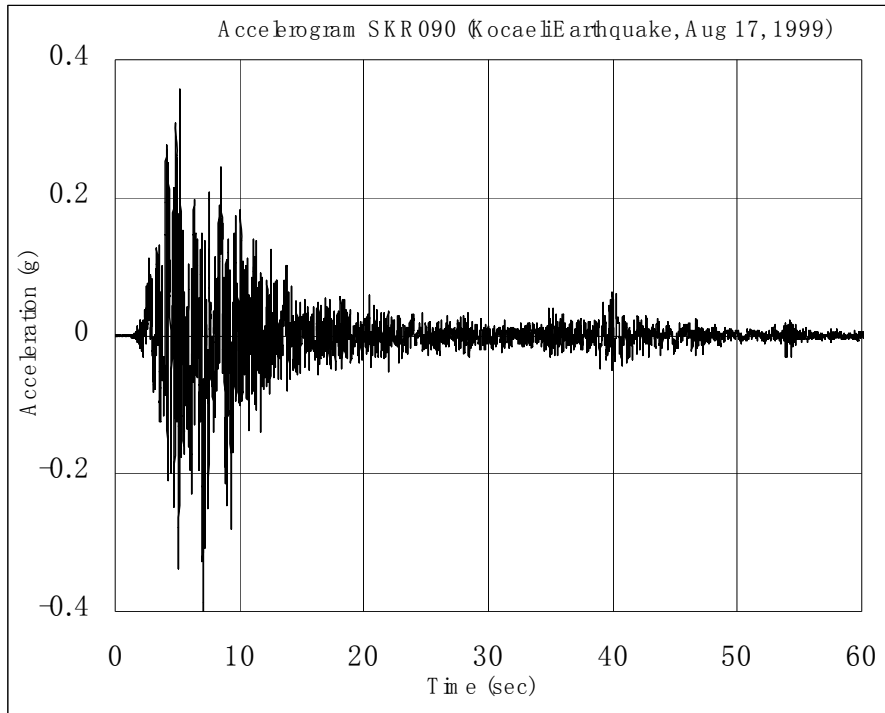

Figure A.1   Accelerations Recorded in Arcelic (000 Component)
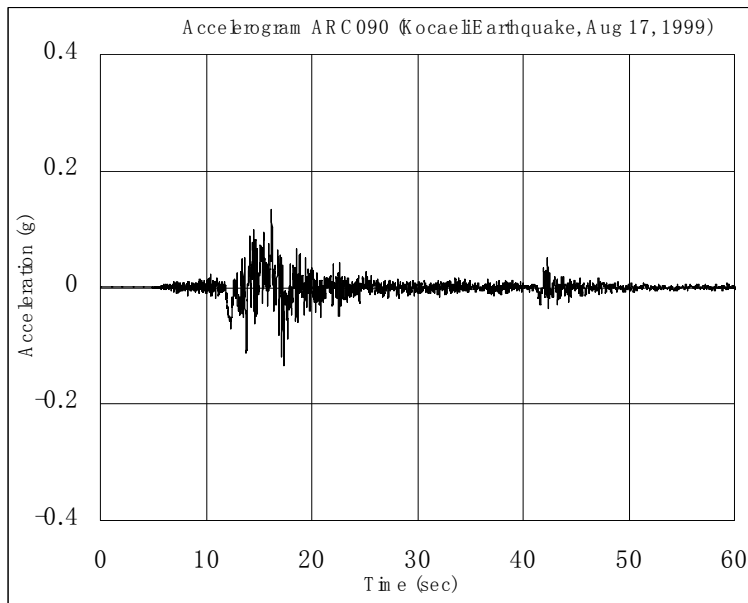
Figure A.2   Accelerations Recorded in Arcelic (090 Component)
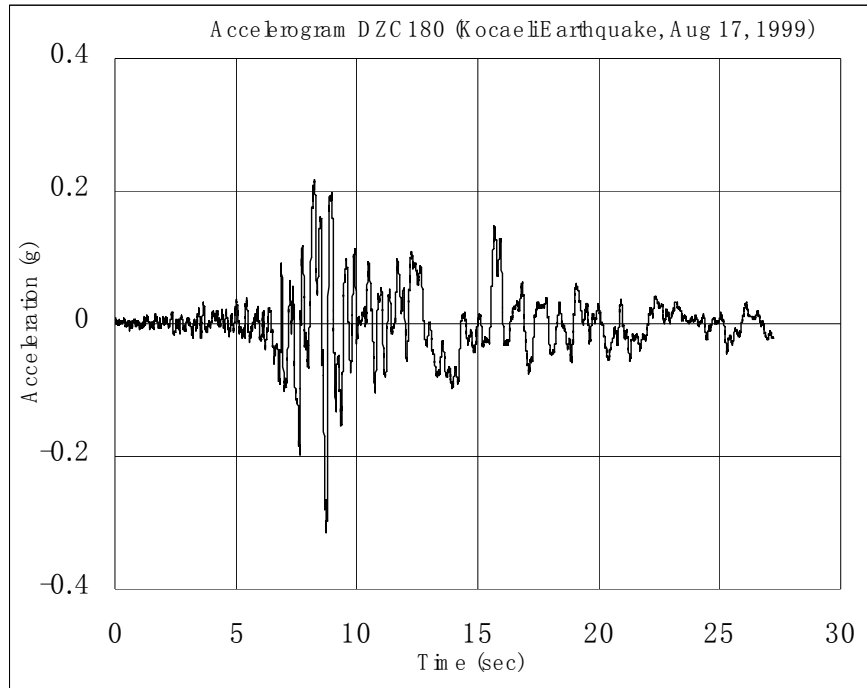
Figure A.3   Accelerations Recorded in Düzce (180 Component)
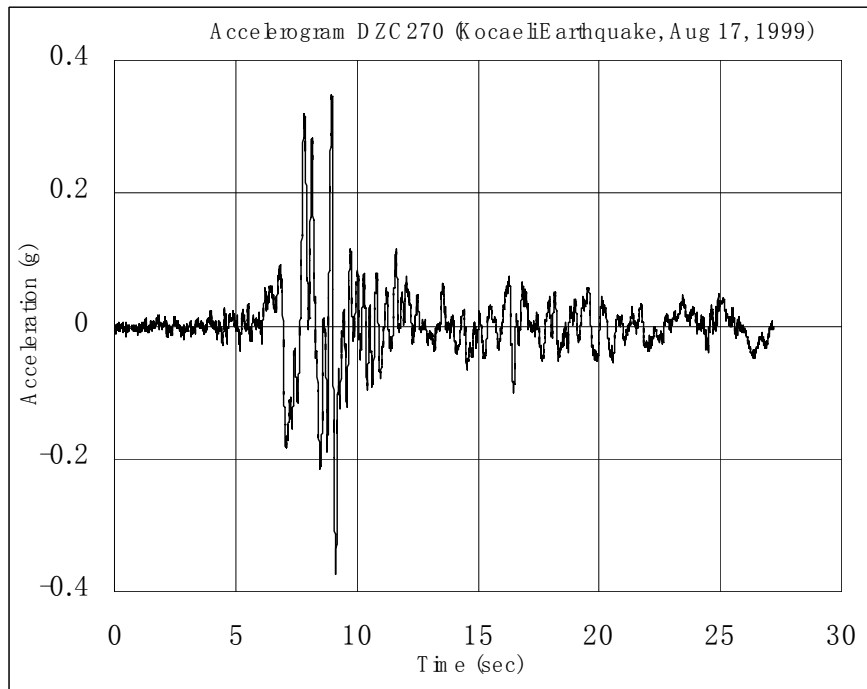
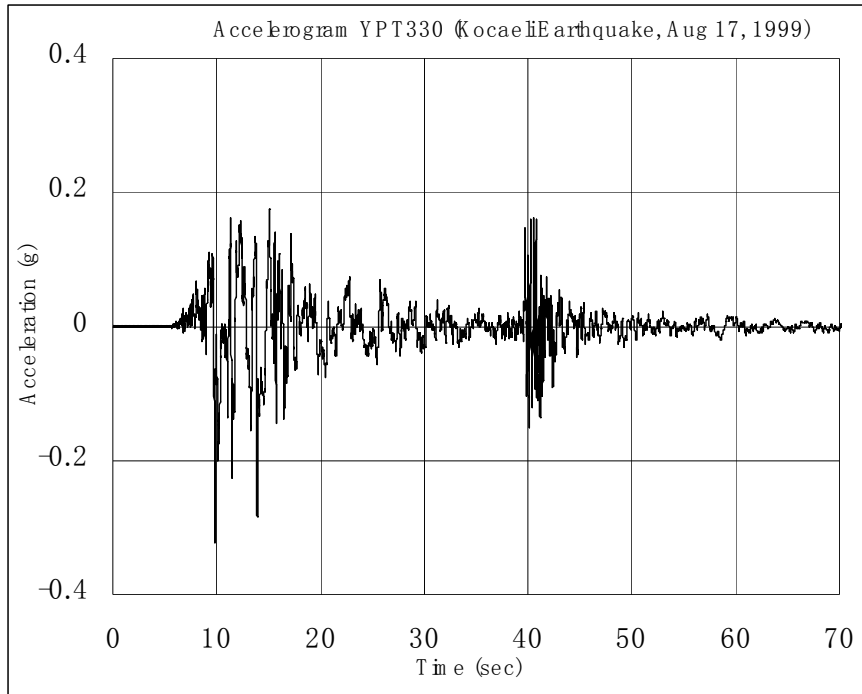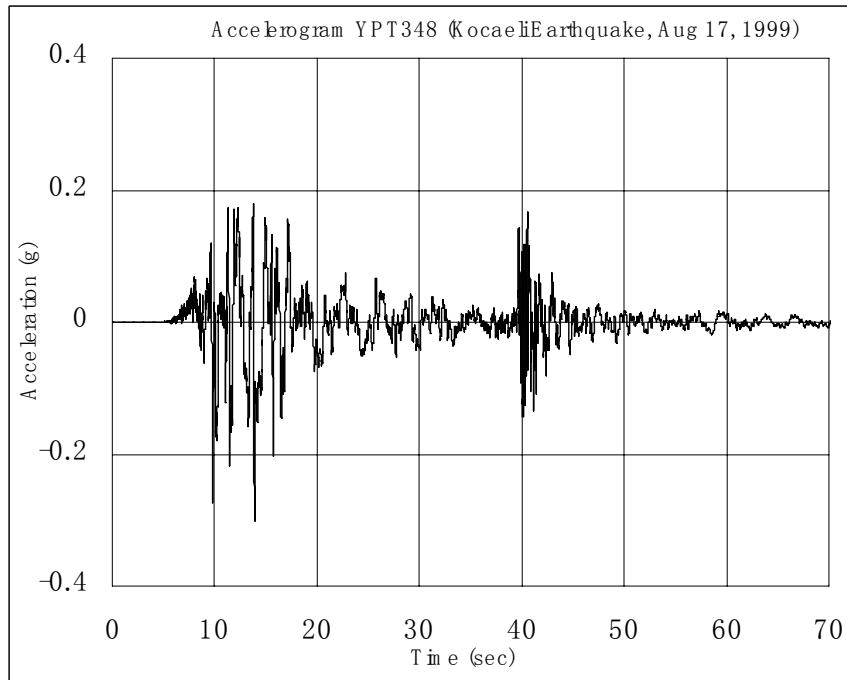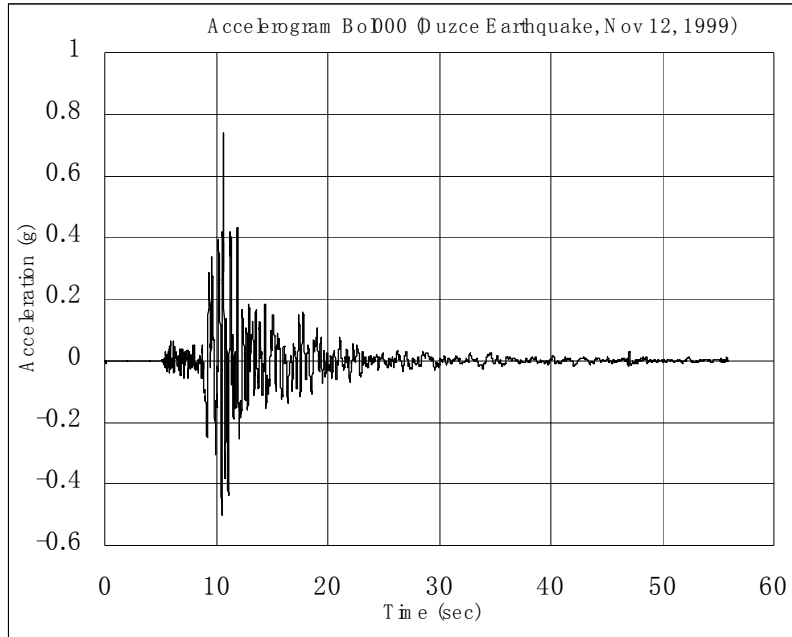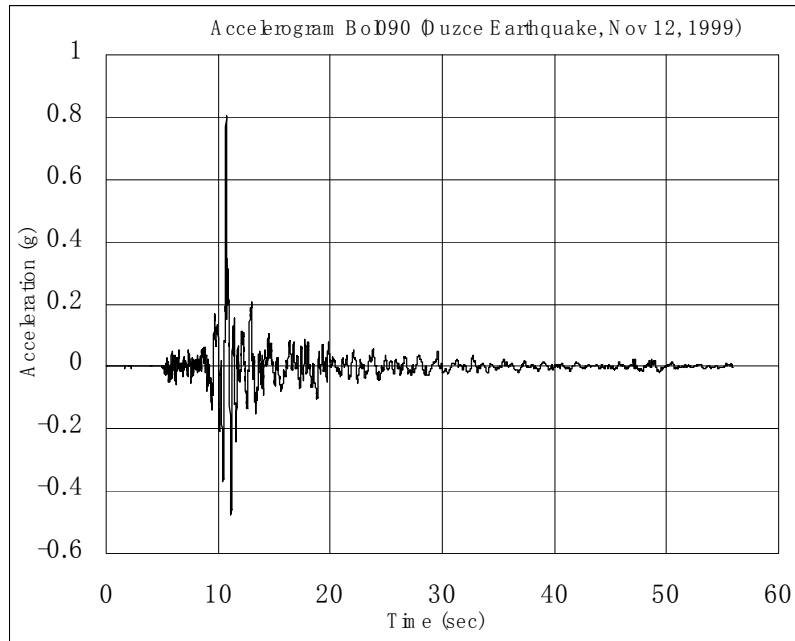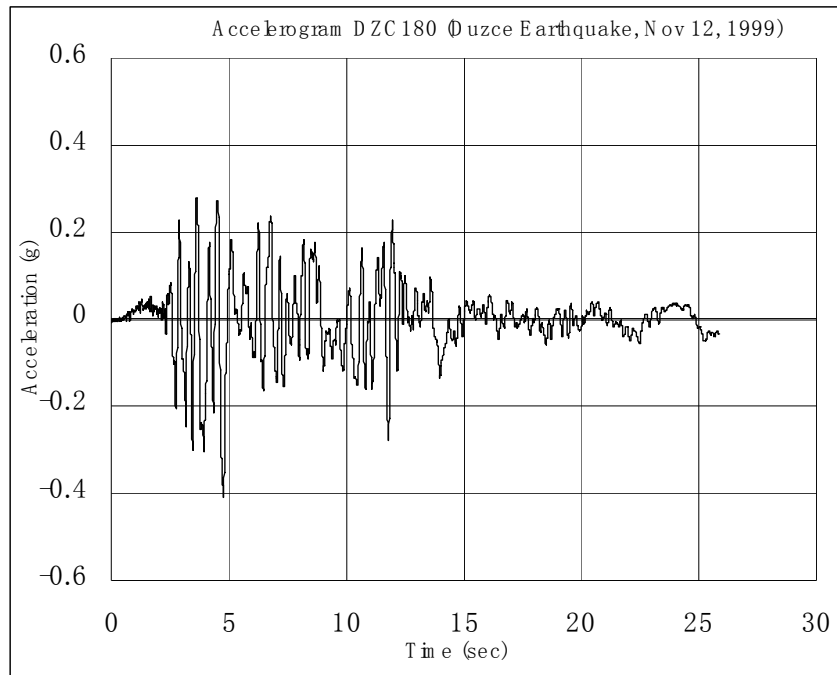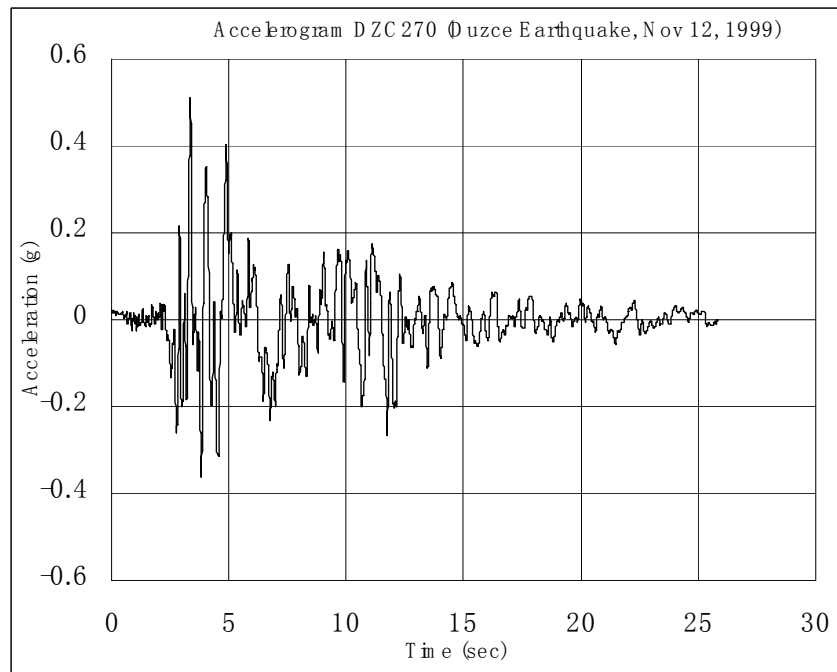Figure A.4   Accelerations Recorded in Düzce (270 Component)

136

Accelerogram GBZ000 (Kocaeli Earthquake, Aug 17, 1999)
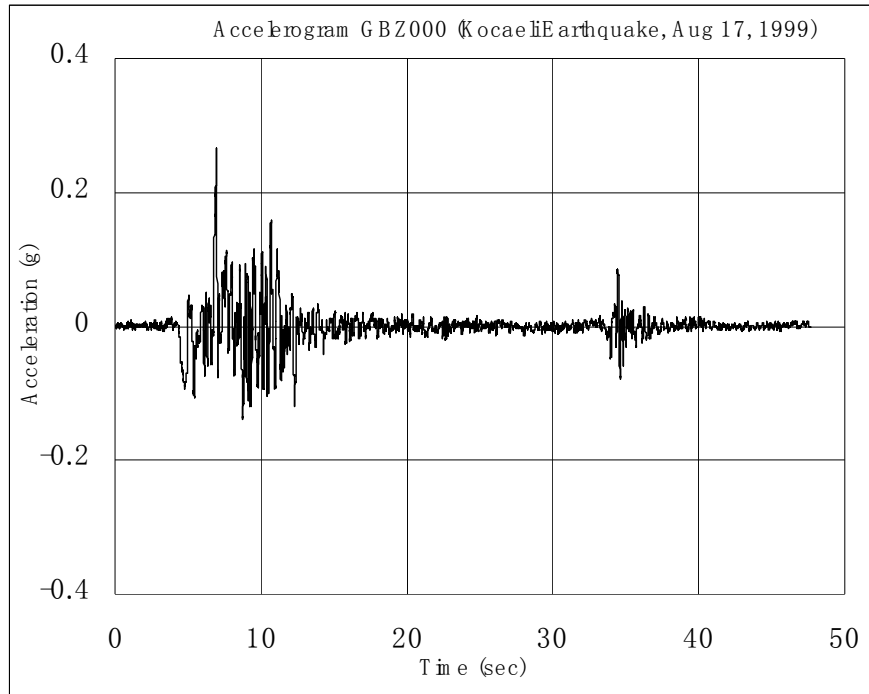
Figure A.5   Accelerations Recorded in Gebze (000 Component)

Accelerogram GBZ270 (Kocaeli Earthquake, Aug 17, 1999)
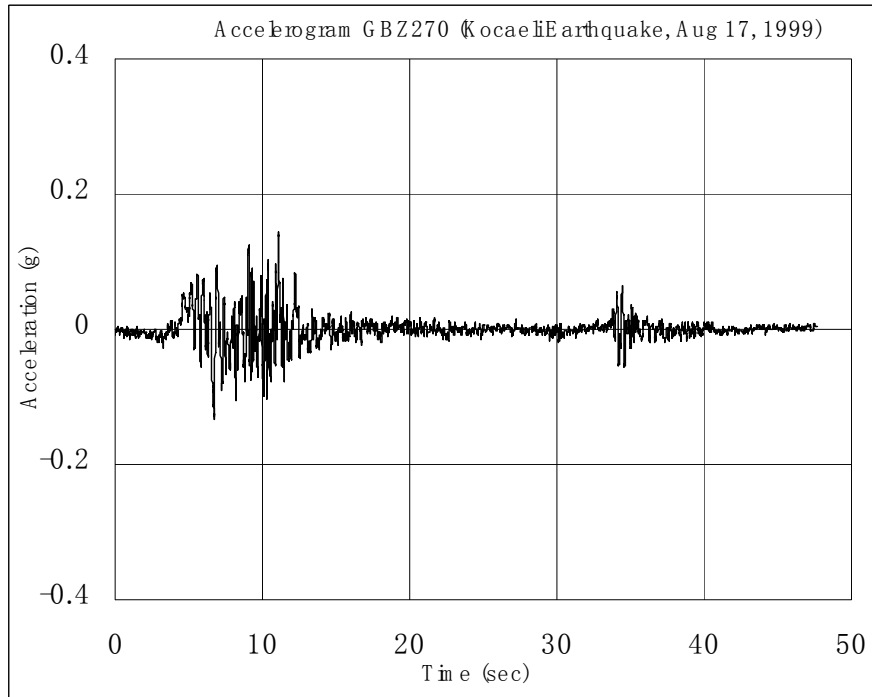
Figure A.6   Accelerations Recorded in Gebze (270 Component)

137
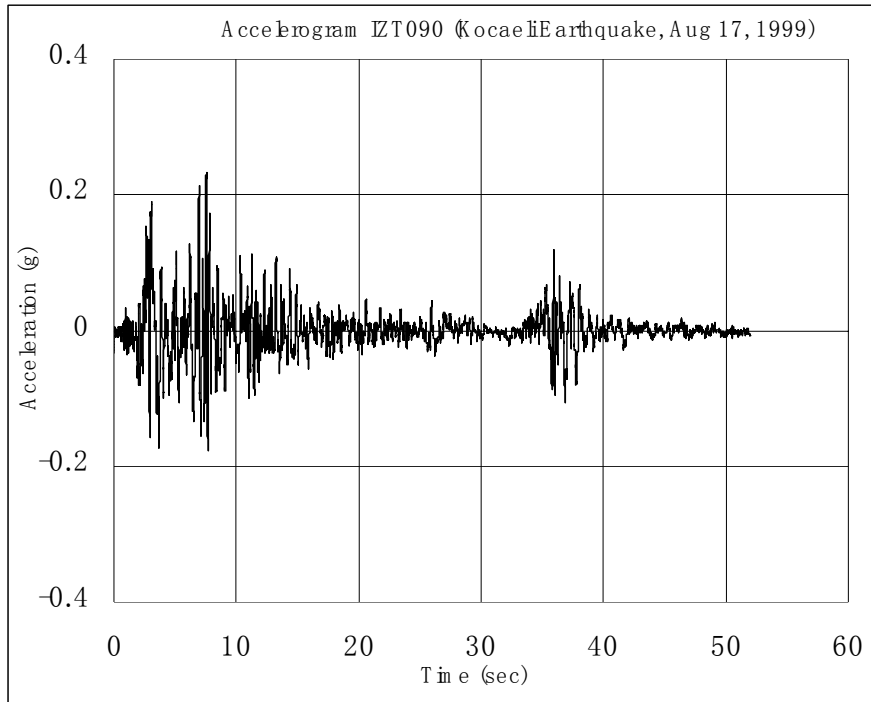
Figure A.7   Accelerations Recorded in Izmit (090 Component)

Figure A.8   Accelerations Recorded in Izmit (180 Component)

138

Figure A.9   Accelerations Recorded in Sakarya (090 Component)

Accelerogram YPT330 (Kocaeli Earthquake, Aug 17, 1999)

Figure A.10   Accelerations Recorded in Yarimca (330 Component)

Accelerogram YPT348 (Kocaeli Earthquake, Aug 17, 1999)

Figure A.11   Accelerations Recorded in Yarimca (348 Component)

140

A.2 ACCELERATION RECORDS FORM DÜZCE EARTHQUAKE

Figure A.12   Accelerations Recorded in Bolu (000 Component)

Figure A.13   Accelerations Recorded in Bolu (090 Component)

141

Figure A.14   Accelerations Recorded in Düzce (180 Component)

Figure A.15   Accelerations Recorded in Düzce (270 Component)

142

Appendix B: Elastic Response Spectra

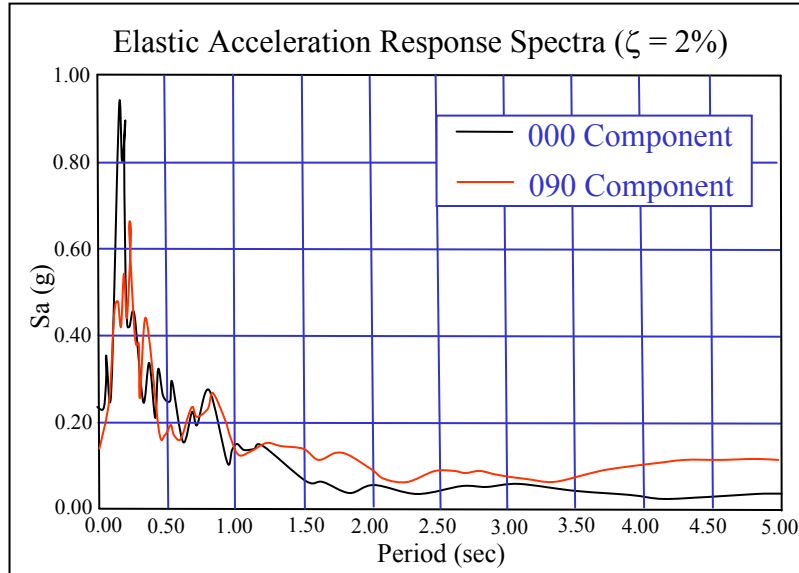**B.1 ELASTIC ACCELERATION RESPONSE SPECTRA FROM KOCAELI EARTHQUAKE**

Figure B.1 Acceleration Response Spectra for Ground Motion in Arcelik
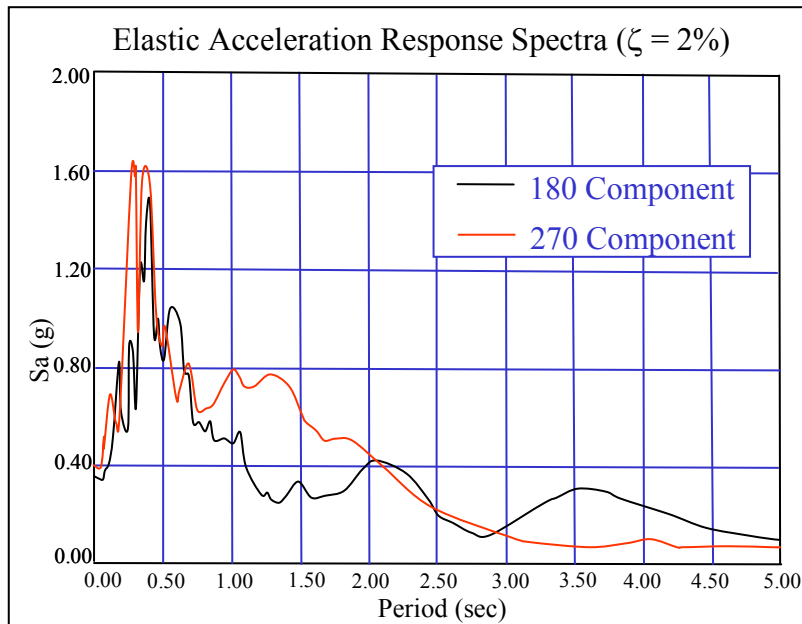

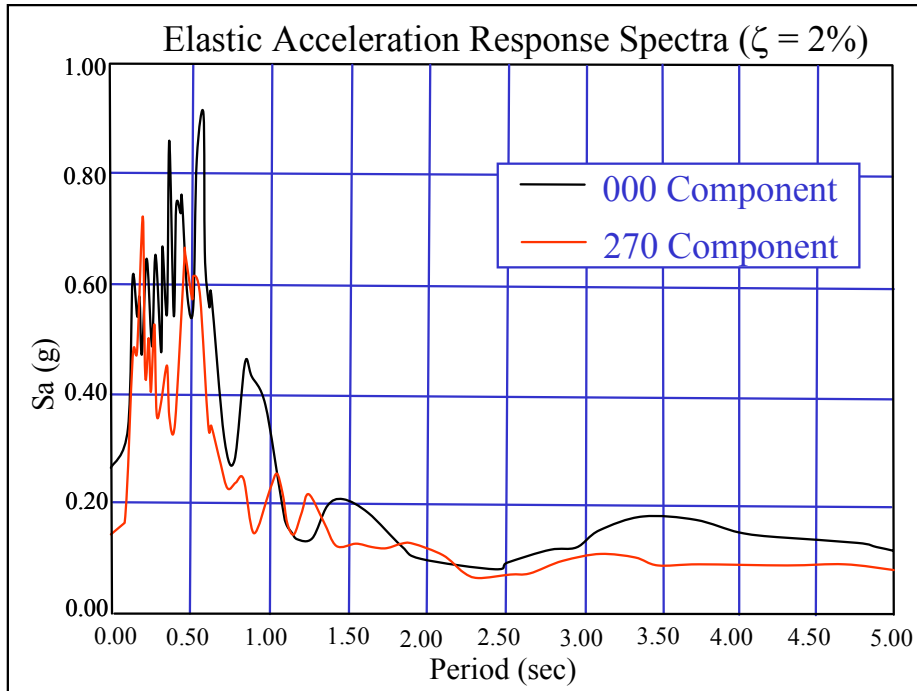Figure B.2 Acceleration Response Spectra for Ground Motion in Düzce

Figure B.3 Acceleration Response Spectra for Ground Motion in Gebze
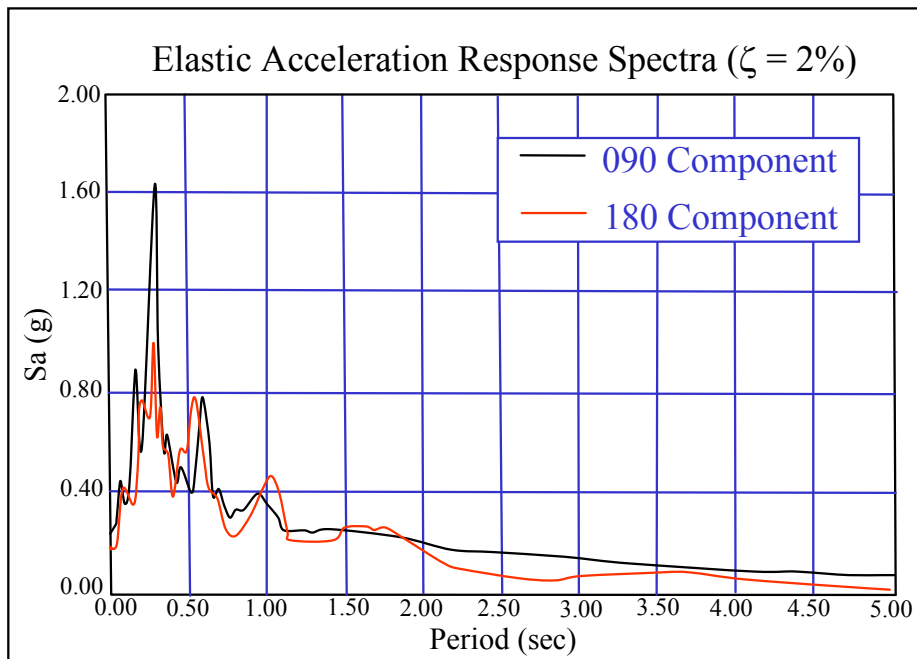

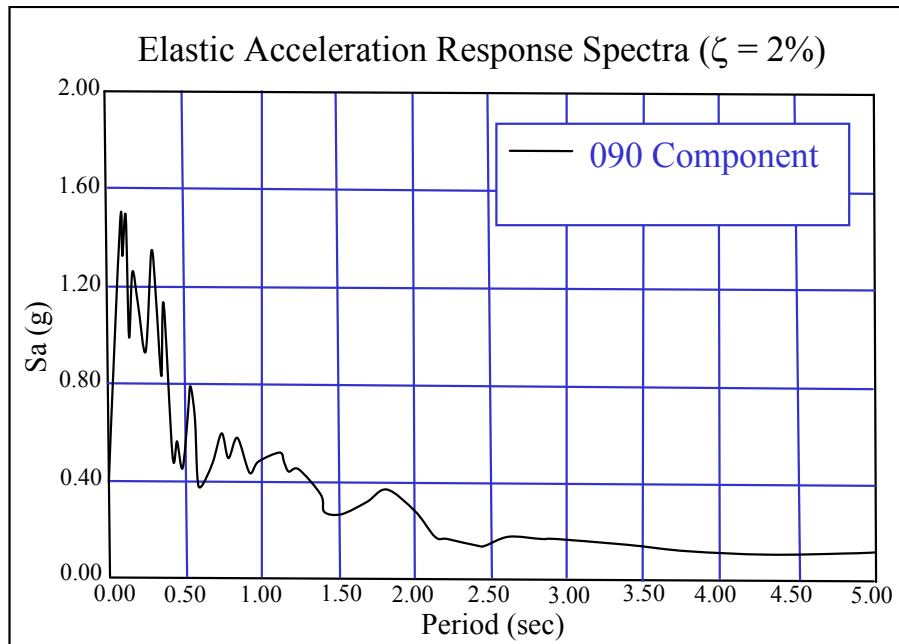Figure B.4 Acceleration Response Spectra for Ground Motion in Izmit

144

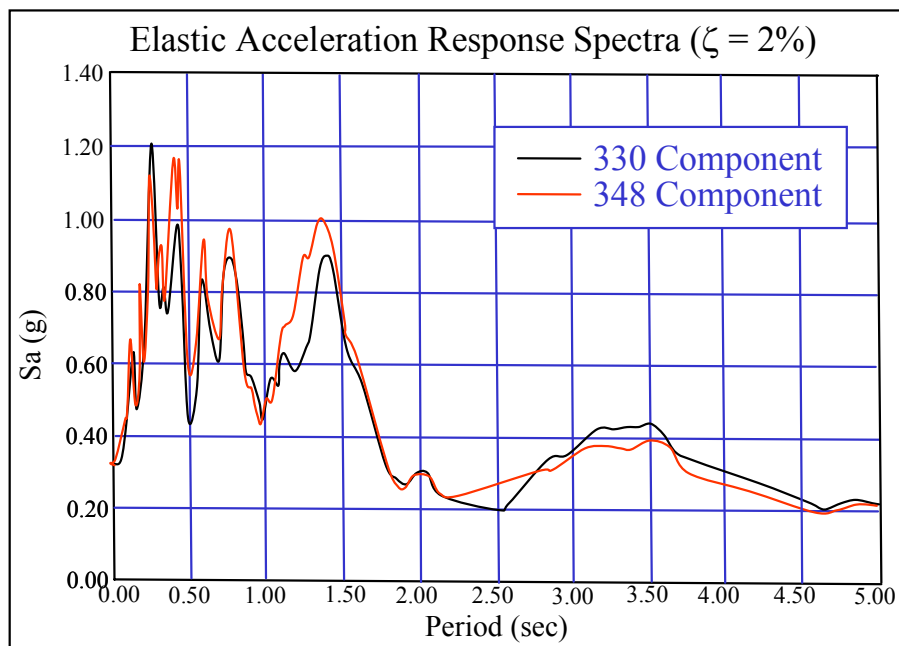Figure B.5 Acceleration Response Spectra for Ground Motion in Sakarya

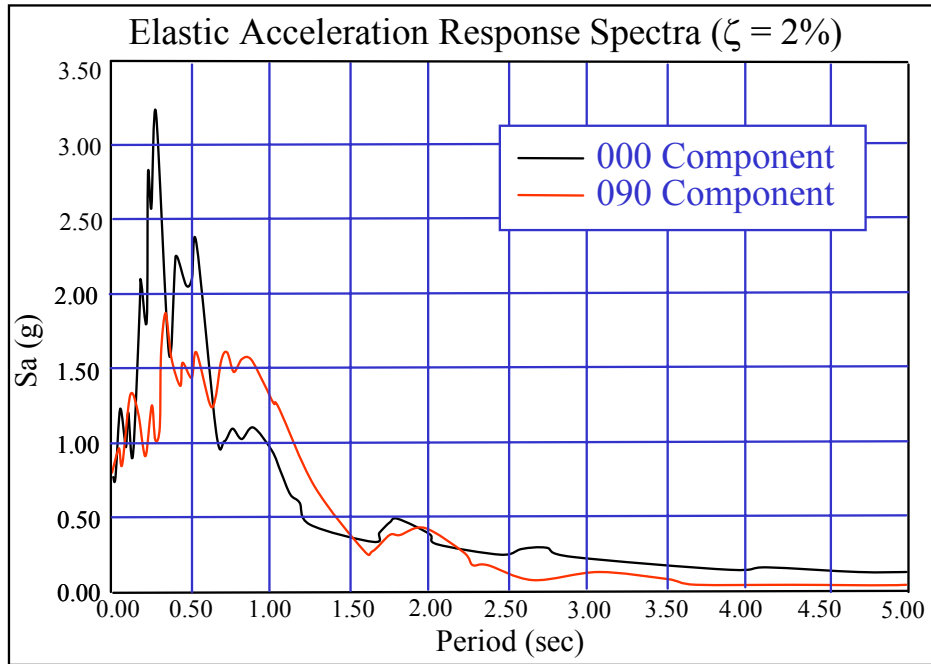Figure B.6 Acceleration Response Spectra for Ground Motion in Yarimca

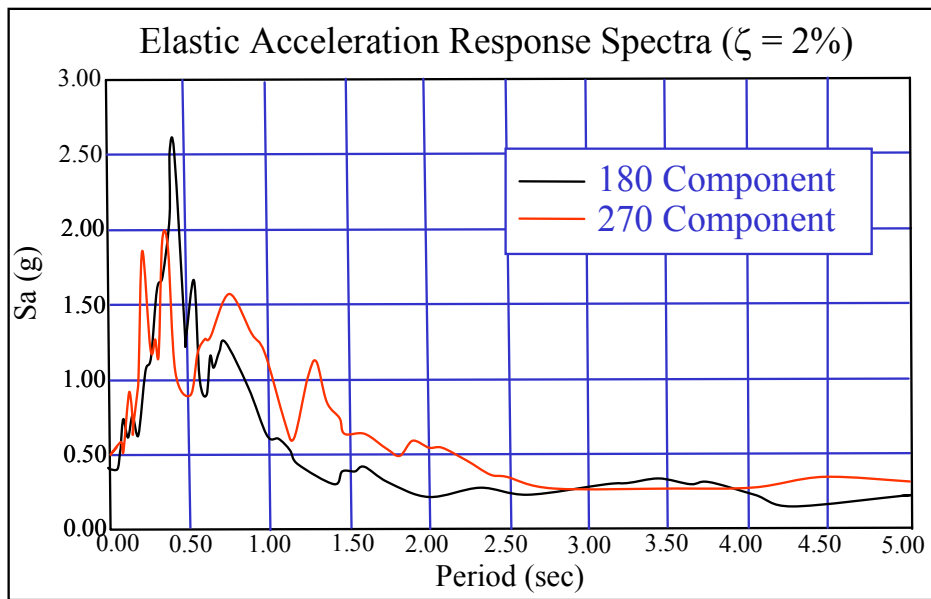Figure B.7 Acceleration Response Spectra for Ground Motion in Bolu

Figure B.8 Acceleration Response Spectra for Ground Motion in Düzce

146

Appendix C: Seismic Analysis Methods

C.1 GENERAL PRINCIPLE

Earthquakes could come in any directions. When an earthquake comes in a direction other than the main axial directions of a structure, the structure will respond in longitudinal and transverse direction simultaneously. This kind of coupling effect on structures and structural members will complicate the structural analyses.

For a building with a rectangular plan, the measure usually taken in engineering is skirting around the coupling effects. Instead, only considered are the structural responses with ground motions coming in the longitudinal and transverse directions. If the structure is proven adequate for the considered earthquakes in both main directions, it is then believed to be able to survive the earthquakes coming in any directions.

The analyses on the one-story industrial buildings conducted in this study follow this general principle, i.e. only the structural responses under the earthquakes coming in the longitudinal and transverse directions are analyzed. The final rehabilitation scheme is built on the basis of the analysis results assuming earthquakes coming in these two directions.

C.2 MODAL ANALYSIS

The modal analysis focuses on the linear elastic behavior of the structure. The basic theory of modal analysis used in this study is summarized as follows.

After a discrete structural analytical model with degree of freedom N has been constructed, the governing equation of the dynamic response of the structure to the ground motion is written as:

$$[M]\{\ddot{u}_t\} + [C]\{\dot{u}_t\} + [K]\{u_t\} = \{0\}$$

(C.1)

where [M], [C] and [K] are respectively the mass matrix, damping matrix and initial stiffness matrix of the structure model, $\{u_t\}, \{\dot{u}_t\}$ and $\{\ddot{u}_t\}$ are respectively the vectors of the absolute nodal displacements, velocities and accelerations. $\{0\}$ indicates that there is no excitation other than the ground motion.

Denoting the displacement relative to the moving ground as $\{u\}$ and the motion of ground as u_g, the total nodal displacement vector can be written as:

$$\{u_t\} = \{u\} + \{1\}u_g \qquad \text{(C.2)}$$

where $\{1\}$ is a vector with all components being 1.

Noticing that damping and stiffness matrices are corresponding to the velocities and displacements relative to each other, the rigid body motion does not induce any damping or elastic forces, i.e. $[C]\{1\} = \{0\}$ and $[K]\{1\} = \{0\}$. Using these two equations together with Eq. C.2 in Eq. C.1, the governing equation is expressed in the structural motion relative to the ground:

$$[M]\{\ddot{u}\} + [C]\{\dot{u}\} + [K]\{u\} = -[M]\{1\}\ddot{u}_g \qquad \text{(C.3)}$$

The relative displacement vector at any time can be regarded as a linear combination of the mode shapes.

$$\{u\} = [\Phi]\{q\} \qquad \text{(C.4)}$$

where $[\Phi]$ is a matrix comprising the mode shapes, in which the ith column, notated as $\{\varphi_i\}$, represents the shape of mode i, $\{q\}$ can be considered as the displacement vector measured in a new coordinate system, in which the base vectors are in the directions of mode shape vectors.

Using Eq. C.4 in Eq. C.3:

$$[M][\Phi]\{\ddot{q}\} + [C][\Phi]\{\dot{q}\} + [K][\Phi]\{q\} = -[M]\{1\}\ddot{u}_g \qquad \text{(C.5a)}$$

Multiplying both sides of Eq. C.5 with the transposition of $[\Phi]$:

$$[\Phi]^T[M][\Phi]\{\ddot{q}\} + [\Phi]^T[C][\Phi]\{\dot{q}\} + [\Phi]^T[K][\Phi]\{q\} = -[\Phi]^T[M]\{1\}\ddot{u}_g \qquad \text{(C.5b)}$$

148

In Eq.C.5b, because the mode shapes are orthogonal to each other about the mass matrix [M] and stiffness matrix [K], i.e. $\{\varphi_i\}^T[M]\{\varphi_j\} = 0$ and $\{\varphi_i\}^T[K]\{\varphi_j\} = 0$ unless i = j, the products $[\Phi]^T[M][\Phi]$ and $[\Phi]^T[K][\Phi]$ are both diagonal matrixes, with those components that are not in their main diagonal to be zero. If the Rayleigh damping form is used, matrix [C] can be interpreted as a linear combination of [M] and [K]:

$$[C] = \beta_1[M] + \beta_2[K] \tag{C.6}$$

where β_1 and β_2 are predefined constants, the product $[\Phi]^T[C][\Phi]$ then can also be transformed into a diagonal matrix. Rayleigh damping has been proven an acceptable form for the modal analyses of multi-degree-freedom systems.

With Raileigh damping, Eq. C.5 can be written as N equations of the form:

$$m_{p,i}\ddot{q}_i + c_{e,i}\dot{q}_i + k_{e,i}q_i = -\mu_i\ddot{u}_g , \quad i = 1, 2, 3...N \tag{C.7}$$

where:

$$m_{p,i} = \{\varphi_i\}^T[M]\{\varphi_i\} = \sum_{j=1}^{N}M_{j,j}\varphi_{i,j}^2 \quad \text{participating mass of mode i;}$$

$$c_{e,i} = \{\varphi_i\}^T[C]\{\varphi_i\} \quad \text{effective damping coefficient for mode i;}$$

$$k_{e,i} = \{\varphi_i\}^T[K]\{\varphi_i\} \quad \text{effective stiffness of mode i;}$$

$$\mu_i = \sum_{j=1}^{N}M_{j,j}\varphi_{i,j}$$

Defining the ratio $r_i = \dfrac{\mu_i}{m_{p,i}}$ as participation factor of model i, and dividing both sides of Eq. C.7 by $m_{p,i}$:

$$\ddot{q}_i + \frac{c_{e,i}}{m_{p,i}}\dot{q}_i + \frac{k_{e,i}}{m_{p,i}}q_i = -r_i\ddot{u}_g , \quad i = 1, 2, 3...N \tag{C.8}$$

Further, defining angular frequency $\omega_i = \sqrt{\dfrac{k_{e,i}}{m_{p,i}}}$ and effective damping ratio $\zeta_i = \dfrac{c_{e,i}}{2m_{p,i}\omega_i}$, Eq. C.8 can be written in the form:

$$\ddot{q}_i + 2\zeta_i\omega_i\dot{q}_i + \omega_i^2 q_i = -r_i\ddot{u}_g , \quad i = 1, 2, 3...N \tag{C.9}$$

149

The participation factor r_i is dependant on the shape as well as the scale of $\{\varphi_i\}$. If $\{\varphi_i\}$ represents a mode shape of a MDOF system, the product of $\{\varphi_i\}$ and an arbitrary nonzero scalar α must be the shape of the same mode of this system. Apparently, $\alpha\{\varphi_i\}$ leads to a different participation factor r_i than that of $\{\varphi_i\}$. From the definitions of ω_i and ζ_i, it can be stated that ω_i and ζ_i are independent of the scale of the mode shape.

Compare Eq. C.9 with the differential equation for a SDOF system:

$$\ddot{u} + 2\zeta\,\omega\dot{u} + \omega^2 u = -\ddot{u}_g \tag{C.10}$$

The only difference between Eq. C.9 and C.10 is the participating factor r_i. As any arbitrary displacement shape may be represented as a linear combination of the mode shapes, Eq. C.9 and C.10 actually provide a way to solve seismic response of MDOF system by linearly combining a series of responses of different SDOF systems. For a particular ground motion $\ddot{u}_g(t)$, if $u(t)$ is the response of a SDOF system with frequency ω_i and damping ratio ζ_i, then $r_i u(t)\{\varphi_i\}$ must be the response of the ith mode of the MDOF structure.

In the same way, if the maximum displacement of a SDOF system with ω_i and ζ_i is determined as $S_{d,i}$ using the displacement response spectrum, then the spectral displacements of the corresponding mode of the MDOF system will be $r_i S_{d,i}\{\varphi_i\}$. Generally, the response of a MDOF system is dominated by several lowest modes, therefore even for a system with a large number of DOF, the modes required to be taken into account to estimate the structural seismic response would be limited. The number of modes included in the calculation is usually determined by effective mass $m_{e,i}$, which is defined as:

$$m_{e,i} = \frac{\left(\sum_{j=1}^{N} M_{j,j} \varphi_{i,j} \right)^2}{\left(\sum_{j=1}^{N} M_{j,j} \varphi_{i,j}^2 \right)}$$

(C.11)

In the modal analyses of this study, a sufficient number of modes are included such that at least 90% of the total mass of the structure is under consideration.

The modal maxima of the considered modes determined from the response spectrum need to be combined in some way to represent the maximum response of the actual structure, because the modal maxima of different modes do not occur at the same time. The procedure used in this study is called Square Root of the Sum of the Squares (SRSS) developed by Newmark. If the modal maxima corresponding to the considered modes are $d_1, d_2, d_3 \cdots d_n$, the maximum total response of the structure is estimated using: $d = \sqrt{d_1^2 + d_2^2 + d_3^2 + \cdots + d_n^2}$. For structures with well separated frequencies, the SRSS combination of modal maxima is within ±10-15% of the actual maximum total response.

From the introduction above, it can be concluded that if the constant damping ratio 2% is used for all the modes of a structures, the key features that determine the structural response are the angular frequencies and corresponding mode shapes. In this study, modal analyses are conducted using SAP2000 program mainly to determine the maximum displacements of structures.

C.3 STATIC ANALYSIS

This type of method consists of two sub-types: equivalent lateral force method and displacement-controlled push-over analysis. A structural analytical model, which could include the inelastic properties of structural members, is required for both kinds of static methods.

The equivalent lateral force method usually follows the steps listed below:

1)   Develop elastic response spectra (acceleration and displacement) based on the earthquake history in a particular geographic region.

2)   Estimate the fundamental period T of the structure under analysis.

3)   Determine design base shear from response spectrum using:

$$V = \frac{S_a \times m}{R}$$

where V is the maximum design base shear, S_a is the spectral acceleration corresponding to the fundamental period T, m is the mass of the structure under consideration, R is an experiential force reducer when the inelastic properties are included in the analytical structural model. $S_a \times m$ is actually the maximum base shear that an elastic SDOF system with mass m and fundamental period T would experience during the considered earthquakes. When a structure behaves inelastically, the maximum base shear should be less than $S_a \times m$, and then R is larger than 1.0. If inelasticity is not considered, R should be set to 1.0.

4)   Distribute the base shear V to the structure (horizontally and vertically) in a proper pattern.

The load pattern affects the structural response dramatically. The two main factors considered in the load pattern are mass distribution and the vibration shape of the first mode of the structure. Usually, the modal shape is estimated very coarsely, but it might be adequate for a primary design.

5)   Run static analysis and investigate the behaviors of structure as well as structural members (displacements, deformations, internal forces, etc.).

As can be seen, all the procedure of the equivalent lateral force method is based on the estimation of the base shear that the structure could see during considered earthquakes. If a structure responds inelastically, it is actually difficult to estimate the

152

structural response based on the forces with a high accuracy because the structure becomes too sensitive to forces after yielding. In order to ensure the safety of the structure, engineers have to use smaller force reducer R which leads to more conservative designs.

The researches have revealed that the responses of structures could be calculated more reliably based on displacements instead of forces, and the displacements of structures under earthquakes could be estimated with fairly high accuracy (Shimazaki and Sozen, 1984). The displacement-controlled push-over analysis was developed based on the structural displacement estimation, and it is used for this study. With acceptable simplifications, the displacement-controlled push-over analyses of one-story precast industrial buildings could be performed with high efficiency and high accuracy. Appendix C only summarizes the main steps taken by the displacement-controlled push-over analysis, the detailed modeling and formulation are illustrated in Chapter 5.

The displacement-controlled push-over analysis used in this study assumes the structural response is dominated by the first mode, i.e. the effective mass ration of the first mode is larger than 75%, and the effect of all the higher modes is negligible. The steps taken by displacement controlled push-over analyses are given below:

1)   Develop elastic response spectra (acceleration and displacement).

2)   Estimate the fundamental period T. With a simplified model (shown in Chapter 5) of the prototype building, T can be quickly estimated with a great accuracy.

3)   Select a control node close to the roof center of the prototype building. The displacement of this control node will be monitored through the push-over.

4)   Estimate the first mode shape $\{\varphi_1\}$, This can be accomplished easily with the simplified model described in Chapter 5.

5)   Determine load pattern based on mass distribution and the shape of the first mode, $f_j = \eta M_{j,j} \varphi_{1,j}$, where η is uniform throughout the structure.

153

6)   Calculate the target displacement Δ_t at the control point. With the estimated period T, the spectral displacement S_d can be determined with the spectra shown in section 2.3. According to the introduction in section C.2, the maximum displacement for this MDOF system should be $r_1 S_d \{\varphi_1\}$. The maximum displacement corresponding to the control node is set to Δ_t.

7)   Increase η from 0, but keep the load pattern, and monitor the displacement of the control node until the target displacement Δ_t is reached;

8)   Investigate the behaviors of structure as well as structural members (displacements, deformations, internal forces, etc.).

As static analysis is the most widely used in real engineering, the development of a feasible static method is of great value. Just like modal analysis, the estimation of period and shape of the fundamental mode plays an essential role in static analyses.

C.4   TIME HISTORY ANALYSIS

To perform a time history analysis on a finite element model, it is necessary to discretize the forcing function and the response. For seismic analysis, the forcing function is given in the form of acceleration of the ground motion, which is usually provided to the structural engineers at discrete instants in time. Therefore, the major concern in performing a time history analysis is the discretization of the system response.

The equilibrium equation of a MDOF system with inelasticity has the same form as Eq. C.3, in which only the linear elastic behavior is considered.

$$[M]\{\ddot{u}(t)\} + [C]\{\dot{u}(t)\} + [K]\{u(t)\} = -[M]\{1\}\ddot{u}_g(t)$$
(C.12)

But now, the stiffness matrix [K] is not constant any more, instead, it varies with the displacement {u} inelastically. Therefore, the numerical analysis has to be performed by iterations, and [K] will be updated in each step.

Given all the response and ground motion information at time t_n, the three response quantities that are desired at time t_{n+1} are the displacement, velocity and the acceleration of the system. It should be mentioned that in an inelastic case, the stiffness matrix [K] is generally varying between time t_n and t_{n+1}. In this study, [K] calculated with the displacement at time t_n is used as constant through the time interval between t_n and t_{n+1}. This might bring some error, but if the time step size $\Delta t = t_{n+1} - t_n$ is small enough, this approximation should be acceptable. Actually, in this study, the time step size is selected as short as 0.0001s, much smaller than the general size (0.01s) selected for linear elastic analyses.

The other two equations simultaneously working with Eq. C.12 to compute the response at time t_{n+1} are given as:

$$\{\dot{u}(t)\} = \frac{d\{u(t)\}}{dt}, \ \{\ddot{u}(t)\} = \frac{d\{\dot{u}(t)\}}{dt} \tag{C.13a}$$

Eq. C.13 can be rewritten in integrals instead of the differential forms:

$$\{\dot{u}_{n+1}\} = \{\dot{u}_n\} + \int_{t_n}^{t_{n+1}} \{\ddot{u}(s)\}ds, \ \{u_{n+1}\} = \{u_n\} + \int_{t_n}^{t_{n+1}} \{\dot{u}(s)\}ds \tag{C.13b}$$

The equilibrium equation Eq. C.12 for the response at time t_{k+1} then can be written as:

$$[M]\{\ddot{u}_{n+1}\} + [C]\{\dot{u}_{n+1}\} + [K_n]\{u_{n+1}\} = -[M]\{1\}\ddot{u}_{g,n+1} \tag{C.14}$$

To discretize the integrands in Eq. C.13b, it is necessary to approximate the continuous acceleration function $\{\ddot{u}(t)\}$. In this study, this is carried out using Newmark-β method, the most common numerical integration method used by structural engineers. According to this method, Eq. C.13b is replaced by:

$$\{\dot{u}_{n+1}\} = \{\dot{u}_n\} + (1-\delta)\Delta t\{\ddot{u}_n\} + \delta\Delta t\{\ddot{u}_{n+1}\} \tag{C.15a}$$

$$\{u_{n+1}\} = \{u_n\} + \{\dot{u}_n\}\Delta t + (0.5-\alpha)(\Delta t)^2\{\ddot{u}_n\} + \alpha(\Delta t)^2\{\ddot{u}_{n+1}\} \tag{C.15b}$$

where δ and α are predefined constants. Substituting Eq. C.15 into Eq. C.14 gives an equation in which only $\{\ddot{u}_{n+1}\}$ is unknown. Solving the equation for $\{\ddot{u}_{n+1}\}$ and using the result back to Eq. C.15, the other two concerned quantities, $\{\dot{u}_{n+1}\}$ and $\{u_{n+1}\}$ at time t_{n+1} can be calculated. Then a new iteration step starts for the response at time t_{n+2} and so on.

One major concern that must be addressed when performing a time history analysis by numerical iterations is the numerical stability. In the Newmark-β method, the selection of the constants δ and α dramatically affects the convergence of the solution. In structural dynamics, the combination of $\delta = 0.5$ and $\alpha = 0.25$ are generally used because it has been shown to have a high degree of numerical stability. For this reason, this combination is selected for the time history analyses of this study. With this selection, Eq. C.15 becomes:

$$\{\dot{u}_{n+1}\} = \{\dot{u}_n\} + \frac{1}{2}(\{\ddot{u}_n\} + \{\ddot{u}_{n+1}\})\Delta t \qquad (C.16a)$$

$$\{u_{n+1}\} = \{u_n\} + \{\dot{u}_n\}\Delta t + \frac{1}{4}(\{\ddot{u}_n\} + \{\ddot{u}_{n+1}\})(\Delta t)^2 \qquad (C.16b)$$

Newmark-β method then turns out as so-called constant-average-acceleration method, which assumes that the acceleration is constant within each time interval, and its magnitude is equal to the average of the acceleration at the beginning and at the end of the time interval, i.e.

$$\{\ddot{u}(t)\} = \frac{1}{2}(\{\ddot{u}_n\} + \{\ddot{u}_{n+1}\}) \qquad t_n \le t \le t_{n+1} \qquad (C.17)$$

Using Eq. C.16 in Eq. Eq. C.14 gives the linear equation group for unknown $\{\ddot{u}_{n+1}\}$ in the form:

$$[A]\{\ddot{u}_{n+1}\} = \{f\} \qquad (C.18)$$

where:

$$[A] = [M] + \frac{\Delta t}{2}[C] + \frac{(\Delta t)^2}{4}[K_n] \qquad (C.19a)$$

156

$$\{f\} = -[M]\{1\}\ddot{u}_{g,n+1} - [C]\left(\{\dot{u}_n\} + \frac{\Delta t}{2}\{\ddot{u}_n\}\right) - [K_n]\left(\{u_n\} + \Delta t\{\dot{u}_n\} + \frac{(\Delta t)^2}{4}\{\ddot{u}_n\}\right) \quad \text{(C.19b)}$$

By solving Eq. C.19, and substituting the result into Eq. C.16, all the response quantities at time t_{n+1} are obtained. As described, both the formulating and the computation implementation of time history analysis are much more complicated than the process of the static method. As a large number of iterations are usually involved in the analysis on a single ground motion record, the time history analysis takes a lot of computation time and apparently it can hardly be used in the primary design.

Appendix D: Stress Distribution in Strengthening Steel Plates

Case 1, Applied Forces (unit: KN)
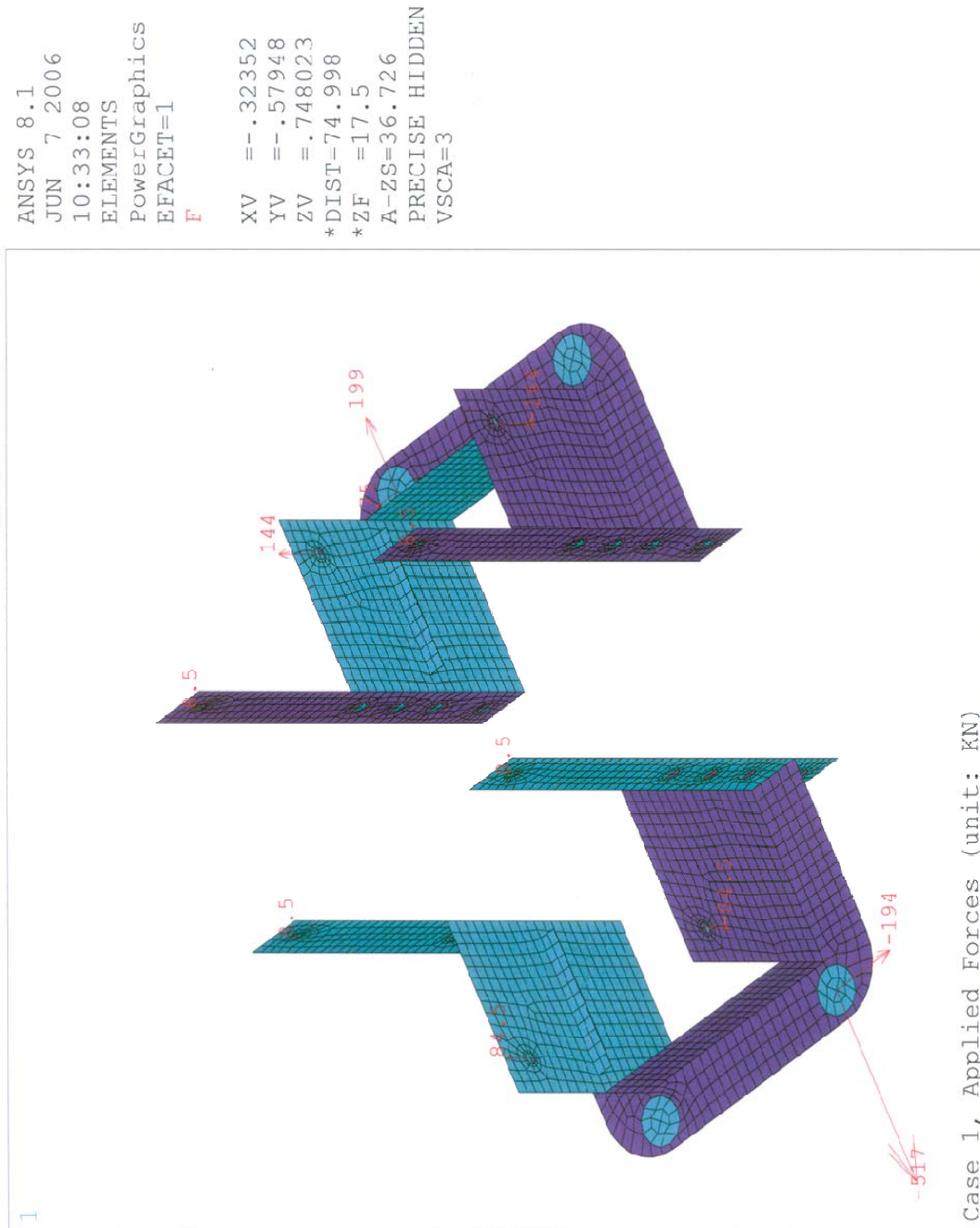
Figure D.1 Applied Forces of Case 1

158

ANSYS 8.1
JUN 7 2006
10:40:44
ELEMENT SOLUTION
STEP=1
SUB =1
TIME=1
SEQV (NOAVG)
MIDDLE
PowerGraphics
EFACET=1
DMX =.266224
SMN =.001424
SMX =32.826
.001424
3.649
7.296
10.943
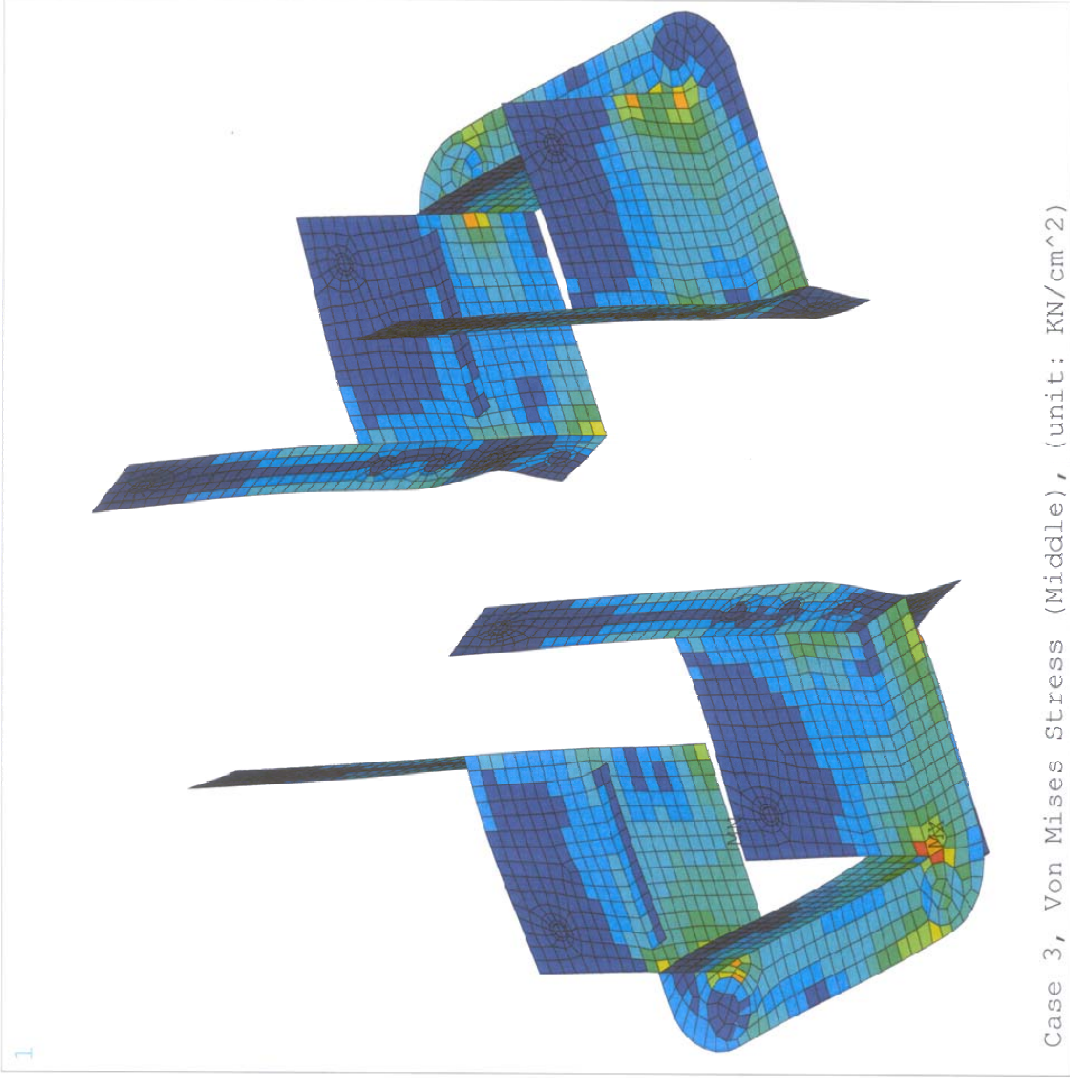14.59
18.237
21.885
25.532
29.179
32.826
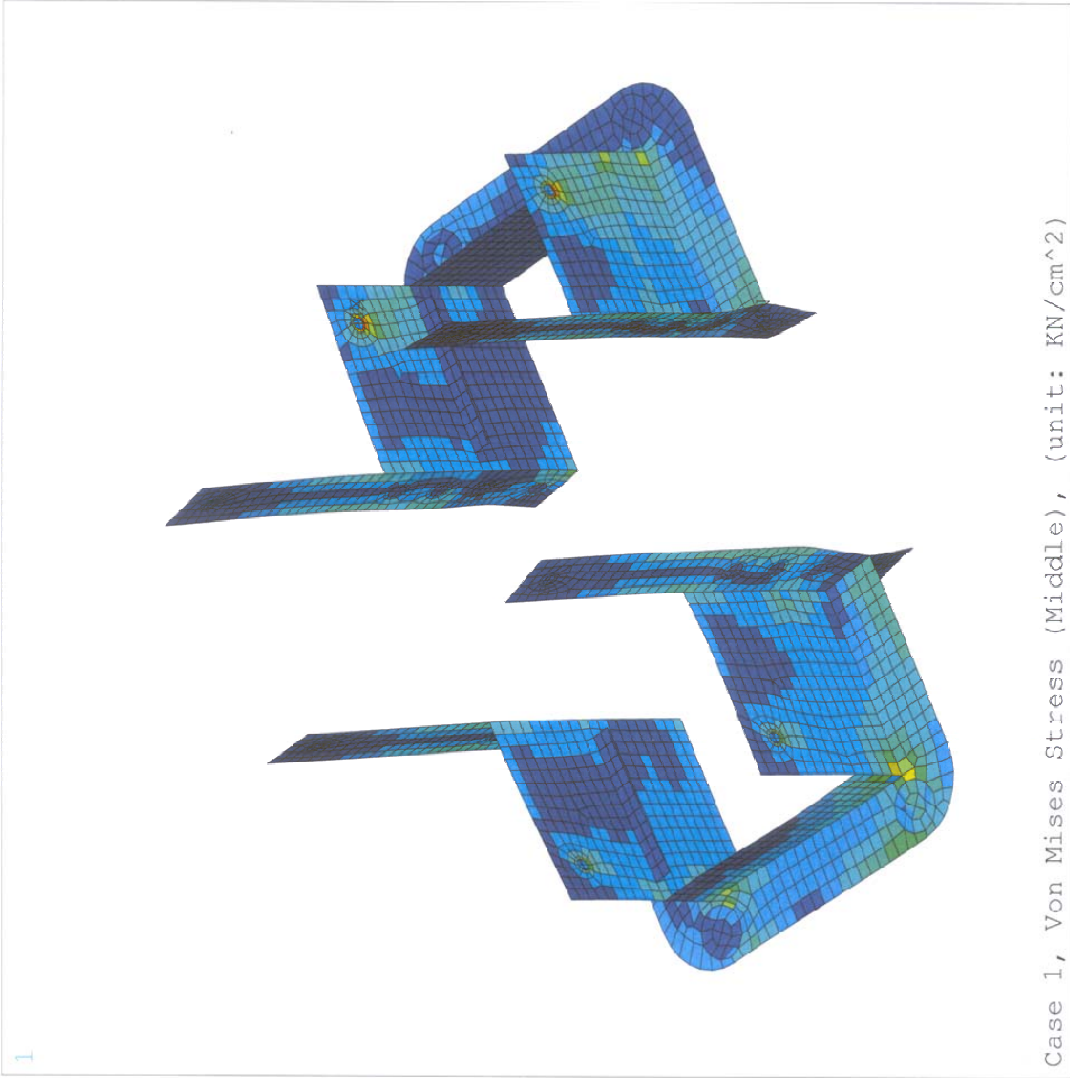
Case 1, Von Mises Stress (Middle), (unit: KN/cm^2)

Figure D.2 Von Mises Stress (Middle) of case 1

159

```
ANSYS 8.1
JUN  7 2006
10:38:14
ELEMENT SOLUTION
STEP=1
SUB =1
TIME=1
SEQV    (NOAVG)
PowerGraphics
EFACET=1
DMX =.266224
SMN =.0325
SMX =34.5
        .0325
        3.862
        7.692
        11.522
        15.351
        19.181
        23.011
        26.841
        30.67
        34.5
```
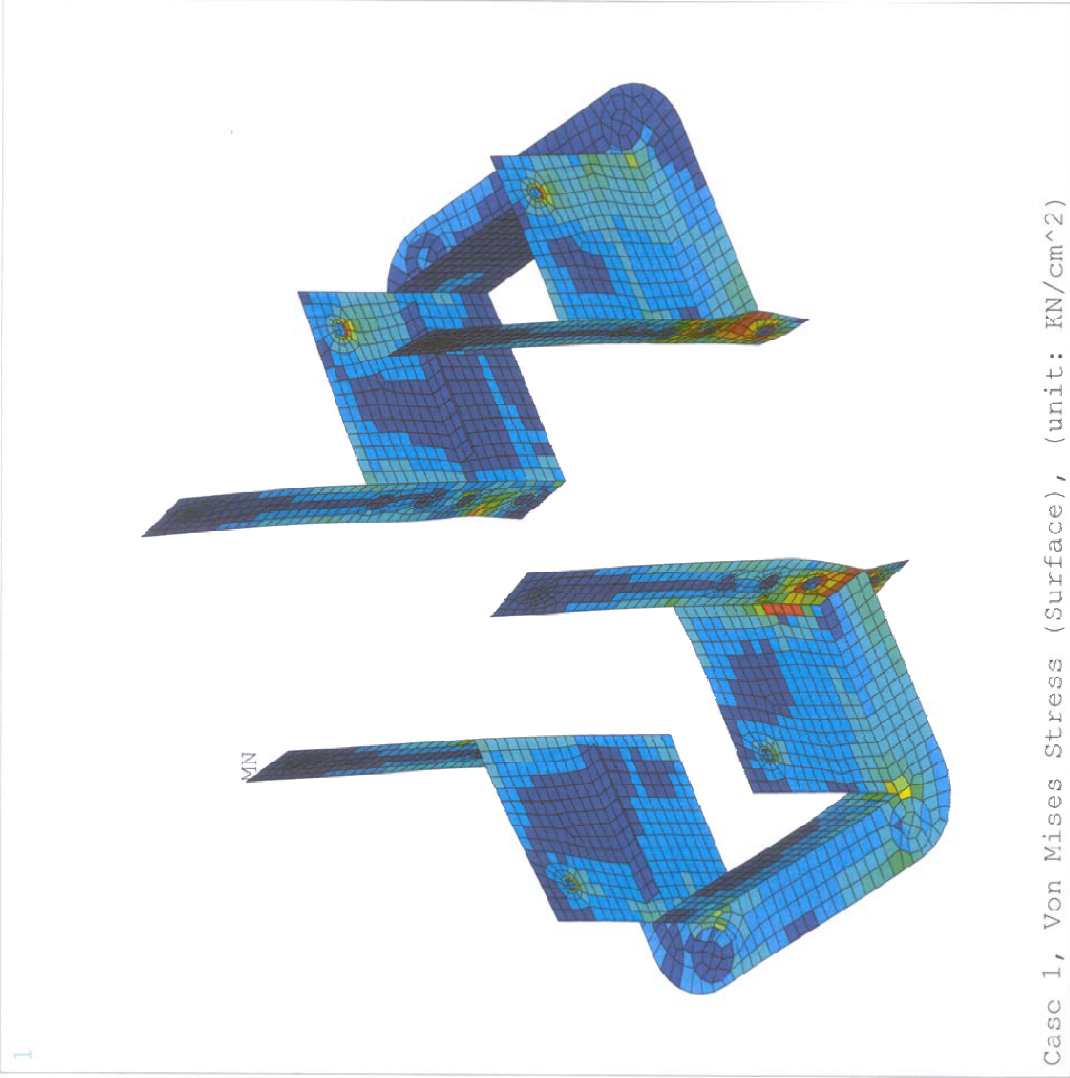
Case 1, Von Mises Stress (Surface), (unit: KN/cm^2)

Figure D.3 Von Mises Stress (Surface) of case 1

ANSYS 8.1
JUN 7 2006
10:53:23
ELEMENTS
PowerGraphics
EFACET=1
REAL NUM
F

XV =-.373889
YV =-.636534
ZV =.67456
*DIST=75.579
*XF =8.971
*YF =-4.628
*ZF =18.105
A-ZS=40.255
PRECISE HIDDEN
VSCA=2
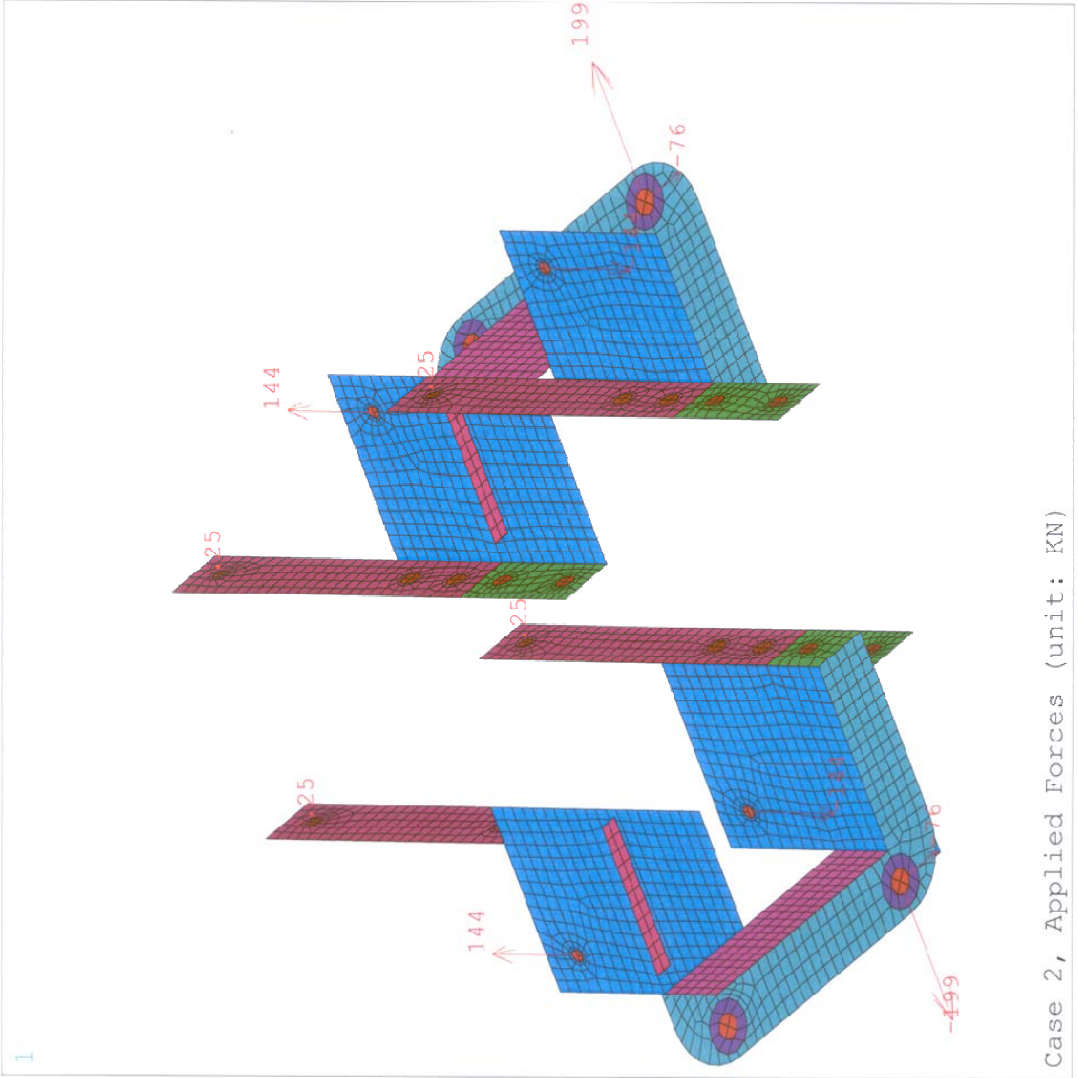
Case 2, Applied Forces (unit: KN)
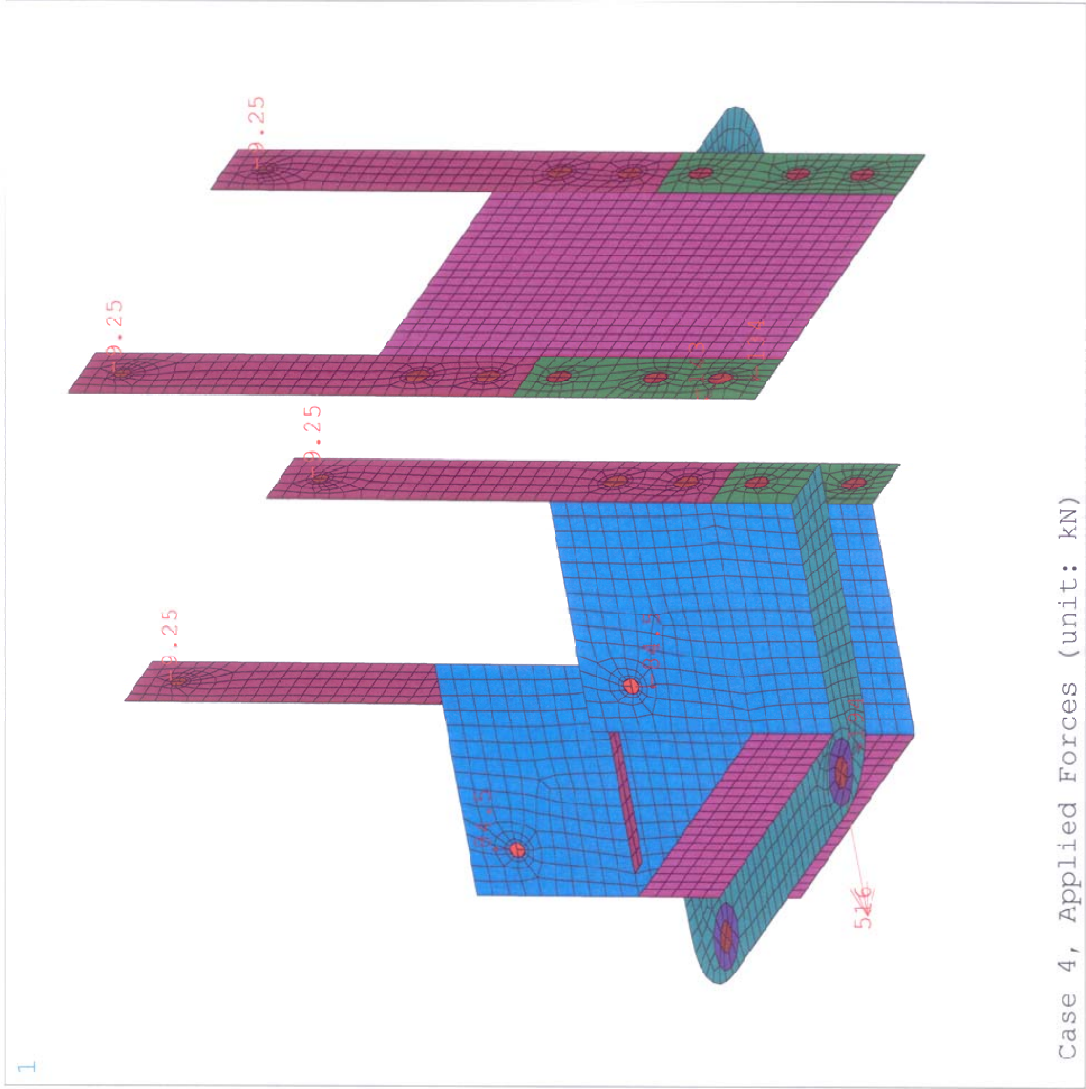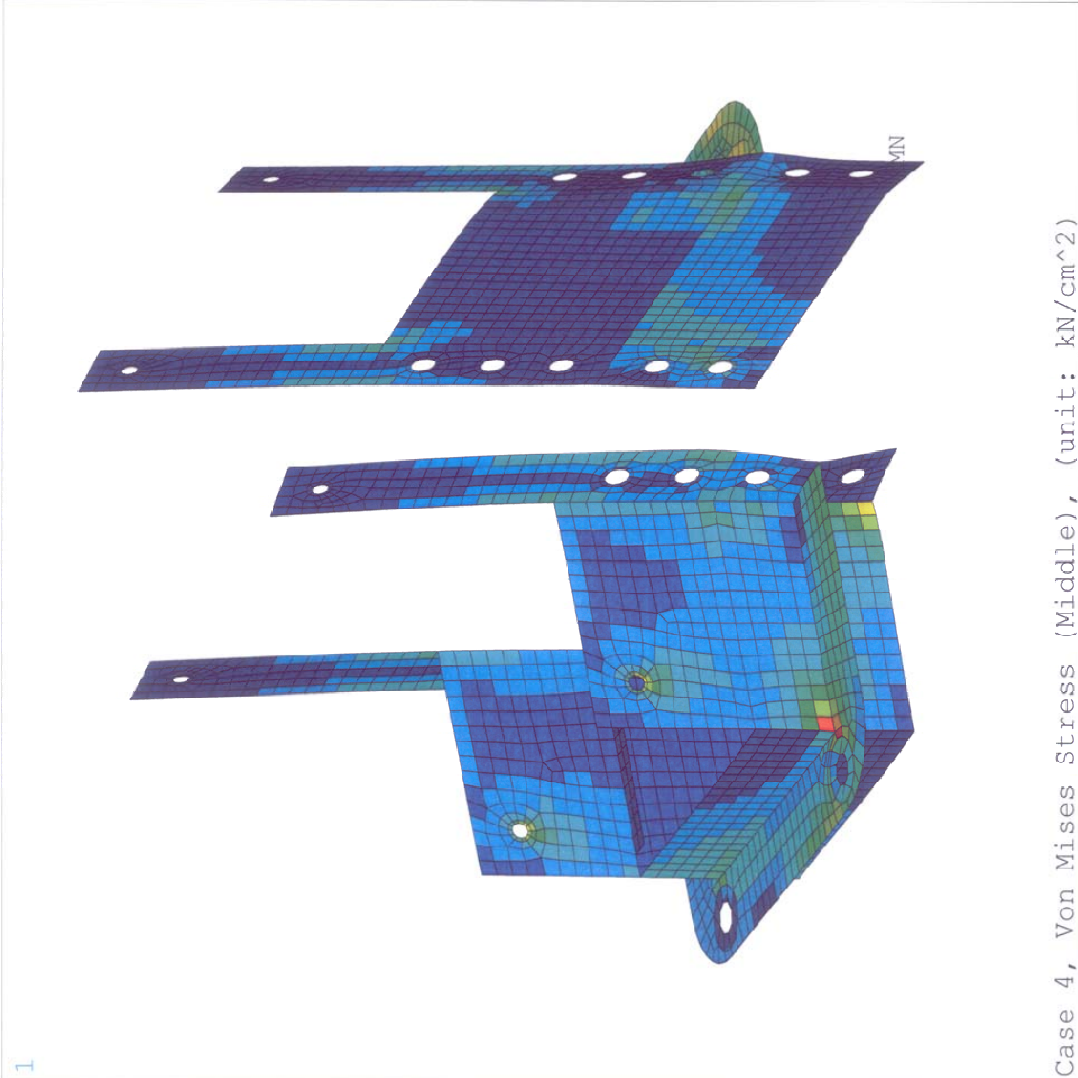
Figure D.4 Applied Forces of Case 2

161

ANSYS 8.1
JUN 7 2006
10:58:25
ELEMENT SOLUTION
STEP=1
SUB =1
TIME=1
SEQV (NOAVG)
MIDDLE
PowerGraphics
EFACET=1
DMX =.036426
SMN =.001106
SMX =32.997

.001106
3.667
7.334
11
14.666
18.332
21.998
25.665
29.331
32.997
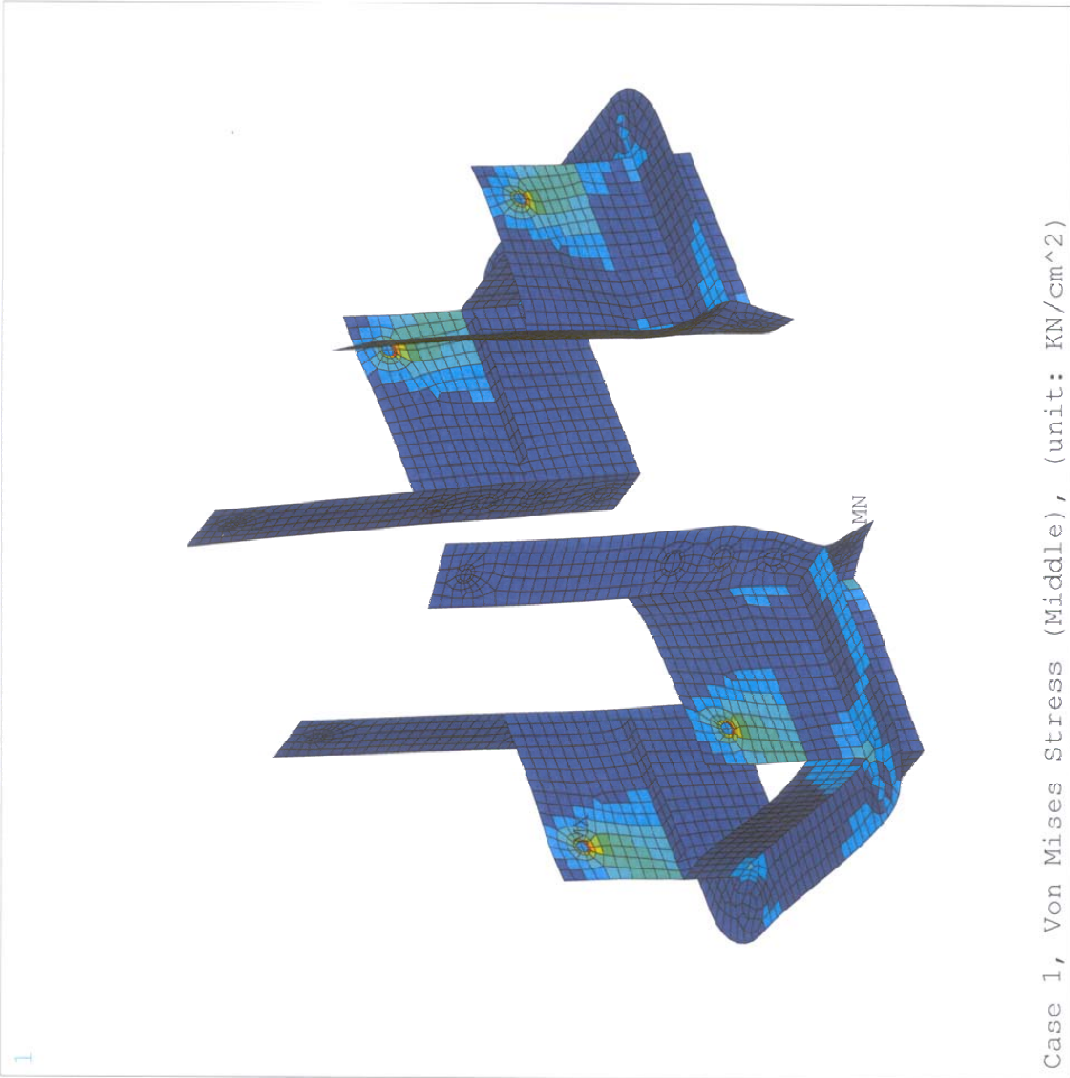
Case 1, Von Mises Stress (Middle), (unit: KN/cm^2)

Figure D.5 Von Mises Stress (Middle) of case 2

162

ANSYS 8.1
JUN 7 2006
10:57:54
ELEMENT SOLUTION
STEP=1
SUB =1
TIME=1
SEQV   (NOAVG)
PowerGraphics
EFACET=1
DMX = .036426
SMN = .001147
SMX =33.165
     .001147
    3.686
    7.371
    11.056
    14.741
    18.426
    22.11
    25.795
    29.48
    33.165
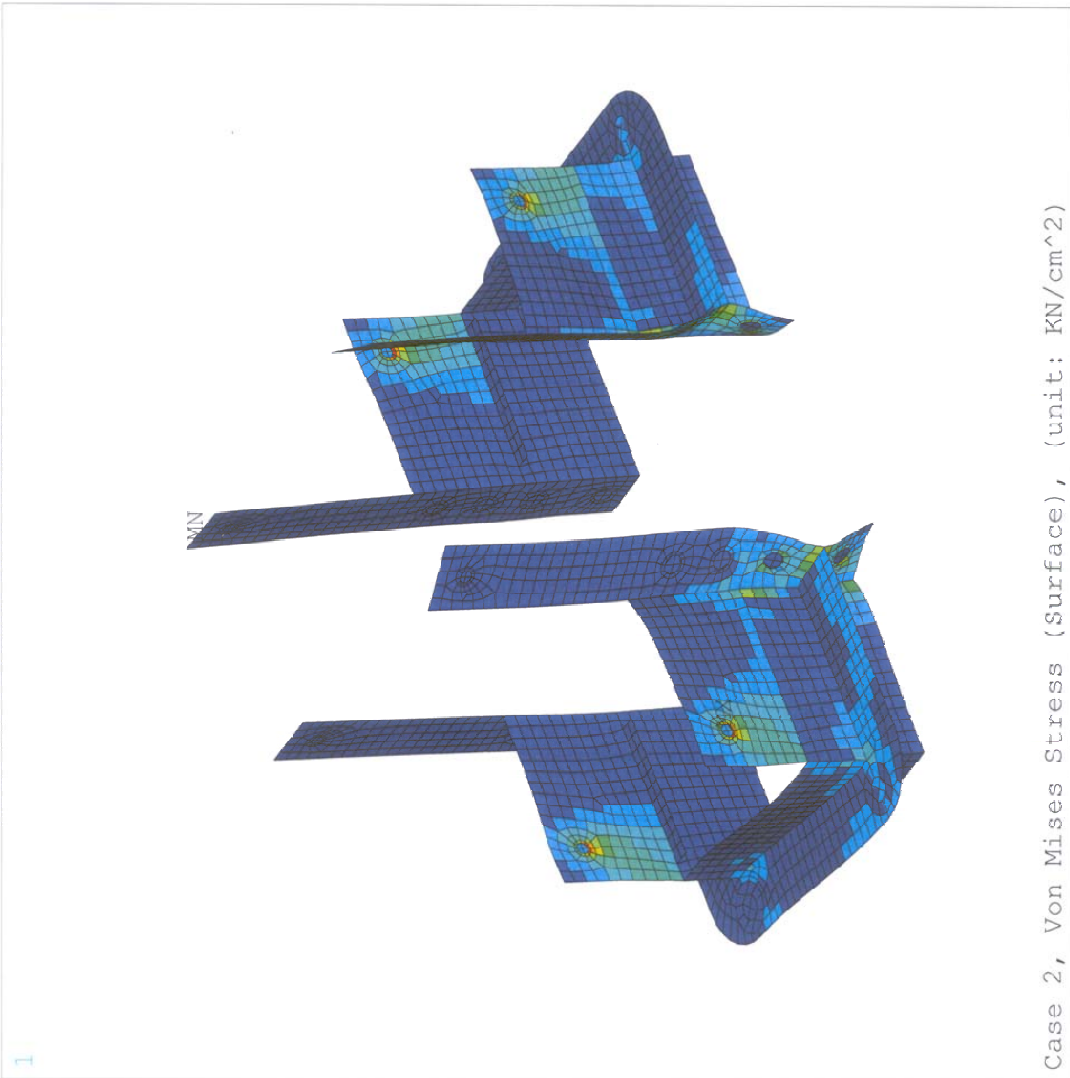
Case 2, Von Mises Stress (Surface), (unit: KN/cm^2)

Figure D.6 Von Mises Stress (Surface) of case 2

163

ANSYS 8.1
JUN 7 2006
11:20:42
ELEMENTS
PowerGraphics
EFACET=1
REAL NUM

F

XV =-.288088
YV =-.674376
ZV =.679869
*DIST=66
*ZF =-17.5
A-ZS=34.01
PRECISE HIDDEN
VSCA=2
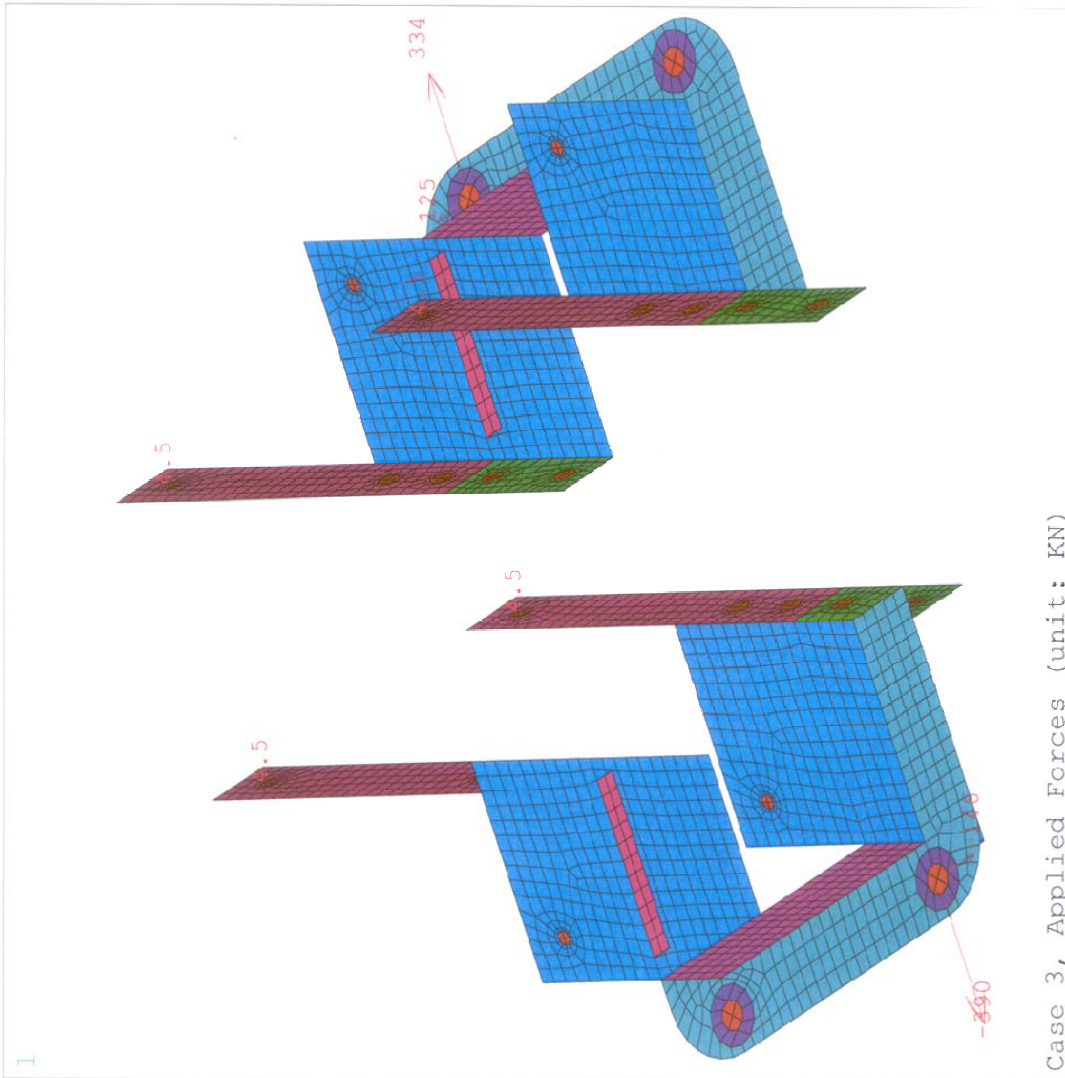
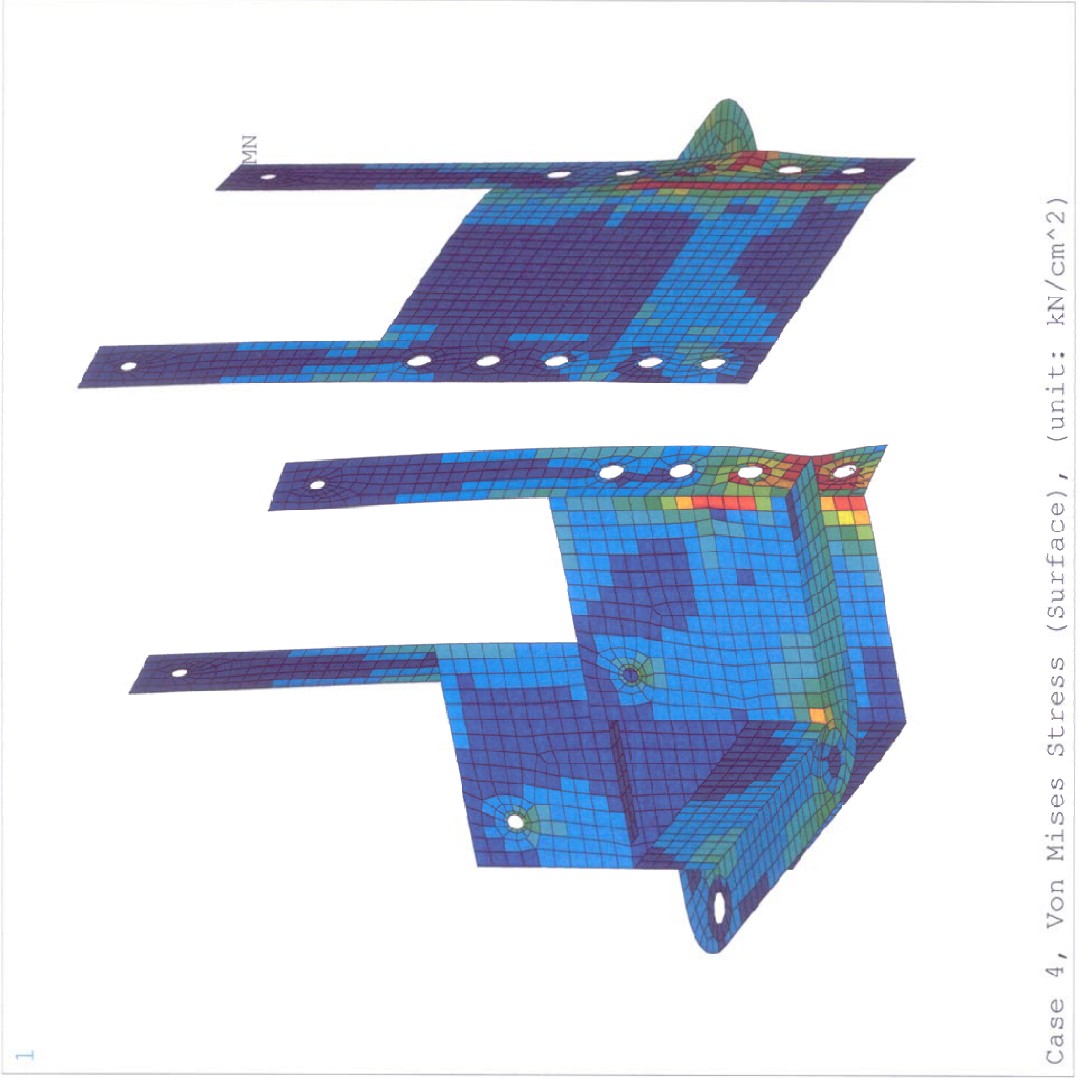Case 3, Applied Forces (unit: KN)

Figure D.7 Applied Forces of Case 3

164

Figure D.8 Von Mises Stress (Middle) of case 3

ANSYS 8.1
JUN 7 2006
11:25:02
ELEMENT SOLUTION
STEP=1
SUB =1
TIME=1
SEQV   (NOAVG)
PowerGraphics
EFACET=1
DMX =.138944
SMN =.007855
SMX =34.5

.007855
3.84
7.673
11.505
15.338
19.17
23.003
26.835
30.668
34.5
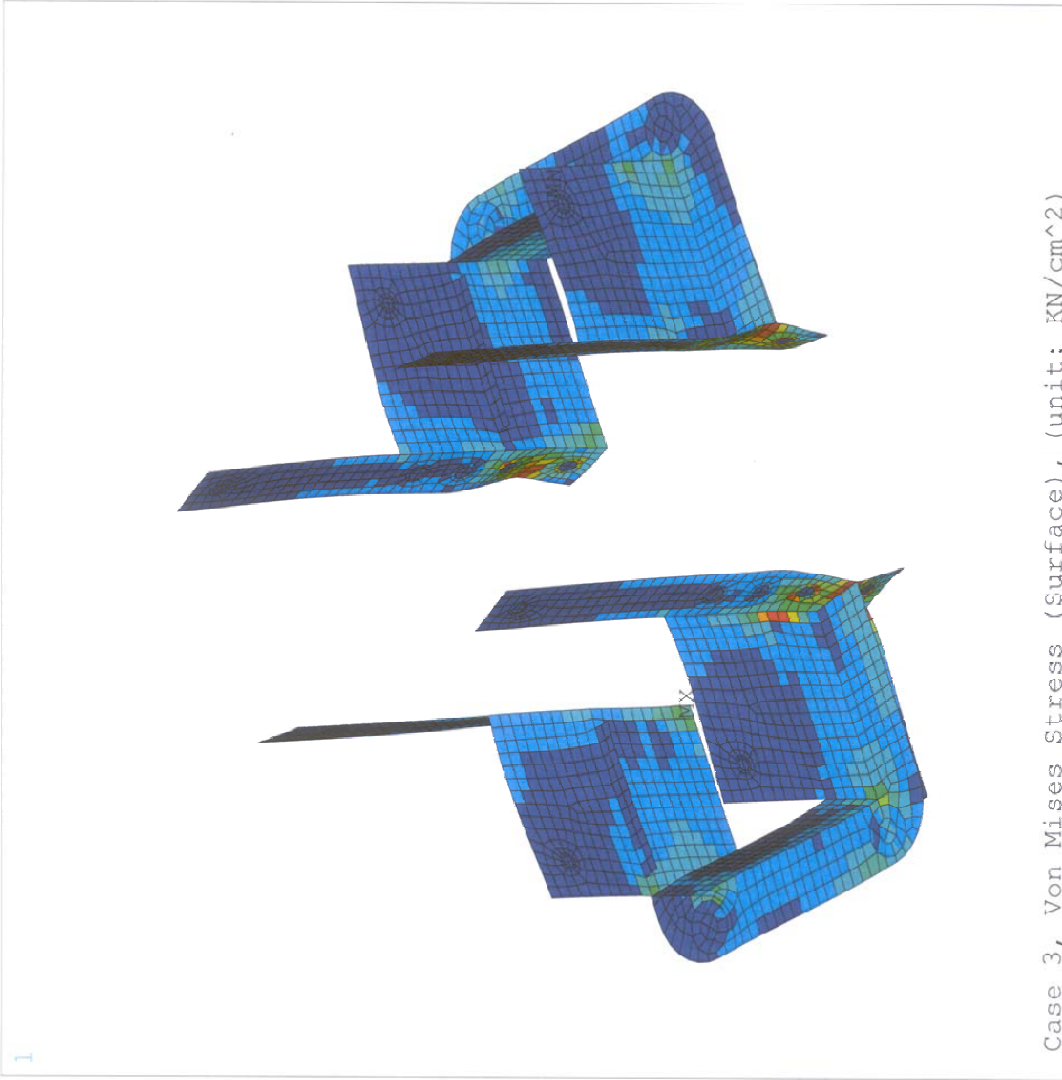
Case 3, Von Mises Stress (Surface), (unit: KN/cm^2)

Figure D.9 Von Mises Stress (Surface) of case 3

166

ANSYS 8.1
JUL 25 2006
18:31:09
ELEMENTS
PowerGraphics
EFACET=1
REAL NUM
F

XV   =.431002
YV   =.827319
ZV   =-.36025
DIST=62.461
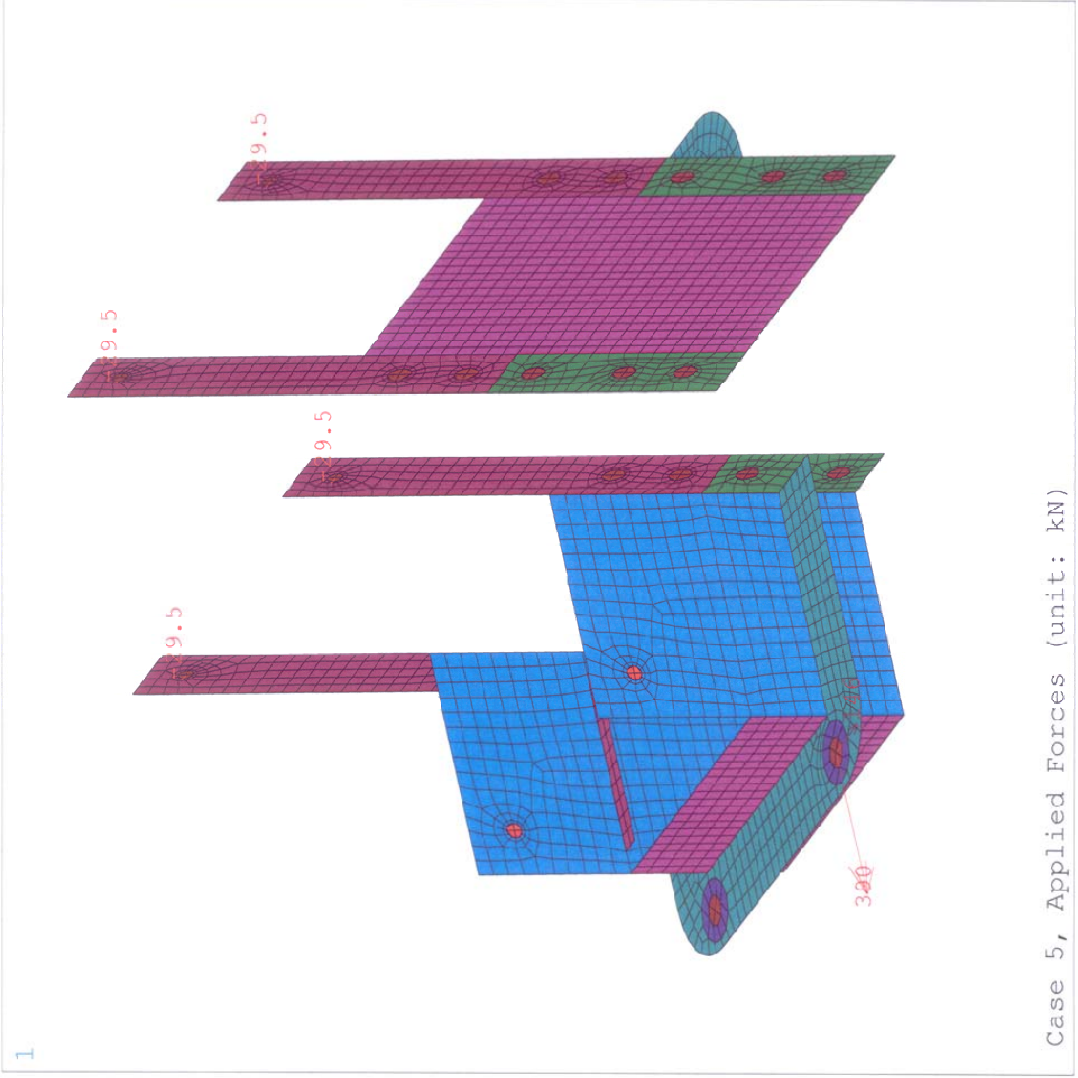XF   =15
ZF   =12.5
A-ZS=-124.88
PRECISE HIDDEN
VSCA=2

Case 4, Applied Forces (unit: kN)

Figure D.10 Applied Forces of Case 4

Figure D.11 Von Mises Stress (Middle) of case 4

Figure D.12 Von Mises Stress (Surface) of case 4
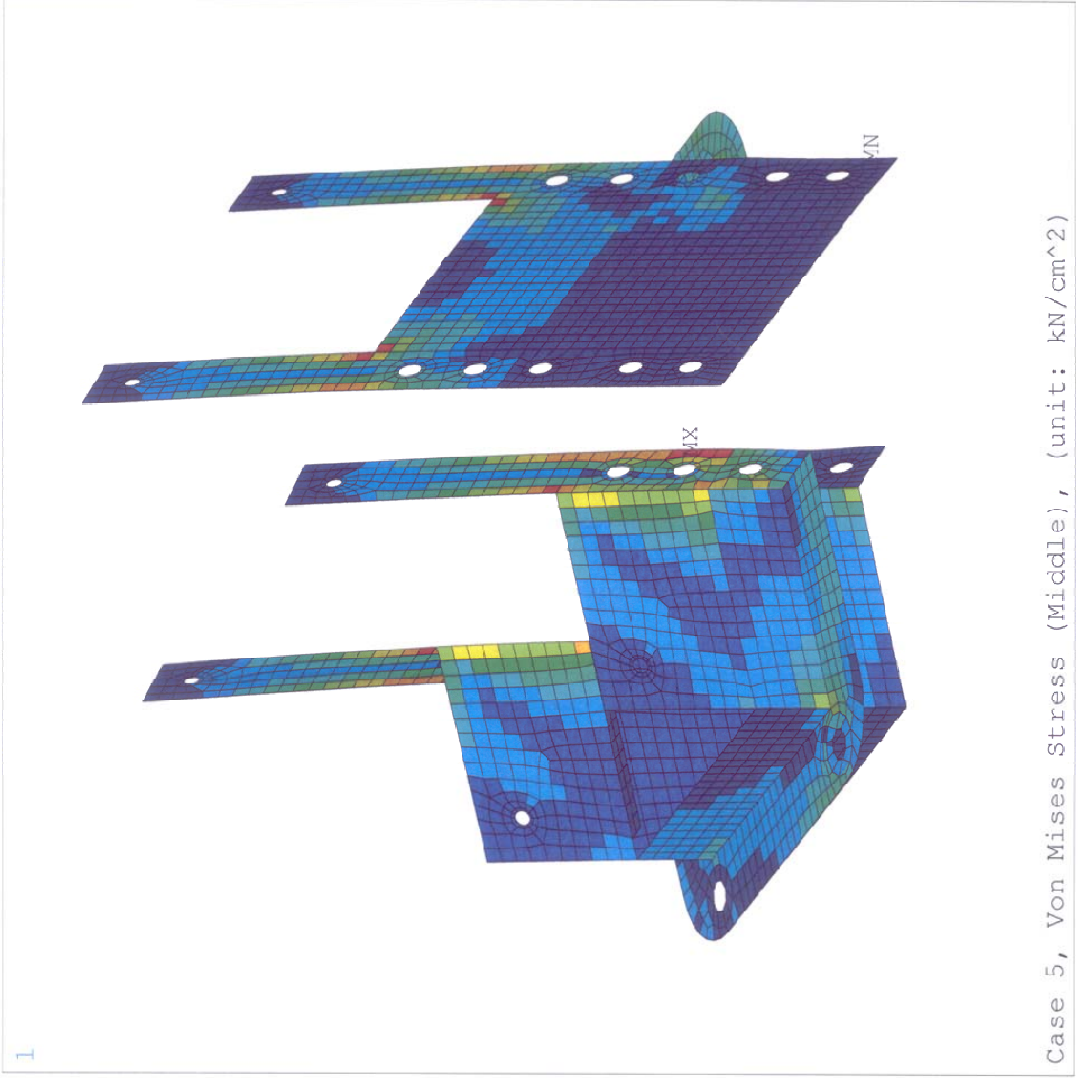
Case 4, Von Mises Stress (Surface), (unit: kN/cm^2)

ANSYS 8.1
JUL 25 2006
18:36:58
ELEMENT SOLUTION
STEP=1
SUB =1
TIME=1
SEQV   (NOAVG)
PowerGraphics
EFACET=1
DMX =.196199
SMN =.023263
SMX =34.5
        .023263
        3.854
        7.685
        11.516
        15.346
        19.177
        23.008
        26.839
        30.669
        34.5

Figure D.13 Applied Forces of Case 5

ANSYS 8.1
JUL 25 2006
18:41:52
ELEMENTS
PowerGraphics
EFACET=1
REAL NUM

XV   =.418774
YV   =.814379
ZV   =.401765
DIST=64.301
XF   =15
ZF   =12.5
A-ZS=-127.172
PRECISE HIDDEN
VSCA=2

Case 5, Applied Forces (unit: kN)

ANSYS 8.1
JUL 25 2006
18:44:35
ELEMENT SOLUTION
STEP=1
SUB =1
TIME=1
SEQV   (NOAVG)
MIDDLE
PowerGraphics
EFACET=1
DMX =.553397
SMN =.017334
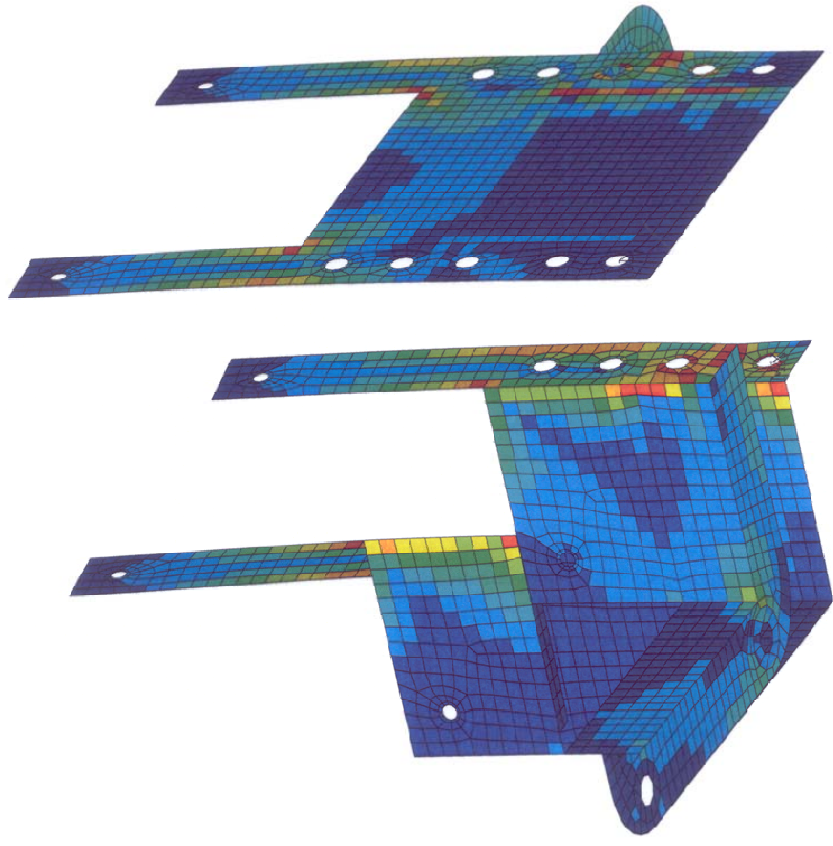SMX =32.137

.017334
3.586
7.155
10.724
14.293
17.862
21.431
25
28.568
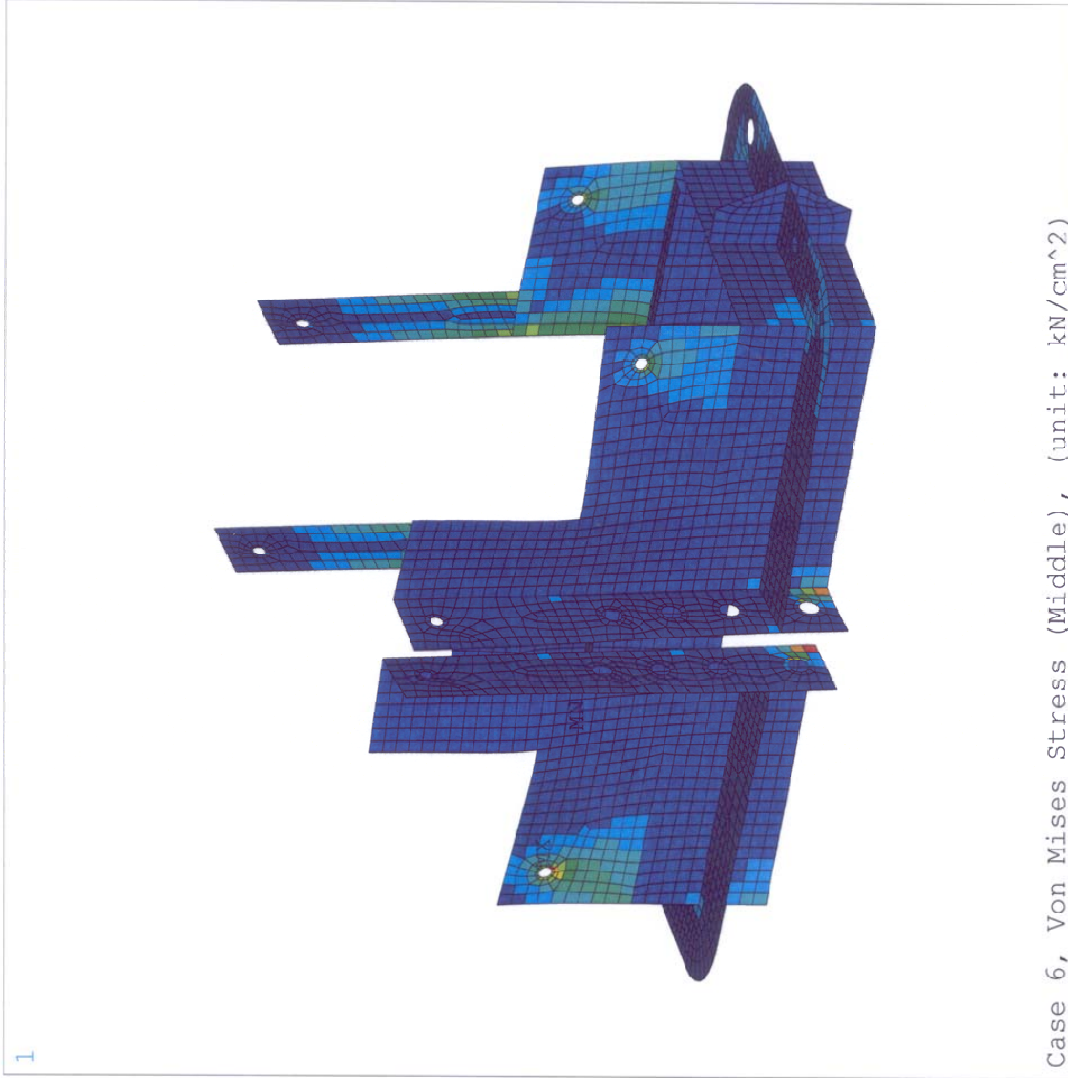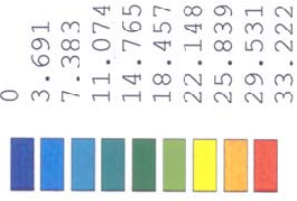32.137

Case 5, Von Mises Stress (Middle), (unit: kN/cm^2)

Figure D.14 Von Mises Stress (Middle) of case 5

171

ANSYS 8.1
JUL 25 2006
18:45:16
ELEMENT SOLUTION
STEP=1
SUB =1
TIME=1
SEQV   (NOAVG)
PowerGraphics
EFACET=1
DMX =.553397
SMN =.009914
SMX =34.5

.009914
3.842
7.674
11.507
15.339
19.171
23.003
26.836
30.668
34.5

Case 5, Von Mises Stress (Surface),   (unit: kN/cm^2)

Figure D.15 Von Mises Stress (Surface) of case 5

172

ANSYS 8.1
JUL 25 2006
18:50:50
ELEMENTS
PowerGraphics
EFACET=1
REAL NUM
F

XV =.546741
YV =-.792968
ZV =.268842
DIST=74.989
ZF =-17.5
A-ZS=-68.819
PRECISE HIDDEN

Case 6, Applied Forces (unit: kN)

Figure D.16 Applied Forces of Case 6

173

ANSYS 8.1
JUL 25 2006
18:53:49
ELEMENT SOLUTION
STEP=1
SUB =1
TIME=1
SEQV   (NOAVG)
MIDDLE
PowerGraphics
EFACET=1
DMX =.717008
SMX =33.222

0
3.691
7.383
11.074
14.765
18.457
22.148
25.839
29.531
33.222

Case 6, Von Mises Stress (Middle), (unit: kN/cm^2)
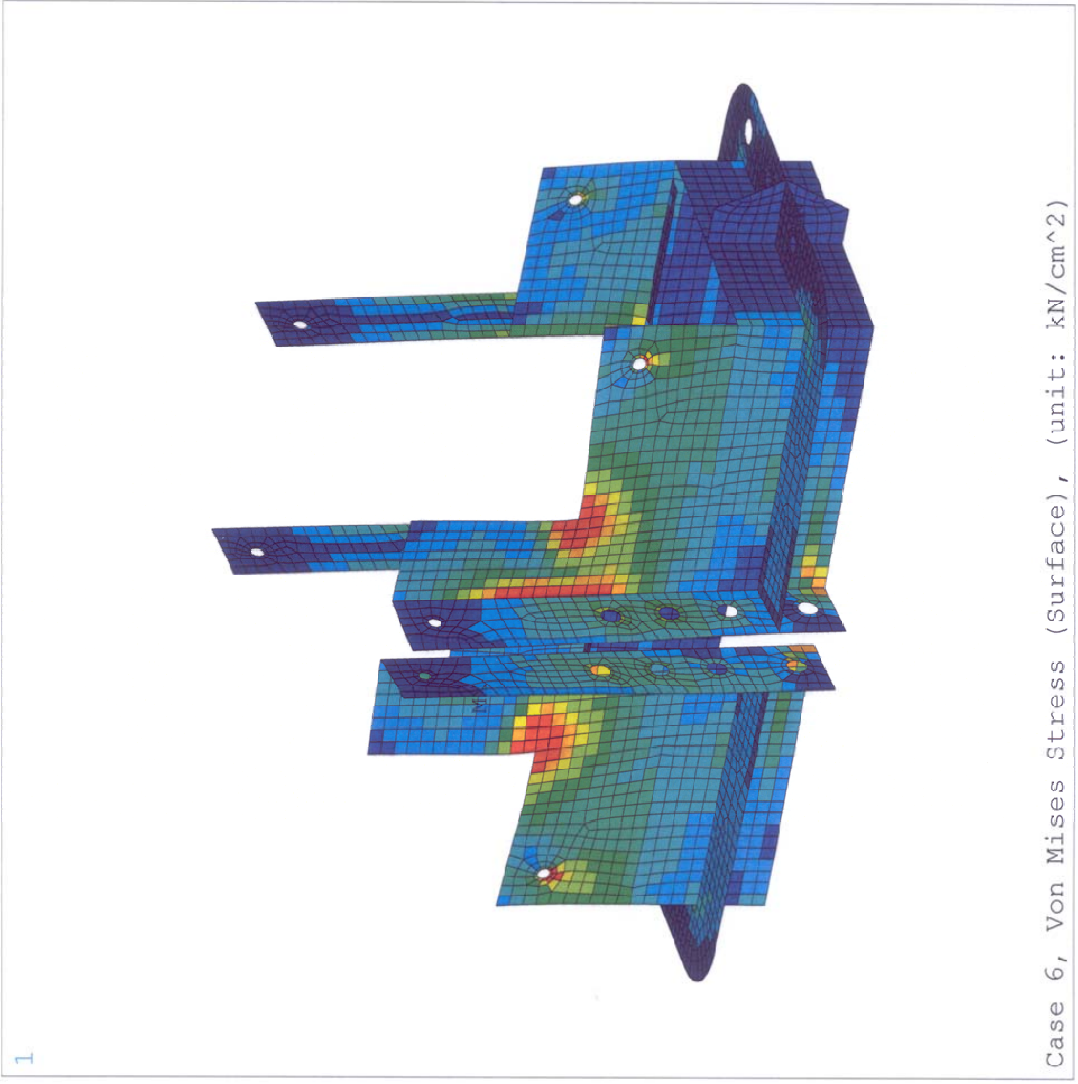
Figure D.17 Von Mises Stress (Middle) of case 6

174

Figure D.18 Von Mises Stress (Surface) of case 6

ANSYS 8.1
JUL 25 2006
18:57:54
ELEMENTS
PowerGraphics
EFACET=1
REAL NUM

F

XV =-.632238
YV =-.720778
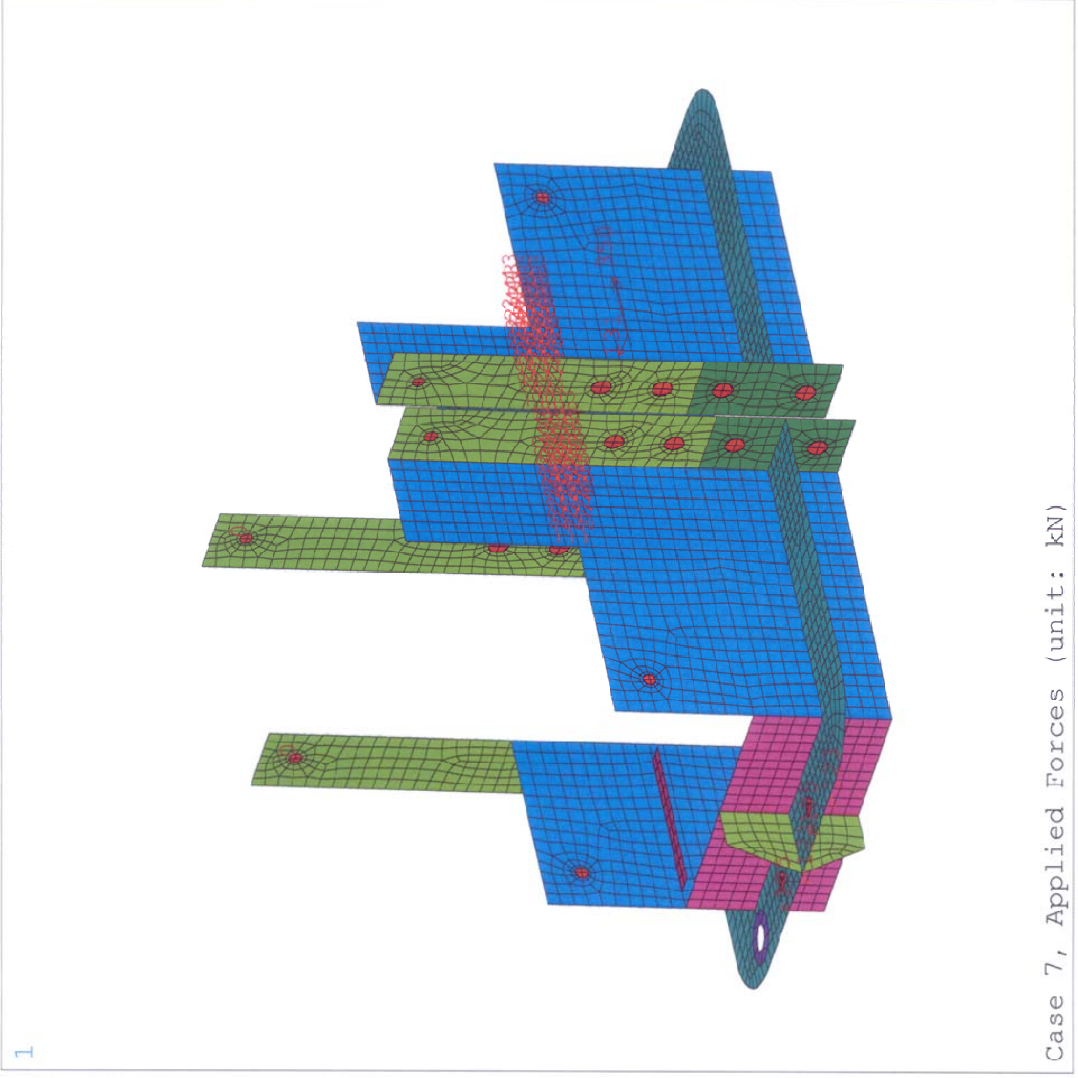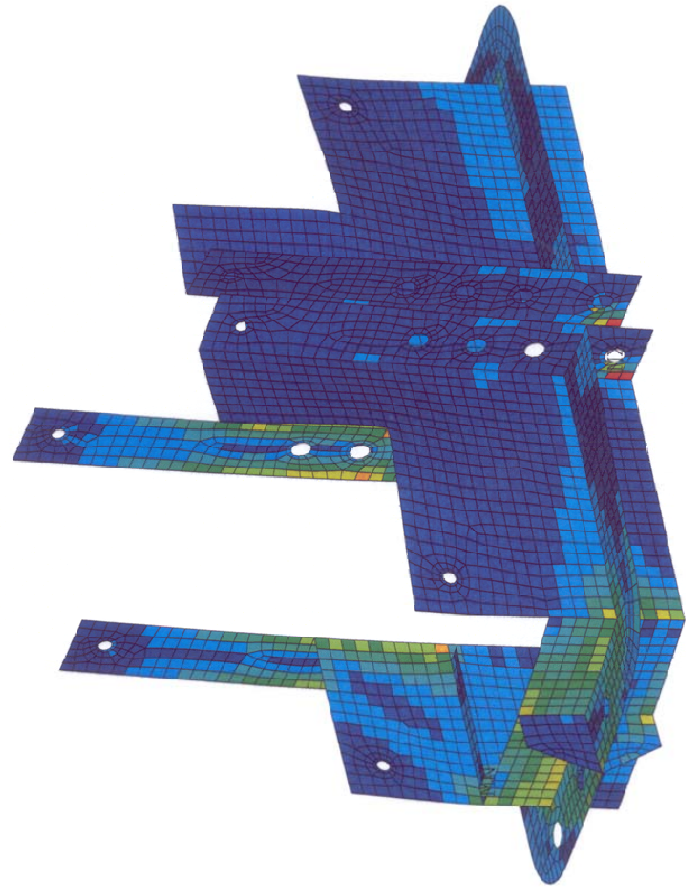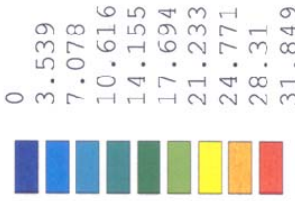ZV =.284173
DIST=74.337
ZF =-17.5
A-ZS=70.685
PRECISE HIDDEN

Case 7, Applied Forces (unit: kN)

Figure D.19 Applied Forces of Case 7

176

ANSYS 8.1
JUL 25 2006
19:00:13
ELEMENT SOLUTION
STEP=1
SUB =1
TIME=1
SEQV   (NOAVG)
MIDDLE
PowerGraphics
EFACET=1
DMX =.804804
SMX =31.849

0
3.539
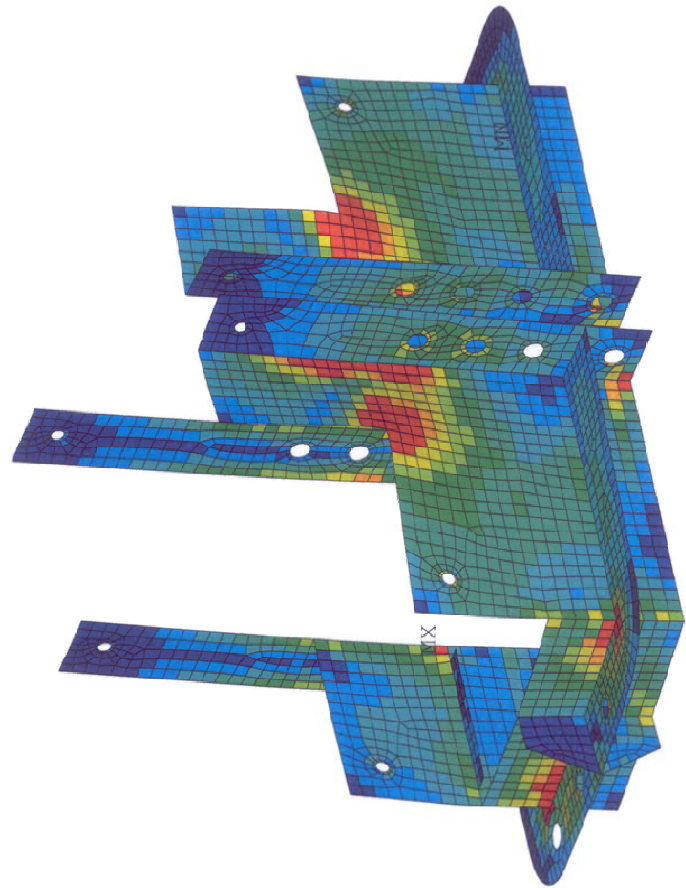7.078
10.616
14.155
17.694
21.233
24.771
28.31
31.849

Case 7, Von Mises Stress (Middle), (unit: kN/cm^2)

Figure D.20 Von Mises Stress (Middle) of case 7

177

ANSYS 8.1
JUL 25 2006
19:00:57
ELEMENT SOLUTION
STEP=1
SUB =1
TIME=1
SEQV   (NOAVG)
PowerGraphics
EFACET=1
DMX =.804804
SMN =.040945
SMX =34.5
    .040945
    3.87
    7.699
    11.527
    15.356
    19.185
    23.014
    26.842
    30.671
    34.5

Case 7, Von Mises Stress (Surface), (unit: kN/cm^2)

Figure D.21 Von Mises Stress (Surface) of case 7

178

ANSYS 8.1
JUL 25 2006
19:04:47
ELEMENTS
PowerGraphics
EFACET=1
REAL NUM

F

XV =.602933
YV =-.759627
ZV =.243802
*DIST=64.102
*XF =7.052
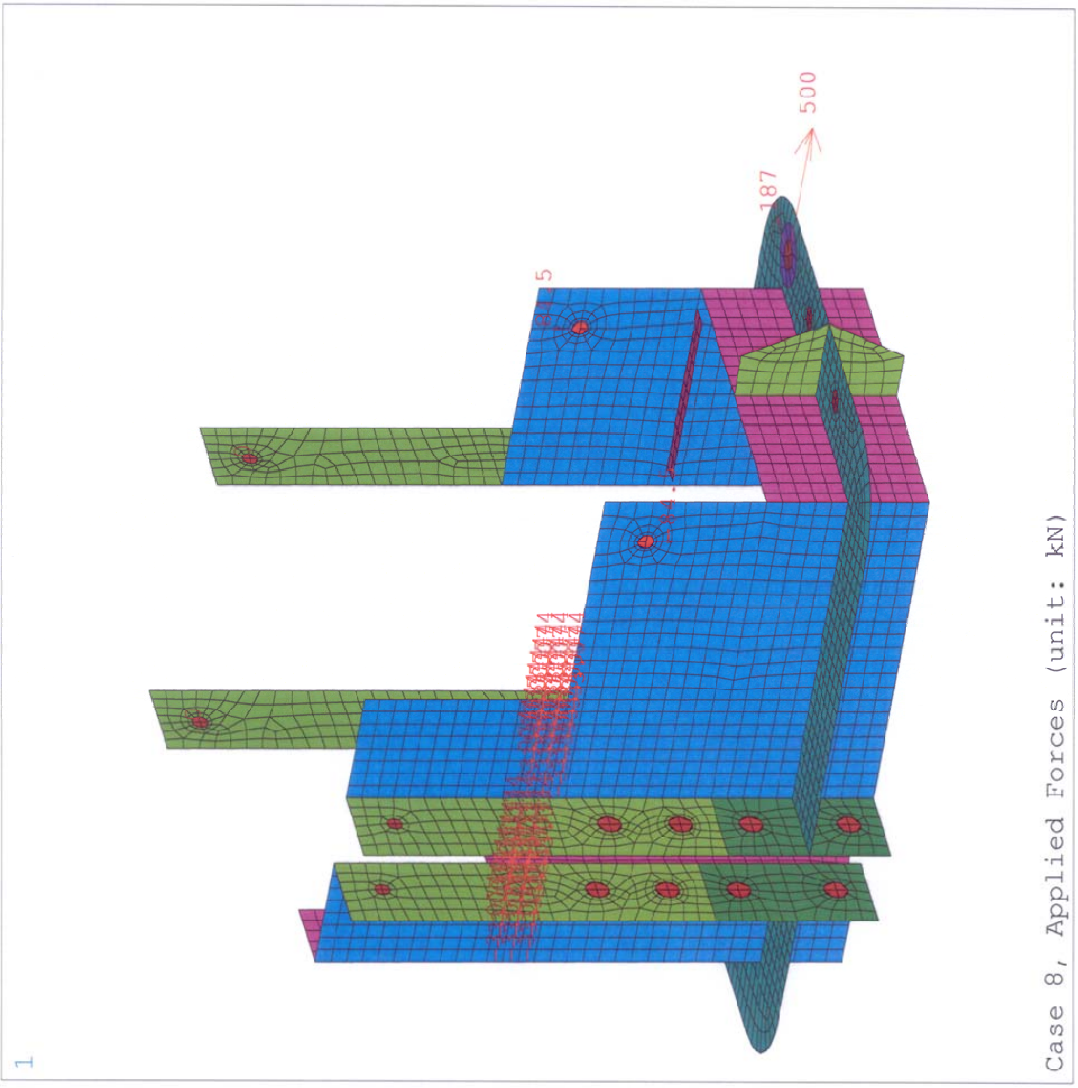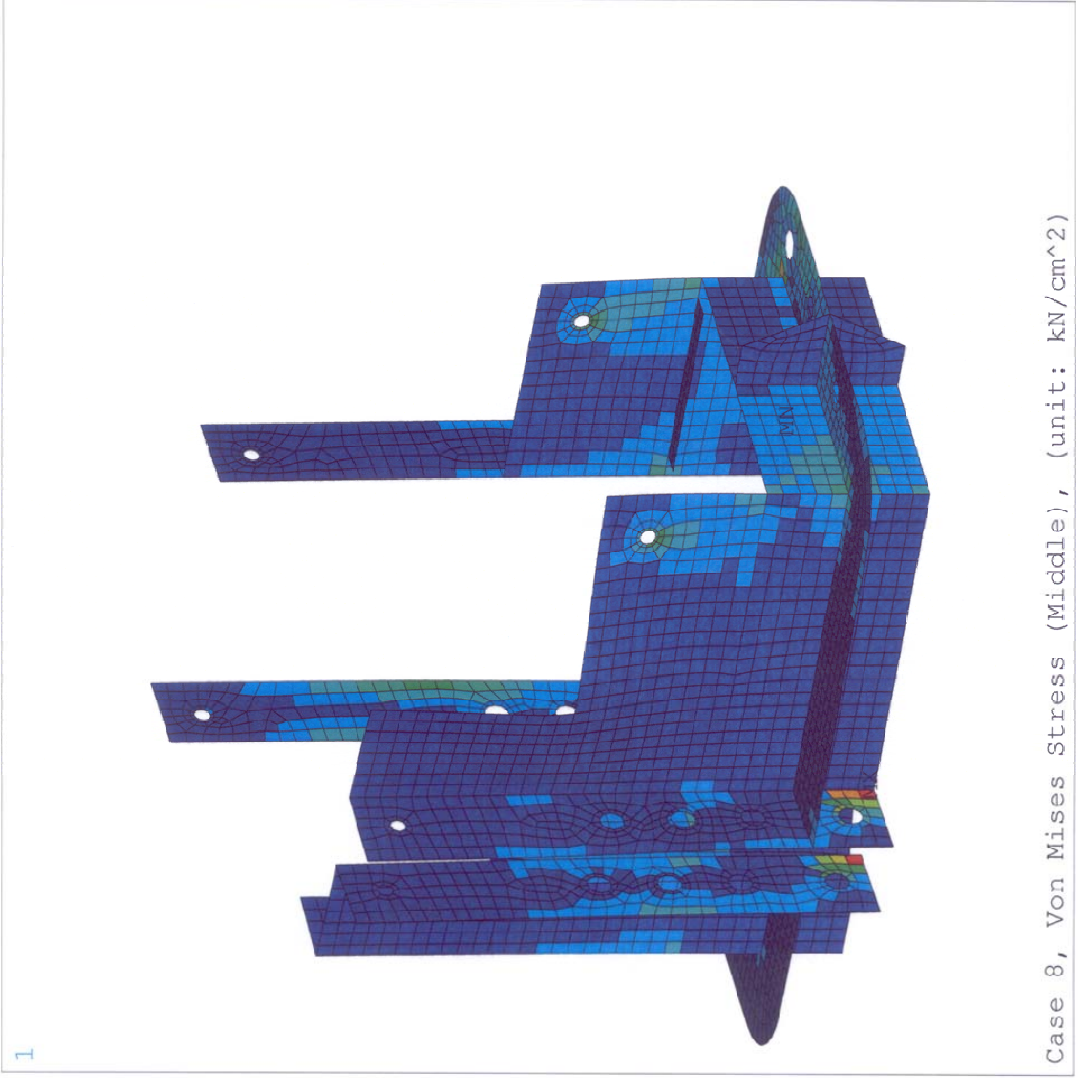*YF =25.475
*ZF =12.5
A-ZS=-72.69
PRECISE HIDDEN
VSCA=2

Case 8, Applied Forces (unit: kN)

Figure D.22 Applied Forces of Case 8

179

ANSYS 8.1
JUL 25 2006
19:07:57
ELEMENT SOLUTION
STEP=1
SUB =1
TIME=1
SEQV   (NOAVG)
MIDDLE
PowerGraphics
EFACET=1
DMX =.831686
SMN =.010181
SMX =34.496
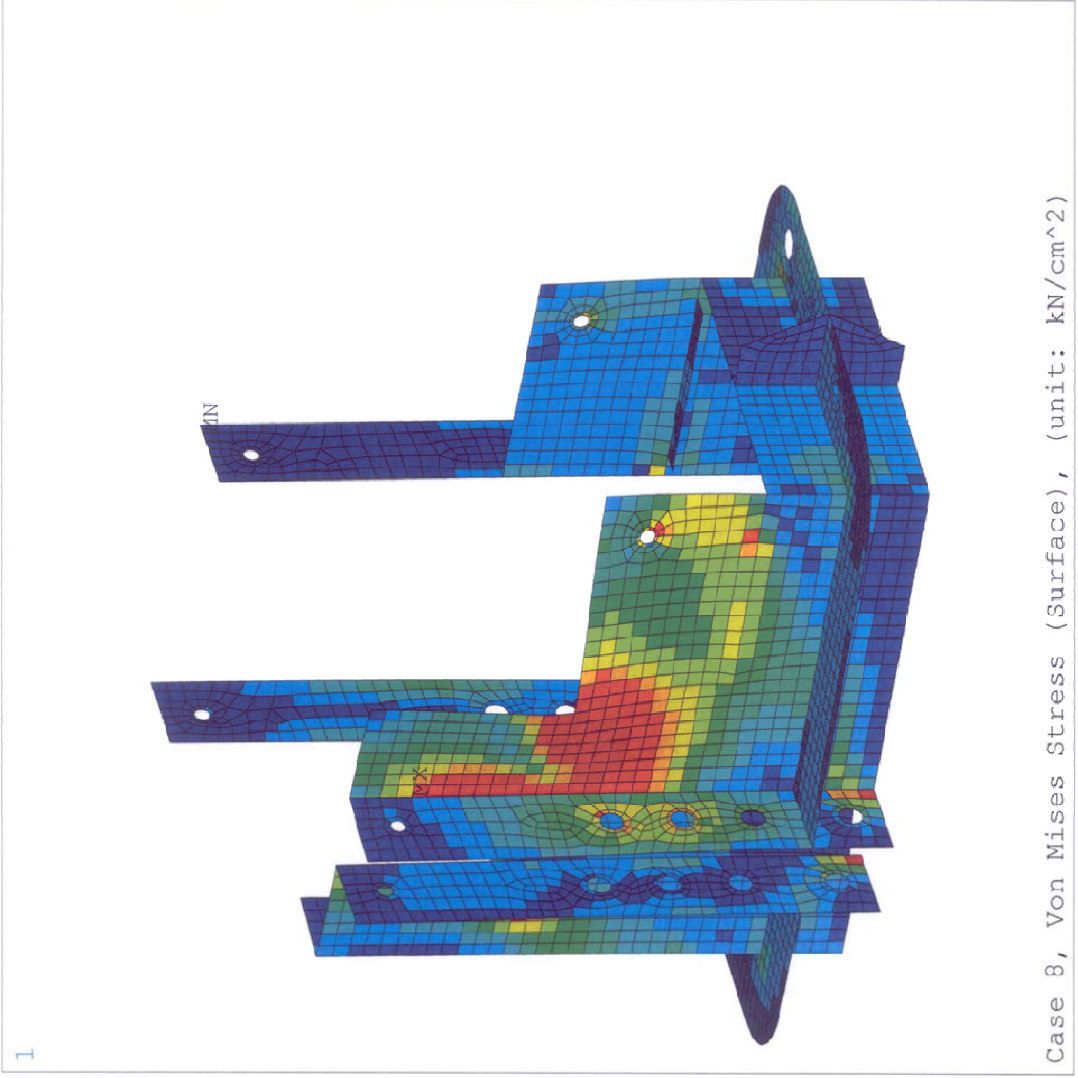   .010181
    3.842
    7.674
    11.506
    15.337
    19.169
    23.001
    26.833
    30.665
    34.496

Case 8, Von Mises Stress (Middle), (unit: kN/cm^2)

Figure D.23 Von Mises Stress (Middle) of case 8

180

ANSYS 8.1
JUL 25 2006
19:07:34
ELEMENT SOLUTION
STEP=1
SUB =1
TIME=1
SEQV   (NOAVG)
PowerGraphics
EFACET=1
DMX =.831686
SMN =.020715
SMX =34.5

.020715
3.852
7.683
11.514
15.345
19.176
23.007
26.838
30.669
34.5

Case 8, Von Mises Stress (Surface), (unit: kN/cm^2)

Figure D.24 Von Mises Stress (Surface) of case 8

181

Figure D.25 Applied Forces of Case 9

ANSYS 8.1
JUL 25 2006
19:17:43
ELEMENT SOLUTION
STEP=1
SUB =1
TIME=1
SEQV   (NOAVG)
MIDDLE
PowerGraphics
EFACET=1
DMX =.655772
SMX =34.497

0
3.833
7.666
11.499
15.332
19.165
22.998
26.831
30.664
34.497

Case 9, Von Mises Stress (Middle), (unit: kN/cm^2)
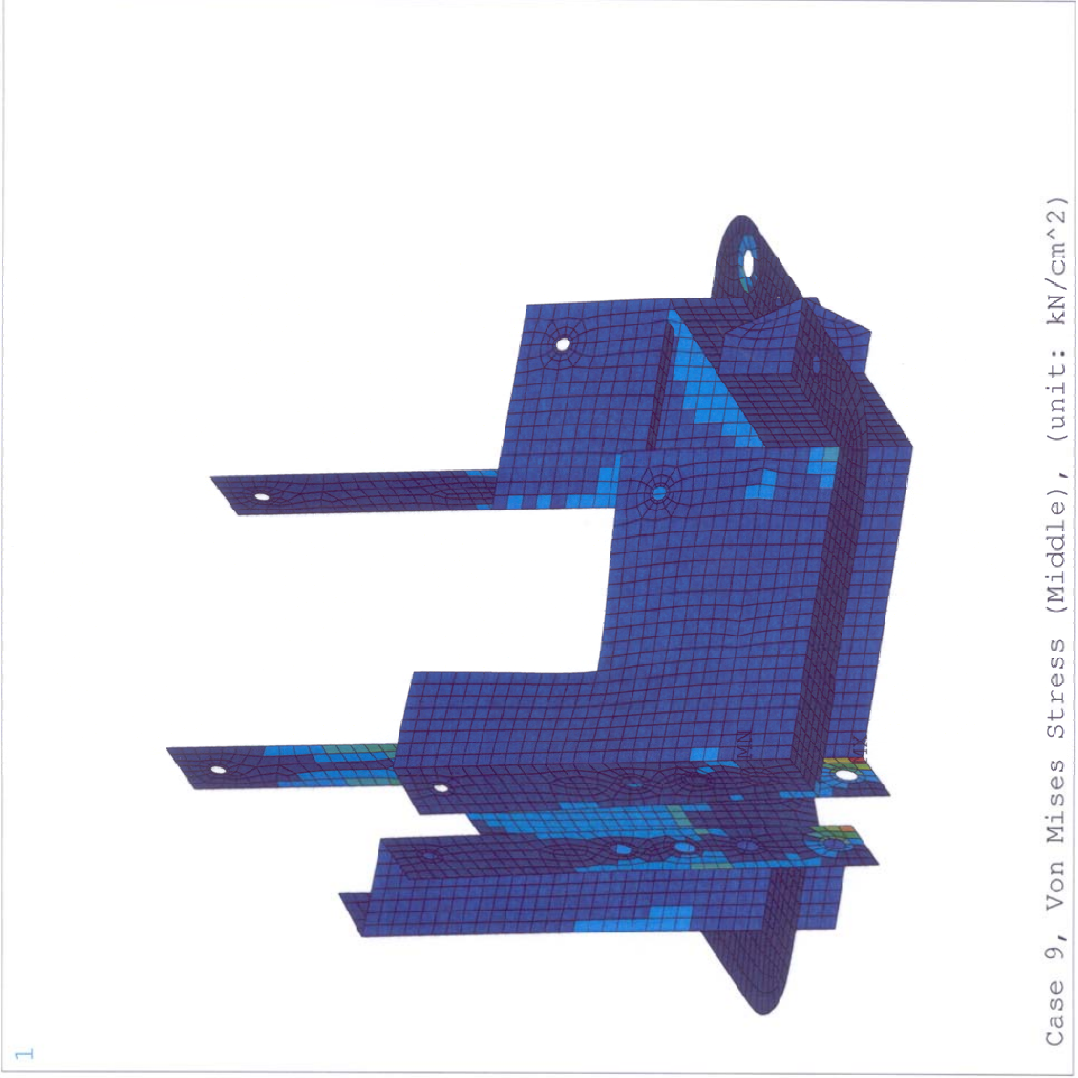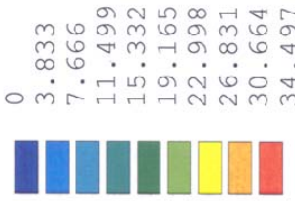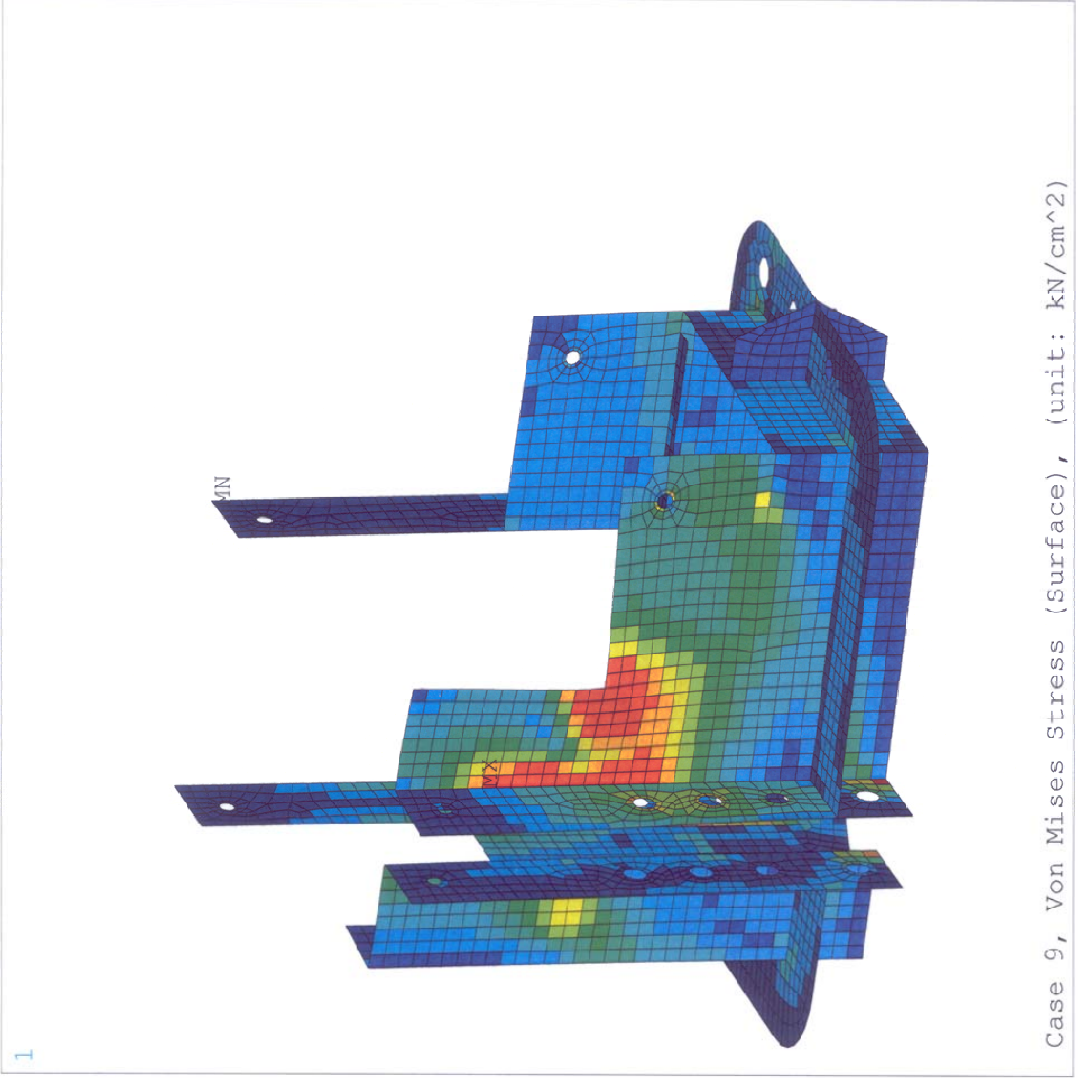
Figure D.26 Von Mises Stress (Middle) of case 9

183

ANSYS 8.1
JUL 25 2006
19:13:19
ELEMENT SOLUTION
STEP=1
SUB =1
TIME=1
SEQV   (NOAVG)
PowerGraphics
EFACET=1
DMX =.655618
SMN =.01714
SMX =34.5

.01714
3.849
7.68
11.511
15.343
19.174
23.006
26.837
30.669
34.5

Case 9, Von Mises Stress (Surface), (unit: kN/cm^2)

Figure D.27 Von Mises Stress (Surface) of case 9

184

References

ACI 318-05 / ACI 318R-05 (2005), Building Code and Commentary. ACI Committee 318, American Concrete Institute, Farmington Hills, Michigan.

Anderson, J. G. (Coordinator) (2000). "1999 Kocaeli, Turkey, Earthquake Reconnaissance Report," Chapter 6. Implications for Seismic Hazard Analysis. *Earthquake Spectra*, Vol. 16 (Supplement A), pp. 113-137. December 2000. Earthquake Engineering Research Institute.

ASCE 7-05 (2006), Minimum Design Loads for Buildings and Other Structures. American Society of Civil Engineers, Reston, Virginia.

Aschheim, M. (Coordinator) (2000). "1999 Kocaeli, Turkey, Earthquake Reconnaissance Report," Chapter 11. Performance of Buildings. *Earthquake Spectra*, Vol.16 (Supplement A), pp. 237-279. December 2000. Earthquake Engineering Research Institute.

Ataköy, H. (1999). "17 August Marmara Earthquakes and the Precast Concrete Structures Built by TPCA Members." Turkish Precast Association. Ankara, Turkey. 12p.

Code for the Buildings to be Built in Disaster Areas, Ministry of Construction, January 1998, Ankara (in Turkish).

Elwood, K. J., and Moehle, J. P. (2003), "Shake Table Test and Analitical Studies on the Gravity Load Collapse of Reinforced Concrete Frames." *PEER Report* 2003/01, Pacific Earthquake Engineering Research Center, University of California, Berkeley.

Ersoy, U., T. Tankut, and G. Özcebe (1999). "Damages Observed in the Precast Frames Structures in the 1998 Ceyhan Earthquake and their Rehabilitation," Department of Civil Engineering, Middle East Technical University, Ankara, Turkey.

FEMA 356 (2000), Prestandard and Commentary for the Seismic Rehabilitation of Buildings, Federal Emergency Management Agency, FEMA 500 C Street SW, Washington, D.C.

Johnson, G. (Coordinator) (2000). "1999 Kocaeli, Turkey, Earthquake Reconnaissance Report," Chapter 14. Industrial Facilities. *Earthquake Spectra*, Vol. 16 (Supplement A), pp. 311-350. December 2000. Earthquake Engineering Research Institute.

Karsan, I.D., and Jirsa, J.O. (1969). "Behavior of Concrete under Compressive Loadings," *Journal of the Structural Division*, Vol. 95 (12), pp. 2543–2563. 1969, ASCE.

Karaesmen, E. (2001). "Prefabrication in Turkey: Facts and Figures," Department of Civil Engineering, Middle East Technical University, Ankara, Turkey.

Kent, D.C., and Park, R. (1971). "Flexural Members with Confined Concrete," *Journal of the Structural Division*, Vol. 97 (7), pp. 1969-1990. July 1971. ASCE.

Lettis, W. (Coordinator) (2000). "1999 Kocaeli, Turkey, Earthquake Reconnaissance Report", Chapter 1. Geology and Seismicity. *Earthquake Spectra*, Vol. 16 (Supplement A), pp. 1-9. December 2000. Earthquake Engineering Research Institute.

Moehle, J. P. (1992). "Displacement-Based Design of RC Structures Subjected to Earthquakes". *Earthquake Spectra,* Vol. 8, No. 3: 403-428. 1992. Earthquake Engineering Research Institute.

Posada, M. (2001). "Performance of Precast Industrial Buildings during the 1999 Earthquakes in Turkey." M.S. Thesis, Department of Civil Engineering, University of Texas at Austin.

Scawthorn, C. and Johnson, G. S. (2000). "Preliminary Report Kocaeli (Izmit) Earthquake of 17 August 1999." *Engineering Structures*, Vol. 22, pp. 727-745.

Shimazaki, K. and Sozen, M.A. (1984). "Seismic Drift of Reinforced Concrete Structures. Research Reports," Hanzama-Gumi, Ltd., Tokyo, Japan, pp. 145-166 (in Japanese).

Paz, M. (2004). Structural Dynamics: Theory and Computation. 5th Edition, Boston.

Taucer, F.F., Spacone, E., and Filippou, F.C. (1991). "A Fiber Beam-Column Element for Seismic Response Analysis of Reinforced Concrete Structures." *EECR Report* 91/17, Earthquake Engineering Research Center, University of California, Berkeley.

TS-9967, Design Construction and Erection Methods for Precast Reinforced and Prestressed Members, Structures and Buildings, Turkish Standards Institute, 1993, Ankara (in Turkish).